

---

# **METABOLOMICS AS A MEANS TO CONTROL HUMAN BACTERIAL INFECTIONS USING A FORMYL PEPTIDE RECEPTOR ANTAGONIST**

---

**Paola Cuomo**

Dottorato in Biotecnologie – XXXIV ciclo

Università di Napoli Federico II







Dottorato in Biotecnologie – XXXIV ciclo

Università di Napoli Federico II



---

# **METABOLOMICS AS A MEANS TO CONTROL HUMAN BACTERIAL INFECTIONS USING A FORMYL PEPTIDE RECEPTOR ANTAGONIST**

---

**Paola Cuomo**

Dottorando: Paola Cuomo  
Relatore: Prof. Rosanna Capparelli  
Correlatori: Dr. Andrea Motta  
Dr. Andrea Fulgione  
Coordinatore: Prof. Marco Moracci

Settore Scientifico Disciplinare MED/04



“Chi ha un perché  
abbastanza forte, può  
superare qualsiasi  
come” (Nietzsche)



## **ACKNOWLEDGEMENTS**

I gratefully acknowledge my supervisor Prof. Rosanna Capparelli for her guidance and support throughout the project.

I'm extremely thankful to Dr. Chiara Medaglia for her assistance and contribution to realize part of this work.

I would like to thank Prof. Mauro Maniscalco and Dr. Andrea Motta for giving me the opportunity to approach the world of research and achieve this objective. Thank you for your support.

I also thank Dr. Debora Paris for her scientific support, advice and encouragement to never give up.

Lastly, I deeply thank my family for being so understanding and supportive during the whole period of this project.

## TABLE OF CONTENTS

<b><u>RIASSUNTO</u></b> .....	1
<b><u>SUMMARY</u></b> .....	7
<b><u>INTRODUCTION</u></b> .....	9
Metabolomics: the revolution of -omics sciences	10
- Metabolomics approach	12
- Clinical applications of metabolomics	13
Inflammation: host immune response	14
<i>Helicobacter pylori</i> infection	15
Aim of thesis	17
<b><u>CHAPTER 1: Metabolomics: a tool to assess in vitro response to <i>Helicobacter pylori</i> infection and reveal the causal role of <i>Helicobacter pylori</i> infection in extra-gastric diseases</u></b> .....	22
1.1 An In Vitro Model to Investigate the Role of <i>Helicobacter pylori</i> in Type 2 Diabetes, Obesity, Alzheimer's Disease and Cardiometabolic Disease	25
<b><u>CHAPTER 2: The role of Formyl peptide receptors in permanent and low-grade inflammation: <i>Helicobacter pylori</i> infection as a model</u></b> .....	38
<b><u>CHAPTER 3: Marine biomolecules: a new challenge for biotechnological applications. The effects of the algal alkaloid Caulerpin in modulating Formyl peptide receptors expression in <i>Helicobacter pylori</i> infection</u></b> .....	53
3.1 Marine natural products	54
3.2 Green algae: source of bioactive secondary metabolites	54
3.2.1 Caulerpin: green algal secondary metabolite	55

3.3 Biotechnological applications of Caulerpin as potential FPRs antagonist	56
---	----

3.4 Caulerpin mitigates <i>Helicobacter pylori</i> -induced inflammation via Formyl peptide receptors	60
---	----

<b><u>CHAPTER 4: Metabolomics: A footprinting metabolic approach to assess cell response to Caulerpin treatment in modulating <i>Helicobacter pylori</i> systemic effects</u></b>	<b>85</b>
---	-----------

4.1 Introduction	86
------------------	----

4.2 Materials and methods	87
4.2.1 Cell culture	87
4.2.2 <i>Helicobacter pylori</i> culture filtrate preparation	87
4.2.3 Cell culture for footprinting metabolite profiling by NMR analysis	87
4.2.4 NMR sample preparation	88
4.2.5 NMR spectra acquisition	88
4.2.6 NMR data processing	88
4.2.7 Network analysis	89
4.2.8 Statistical analysis	89

4.3 Results and Discussion	90
4.3.1 <i>Helicobacter pylori</i> culture filtrate may promote a systemic metabolic reprogramming	90
4.3.2 Caulerpin may recover the <i>Helicobacter pylori</i> culture filtrate-induced metabolic changes	95

4.4 Conclusion	99
----------------	----

<b><u>CONCLUDING REMARKS</u></b>	<b>104</b>
----------------------------------	------------

<b><u>APPENDIX</u></b>	<b>107</b>
------------------------	------------

## **RIASSUNTO**



*Helicobacter pylori* (*H. pylori*) è un batterio microaerofilo Gram-negativo, in grado di stabilire un'infezione gastrica cronica. Nonostante lo stomaco possieda un pH estremamente basso, tale da impedire la crescita della maggior parte delle forme microbiche, *H. pylori* ha sviluppato particolari caratteristiche microbiologiche che, gli consentono di sopravvivere e colonizzare la mucosa gastrica, provocando l'insorgenza di diverse patologie, tra cui: gastriti croniche, ulcere, linfoma di MALT (Mucosal Associated Lymphoid Tissue) e neoplasie gastriche.

*H. pylori* ha una caratteristica forma elicoidale che, insieme ai flagelli che lo costituiscono, gli consente di raggiungere lo strato di muco che riveste le cellule epiteliali gastriche, laddove si annida sfuggendo all'azione distruttiva del pH gastrico. La sua capacità di produrre enormi quantità di enzima ureasi, inoltre, gli consente di idrolizzare l'urea in ammoniaca ( $\text{NH}_3$ ) e anidride carbonica ( $\text{CO}_2$ ), così da neutralizzare l'acidità dell'ambiente gastrico. Queste caratteristiche rendono *H. pylori* un batterio responsabile di una malattia endemica in tutto il mondo, considerata la più comune tra le patologie batteriche. Circa il 50% della popolazione mondiale ne risulta affetta, con una maggiore prevalenza nelle aree geografiche industrialmente poco sviluppate e con scarse condizioni igienico-sanitarie. Sebbene la maggior parte delle persone infettate non manifesti sintomi; una minoranza di persone (20%) sviluppa importanti patologie gastroduodenali.

La diversa manifestazione dell'infezione dipende da diversi fattori quali: la risposta dell'ospite, la virulenza del batterio e i fattori ambientali.

Ogni volta che un microorganismo patogeno entra in contatto con l'uomo, questo interviene attivando la risposta immunitaria innata. Quest'ultima si realizza in due fasi: la prima è caratterizzata dall'azione di elementi non specifici e non inducibili dell'ospite, tra cui barriere fisiche e fisiologiche (cute, mucose, pH gastrico), il cui compito è quello di impedire l'ingresso del patogeno; la seconda invece è caratterizzata da elementi effettori dotati di recettori (Pattern Recognition Receptors, PRRs) capaci di riconoscere strutture molecolari conservate del patogeno (Pathogen Associated Molecular Patterns, PAMPs), i quali danno il via ai meccanismi di difesa dell'ospite che portano alla risposta infiammatoria.

L'infiammazione è una delle modalità più efficaci di risposta dell'ospite ad agenti esterni. Tuttavia, se non appropriatamente contenuta, può condurre ad alterazioni sistemiche e danni tissutali

più gravi di quelli prodotti dall'insulto. Numerose evidenze scientifiche infatti, riportano una profonda associazione tra meccanismi infiammatori e patologie con un elevato tasso di morbosità e mortalità.

Generalmente, la principale sfida per un microorganismo patogeno è quella di evitare la sua eliminazione da parte del sistema immunitario. La capacità di *H. pylori* di stabilire un'infezione persistente, indica la sua abilità di eludere le difese dell'ospite, sviluppando esso stesso dei meccanismi di difesa. *H. pylori*, infatti, sopravvive nel lume acido dello stomaco, posizionandosi oltre la portata dei comuni sistemi di riconoscimento dell'ospite. Ciò nonostante, promuove ugualmente l'attivazione del sistema immunitario, inducendo una risposta infiammatoria moderata, ma persistente, causa delle numerose complicazioni cliniche associate all'infezione.

L'infiammazione cronica ha un ruolo patogenetico determinante nell'insorgenza del cancro gastrico associato all'infezione da *H. pylori*. In aggiunta, studi recenti hanno evidenziato il ruolo dell'infiammazione associata all'infezione non solo nell'alterazione dei processi biologici che caratterizzano il lume gastrico, ma anche di quelli esterni all'ambiente gastrico, provocando importanti manifestazioni extra-gastriche (Capitolo 1).

In assenza di una adeguata strategia vaccinale che miri a prevenire la diffusione del patogeno, la terapia antibiotica resta l'unica arma a disposizione per contrastare l'infezione e le manifestazioni cliniche che ne derivano. Sfortunatamente, la rapida diffusione dell'antibiotico resistenza sta avendo un forte impatto negativo sui trattamenti farmacologici disponibili, compromettendone l'efficacia e contribuendo al dilagare dell'infezione.

In questo scenario, *H. pylori* rappresenta una seria minaccia per la salute dell'uomo, contro la quale sono necessarie strategie farmacologiche alternative.

Il presente lavoro di tesi ha come scopo principale quello di **individuare nuovi agenti terapeutici per il controllo dell'infezione da *Helicobacter pylori*, che abbiano come obiettivo la modulazione della risposta immunitaria innata, utilizzando come target farmacologico i recettori per i peptidi formilati (FPRs)** (Capitoli 2 e 3).

I recettori per i peptidi formilati sono PRRs (Capitolo 2), il cui nome deriva dalla capacità di legare peptidi formilati, sia di derivazione

batterica (PAMPs), sia di derivazione mitocondriale (Damage Associated Molecular Patterns, DAMPs), partecipando pertanto alla patogenesi delle infezioni e delle patologie infiammatorie. Essi appartengono alla famiglia dei recettori accoppiati a proteine G ( $G_i$ ), i quali attraverso l'attivazione delle proteine G eterotrimeriche, riescono a convertire stimoli extracellulari in risposte intracellulari. Di conseguenza, tali recettori appaiono coinvolti in numerosi processi fisiologici e patologici, costituendo importanti target per lo sviluppo di nuovi agenti terapeutici. Si tratta di recettori ad attività chemiotattica, particolarmente coinvolti nei processi infiammatori, di cui l'uomo possiede tre differenti isoforme: FPR1, FPR2 o FPRL1 e FPR3 o FPRL2. Tutti e tre i recettori sono espressi a livello dei monociti, ma solo FPR1 e FPR2 si trovano a livello della membrana dei neutrofili. Inoltre, FPR1 è espresso a livello degli astrociti, delle cellule della microglia, degli epatociti e delle cellule dendritiche immature. FPR2 invece, oltre alle cellule che esprimono FPR1, si trova anche sui fagociti, leucociti, cellule epiteliali ed endoteliali. Pertanto, FPR2 è tra i tre recettori, quello con una maggiore promiscuità in termini di distribuzione tissutale e non solo. Al contrario di FPR1 e FPR3, FPR2 può rispondere ad un elevato numero di ligandi di origine esogena o endogena e caratterizzati da una cospicua diversità strutturale.

È interessante notare inoltre, che FPR2 può legare un ampio numero di molecole di origine sintetica, rappresentando in tal senso, un importante strumento per lo sviluppo di nuovi farmaci.

I recettori per i peptidi formilati contribuiscono in misura significativa al processo patologico associato all'infezione da *H. pylori*. Quest'ultimo infatti, produce un peptide ad attività antimicrobica [Hp(2-20)], il quale interagendo con FPR2 favorisce la colonizzazione e infiammazione della mucosa gastrica. L'interazione tra Hp(2-20) e FPR2 attiva una cascata del segnale a valle che culmina nella risposta infiammatoria, partecipando alla severità dell'infezione.

Sulla base di quanto riportato, l'attività di ricerca si è focalizzata sulla **identificazione e caratterizzazione di composti di origine naturale capaci di antagonizzare FPR2** e quindi inibirne la cascata di trasduzione del segnale.

Negli ultimi anni l'invasione del Mar Mediterraneo da parte di specie "aliene" o alloctone ha rappresentato un problema di portata mondiale, modificando la struttura degli habitat e provocando la distribuzione degli organismi autoctoni, con importanti conseguenze ecologiche, sociali ed economiche. Solitamente queste specie per potere sopravvivere in ambienti non nativi, producono metaboliti secondari i quali spesso possiedono importanti proprietà biologiche. In questo scenario, l'utilizzo di questi prodotti rappresenta una valida e sostenibile alternativa all'impiego di molecole biologicamente attive di origine sintetica.

Un approccio di tale tipo contribuisce alla realizzazione di un processo di sostenibilità economica e soprattutto ambientale.

La Caulerpina è un alcaloide prodotto dall'alga verde *Caulerpa cylindracea*, nativa dell'Australia e invasiva nel Mediterraneo.

La possibilità di utilizzare la Caulerpina come potenziale antagonista del recettore FPR2, per ridurre il processo infiammatorio associato all'infezione da *H. pylori*, è stata valutata sulla base di diversi elementi: (i) riconosciuta attività antinfiammatoria; (ii) scarsa tossicità; (iii) presenza di nuclei indolici nella struttura chimica.

Da sempre gli indoli sono composti di notevole interesse farmaceutico; inoltre è riportato che antagonisti dei recettori per i peptidi formilati finora noti (prevalentemente peptidi), contengono nella loro struttura nuclei indolici.

La potenzialità della Caulerpina nell'interagire e antagonizzare FPR2 è stata esaminata eseguendo test *in silico* e *in vitro*. Questi ultimi hanno evidenziato un'interessante capacità della molecola nel ridurre la risposta infiammatoria associata all'infezione da *H. pylori*, modulando il pathway del segnale del recettore FPR2.

Accanto a tali indagini, l'approccio metabolomico mediante Risonanza Magnetica Nucleare (NMR) e analisi multivariata è stato condotto per valutare l'efficacia della Caulerpina e la sua capacità di ridurre il rischio di patologie extra-gastriche associate all'infezione (Capitolo 4).

In conclusione, il seguente lavoro di tesi apre la strada al possibile impegno della Caulerpina da parte dell'industria farmaceutica, come potenziale agente ad attività antinfiammatoria da impiegare nella terapia contro l'infezione da *Helicobacter pylori*, riducendo i rischi clinici associati. In aggiunta, l'importanza dei recettori per i peptidi formilati rende la Caulerpina un potenziale candidato per il trattamento di svariate patologie infiammatorie, non necessariamente di origine microbica.



## **SUMMARY**

*Helicobacter pylori* (*H. pylori*) is a major human pathogen causing chronic infection, which generates a state of persistent inflammation, leading to severe gastric and extra-gastric outcomes. In the absence of effective vaccines, treatment of chronic *H. pylori* infection is the favorite approach for preventing the subsequent clinical implications. However, *H. pylori* eradication is a difficult clinical practice. Increasing antibiotic resistance, as well as the capacity of *H. pylori* to successfully evade the host immune system, make it a serious threat for human health. Consequently, novel pharmacological strategies are needed.

The present PhD thesis focuses on the **identification of new therapeutic agents for the management of *H. pylori* infection, modulating the host innate immune response, by targeting the Formyl peptide receptors (FPRs).**

FPRs participate to the host defense by orchestrating the inflammatory response. They have been widely recognized to play critical roles in inflammation-associated diseases. Thus, treatment with FPRs-modulation may be helpful to reduce *H. pylori*-associated inflammation and prevent the related clinical complications. Among FPRs, our attention was focused on FPR2, as the most attractive and promiscuous target.

In this thesis the **valorization of invasive marine biomasses for the production of natural anti-inflammatory agents, able to target FPRs**, was investigated. Caulerpin, a bis-indole alkaloid isolated from algae of the genus *Caulerpa*, was identified as potential FPR2 inhibitor. By performing both *in silico* and *in vitro* studies, the efficacy of Caulerpin in modulating the immune response against *H. pylori*, by reverting the FPR2-related signaling cascade, was explored. Moreover, a holistic and omics approach, consisting in metabolomics analysis, was applied as a means useful to examine the role of Caulerpin in attenuating the *H. pylori*-induced inflammation and the related adverse clinical outcomes. This study might pave the way for a possible future use of Caulerpin as promising therapeutic or adjuvant anti-inflammatory agent against *H. pylori* infection.

## **INTRODUCTION**



## Metabolomics: the revolution of *-omics* sciences

In the last decades, several advances have been made in biological research. The complete sequence of the human genome (Liolios et al., 2006), the development of *high-throughput* technologies and the access to large-scale datasets enabled important advances in both medicine and biology, giving rise to the *-omics* sciences.

The term “*omics*” is used to address all disciplines (genomics, transcriptomics, proteomics and metabolomics) that provide a global assessment of a set of biological molecules (Hasin et al., 2017) and favor the global analysis of changes in gene sequences (genomics), gene expression (transcriptomics), gene products (proteomics), and a readout of the physiological cell state (metabolomics) *via* final products (Hedge et al., 2009).

Human diseases, including inflammatory pathologies, are complex and multifactorial. They are generally characterized by changes of the host cell gene expression and/or their products. In this context, *omics* sciences represent a valid comprehensive approach for understanding the molecular mechanisms of diseases, as well as the effects of potential treatments (Nemutulu et al., 2012), thus overcoming the “reductionistic method” (Van Regenmortel, 2004).

The recent and ever more growing interest in metabolomics completed the *omics* revolution, generating an integrated and coordinated system, where a biological process is investigated as a whole (Joyce and Palsson, 2006).

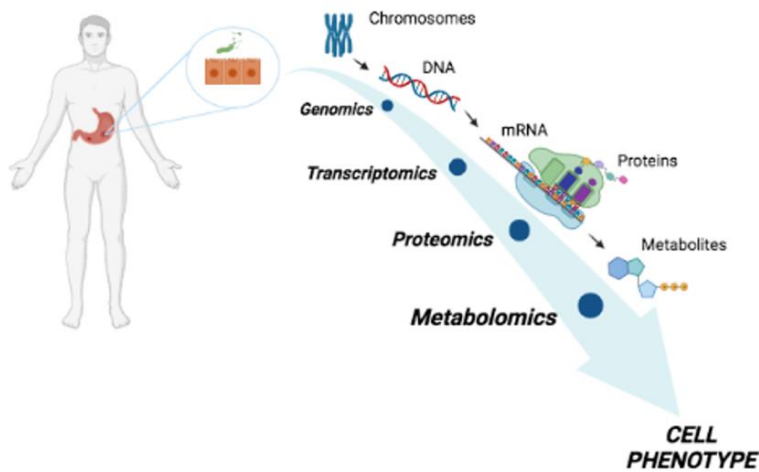


**Figure 1.** Schematic overview of the omics sciences related to the gastric cell response to *Helicobacter pylori* infection. Metabolomics is located at the bottom of the omics cascade, converging in the understanding of the cell phenotype and function.

Metabolomics identifies and quantifies a set of metabolites (small molecules produced by enzymatic reactions), which represent the end product of the cell metabolism (the metabolome) (Alonso and Marsal, 2015). Unlike genes and proteins, which can be modified epigenetically or post-translationally, respectively, metabolites give an instant picture of the biochemical state of cells, tissues or other biological samples. Metabolites are the ultimate response of a biological system to genetic changes and environmental stimuli (Zhang et al., 2013). Therefore, as shown in the Figure 1, metabolomics is highly informative to explore cell phenotype and function.

Metabolites can be classified into primary or secondary metabolites. Primary metabolites are present in all living cells and play key roles in the survival of the organism, while secondary metabolites are optional for the organism's life. Primary metabolites are directly involved in metabolic pathways responsible for providing energy for cell growth (Figure 2). Thus, characterization of endogenous or exogenous metabolites and the analysis of their interactions represents a significant contribution to the understanding of the cellular state at a given condition.

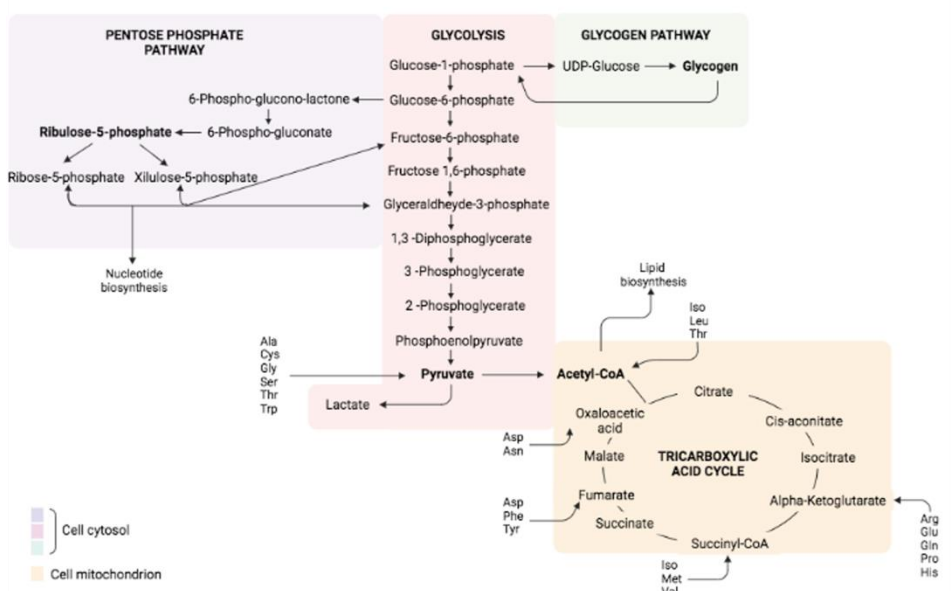


**Figure 2.** Key metabolic pathways and their interconnection.

## - Metabolomics approach

To achieve a comprehensive analysis of metabolites, several approaches exist, which can be classified as targeted and untargeted. Each metabolomics approach allows the identification and quantification of metabolites. However, they differ in the experimental design, sample preparation and number of metabolites detected.

The targeted approach is a hypothesis-driven technique (Schrimpe-Rutledge et al., 2016). It is used to identify and quantify one specific metabolite or a limited set of known metabolites (Bingol, 2018). In detail, the identity of target metabolite is established by comparing acquired data with available databases and then confirmed by analyzing pure reference compounds (Bingol, 2018). Additionally, through the use of internal chemically defined standards, metabolites of interest can be quantified. Contrary to the untargeted approach, the sample preparation procedure is generally optimized according to the class of metabolites under investigation and often includes steps such as metabolite concentration and/or interferences removal (Álvarez-Sánchez et al., 2010).

The untargeted metabolomics approach instead, is a non-hypothesis-driven technique (Schrimpe-Rutledge et al., 2016). It can analyze a large number of metabolites simultaneously, including unknown ones, and identify unexpected changes. To detect the highest number of metabolites and simultaneously make more manageable the extensive dataset of signals, untargeted metabolomics requires advanced and multiple analytical techniques (Roberts et al., 2012). It may require specific procedures for sample preparation (Álvarez-Sánchez et al., 2010) and more time to process the wide set of acquired data. Moreover, one of its major challenges is the identification of unknown chemical compounds (Roberts et al., 2012). Despite these limitations, untargeted metabolomics is considered the true omics approach, providing information about the metabolic fingerprinting (intracellular metabolome or endo-metabolome) or footprinting (extracellular metabolome or exo-metabolome) of a particular condition.

#### **- Clinical applications of metabolomics**

Metabolomics has several possible applications in many fields, including plant and food sciences, microbiology and clinics. The recent advent of precision medicine has made metabolomics one of the most powerful biomedical strategies.

In this regard, by identifying metabolic pathways of diseases, metabolomics can be used to understand disease mechanisms and detect new targets for drug development (Nicholson and Lindon, 2008; Wishart, 2016). In addition, metabolomics can provide potential biomarkers, which may be used for disease diagnosis and prediction, and to screen the activity of therapeutic treatments (Wishart, 2016). Finally, by identifying individual metabolic profiles, metabolomics can predict the response of an individual to a novel pharmacological treatment, revealing its efficacy or toxicity, or to develop personalized treatment (pharmacometabolomics).

The present work of thesis focuses on the study of cell metabolites, as a means to explore systemic changes associated with *Helicobacter pylori* (*H. pylori*)-induced inflammation and investigate the effectiveness of a potential treatment for the modulation of the *H. pylori*-stimulated inflammatory response.

## Inflammation: host immune response

To maintain the homeostasis and survive to harmful external stimuli, such as bacteria, multicellular organisms have developed defense mechanisms, which can be distinguished into constitutive and inducible ones (Albiger et al., 2007).

Host constitutive defense mechanisms consist in physical (skin and mucosae), mechanical (ciliated cells of the respiratory tract), and biological (tears, antibacterial enzymes) barriers, while inducible mechanisms include the innate and adaptative immune system. When bacterial infection occurs, these two systems are consecutively activated.

Innate immune system is the most important and ancient element of the host defense (van der Heijden et al., 2018). It can detect pathogens by a set of Pattern Recognition Receptors (PRRs) expressed by myeloid cells (monocytes, macrophages, neutrophils and dendritic cells) and epithelial cells (Netea et al., 2017). PRRs can recognize microbial structures of both pathogens (Pathogen Associated Molecular Patterns, PAMPs) and symbiotic microbiota (Microbial Associated Molecular Patterns, MAMPs). Microbiome is known to play critical roles in host health, contributing to regulate normal cell functions (Zheng et al., 2020). Hypothesis suggest that PRRs have evolved to favor host-microbial symbiont coexistence. Based on this consideration, PRRs tolerate microbial self (Chu and Mazmanian, 2013), while during infection, PRRs trigger diverse events which culminate in the inflammatory response.

Formyl peptide receptors (FPRs) are PRRs expressed by immune cells, which contribute to preserve the host from pathogens. Non-immune cells also express FPRs. This class of receptors, in fact, can exert functions which extend beyond the immune ones (Bush et al., 2021). They are known to coordinate pathophysiological responses to different stimuli, modulating the inflammatory response and participating to numerous severe diseases (Figure 3).

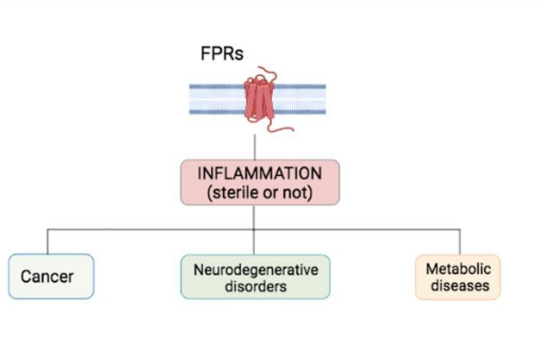


**Figure 3.** Role of FPRs in chronic inflammatory diseases.

Inflammation is a biological process leading to injury removal and homeostasis return. If not self-limited, inflammation may become a serious problem for the host rather than the pathogen (Barton, 2008). This is the case of *H. pylori*, which can establish a persistent infection. To colonize chronically the gastric mucosa, *H. pylori* has to control the host immune system, inducing as well as eluding the inflammation. To escape the host immune system, *H. pylori* reduces the activation of Toll-like receptor 4 (TLR4) modifying the lipid core A domain of its lipopolysaccharide (LPS) (Cullen et al., 2011), while to induce inflammation, it activates host transcription factors. In this context FPRs have a critical role.

### ***Helicobacter pylori* infection**

*H. pylori* is a Gram-negative bacterium, which was first described by B. J. Marshall and R. Warren in the early 1980s. They isolated spiral bacteria, later identified as *H. pylori* from inflamed human gastric biopsies, and demonstrated a direct relationship between *H. pylori* infection and peptic ulcer diseases (Ahmed, 2005; Kusters et al., 2006). *H. pylori* is a well-known human pathogen, responsible for one of the most common chronic bacterial infections. It colonizes the human stomach of approximately 50% of the population worldwide, with a higher rate of infection in developing countries because of different socio-economic and hygienic conditions (White et al., 2015). In most cases, the infection is asymptomatic and is acquired during the early childhood (Aguilera Matos et al., 2020). In the absence of an effective treatment, the infection can persist lifelong,

eliciting chronic gastric inflammation, which may evolve into duodenal ulcer, gastric mucosa associated lymphoid tissue (MALT) lymphoma and gastric cancer (White et al., 2015; Savoldi et al., 2018).

Bacterial virulence, environmental parameters and host genetic factors influence the clinical outcome of the *H. pylori* infection (Pachathundikandi et al., 2013). When *H. pylori* enters the host stomach, urease is critical to initiate a successful colonization of the gastric acid environment, concluded by flagella and bacterial adhesins (Kao et al., 2016). Flagella play a pivotal role in moving *H. pylori* toward the mucus layer to gastric epithelium cells (Kao et al., 2012), while bacterial adhesins (SabA, BabA, Hsp60) favor the interaction between *H. pylori* and host gastric cells (Kao et al., 2016). Finally, after host colonization, bacterial virulence factors are critical to establish a persistent infection.

The main virulence determinants produced by *H. pylori* are the vacuolating cytotoxin (VacA) and the cytotoxin associated gene A (CagA). All strains of *H. pylori* harbor the *VacA* gene, which enables *H. pylori* survival and persistence in the human stomach (Cover and Blanke, 2005). Not all *H. pylori* strains contain the *CagA* gene, suggesting its effective role in the virulence of individual *H. pylori* strains. Upon phosphorylation, CagA protein activates signal transduction pathways, resulting in pro-inflammatory and mitogenic responses (Sheikh et al., 2018).

Interestingly, *H. pylori* produces a cecropin-like peptide [Hp(2-20)] with high antimicrobial properties. Hp(2-20) confers to *H. pylori* a competitive advantage over other bacteria, making easier both the colonization and persistence in the gastric environment (Bylund et al., 2001). Moreover, Hp(2-20) interacts with host cell receptors (Formyl peptide receptors, FPRs), triggering a pro-inflammatory response (Bylund et al., 2001). As a consequence, Hp(2-20) contributes to *H. pylori* virulence and together with VacA and CagA stimulate gastric mucosal inflammation, which might promote premalignant changes, increasing the risk of severe gastric diseases (Hou et al., 2017; Abdullah et al., 2019).

*H. pylori* infection can also cause systemic or extra-gastric diseases. Emerging evidences suggest that *H. pylori* increases the risk of chronic diseases, including insulin resistance, diabetes, obesity, cardiovascular and neurological diseases (Gravina et al., 2018).

The reason why *H. pylori* is recognized as risk factor for extra-gastric diseases is still unclear. It is assumed that the persistent and low-

grade inflammatory state induced by *H. pylori* infection plays a key role. Chronic inflammation leads to a continuous release of pro-inflammatory cytokines, thus altering cell homeostasis and affecting both glucose and lipid metabolism, which could result in insulin resistance and associated diseases (Esposito and Giugliano, 2004). Insulin resistance, in turn, enhance the inflammatory state as a consequence of reduced anti-inflammatory effects of insulin.

*H. pylori* eradication could be a clear solution to control both gastric and extra-gastric risks (Gravina et al., 2020). Nevertheless, the emergence of antibiotic resistant strains has harmful effects on the efficacy of *H. pylori* treatment, making difficult bacterium eradication. In this context, novel therapeutic approaches are needed.

## Aim of thesis

The objectives of the present thesis are the identification and characterization of natural products, isolated from living organisms, able to modulate the inflammation induced by *H. pylori* and the related clinical outcomes.

Formyl peptide receptors (FPRs) have been chosen as pharmacological target. Among the three FPRs, FPR2 is the one that responds to numerous structurally different ligands of both exogenous and endogenous origins, and that plays important roles in inflammation and pathogenesis of infections and inflammatory disorders. FPR2 also responds to a wide range of synthetic ligands, which is of great utility for pharmacological applications.

Caulerpin, one of the three major secondary metabolites produced by the macroalga *Caulerpa cylindracea*, was tested as potential candidate able to limit the *H. pylori*-induced inflammatory response, through FPR2-related signaling pathway. Caulerpin is a defensive metabolite which has contributed to the colonization of the Mediterranean Sea by *Caulerpa cylindracea*, causing ecological, economic and social problems (Del Coco et al., 2018; Miccoli et al., 2021). Exploitation of Caulerpin for biotechnological utilization in pharmaceutical industry offers multiple advantages: 1) avoids chemical compounds synthesis, decreasing environmental and human-health risks; 2) favors the utilization and recovery of algae



biomass, limiting the invasiveness threat; 3) contributes to the circular economy.

The research activities went through three main steps:

**1) *Metabolite profiling and metabolomics as a tool for a comprehensive analysis of cell response to *H. pylori* stimuli.***

The aim of this first step was to conduct a comprehensive analysis of biochemical changes (intracellular and extracellular) that the *H. pylori*-associated inflammation promotes and identify its role in metabolic disorders (Obesity, Diabetes and Cardiovascular Diseases) and neurological diseases (Alzheimer's disease).

**2) *Screening of natural compound libraries for the identification of anti-inflammatory agents targeting FPR2.***

The aim of this second step was to search for novel and natural FPR2 antagonists, showing significant contribution in controlling the *H. pylori*-associated inflammation and the resulting clinical adverse effects. Caulerpin was selected as potential candidate, then confirmed by biological assays.

**3) *Metabolite profiling and metabolomics as a tool for a comprehensive analysis of cell response to Caulerpin treatment.***

The aim of this third step was to validate the efficacy of Caulerpin in mitigating *H. pylori*-associated systemic effects, pointing out the importance of metabolomics in drug discovery. For this purpose, footprinting metabolomics was performed.

## References

- Abdullah, M.; Greenfield, L.K.; Bronte-Tinkew, D.; Capurro, M.I.; Rizzuti, D.; Jones, N.L. VacA promotes CagA accumulation in gastric epithelial cells during *Helicobacter pylori* infection. *Sci Rep.* **2019**; 9(1):38.
- Aguilera Matos, I.; Diaz Oliva, S.E.; Escobedo, A.A.; Villa, Jiménez, O.M.; Velazco, Villaurrutia, Y.D.C. *Helicobacter pylori* infection in children. *BMJ Paediatr* **2020**; 4(1): e000679.
- Ahmed, N. 23 years of the discovery of *Helicobacter pylori*: is the debate over? *Ann Clin Microbiol Antimicrob.* **2005**; 4:17.
- Albiger, B.; Dahlberg, S.; Henriques-Normark, B.; Normark, S. Role of the innate immune system in host defence against bacterial infections: focus on the Toll-like receptors. *J Intern Med.* **2007**; 261(6):511-28.
- Alonso, A.; Marsal, S.; Julià, A. Analytical methods in untargeted metabolomics: state of the art in 2015. *Front Bioeng Biotechnol.* **2015**; 3:23.
- Álvarez-Sánchez, B.; Priego-Capote, F.; Luque de Castro, M.D. Metabolomics analysis II. Preparation of biological samples prior to detection. *Trends Anal Chem.* **2010**; 29:120–7.
- Barton GM. A calculated response: control of inflammation by the innate immune system. *J Clin Invest.* **2008**; 118(2):413-20.
- Bingol, K. Recent Advances in Targeted and Untargeted Metabolomics by NMR and MS/NMR Methods. *High Throughput.* **2018**; 7(2):9.
- Busch, L.; Vieten, S.; Brödel, S.; Endres, K.; Bufe, B. Emerging contributions of formyl peptide receptors to neurodegenerative diseases. *Biol Chem.* **2021**; 403(1):27-41.
- Bylund, J.; Christophe, T.; Boulay, F.; Nyström, T.; Karlsson, A.; Dahlgren, C. Proinflammatory activity of a cecropin-like antibacterial peptide from *Helicobacter pylori*. *Antimicrob Agents Chemother.* **2001**; 45(6):1700-4.
- Chu, H.; Mazmanian, S.K. Innate immune recognition of the microbiota promotes host-microbial symbiosis. *Nat Immunol.* **2013**; 14(7):668-75.
- Cover, T.L.; Blanke, S.R. *Helicobacter pylori* VacA, a paradigm for toxin multifunctionality. *Nat Rev Microbiol.* **2005**; 3(4):320-32.
- Cullen, T.W.; Giles, D.K.; Wolf, L.N.; Ecobichon, C.; Boneca, I.G.; Trent, M.S. *Helicobacter pylori* versus the host: remodeling of the bacterial outer membrane is required for survival in the gastric mucosa. *PLoS Pathog.* **2011**; 7(12):e1002454.
- Del Coco, L.; Felling, S.; Girelli, C.R.; Angilè, F.; Magliozzi, L.; Almada, F.; D'Aniello, B.; Mollo, E.; Terlizzi, A.; Fanizzi, F.P. <sup>1</sup>H NMR Spectroscopy and MVA to Evaluate the Effects of Caulerpin-Based Diet on *Diplodus sargus* Lipid Profiles. *Mar Drugs.* **2018**; 16(10):390.
- Esposito, K.; Giugliano, D. The metabolic syndrome and inflammation: association or causation? *Nutr Metab Cardiovasc Dis.* **2004**; 14(5):228-32.

- Gravina, A.G.; Priadko, K.; Ciamarra, P.; Granata, L.; Facchiano, A.; Miranda, A.; Dallio, M.; Federico, A.; Romano, M. Extra-Gastric Manifestations of *Helicobacter pylori* Infection. *J Clin Med*. **2020**; 9(12):3887.
- Gravina, A.G.; Zagari, R.M.; De Musis, C.; Romano, L.; Loguercio, C.; Romano, M. *Helicobacter pylori* and extragastric diseases: A review. *World J Gastroenterol*. **2018**; 24(29):3204-3221.
- Hasin, Y.; Seldin, M.; Lusis, A. Multi-omics approaches to disease. *Genome Biol*. **2017**; 18(1):83.
- Hegde, P.S.; White, I.R.; Debouck, C. Interplay of transcriptomics and proteomics. *Curr Opin Biotechnol*. **2003**; 14(6):647-51.
- Hou, X.L.; Ji, C.D.; Tang, J.; Wang, Y.X.; Xiang, D.F.; Li, H.Q.; Liu, W.W.; Wang, J.X.; Yan, H.Z.; Wang, Y.; Zhang, P.; Cui, Y.H.; Wang, J.M.; Bian, X.W.; Liu, W. FPR2 promotes invasion and metastasis of gastric cancer cells and predicts the prognosis of patients. *Sci Rep*. **2017**; 7(1):3153.
- Joyce, A.R.; Palsson, B.Ø. The model organism as a system: integrating 'omics' data sets. *Nat Rev Mol Cell Biol*. **2006**; 7(3):198-210.
- Kao, C.Y.; Sheu, B.S.; Sheu, S.M.; Yang, H.B.; Chang, W.L.; Cheng, H.C.; Wu, J.J. Higher motility enhances bacterial density and inflammatory response in dyspeptic patients infected with *Helicobacter pylori*. *Helicobacter*. **2012**; 17(6):411-6.
- Kao, C.Y.; Sheu, B.S.; Wu, J.J. *Helicobacter pylori* infection: An overview of bacterial virulence factors and pathogenesis. *Biomed J*. **2016**; 39(1):14-23.
- Kusters, J.G.; van Vliet, A.H.; Kuipers, E.J. Pathogenesis of *Helicobacter pylori* infection. *Clin Microbiol Rev*. **2006**; 19(3):449-90.
- Liolios, K.; Tavernarakis, N.; Hugenholtz, P.; Kyrpides, N.C. The Genomes On Line Database (GOLD) v.2: a monitor of genome projects worldwide. *Nucleic Acids Res*. **2006**; 34(Database issue): D332-4.
- Miccoli A, Mancini E, Boschi M, Provenza F, Lelli V, Tiralongo F, Renzi M, Terlizzi A, Bonamano S, Marcelli M. Trophic, Chemo-Ecological and Sex-Specific Insights on the Relation Between *Diplodus sargus* (Linnaeus, 1758) and the Invasive *Caulerpa cylindracea* (Sonder, 1845). *Front. Mar. Sci*. **2021**; 8:680787.
- Nemutlu, E.; Zhang, S.; Juranic, N.O.; Terzic, A.; Macura, S.; Dzeja, P. <sup>18</sup>O-assisted dynamic metabolomics for individualized diagnostics and treatment of human diseases. *Croat Med J*. **2012**; 53(6):529-34.
- Netea, M.G.; Balkwill, F.; Chonchol, M.; Cominelli, F.; Donath, M.Y.; Giamarellos-Bourboulis, E.J.; Golenbock, D.; Gresnigt, M.S.; Heneka, M.T.; Hoffman, H.M. A guiding map for inflammation. *Nat Immunol*. **2017**; 18(8):826-831.
- Nicholson, J.K.; Lindon, J.C. Systems biology: Metabonomics. *Nature*. **2008**; 455(7216):1054-6.
- Pachathundikandi, S.K.; Tegtmeyer, N.; Backert, S. Signal transduction of *Helicobacter pylori* during interaction with host cell protein receptors of epithelial and immune cells. *Gut Microbes*. **2013**; 4(6):454-74.

- Roberts, L.D.; Souza, A.L.; Gerszten, R.E.; Clish, C.B. Targeted metabolomics. *Curr Protoc Mol Biol.* **2012**; 30(2):1-24.
- Savoldi, A.; Carrara, E.; Graham, D.Y.; Conti, M.; Tacconelli, E. Prevalence of Antibiotic Resistance in *Helicobacter pylori*: A Systematic Review and Meta-analysis in World Health Organization Regions. *Gastroenterology.* **2018**; 155(5):1372-1382.e17.
- Schrimpe-Rutledge, A.C.; Codreanu, S.G.; Sherrod, S.D.; McLean, J.A. Untargeted Metabolomics Strategies-Challenges and Emerging Directions. *J Am Soc Mass Spectrom.* **2016**; 27(12):1897-1905.
- Sheikh, A.F.; Yadyad, M.J.; Goodarzi, H.; Hashemi, S.J.; Aslani, S.; Assarzadegan, M.A.; Ranjbar, R. CagA and vacA allelic combination of *Helicobacter pylori* in gastroduodenal disorders. *Microb Pathog.* **2018**; 122:144-150.
- van der Heijden, C.D.C.C.; Noz, M.P.; Joosten, L.A.B.; Netea, M.G.; Riksen, N.P.; Keating, S.T. Epigenetics and Trained Immunity. *Antioxid Redox Signal.* **2018**; 29(11):1023-1040.
- Van Regenmortel, M.H. Reductionism and complexity in molecular biology. Scientists now have the tools to unravel biological and overcome the limitations of reductionism. *EMBO Rep.* **2004**; 5(11):1016-20.
- White, J.R.; Winter, J.A.; Robinson, K. Differential inflammatory response to *Helicobacter pylori* infection: etiology and clinical outcomes. *J Inflamm Res.* **2015**; 8:137-47.
- Wishart, D.S. Emerging applications of metabolomics in drug discovery and precision medicine. *Nat Rev Drug Discov.* **2016**; 15(7):473-84.
- Zhang, A.; Sun, H.; Xu, H.; Qiu, S.; Wang, X. Cell metabolomics. *OMICS.* **2013**; 17(10):495-501.
- Zheng, D.; Liwinski, T.; Elinav, E. Interaction between microbiota and immunity in health and disease. *Cell Res.* **2020**; 30(6):492-506.

## **CHAPTER 1**

***Metabolomics: a tool to assess in vitro response to Helicobacter pylori infection and investigate on the causal role of Helicobacter pylori infection in extra-gastric diseases***

In this chapter, NMR-based metabolomics investigation on *H. pylori*-induced inflammation and its role as risk factor for extra-gastric diseases (Diabetes, Obesity, Cardiovascular diseases and Alzheimer's disease) are described. Additional information on the contribution of *H. pylori* infection in developing metabolic and neurodegenerative diseases is also provided by exploring the expression level of the major genes involved in metabolic and inflammatory pathways.

Diabetes, Obesity, Cardiovascular disease and Alzheimer's disease belong to the family of chronic pathologies (Rao et al., 2014; Procaccini et al., 2016), which are characterized by a progressive dysfunction of metabolic and physiological functions, in response to chronic exposure to environmental or biological factors. It is now widely recognized that chronic inflammation is the major etiological component leading to such chronic manifestations (Furman et al., 2019), and that persistent *H. pylori* infection, as cause of low-grade chronic inflammation, is a risk factor (Franceschini et al., 2019; Pellicano et al., 2020).

Inflammation protects the host from bacteria, viruses or non-microbial injuries (Kotas and Medzhitov, 2015). Shift from short to long-term inflammatory response causes serious tissue and organ damages, increasing the risk for chronic pathologies (Fullerton and Gilroy, 2016). Inflammation also promotes metabolic changes to ensure a suitable energy supply and favor immune system activities (Fuman et al., 2019).

In this context, metabolomics, by revealing the molecular phenotype of particular pathophysiological conditions, appears as the most advantageous strategy to investigate biochemical alterations responsible for metabolic dysfunctions underlying *H. pylori*-induced inflammation and the derived consequences.

## References

- Franceschi, F.; Covino, M.; Roubaud Baudron, C. Review: *Helicobacter pylori* and extragastric diseases. *Helicobacter*. **2019**; 24 Suppl 1: e12636.
- Fullerton, J.N.; Gilroy, D.W. Resolution of inflammation: a new therapeutic frontier. *Nat Rev Drug Discov*. **2016**; 15(8):551-67.
- Furman, D.; Campisi, J.; Verdin, E.; Carrera-Bastos, P.; Targ, S.; Franceschi, C.; Ferrucci, L.; Gilroy, D.W.; Fasano, A.; Miller, G.W.; et al. Chronic inflammation in the etiology of disease across the life span. *Nat Med*. **2019**; 25(12):1822-1832.
- Kotas, M.E.; Medzhitov, R. Homeostasis, inflammation, and disease susceptibility. *Cell*. **2015**; 160(5):816-827.
- Pellicano, R.; Ianiro, G.; Fagoonee, S.; Settanni, C.R.; Gasbarrini, A. Review: Extragastric diseases and *Helicobacter pylori*. *Helicobacter*. **2020**; 25 Suppl 1: e12741.
- Procaccini, C.; Santopaolo, M.; Faicchia, D.; Colamatteo, A.; Formisano, L.; de Candia, P.; Galgani, M.; De Rosa, V.; Matarese, G. Role of metabolism in neurodegenerative disorders. *Metabolism*. **2016**; 65(9):1376-90.
- Rao, D.P.; Dai, S.; Lagacé, C.; Krewski, D. Metabolic syndrome and chronic disease. *Chronic Dis Inj Can*. **2014**; 34(1):36-45.

# 1.1 An In Vitro Model to Investigate the Role of *Helicobacter pylori* in Type 2 Diabetes, Obesity, Alzheimer's Disease and Cardiometabolic Disease



International Journal of  
Molecular Sciences



Article

## An In Vitro Model to Investigate the Role of *Helicobacter Pylori* in Type 2 Diabetes, Obesity, Alzheimer's Disease and Cardiometabolic Disease

Paola Cuomo <sup>1,†</sup>, Marina Papaiani <sup>1,†</sup>, Clementina Sansone <sup>2</sup>, Antonio Iannelli <sup>3,4</sup>,  
Domenico Iannelli <sup>1,\*</sup>, Chiara Medaglia <sup>5</sup>, Debora Paris <sup>6</sup>, Andrea Motta <sup>6</sup>  
and Rosanna Capparelli <sup>1,\*</sup>

<sup>1</sup> Department of Agriculture Sciences, University of Naples "Federico II", via Università, 100-Portici, 80055 Naples, Italy; paola.cuomo@unina.it (P.C.); marina.papaiani@unina.it (M.P.)

<sup>2</sup> Department of Marine Biotechnology, Stazione Zoologica Anton Dohrn, 80121 Naples, Italy; clementina.sansone@szn.it

<sup>3</sup> Department of Digestive Surgery, Université Côte d'Azur, Campus Valrose, Batiment L, Avenue de Valrose, 28-CEDEX 2, 06108 Nice, France; iannelli.a@chu-nice.fr

<sup>4</sup> Inserm, U1065, Team 8 "Hepatic Complications of Obesity and Alcohol", Route Saint Antoine de Ginestière 151, BP 2 3194, CEDEX 3, 06204 Nice, France

<sup>5</sup> Department of Microbiology and Molecular Medicine, University of Geneva Medical School, rue du Général-Dufour, 1211 Genève, Switzerland; chiara.medaglia@unige.ch

<sup>6</sup> Institute of Biomolecular Chemistry, National Research Council, via Campi Flegrei, 34-Pozzuoli, 80078 Naples, Italy; dparis@icb.cnr.it (D.P.); andrea.motta@icb.cnr.it (A.M.)

\* Correspondence: domenico.iannelli1935@gmail.com (D.I.); capparelli@unina.it (R.C.)

† These authors contributed equally to this work.

Received: 7 October 2020; Accepted: 4 November 2020; Published: 8 November 2020



**Abstract:** *Helicobacter pylori* (*Hp*) is a Gram-negative bacterium colonizing the human stomach. Nuclear Magnetic Resonance (NMR) analysis of intracellular human gastric carcinoma cells (MKN-28) incubated with the *Hp* cell filtrate (*Hpcf*) displays high levels of amino acids, including the branched chain amino acids (BCAA) isoleucine, leucine, and valine. Polymerase chain reaction (PCR) Array Technology shows upregulation of mammalian Target Of Rapamycin Complex 1 (mTORC1), inflammation, and mitochondrial dysfunction. The review of literature indicates that these traits are common to type 2 diabetes, obesity, Alzheimer's diseases, and cardiometabolic disease. Here, we demonstrate how *Hp* may modulate these traits. *Hp* induces high levels of amino acids, which, in turn, activate mTORC1, which is the complex regulating the metabolism of the host. A high level of BCAA and upregulation of mTORC1 are, thus, directly regulated by *Hp*. Furthermore, *Hp* modulates inflammation, which is functional to the persistence of chronic infection and the asymptomatic state of the host. Finally, in order to induce autophagy and sustain bacterial colonization of gastric mucosa, the *Hp* toxin VacA localizes within mitochondria, causing fragmentation of these organelles, depletion of ATP, and oxidative stress. In conclusion, our in vitro disease model replicates the main traits common to the above four diseases and shows how *Hp* may potentially manipulate them.

**Keywords:** *Helicobacter pylori*; mTORC1; branched chain amino acids; inflammation; mitochondrial dysfunction

### 1. Introduction

*Helicobacter pylori* (*Hp*) is a Gram-negative bacterium colonizing the human gastric mucosa. It is transmitted orally, often within the family. Colonizing about one half of the world's population,



*Hp*, can be classified as one of the most successful human pathogens [1,2]. Genetic diversity and efficient evasion of host innate and adaptive immune responses contribute to this success [3]. Genetic diversity of *Hp* originates from a high mutation rate, and is favored by the absence of a DNA mismatch repair mechanism and acquisition of DNA from other strains [3]. The *Hp* lipopolysaccharide escapes binding by antimicrobial peptides and detection by Toll-like receptors (TLRs) by removing phosphate groups from the lipid A [4]. VacA modulates T-cell proliferation by inhibiting nuclear translocation of the T transcription factor NF-AT [5]. *Hp* can persist for decades asymptotically, but carriers are at risk of developing gastritis, duodenal ulcers, non-Hodgkin's lymphoma, or gastric adenocarcinoma. Finally, epidemiological studies suggest that *Hp* may cause extra gastric diseases [6].

Often, bacteria colonize the host by exploiting its metabolism [7]. For this purpose, *Hp* uses mTORC1, which is the complex sensing the conditions for cellular survival. mTORC1 is active when nutrients are abundant, and inactive when they are scarce [8]. In the early phase of host colonization, the *Hp* toxin VacA inhibits mTORC1 expression and activates autophagy to gain the nutrients needed to colonize the gastric mucosa [9]. Once this phase is terminated, autophagy would obstruct the chronic infection. To prevent this condition, CagA (a toxin antagonistic to VacA) activates mTORC1 [10]. The branched chain amino acids (BCAA) leucine, isoleucine, and valine, together with insulin, actively participate to mTORC1 activation [11]. *Hp*, through a clever use of two antagonistic toxins, modulates mTORC1 and, consequently, the metabolism of its host. Furthermore, in order to induce autophagy and sustain colonization of gastric mucosa, VacA localizes within the mitochondria by causing mitochondrial DNA mutations in the gastric cells, mitochondrial fragmentation, depletion of ATP, and oxidative stress [12]. Finally, to facilitate chronic infection and persistence of the host asymptomatic state, *Hp* modulates inflammation. However, this unstable equilibrium often fails. Inflammation is the most frequent cause of the passage from the asymptomatic state to that of disease [13].

We just described how upregulation of mTORC1, high levels of BCAA, inflammation, and mitochondrial dysfunctions characterize *Hp* infection. According to current literature, the same traits characterize the metabolic diseases known as type 2 diabetes (T2D), obesity (OB), Alzheimer's disease (AD), and cardiometabolic disease (CMD) [14–17]. It seemed, therefore, feasible to investigate whether *Hp* may potentially predispose to the above diseases.

Epidemiological studies have several limitations. They require the enrollment of a large number of patients, and known and unknown confounding factors make results difficult to replicate [18]. Analysis of the cellular metabolic profile of in vitro cultured cells has detected yeast mutants that conventional methods failed to identify [19], while the medium from cultured human muscle cells identified creatine as a biomarker of human mitochondrial disease [20]. Inspired by these results, we tested whether nuclear magnetic resonance (NMR) metabolomics and microarray analysis of the human gastric carcinoma cells MKN-28, incubated for 2 h with the *Hp* cell filtrate (*Hpcf*), might identify the traits that current literature recognizes as biomarkers of patients with one of the four diseases listed above. MKN-28 incubated with *Hpcf* showed high levels of BCAA, upregulation of mTORC1, mitochondrial dysfunction, and inflammation. Here, we show that these traits are all referable, at least in part, to *Hp*.

## 2. Results

### 2.1. NMR-Based Metabolomics Analysis

The in vitro metabolic effects of *Hpcf* on the MKN-28 cells were investigated by performing NMR-based intracellular and extracellular metabolomics analysis of the MKN-28 cells. Intracellular analysis compared MKN-28 cells incubated and not with the *Hpcf* of the culture medium used to grow *Hp*. We first applied the unsupervised Principal Component Analysis (PCA) to verify the homogeneity of samples and then the supervised orthogonal projection to latent structure analysis (OPLS-DA) to

explore the intracellular metabolic profiles. The score plot (Figure 1A) shows a distinct separation between the two sample classes along the first component  $t[1]$ .

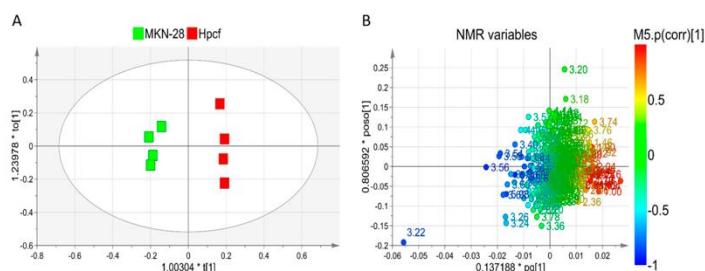


**Figure 1.** OPLS-DA of MKN-28 cell samples. (A) Scores plot showing the distinct separation between MKN-28 cells incubated (red squares) and not incubated (green squares) with *Hpcf*. The X-axis title represents the factor multiplied (\*) the principal predictive component  $t[1]$  which better approximates the dataset variation correlated with samples classification. On the ordinate axis, the title represents the factor multiplied (\*) the orthogonal component  $t[1]$  which accounts for intraclass variation. (B) Loadings plot of nuclear magnetic resonance (NMR) variables (chemical shift) referred to metabolites responsible for between-classes separation and characterized by  $|p(\text{corr})|$  value  $> 0.7$ .

In particular, the extracts of MKN-28 cells incubated with *Hpcf* are placed at  $t[1]$  positive coordinates, while the extracts of the MKN-28 cells non-incubated with *Hpcf* are placed at  $t[1]$  negative coordinates. To discriminate between the two groups of samples, we used the NMR loadings plot variables with correlation loading values  $|p(\text{corr})| > 0.7$  (Figure 1B). Cells incubated with *Hpcf* when compared with non-incubated cells show higher levels of the amino acids phenylalanine, tyrosine, glutamate, proline, leucine, alanine, valine, and isoleucine, the short chain fatty acids acetate and propionate, saturated fatty acids, sialic acid, and lower levels of taurine (Figures 2A and 3A,B).

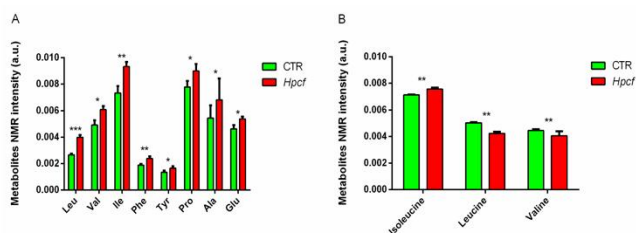


**Figure 2.** (A) Intracellular amino acid concentration differences (leucine, valine, isoleucine, phenylalanine, tyrosine, proline, and alanine) detected in MKN-28 cells incubated (red columns) or not incubated (green columns) with *Hpcf*. (B) Extracellular BCAA (leucine, isoleucine, and valine) concentration differences detected in culture medium of MKN-28 cells incubated (red columns) or not incubated (green columns) with *Hpcf*. Some *Hp* strains synthesizes isoleucine. Our strain is one of the strains that justify its upregulation. The X-axis reports a single amino acid and the Y-axis reports the bucket variation corresponding to the specific amino acid scaled to the total NMR spectral area. Intensity of amino acids is expressed in arbitrary units and represented as means  $\pm$  SD (\*  $p < 0.5$ , \*\*  $p < 0.01$ , \*\*\*  $p < 0.001$ ) calculated from two experiments in which each is performed in quadruplicate.

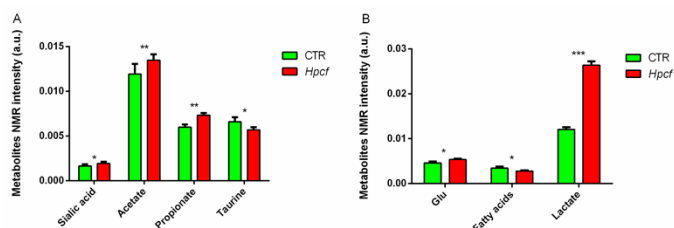


**Figure 3.** (A) Metabolite concentration differences (sialic acid, acetate, propionate, and taurine) detected in MKN-28 cells incubated (red columns) or not incubated with *H. pylori* cell filtrate (*Hpcf*). (B) Metabolite concentration differences (glutamate, fatty acids, and lactate) detected in MKN-28 cells incubated (red columns) or not incubated with *H. pylori* cell filtrate (*Hpcf*). The X-axis reports a single metabolite and the Y-axis reports the bucket variation corresponding to the specific metabolite scaled to the total NMR spectral area. Intensity of metabolites is expressed as arbitrary units and represented as means  $\pm$  SD (\*  $p < 0.5$ , \*\*  $p < 0.01$ , \*\*\*  $p < 0.001$ ) calculated from two experiments with each performed in quadruplicate.

## 2.2. Helicobacter Pylori Alters the Amino Acids Metabolism

The literature describes a study where two independent cohorts with each consisting of more than 3000 normoglycemic participants being followed for 12 years. High plasma levels of BCAA, and of the two aromatic amino acids (AAA) tyrosine and phenylalanine (out of 60 metabolites) could predict the development of T2D in the enrolled participants as early as 12 years in advance from the onset of the disease [21]. Numerous independent studies confirm the association of high plasma levels of BCAA with T2D [22] and OB [23].

Incubated with *Hpcf* for 2 h, the human MKN-28 gastric cells show altered expression levels of 13 metabolites (Figures 2A and 3A,B) including the five amino acids listed above, which are all expressed at high levels (Figure 2A). These findings, obtained using cells cultured in vitro, replicate the results of the studies carried out on humans and cited above. Furthermore, a recent longitudinal study carried out on a large Japanese population demonstrates that, in addition to the above amino acids, alanine and proline, which are positively associated with visceral fat deposition, while glycine is negatively associated [24]. Our study replicates these results (Figure 2A). The probability that seven out of the 20 (0.35) amino acids upregulated in the studies reported above, and, in the present one, are instead upregulated by chance at  $8 \times 10^{-8}$ .

Mammals lack the enzymes needed for the synthesis of BCAA [14]. The increased plasma levels of BCAA detected in patients with T2D or OB may result from two potential mechanisms. One claims that an excess of dietary BCAA activates the mTORC1 complex. The alternative mechanism suggests that high levels of BCAA alter the metabolism by causing mitochondrial dysfunction of pancreatic islet  $\beta$  cells [22]. MKN-28 cells incubated with *Hpcf* display upregulation of mTORC1 and mitochondrial dysfunction (Table 1). Therefore, these data indicate that cell culture may fruitfully be used to investigate whether *Hp* influences apparently different diseases. Zucker-obese rats display lower muscle glycine levels compared to Zucker-lean rats. However, when Zucker-obese rats are fed on a BCAA-restricted diet, their muscle glycine levels become normal. These results argue that BCAA metabolism may somehow interfere with that of glycine and, at the same time, give plausibility to the negative association of glycine with BCAA reported above.

**Table 1.** Genes of mammalian Target Of Rapamycin (*mTOR*) signaling, inflammatory, and oxidative stress pathways detected by polymerase chain reaction (PCR) array technology and differently expressed in MKN-28 cells incubated with *Hpcf* for 1 or 2 h. Variation of gene expression levels is reported as fold regulation. Values > |2| are considered statistically significant.

Pathway Name	Gene ID	Gene Name	Fold Regulation 1 h	Fold Regulation 2 h
<i>mTOR</i> signaling pathway	<i>RPTOR</i>	Regulatory associated protein of mTOR complex 1	−1.42	286.04
	<i>MLST8</i>	mTOR associated protein, LST8 homolog ( <i>S. cerevisiae</i> )	−1.42	398.95
	<i>AKT1</i>	V-akt murine thymoma viral oncogene homolog 1	−1.42	50.13
	<i>AKT2</i>	V-akt murine thymoma viral oncogene homolog 2	−1.42	504.97
	<i>INSR</i>	Insulin receptor	−1.42	257.79
	<i>IRS1</i>	Insulin receptor substrate 1	−1.42	278.22
	<i>PLD1</i>	Phospholipase D1, phosphatidylcholine-specific	−6.31	130.70
	<i>RPS6KA2</i>	Ribosomal protein S6 kinase, 90 kDa, polypeptide 2	−1.24	3.37
	<i>PDPK1</i>	3-phosphoinositide dependent protein kinase-1	−1.53	28.25
	<i>PIK3CB</i>	Phosphoinositide-3-kinase, catalytic, beta polypeptide	−1.42	16.34
	<i>PIK3CD</i>	Phosphoinositide-3-kinase, catalytic, delta polypeptide	3.37	184.83
	<i>PIK3CG</i>	Phosphoinositide-3-kinase, catalytic, gamma polypeptide	−1.42	215.28
	<i>CHUK</i>	Conserved helix-loop-helix ubiquitous kinase	−4.08	181.03
	<i>EIF4E</i>	Eukaryotic translation initiation factor 4E	−1.42	922.92
	<i>HIF1A</i>	Hypoxia inducible factor 1, alpha subunit	192.93	955.47
Inflammatory pathway	<i>CXCL8</i>	Interleukin 8	−3.29	2.96
	<i>IL-6</i>	Interleukin 6	14.45	114.56
	<i>TLR2</i>	Toll-like receptor 2	58	72.18
	<i>TLR9</i>	Toll-like receptor 9	3.29	134.55
	<i>TNF</i>	Tumor necrosis factor	12.9	154.26
Oxidative stress pathway	<i>ATOX1</i>	ATX1 antioxidant protein 1 homolog (yeast)	3.57	37.69
	<i>GPX2</i>	Glutathione peroxidase 2 (gastrointestinal)	3.57	37.69
	<i>GPX4</i>	Glutathione peroxidase 4 (gastrointestinal)	3.57	37.69
	<i>GSS</i>	Glutathione synthetase	3.57	9.54
	<i>NOX5</i>	NADPH oxidase. EF-hand calcium binding domain 5	3.57	7.54
	<i>SOD1</i>	Superoxide dismutase 1. soluble	−28.68	−9.67
	<i>SOD2</i>	Superoxide dismutase 2. mitochondrial	3.96	4.04

BCAA and glutamate are the two pathways more often altered in patients with AD [25]. High levels of isoleucine are associated with AD and high levels of valine are associated with reduced risk of AD. The latter result has been confirmed in the longitudinal Rotterdam study [26]. BCAA cross the blood-brain barrier through the large neutral amino acid transporter LAT1 in competition with AAA [27]. When the plasma level of BCAA is chronically elevated, BCAA uptake in the brain is favored at the expense of tryptophan, which is the precursor of serotonin and a molecule with multiple functions. It reduces amyloid- $\beta$  (A $\beta$ ) production (the hallmark of AD), protects neural survival, and stabilizes the mood [28]. Furthermore, the enzyme-branched chain amino acid transaminase (BCAT) converts BCAA to glutamate. Heightened levels of glutamate cause neuronal death by excitotoxicity (nerve cells death by glutamate overactivation). Finally, mTORC1 activation and mitochondrial dysfunction have a role in AD. The former enhances the *tau*-induced neurodegeneration, and apoptosis of post-mitotic neurons while the latter provokes A $\beta$  plaque formation [29]. In conclusion, high levels of isoleucine, valine, and glutamate (Figure 2A), mTORC1 activation (Table 1), and mitochondrial dysfunction (Table 1) reported in this study successfully recapitulate in vitro what is described in human studies. Of note, the convergent dysmetabolism (high levels of isoleucine, valine, and glutamate) common to T2D, OB, and AD is confirmed by the efficacy in AD patients of drugs used to treat T2D and other metabolic diseases [14].

In addition to T2D, OB, and AD, recently high levels of BCAA have also been shown to have a critical role in the pathogenesis of heart failure [15]. Studies in a mouse model have demonstrated that accumulation of BCAA requires inhibition of the BCAA-degradation-gene Kruppel-like factor 15 (KLF15). The subsequent intra-myocardial accumulation of BCAA upregulates mTORC1 that activates protein synthesis, cardiac hypertrophy, and heart failure. In a mouse model, pharmacologically induced BCAA catabolism significantly re-establishes the cardiac function [30]. Significantly, suppression of BCAA catabolism and accumulation of BCAA have also been observed in humans with heart failure. With regard to mitochondrial function, accumulation of lipids in the heart and hyperglycemia lead to impaired mitochondrial phosphorylation [31].

### 2.3. MKN-28 Cells Uptake BCAA from Culture Medium

The four diseases listed above have high levels of BCAA as a common feature. Mammalian cells as well as *Hp* cannot synthesize essential amino acids (which include BCAA). To shed light on the origin of the high levels of BCAAs observed in our experiments, we tested the hypothesis that they may derive from the depletion of culture medium by the MKN-28 cells. Following incubation with *Hpcf*, the MKN-28 cells display increased concentration of BCAA, while the extracellular medium shows reduced concentration of BCAA (Figure 2A,B). Since both *Hp* and MKN-28 cells are auxotrophic for essential amino acids, the above interpretation seems plausible.

### 2.4. *Helicobacter Pylori* Induces Inflammation and Oxidative Stress

*Hp* infection induces inflammation via activation of *NF- $\kappa$ B*. In our study, cell inflammation is confirmed by the upregulation of the *IL-8*, *TNF- $\alpha$* , *IL-6*, *TLR2*, and *TLR9* genes expressed by the MKN-28 cells incubated with *Hpcf* (Table 1). These cytokines characterize *Hp* infection and are part of a panel validated to detect inflammation in patients with chronic diseases [32]. If not controlled, inflammation may damage the gastric cells. In our study, we find several metabolites controlling the inflammation triggered by *Hp*. Taurine curbs the excess of Reactive oxygen species (ROS) produced by mitochondria [33]. The reduced level of this metabolite (Figure 3A) may indicate that part of it has been used to control the high levels of ROS produced by the mitochondria. One more signature in the same direction is sialic acid, expressed at a high level (Figure 3A). This metabolite assists the immune system to discriminate between the self and non-self [34]. Inflammation is also regulated by intracellular (acetate and propionate) and the extracellular (lactate) metabolites (Figure 3A,B). Acetate and propionate modulate the gastric mucosa inflammation [35]. Lactate, the product of the

catabolism of glucose under anaerobic conditions, induces expression of anti-inflammatory genes, and promotes macrophage polarization [36].

High levels of BCAAs (Figure 2A) and FA (Figure 3B) cause accumulation of catabolic intermediates (propionyl CoA and succinyl CoA) and incompletely oxidized FA contribute to the mitochondrial stress [37]. PCR array technology displayed upregulation of the main genes involved in the cell oxidative stress (Table 1). In particular, upregulation of *SOD2*, and downregulation of *SOD1*, point out the involvement of mitochondria in the production of ROS (Figure 4). Mitochondrial dysfunction is further confirmed by the high level of glutamate, which is tightly correlated with mitochondrial stress [35] (Figure 3B).

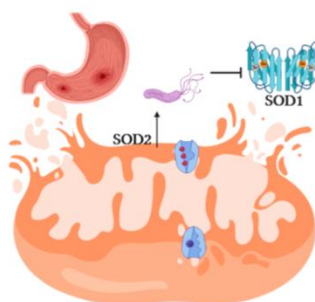


**Figure 4.** Schematic representation of superoxide dismutase 1 (*SOD1*) and superoxide dismutase 2 (*SOD2*) genes modulated by *Hp*. Downregulation of *SOD1* and upregulation of *SOD2* point out the involvement of mitochondria in ROS production.

BCAA are required for the activation of mTORC1 [38]. PCR array technology showed up-regulation of both the *RPTOR* and *MLST8* subunits of mTORC1 after 2 h of *Hpcf* treatment, with key genes implicated in the regulation of the mTORC1 (*AKT1*, *AKT2*, *INSR*, *IRS1*, *PLD1*, and *RPS6KA2*) being significantly up-regulated ( $p$ -value  $\leq 0.0001$ ). Significantly, upregulated genes include *AKT1*-involved in the inhibition of protein breakdown-and *INSR*-sensing the concentration of insulin outside the cell and transmits this signal through the *PI3K/Akt/mTORC1* pathway [39]. Finally, mTORC1 activation is confirmed by the overexpression of the positive effectors *CHUK*, *EIF4E*, and *HIF1A* (Table 1).

We can conclude that high levels of BCAA (Figure 2A), activation of mTORC1, impaired mitochondrial activity, and inflammation (Table 1) are dominant traits common to the four diseases under investigation, and all potentially referable to *Hp*.

### 3. Discussion

Cellular homeostasis is heavily dependent upon a balanced regulation of mTORC1. Thus, deregulation of this complex inevitably leads to many diseases, including metabolic diseases. Though mTORC1 can be modulated by several factors, amino acids are condition necessary and sufficient for promoting cellular anabolic metabolism and mTORC1 activation [40]. Upon incubation with *Hpcf*, MKN-28 cells show high levels of amino acids (Figure 2A). This result, also observed in the AGS human cell line, reflects the demand of nutrients by *Hp* [41]. At the same time, it displays the tight connection linking mTORC1 activation, high amino acids concentrations, and *Hp* infection.

In the absence of inflammation, immune cells exploit an anabolic metabolism modulated by mTORC1 tempered by *c-MYC*. In the presence of inflammation, *c-MYC* is suppressed and mTORC1 moves under the control of *HIF1a* [42]. This finding indicates that cell replication and inflammation both



depend upon mTORC1, but are regulated by *c-MYC* in the absence of inflammation and *HIF1 $\alpha$*  in the presence of inflammation. In addition of inducing anabolic metabolism, inflammation inhibits *AMPK*, which is the activator of catabolic metabolism [43]. In our study, upregulation of *HIF1 $\alpha$*  and mTORC1 indicates that MKN-28 cells, upon incubation with *Hpcf*, express the mTORC1-*HIF1 $\alpha$* -regulated inflammatory phenotype (Table 1). Induction of *TNF- $\alpha$*  and *IL-6* (Table 1) confirms the suppression of *AMPK*, which is a condition required for expression of these cytokines. Enhanced glycolysis via activation of *PIK3* subunits and mTORC1-*HIF1 $\alpha$*  (Table 1) and suppression of *AMPK* further confirm the anabolic state of the MKN-28 cells. Activation of MKN-28 cells by *Hpcf* and expression of the genes modulating mTORC1-*HIF1 $\alpha$*  are one more proof of the tight connection between *Hp* and mTORC1 activation.

As a supervisor of host cell nourishment, mTORC1 is also the target of bacteria. To establish infection, bacteria often need to shift the host cellular metabolism from anabolic to catabolic. Inhibition of mTORC1 by the *Hp* toxin VacA is interpreted as a means used by the bacterium to prevent the production of nutrients needed by immune cells of the host to mount an antibacterial response [12]. Taken alone, inhibition of mTORC1 by VacA may seem at odds with the activation of the same gene by increased concentrations of amino acids. Actually, *Hp* has adopted this strategy to better exploit the resources of the host. Autophagy induced by the VacA toxin is useful to *Hp* during the gastric mucosa colonization phase [44]. However, once *Hp* has colonized the gastric mucosa, autophagy becomes harmful for the survival of bacteria. Therefore, in this phase of infection, VacA is neutralized by CagA [10]. Two virulence factors of *Hp*, acting antagonistically, protect the survival of bacteria during different phases of the infection: a highly rewarding result for *Hp* that, by the same mechanism, can inhibit or activate the host cellular metabolism.

*Hp* directly impacts on mitochondria and inflammation. Mitochondria are involved in ATP production, apoptosis, lipid, and amino acids metabolism [45]. In our in vitro experiment, the signatures of mitochondrial stress are evident as upregulation of the antioxidant superoxide dismutase *SOD2* (Table 1) and those of inflammation as secretion of the pro-inflammatory factors as well as *TNF- $\alpha$*  and *IL-6* genes (Table 1). At this stage, we can conclude that the traits common to the four diseases can all be associated, at least in part, with *Hp*.

Several interesting insights emerge from this study. First, it demonstrates that cell lines can be used successfully to investigate genetic or metabolic disorders. Cell line experiments, compared to studies on patients, offer the advantage of reducing variables, differences in the diet, use of drugs, or genetic heterogeneity, between participants. Second, the study raises the question whether a concerted effort to study the basic biology of diseases with several traits in common (as T2D, OB, AD, and CMT) may be more effective than the traditional approach of studying each disease separately. Third, here, we point out that *Hp* and mammals have lost the genes coding for essential amino acids. Evolution gives some hints about the benefits associated with gene loss [46]. Organisms, bacteria as well as mammals, evolve under changing environmental conditions. If amino acids are available in the environment, the corresponding genes, no longer adaptive, are lost or undergo mutations leading to more adaptive genes. Following this logic, it seems clear that mammals and *Hp* are auxotrophic for essential amino acids. Mammals can obtain essential amino acids from their diet. *Hp* finds them in its niche (the gastric mucosa), which is rich in essential amino acids derived from the diet of the host [7].

Finally, we acknowledge a limit of this study. We describe four traits common to the four diseases and *Hp* infection. However, this finding is not sufficient to attribute to *Hp* a causal role for the above diseases. *Hp* could just be the biomarker of a genetic or metabolic disorder carried by the MKN-28 cell line. It is hard to distinguish between causation and association, especially in the case of highly complex diseases. Despite the fact that high levels of BCAA anticipate of many years T2D, it is not known yet whether BCAA are the cause of T2D or a biomarker of insulin resistance [11]. However, human stem cells-derived organoids [47] from healthy donors and from patients with the above diseases may permit us to repeat the study in a known genetic context and clarify the role of *Hp*.

#### 4. Materials and Methods

##### 4.1. *Helicobacter Pylori*

*Hp* strain ATCC 43504 was grown in Brain Heart Infusion medium (BHI, Oxoid, UK) complemented with 10% Fetal Bovine Serum (FBS, Oxoid, UK) and incubated under microaerophilic condition at 37 °C [48].

##### 4.2. Cell Culture Conditions

The human gastric adenocarcinoma MKN-28 cell line (ATCC, MD, USA) was grown in DMEM/F12 medium, supplemented with 10% FBS, 1% penicillin/streptomycin, and 1% glutamine in a 100-mm culture dish at 37 °C in a 5% CO<sub>2</sub> atmosphere. The reagents were all from Gibco, ThermoFisher, Waltham, MA, USA.

##### 4.3. Cell Culture for Metabolomics Analysis

Confluent 100-mm dishes were incubated for two hours with *Hpcf*, or as a control with BHI medium. The cells were detached from the adherent substrate with trypsin (1.5 mL for 3 min), and washed twice with Phosphate-Buffered Saline (PBS). The mixture, containing detached cells, was transferred into a Falcon tube and centrifuged at 1200 rpm and 25 °C for 3 min. The liquid phase was discarded, and the cell pellet was washed three times with 5 mL of PBS. After the last wash, the cell pellet was frozen in liquid nitrogen and stored at −80 °C until metabolites extraction.

##### 4.4. Metabolites Extraction and NMR Samples Preparation

Combined extraction of polar and hydrophobic metabolites was carried out by using ice-cold methanol/Milli-Q® water/chloroform (1/0.72/1) solvents as described by Papaïanni et al. 2020 [49]. NMR-based intracellular metabolomics analysis and NMR-based extracellular metabolomics analysis were shown as Papaïanni et al., 2020 [50].

##### 4.5. NMR Spectroscopy

NMR spectra were recorded on a Bruker Avance III-600 MHz spectrometer (Bruker BioSpin GmbH, Rheinstetten, Germany) as reported [51].

##### 4.6. RNA Extraction and Real-Time PCR

Gene expression analysis through PCR array technology was performed as described [52]. Briefly, cells ( $2 \times 10^6$ ), used for RNA extraction, were seeded in Petri dishes (100 mm diameter) and treated with *Hpcf*. After 2 h of exposure time, cells were washed directly in the Petri dish by adding cold PBS. Cells were lysed in the Petri dish by adding 1 mL of Trisure Reagent (Bioline, Memphis, TN, USA). RNA was isolated according to the manufacturer's protocol. RNA concentration and purity were assessed using the nanophotometer Nanodrop (Euroclone, Milan, Italy). RNA (200 ng) was reverse transcribed using the RT2 first strand kit (Qiagen, Hilden, Germany), according to the manufacturer's instructions. The qRT-PCR analysis was performed in triplicate using the RT2 Profiler PCR Array kit (Qiagen, Hilden, Germany). Plates were run on a ViiA7 (Applied Biosystems, Foster City, CA, USA) according to the Standard Fast PCR Cycling protocol with 10 µL reaction volumes. Cycling conditions were: 1 cycle initiation at 95.0 °C for 10 min, which was followed by amplification for 40 cycles at 95.0 °C for 15 s and 60.0 °C for 1 min. Amplification data were collected via ViiA 7 RUO Software (Applied Biosystems, Foster City, CA, USA). The cycle threshold (Ct)-values were analysed with PCR array data analysis online software (<http://pcrdataanalysis.sabiosciences.com/pcr/arrayanalysis.php>, Qiagen, Hilden, Germany).



**Author Contributions:** R.C., D.I., A.I., C.M., P.C., and M.P. designed the research. P.C., M.P., and C.S. performed the research. A.M., D.P. analyzed metabolic data. D.I. and R.C. wrote the paper. All authors have read and agreed to the published version of the manuscript.

**Funding:** The authors declare no competing financial interest.

**Acknowledgments:** We thank anonymous reviewers for insightful suggestions that clearly improved the quality of the article.

**Conflicts of Interest:** The authors declare no conflict of interest.

### Abbreviations

<i>Hp</i>	<i>Helicobacter pylori</i>
NMR	Nuclear Magnetic Resonance
<i>Hpcf</i>	<i>Hp</i> cell filtrate
BCAA	Branched chain amino acids
mTORC1	mammalian Target Of Rapamycin Complex 1
TLRs	Tool like receptors
NF-AT	nuclear translocation of the T transcription factor
T2D	Type 2 diabetes
OB	Obesity
AD	Alzheimer's disease
CMD	Cardiometabolic disease
PCA	Principal Component Analysis
OPLS-	Orthogonal partial least squares discriminant analysis
AAA	Aromatic amino acids
ROS	Reactive oxygen species
LAT1	Large neutral amino acid transporter
BCAT	Branched chain amino acid transaminase
KLF15	Kruppel-like factor 15
FBS	Fetal Bovine Serum
BHI	Brain Heart Infusion medium
PBS	Phosphate-Buffered Saline

### References

- Salama, N.R.; Hartung, M.L.; Müller, A. Life in the human stomach: Persistence strategies of the bacterial pathogen *Helicobacter pylori*. *Nat. Rev. Microbiol.* **2013**, *11*, 385–399. [\[CrossRef\]](#)
- Cuomo, P.; Papaiani, M.; Fulgione, A.; Guerra, F.; Capparelli, R.; Medaglia, C. An innovative approach to control *H. Pylori*-induced persistent inflammation and colonization. *Microorganisms* **2020**, *8*, 1214. [\[CrossRef\]](#)
- Cooke, C.L.; Huff, J.L.; Solnick, J.V. The role of genome diversity and immune evasion in persistent infection with *Helicobacter pylori*. *FEMS Immunol. Med. Microbiol.* **2005**, *45*, 11–23. [\[CrossRef\]](#)
- Cullen, T.W.; Giles, D.K.; Wolf, L.N.; Ecobichon, C.; Boneca, I.G.; Trent, M.S. *Helicobacter pylori* versus the Host: Remodeling of the Bacterial Outer Membrane Is Required for Survival in the Gastric Mucosa. *PLoS Pathog.* **2011**, *7*, e1002454. [\[CrossRef\]](#)
- Gebert, B.; Fischer, W.; Weiss, E.; Hoffmann, R.; Haas, R. *Helicobacter pylori* vacuolating cytotoxin inhibits T lymphocyte activation. *Science* **2003**, *301*, 1099–1102. [\[CrossRef\]](#)
- Franceschi, F.; Gasbarrini, A.; Polyzos, S.A.; Kountouras, J. Extragastric Diseases and *Helicobacter pylori*. *Helicobacter* **2015**, *20*, 40–46. [\[CrossRef\]](#)
- Eisenreich, W.; Rudel, T.; Heesemann, J.; Goebel, W. How viral and intracellular bacterial pathogens reprogram the metabolism of host cells to allow their intracellular replication. *Front. Cell. Infect. Microbiol.* **2019**, *9*, 42. [\[CrossRef\]](#)
- Sancak, Y.; Bar-Peled, L.; Zoncu, R.; Markhard, A.L.; Nada, S.; Sabatini, D.M. Ragulator-rag complex targets mTORC1 to the lysosomal surface and is necessary for its activation by amino acids. *Cell* **2010**, *141*, 290–303. [\[CrossRef\]](#) [\[PubMed\]](#)

9. Ansari, S.; Yamaoka, Y. *Helicobacter pylori* virulence factors exploiting gastric colonization and its pathogenicity. *Toxins* **2019**, *11*, 677. [\[CrossRef\]](#) [\[PubMed\]](#)
10. Kim, I.-J.; Lee, J.; Oh, S.J.; Chung, H.J.; Chen, J.; Blanke Correspondence, S.R. *Helicobacter pylori* Infection Modulates Host Cell Metabolism through VacA-Dependent Inhibition of mTORC1. *Cell Host Microbi* **2018**, *23*, 583–593. [\[CrossRef\]](#)
11. Lynch, C.J.; Adams, S.H. Branched-chain amino acids in metabolic signalling and insulin resistance. *Nat. Rev. Endocrinol.* **2014**, *10*, 723–736. [\[CrossRef\]](#)
12. Huang, X.W.; Luo, R.H.; Zhao, Q.; Shen, Z.Z.; Huang, L.L.; An, X.Y.; Zhao, L.J.; Wang, J.; Huang, Y.Z. *Helicobacter pylori* induces mitochondrial DNA mutation and reactive oxygen species level in AGS cells. *Int. J. Med. Sci.* **2011**, *8*, 56–67. [\[CrossRef\]](#)
13. White, J.R.; Winter, J.A.; Robinson, K. Differential inflammatory response to *Helicobacter pylori* infection: Etiology and clinical outcomes. *J. Inflamm. Res.* **2015**, *8*, 137–147.
14. White, P.J.; Newgard, C.B. Branched-chain amino acids in disease. *Science* **2019**, *363*, 582–583. [\[CrossRef\]](#)
15. Shao, D.; Villet, O.; Zhang, Z.; Choi, S.W.; Yan, J.; Ritterhoff, J.; Gu, H.; Djukovic, D.; Christodoulou, D.; Kolwicz, S.C.; et al. Glucose promotes cell growth by suppressing branched-chain amino acid degradation. *Nat. Commun.* **2018**, *9*, 1–17. [\[CrossRef\]](#)
16. Yilmaz, M.I.; Romano, M.; Basarali, M.K.; Elzagallaai, A.; Karaman, M.; Demir, Z.; Demir, M.F.; Akcay, F.; Seyrek, M.; Haksever, N.; et al. The Effect of Corrected Inflammation, Oxidative Stress and Endothelial Dysfunction on Fmd Levels in Patients with Selected Chronic Diseases: A Quasi-Experimental Study. *Sci. Rep.* **2020**, *10*, 9018. [\[CrossRef\]](#)
17. Lowell, B.B.; Shulman, G.I. Mitochondrial dysfunction and type 2 diabetes. *Science* **2005**, *307*, 384–387. [\[CrossRef\]](#)
18. Sul, J.H.; Martin, L.S.; Eskin, E. Population structure in genetic studies: Confounding factors and mixed models. *PLoS Genet.* **2018**, *14*, e1007309. [\[CrossRef\]](#)
19. Allen, J.; Davey, H.M.; Broadhurst, D.; Heald, J.K.; Rowland, J.J.; Oliver, S.G.; Kell, D.B. High-throughput classification of yeast mutants for functional genomics using metabolic footprinting. *Nat. Biotechnol.* **2003**, *21*, 692–696. [\[CrossRef\]](#)
20. Shaham, O.; Slate, N.G.; Goldberger, O.; Xu, Q.; Ramanathan, A.; Souza, A.L.; Clish, C.B.; Sims, K.B.; Mootha, V.K. A plasma signature of human mitochondrial disease revealed through metabolic profiling of spent media from cultured muscle cells. *Proc. Natl. Acad. Sci. USA* **2010**, *107*, 1571–1575. [\[CrossRef\]](#)
21. Wang, T.J.; Larson, M.G.; Vasan, R.S.; Cheng, S.; Rhee, E.P.; McCabe, E.; Lewis, G.D.; Fox, C.S.; Jacques, P.F.; Fernandez, C.; et al. Metabolite profiles and the risk of developing diabetes. *Nat. Med.* **2011**, *17*, 448–453. [\[CrossRef\]](#)
22. Frühbeck, G. Obesity: Screening for the evident in obesity. *Nat. Rev. Endocrinol.* **2012**, *8*, 570–572. [\[CrossRef\]](#)
23. Newgard, C.B.; An, J.; Bain, J.R.; Muehlbauer, M.J.; Stevens, R.D.; Lien, L.F.; Haqq, A.M.; Shah, S.H.; Arlotto, M.; Slentz, C.A.; et al. A Branched-Chain Amino Acid-Related Metabolic Signature that Differentiates Obese and Lean Humans and Contributes to Insulin Resistance. *Cell Metab.* **2009**, *9*, 311–326. [\[CrossRef\]](#)
24. Yamakado, M.; Nagao, K.; Imaizumi, A.; Tani, M.; Toda, A.; Tanaka, T.; Jinzu, H.; Miyano, H.; Yamamoto, H.; Daimon, T.; et al. Plasma Free Amino Acid Profiles Predict Four-Year Risk of Developing Diabetes, Metabolic Syndrome, Dyslipidemia, and Hypertension in Japanese Population. *Sci. Rep.* **2015**, *5*, 11918. [\[CrossRef\]](#)
25. Holčěek, M. Branched-chain amino acids in health and disease: Metabolism, alterations in blood plasma, and as supplements. *Nutr. Metab.* **2018**, *15*, 1–12. [\[CrossRef\]](#)
26. Toledo, J.B.; Arnold, M.; Kastenmüller, G.; Chang, R.; Baillie, R.A.; Han, X.; Thambisetty, M.; Tenenbaum, J.D.; Suhre, K.; Thompson, J.W.; et al. Metabolic network failures in Alzheimer's disease: A biochemical road map. *Alzheimers Dement.* **2017**, *13*, 965–984. [\[CrossRef\]](#)
27. Boado, R.J.; Li, J.Y.; Nagaya, M.; Zhang, C.; Pardridge, W.M. Selective expression of the large neutral amino acid transporter at the blood-brain barrier. *Proc. Natl. Acad. Sci. USA* **1999**, *96*, 12079–12084. [\[CrossRef\]](#)
28. Wang, R.; Reddy, P.H. Role of Glutamate and NMDA Receptors in Alzheimer's Disease. *J. Alzheimers Dis.* **2017**, *57*, 1041–1048. [\[CrossRef\]](#) [\[PubMed\]](#)
29. Song, M.K.; Bischoff, D.S.; Song, A.M.; Uyemura, K.; Yamaguchi, D.T. Metabolic relationship between diabetes and Alzheimer's Disease affected by Cyclo(His-Pro) plus zinc treatment. *BBA Clin.* **2017**, *7*, 41–54. [\[CrossRef\]](#)

30. Ren, J.; Pulakat, L.; Whaley-Connell, A.; Sowers, J.R. Mitochondrial biogenesis in the metabolic syndrome and cardiovascular disease. *J. Mol. Med.* **2010**, *88*, 993–1001. [\[CrossRef\]](#) [\[PubMed\]](#)
31. Lamb, A.; Chen, L.F. Role of the *Helicobacter pylori*-Induced inflammatory response in the development of gastric cancer. *J. Cell. Biochem.* **2013**, *114*, 491–497. [\[CrossRef\]](#)
32. Koelman, L.; Pivovarov-Ramich, O.; Pfeiffer, A.E.H.; Grune, T.; Aleksandrova, K. Cytokines for evaluation of chronic inflammatory status in ageing research: Reliability and phenotypic characterisation. *Immun. Ageing* **2019**, *16*, 11. [\[CrossRef\]](#)
33. Heinz, S.; Freyberger, A.; Lawrenz, B.; Schladt, L.; Schmuck, G.; Ellinger-Ziegelbauer, H. Mechanistic Investigations of the Mitochondrial Complex i Inhibitor Rotenone in the Context of Pharmacological and Safety Evaluation. *Sci. Rep.* **2017**, *7*, 1–13. [\[CrossRef\]](#)
34. Xue, Z.; Zhao, H.; Zhu, R.; Chen, C.; Cao, H.; Han, J.; Han, S. On the use of abiotic sialic acids to attenuate cell inflammation. *Sci. Rep.* **2018**, *8*, 17320. [\[CrossRef\]](#)
35. Paglia, G.; Stochero, M.; Cacciatore, S.; Lai, S.; Angel, P.; Alam, M.T.; Keller, M.; Ralser, M.; Astarita, G. Unbiased Metabolomic Investigation of Alzheimer's Disease Brain Points to Dysregulation of Mitochondrial Aspartate Metabolism. *J. Proteome Res.* **2016**, *15*, 608–618. [\[CrossRef\]](#) [\[PubMed\]](#)
36. Ivashkiv, L.B. The hypoxia-lactate axis tempers inflammation. *Nat. Rev. Immunol.* **2020**, *20*, 85–86. [\[CrossRef\]](#)
37. Newgard, C.B. Interplay between lipids and branched-chain amino acids in development of insulin resistance. *Cell Metab.* **2012**, *15*, 606–614. [\[CrossRef\]](#)
38. Laplante, M.; Sabatini, D.M. Regulation of *mTORC1* and its impact on gene expression at a glance. *J. Cell Sci.* **2013**, *126*, 1713–1719. [\[CrossRef\]](#)
39. Bond, P. Regulation of *mTORC1* by growth factors, energy status, amino acids and mechanical stimuli at a glance. *J. Int. Soc. Sports Nutr.* **2016**, *13*, 8. [\[CrossRef\]](#)
40. Rabanal-Ruiz, Y.; Otten, E.G.; Korolchuk, V.I. *mTORC1* as the main gateway to autophagy. *Essays Biochem.* **2017**, *61*, 565–584.
41. Matsunaga, S.; Nishiumi, S.; Tagawa, R.; Yoshida, M. Alterations in metabolic pathways in gastric epithelial cells infected with *Helicobacter pylori*. *Microb. Pathog.* **2018**, *124*, 122–129. [\[CrossRef\]](#)
42. Liu, L.; Luc, Y.; Martinez, J.; Bi, Y.; Lian, G.; Wang, T.; Milasta, S.; Wang, J.; Yang, M.; Liu, G.; et al. Proinflammatory signal suppresses proliferation and shifts macrophage metabolism from *Myc*-dependent to *HIF1 $\alpha$* -dependent. *Proc. Natl. Acad. Sci. USA* **2016**, *113*, 1564–1569. [\[CrossRef\]](#)
43. Sag, D.; Carling, D.; Stout, R.D.; Suttles, J. Adenosine 5'-Monophosphate-Activated Protein Kinase Promotes Macrophage Polarization to an Anti-Inflammatory Functional Phenotype. *J. Immunol.* **2008**, *181*, 8633–8641. [\[CrossRef\]](#)
44. Ricci, V. Relationship between vaca toxin and host cell autophagy in *Helicobacter pylori* infection of the human stomach: A few answers, Many questions. *Toxins* **2016**, *8*, 203. [\[CrossRef\]](#)
45. Spinelli, J.B.; Haigis, M.C. The multifaceted contributions of mitochondria to cellular metabolism. *Nat. Cell Biol.* **2018**, *20*, 745–754. [\[CrossRef\]](#)
46. D'Souza, G.; Waschina, S.; Pande, S.; Bohl, K.; Kaleta, C.; Kost, C. Less is more: Selective advantages can explain the prevalent loss of biosynthetic genes in bacteria. *Evolution* **2014**, *68*, 2559–2570. [\[CrossRef\]](#) [\[PubMed\]](#)
47. Bartfeld, S.; Bayram, T.; Van De Wetering, M.; Huch, M.; Begthel, H.; Kujala, P.; Vries, P.; Peters, R.; Hans, P.J.C. In vitro expansion of human gastric epithelial stem cells and their responses to bacterial infection. *Gastroenterology* **2015**, *148*, 126–136. [\[CrossRef\]](#)
48. Contaldi, F.; Capuano, F.; Fulgione, A.; Aiese Cigliano, R.; Sanseverino, W.; Iannelli, D.; Medaglia, C.; Capparelli, R. The hypothesis that *Helicobacter pylori* predisposes to Alzheimer's disease is biologically plausible. *Sci. Rep.* **2017**, *7*, 7817. [\[CrossRef\]](#)
49. Papaiani, M.; Paris, D.; Woo, S.L.; Fulgione, A.; Rigano, M.M.; Parrilli, E.; Tutino, M.L.; Marra, R.; Manganiello, G.; Casillo, A.; et al. Plant dynamic metabolic response to bacteriophage treatment after *Xanthomonas campestris* *pv* *campestris* infection. *Front. Microbiol.* **2020**, *11*, 732. [\[CrossRef\]](#)
50. Fulgione, A.; Papaiani, M.; Cuomo, P.; Paris, D.; Romano, M.; Tuccillo, C.; Palomba, L.; Medaglia, C.; De Seta, M.; Esposito, N.; et al. Interaction between *MyD88*, *TIRAP* and *IL1RL1* against *Helicobacter pylori* infection. *Sci. Rep.* **2020**, *10*, 15831. [\[CrossRef\]](#)

51. Papaiani, M.; Cuomo, P.; Fulgione, A.; Albanese, D.; Gallo, M.; Paris, D.; Motta, A.; Iannelli, D.; Capparelli, R. Bacteriophages Promote Metabolic Changes in Bacteria Biofilm. *Microorganisms* **2020**, *8*, 480. [[CrossRef](#)]
52. Sansone, C.; Nuzzo, G.; Galasso, C.; Casotti, R.; Fontana, A.; Romano, G.; Ianora, A. The Marine Dinoflagellate *Alexandrium andersoni* Induces Cell Death in Lung and Colorectal Tumor Cell Lines. *Mar. Biotechnol.* **2018**, *20*, 343–352. [[CrossRef](#)] [[PubMed](#)]

**Publisher's Note:** MDPI stays neutral with regard to jurisdictional claims in published maps and institutional affiliations.



© 2020 by the authors. Licensee MDPI, Basel, Switzerland. This article is an open access article distributed under the terms and conditions of the Creative Commons Attribution (CC BY) license (<http://creativecommons.org/licenses/by/4.0/>).

## **CHAPTER 2**

***The role of Formyl peptide receptors  
in permanent and low-grade  
inflammation: Helicobacter pylori  
infection as a model***

Formyl peptide receptors (FPRs) are a group of the host innate immune receptor family, playing critical roles in infection, inflammation and progression of chronic diseases (Le et al., 2002; Chen et al., 2020). FPRs participate to numerous pathophysiological processes, orchestrating disease initiation, progression and in some cases, disease resolution (Liang et al., 2020). They have been reported to be involved in multiple diseases, such as diabetes, obesity, cardiovascular disease and neurological disorders (Li and Ye, 2013; Caso et al., 2021), suggesting that these receptors might act as potential target for therapeutical intervention.

In this chapter, an extensive description of FPRs and their molecular biology is provided, highlighting their role in *H. pylori*-induced inflammation and related clinical effects.

## References

- Caso, V.M.; Manzo, V.; Pecchillo Cimmino, T.; Conti, V.; Caso, P.; Esposito, G.; Russo, V.; Filippelli, A.; Ammendola, R.; Cattaneo, F. Regulation of Inflammation and Oxidative Stress by Formyl Peptide Receptors in Cardiovascular Disease Progression. *Life* (Basel). **2021**; 11(3):243.
- Chen, T.; Xiong, M.; Zong, X.; Ge, Y.; Zhang, H.; Wang, M.; Won Han, G.; Yi, C., et al. Structural basis of ligand binding modes at the human formyl peptide receptor 2. *Nat Commun.* **2020**; 11(1):1208.
- Le, Y.; Murphy, P.M.; Wang, J.M. Formyl-peptide receptors revisited. *Trends Immunol.* **2002**; 23(11):541-8.
- Li, Y.; Ye, D. Molecular biology for formyl peptide receptors in human diseases. *J Mol Med* (Berl). **2013**; 91(7):781-9.
- Liang, W.; Chen, K.; Gong, W.; Yoshimura, T.; Le, Y.; Wang, Y.; Wang, J.M. The Contribution of Chemoattractant GPCRs, Formylpeptide Receptors, to Inflammation and Cancer. *Front Endocrinol* (Lausanne). **2020**; 11:17.



## Review

# The Role of Formyl Peptide Receptors in Permanent and Low-Grade Inflammation: *Helicobacter pylori* Infection as a Model

Paola Cuomo <sup>1</sup> , Marina Papaiani <sup>1</sup>, Rosanna Capparelli <sup>1,\*</sup> and Chiara Medaglia <sup>2</sup>

<sup>1</sup> Department of Agriculture Sciences, University of Naples Federico II, Portici, 80055 Naples, Italy; paola.cuomo@unina.it (P.C.); marina.papaiani@unina.it (M.P.)

<sup>2</sup> Department of Microbiology and Molecular Medicine, University of Geneva Medical School, 1211 Genève, Switzerland; chiara.medaglia@unige.ch

\* Correspondence: capparel@unina.it



**Citation:** Cuomo, P.; Papaiani, M.; Capparelli, R.; Medaglia, C. The Role of Formyl Peptide Receptors in Permanent and Low-Grade Inflammation: *Helicobacter pylori* Infection as a Model. *Int. J. Mol. Sci.* **2021**, *22*, 3706. <https://doi.org/10.3390/ijms22073706>

Academic Editor: Alessandra Tosco

Received: 28 February 2021

Accepted: 30 March 2021

Published: 2 April 2021

**Publisher's Note:** MDPI stays neutral with regard to jurisdictional claims in published maps and institutional affiliations.



**Copyright:** © 2021 by the authors. Licensee MDPI, Basel, Switzerland. This article is an open access article distributed under the terms and conditions of the Creative Commons Attribution (CC BY) license (<https://creativecommons.org/licenses/by/4.0/>).

**Abstract:** Formyl peptide receptors (FPRs) are cell surface pattern recognition receptors (PRRs), belonging to the chemoattractant G protein-coupled receptors (GPCRs) family. They play a key role in the innate immune system, regulating both the initiation and the resolution of the inflammatory response. FPRs were originally identified as receptors with high binding affinity for bacteria or mitochondria N-formylated peptides. However, they can also bind a variety of structurally different ligands. Among FPRs, formyl peptide receptor-like 1 (FPRL1) is the most versatile, recognizing N-formyl peptides, non-formylated peptides, and synthetic molecules. In addition, according to the ligand nature, FPRL1 can mediate either pro- or anti-inflammatory responses. Hp(2-20), a *Helicobacter pylori*-derived, non-formylated peptide, is a potent FPRL1 agonist, participating in *Helicobacter pylori*-induced gastric inflammation, thus contributing to the related site or not-site specific diseases. The aim of this review is to provide insights into the role of FPRs in *H. pylori*-associated chronic inflammation, which suggests this receptor as potential target to mitigate both microbial and sterile inflammatory diseases.

**Keywords:** *Helicobacter pylori*; formyl peptide receptors; inflammation

## 1. Introduction

The human body is continuously exposed to millions of pathogens, which can enter it through different ways. The immune system, and in particular, innate immunity, has an important role in controlling the infections, representing the front-line defense against invading pathogens [1–3].

Innate immunity is mediated by anatomic barriers (skin and mucosa), physiological functions (pH values, temperature, chemical mediators), and cellular elements [4]. Skin and mucosal surfaces—including the gastrointestinal tract, the respiratory tract, the urogenital tract, and ocular surface—are the earliest sites of host–pathogen interactions, separating the body from the external environment [3,5]. This feature makes them directly involved in preventing the entry of invading microorganisms [3], acting as chemical–physical barriers [6]. Nevertheless, mechanical or chemical cleansing mechanisms provided by anatomic barriers can fail, promoting the action of other innate immune elements—specifically, immune cells, which participate to potentiate the protective role of the mucosal surface. The mucosal immune system, indeed, comprises approximately 80% of all the immune cells (macrophages, monocytes, neutrophils, dendritic cells, B and T cells, and natural killer cells) [6,7], which express specific receptors called pattern recognition receptors (PRRs).

Pattern recognition receptors are germline-encoded receptors, evolutionary selected and conserved. They mediate innate immune recognition by detecting conserved molecular structures associated with pathogens or host tissue/cell damage, also called pathogen-

associated molecular patterns (PAMPs) [8] or damage-associated molecular patterns (DAMPs), respectively.

The activation of pattern recognition receptors initiates the inflammatory response, leading to cytokine, chemokine, prostaglandin, and leukotriene production, as they are key messengers signaling the occurrence of tissue damage.

Inflammation is a complex biological response initiated by the host against a microbial infection or an injury. The aim of this process consists of protecting the host by removing the dangerous stimulus and restoring the damaged tissue, thus favoring the return to the homeostasis [9]. However, if not controlled and self-limited, the inflammatory response may cause severe tissue damage, increasing the microbial pathogenicity [10,11] and contributing to the development of chronic inflammatory diseases [12].

Formyl peptide receptors (FPRs) are a family of pattern recognition receptors, able to recognize principally N-formyl methionine-containing peptides, derived both from bacteria (PAMPs) and mitochondria (DAMPs) [13]. In addition to pattern recognition receptors, formyl peptide receptors regulate the inflammatory reaction by modulating the host defense with regulatory functions in both the initiation and the resolution of inflammation. This suggests their involvement in physiological as well as pathological conditions, making them an important element of the innate immune system with a critical role in human health.

The present review focuses on formyl peptide receptors of the gastrointestinal mucosal immune system, their role in inflammation associated with *Helicobacter pylori* infection, and the possibility of targeting them to modulate *H. pylori*-associated chronic inflammation.

## 2. Formyl Peptide Receptors

### 2.1. Formyl Peptide Receptors: Cell Distribution and Classification

Formyl peptide receptors are a family of classical chemoattractant receptors. Human cells present three different isoforms of FPRs: FPR1, FPR2, or formyl peptide receptor-like 1 (FPRL1), and FPR3 or Formyl peptide receptor-like 2 (FPRL2). Each receptor is encoded by a specific gene of the human FPR gene family (FPR1, FPR2, FPR3) clustered on the chromosomal region 19q13.3 [14]. FPR1, FPR2, and FPR3 genes share high level of sequence homology [9], resulting in receptor similarity. Compared to FPR1, FPRL1 has one additional amino acid, for a total of 351 residues, and a sequence homology corresponding to 69% between the two receptors. Meanwhile, compared to FPR1, FPRL2 has two additional amino acids, for a total of 352, and a sequence homology of 56% [14]. Despite the high sequence identity among the three FPRs, they differ in cell expression, role (Table 1), and ligand recognition (Table 2). Phagocytic cells were the first in which FPRs were identified. Monocytes express the three FPR genes, but their expression can change in differentiating monocytes. Specifically, monocytes differentiating in macrophages maintain FPRL1 expression, while the transition from immature to mature dendritic cells determines the loss of FPR1. The role of FPRs in macrophage and dendritic cell differentiation has been widely investigated, demonstrating that WKYMV (an FPR ligand) negatively regulates LPS-induced dendritic cell differentiation [15,16], while Lipoxin-A4, LL-37, and serum amyloid A protein (SAA) (FPRL1 agonists) mediate macrophage polarization to the anti-inflammatory form M2 [16]. These findings suggest that FPRs play a regulatory function in immune cell differentiation and activation. Unlike monocytes, neutrophils express both FPR1 and FPRL1, but they lack the FPRL2 gene [14]. Recently, adaptive immune cells were discovered to express FPRs. FPRL1 was found in human tonsillar follicular helper T cells, Th1 cells, Th2 cells, Th17 cells, and in naive CD4 T cells (CD3+, CD4+, CD45RA-, CD45RO-, and CCR7+) [16,17].

In addition, FPR expression has also been described in platelets, microglial cells, epithelial cells, hepatocytes, fibroblasts, and endothelial cells, as well as spleen, brain, placenta, liver, and further tissues, demonstrating the almost ubiquitous distribution of these receptors [18]. The wide expression of formyl peptide receptors in immune and



non-immune cells, including various organs and tissues, suggests their involvement in multiple biological functions, with inflammation as the core.

Among the three receptors, formyl peptide receptor-like 1 is the most ubiquitous one. It has been found in different non-myeloid-endothelial cells, epithelial cells, as well as the hepatocyte and tissue-gastrointestinal tract, brain, spleen, female organ tissues, pancreas, and endocrine glands [19,20]. Furthermore, compared to FPR1 and FPRL2, FPRL1 can interact with the highest variety of chemically different ligands, including non-formylated peptides, organic molecules, and lipid mediators [19]. These properties make FPRL1 the most promiscuous formyl peptide receptor, and more generally, G-protein coupled receptor (GPCR), able to elicit different cell responses, with inflammation as the common feature.

## 2.2. FPRs: G-Protein Coupled Receptors

FPRs belong to the family of G-protein coupled receptors (GPCRs), the largest class of cell surface seven-transmembrane proteins. Conventionally, GPCRs are located on the cell surface. However, they can also be expressed in the cell nucleus [46]. Recent studies have demonstrated the nuclear localization of FPRL1 in cancer cell lines [46], providing a further element confirming the versatility of this receptor.

More than 3% of the human genome encodes 800 GPCRs, mainly involved in regulating physiological processes by responding to endogenous ligands, such as hormones, neurotransmitters, chemokines, and calcium ions, or to exogenous ligands, such as odorant molecules and light photons [47,48]. Like hormones and neurotransmitter receptors, GPCRs regulate the communication between the inside and outside of the cells [49], transducing the extracellular signals in cellular response.

GPCRs are coupled to heterotrimeric G proteins, consisting of  $G\alpha$ ,  $G\beta$ , and  $G\gamma$  subunits, which initiate the downstream signaling associated with the receptor. Ligand binding stimulates GPCR conformational change and the activation of the heterotrimeric G proteins, resulting in guanosine triphosphate (GTP)-bound  $G\alpha$  and  $G\beta$ - $\gamma$  subunit dissociation. In the active state, G proteins activate specific enzymes, which in turn generate second messengers, leading to cellular response [50].

Chemotaxis are a common cellular response initiated by GPCRs, expressed on chemotactic cells. This subfamily of G protein-coupled receptors plays an important role in sensing chemoattractant molecules [51], coordinating cell migration at the damaged site, and initiation of the immune response.

N-formylated peptides are one of the first identified chemotactic stimuli [14], exhibiting high affinity for G protein-coupled receptors [51]. This has been demonstrated by the observation that the pertussis toxin inhibits formyl peptide-induced chemotaxis, altering their binding affinity for the receptor [52]. More specifically, the pertussis toxin acts by inducing ADP-ribosylation of the  $\alpha$  subunit of a  $G_i$ -heterotrimeric G protein [53], affecting the molecular shifts responsible for the cell signal translation pathway and specifically inhibiting cell migration.

Based on this evidence, FPRs are  $G_i$  protein-coupled receptors—belonging to the  $\gamma$ -group of rhodopsin-like receptors—able [54] to recognize the presence of bacteria or host cell damage and promote the immune response by activating the chemotaxis.

## 2.3. N-Formylated Peptides: Signal Peptides Detected by FPRs

The capability to distinguish between self and non-self is fundamental for the wellness of the host. The immune system has the essential role of initiating a defensive response against pathogens, by detecting microbial chemical elements: pathogen-associated molecular patterns (PAMPs). Bacterial signal peptides represent an important class of PAMPs, responsible for innate immune system activation by interacting with specific pattern recognition receptors (PRRs). They play a critical role in nascent protein translocation from the cytoplasm to other sites inside or outside the cell [55,56].

**Table 1.** Distribution and roles of formyl peptide receptors (FPRs; FPR1, formyl peptide receptor-like (FPRL)1, and FPRL2) in innate, adaptative, and non-immune cells. The table also reports the formyl peptide receptor expression in organs or tissues, or where it is not well-defined.

	Cells/Tissues	Formyl Peptide Receptors	Role	References
Innate Immune Cell Expression	Neutrophils	FPR1, FPRL1	Chemotaxis, phagocytosis, superoxide generation	[16,21,22]
	Natural killer cells	FPR1, FPRL1	Interferon $\gamma$ production	[16,23]
	Immature dendritic cells	FPR1, FPRL2	Chemotaxis	[15,21,22]
	Mature dendritic cells	FPRL2	Chemotaxis	[15,21,22]
	Monocytes	FPR1, FPRL1, FPRL2	Chemotaxis, pro-inflammatory activity	[16]
	Macrophages	FPR1, FPRL1, FPRL2	Chemotaxis, pro-inflammatory activity	[16]
Adaptative Immune Cell Expression	Naïve CD4 T cells (CD3+, CD4+, CD45RA+, CD45RO−, CCR7+)	FPRL1	Interferon- $\gamma$ production	[16,17]
	Th1 cells	FPRL1	–	[16,17]
	Th2	FPRL1	–	[16,17]
	Th17	FPRL1	–	[16,17]
Non-Immune Cells, Organ/Tissue Expression	Epithelial cells	FPRL1	Chemotaxis	[18,24]
	Endothelial cells	FPRL1	Chemotaxis, angiogenesis, and cell proliferation	[25]
	Microglial cells	FPRL1, FPRL2	Inflammation and neurogenerative activity	[18,26]
	Keratinocytes	FPRL1	Cell proliferation and pro-inflammatory activity	[27]
	Fibroblasts	FPRL1	Chemotaxis and innate immune response stimulation	[28]
	Astrocytes	FPRL1	Inflammation and neurogenerative activity	[18,26]
	Hepatocytes	FPRL1	Chemotaxis, angiogenesis	[18,29]
	Intestinal epithelial cells	FPR1, FPRL1	Cell proliferation, inflammation, and tumorigenesis	[30]
	Brain	FPRL1	Inflammation and neurodegenerative activity	[16–18]
	Spleen	FPRL1, FPRL2	Innate immune response	[16–18]
	Placenta	FPRL1, FPRL2	Innate immune response	[16–18]
	Lung	FPRL1, FPRL2	Innate immune response	[16–18]
	Testis	FPRL1	Innate immune response	[16–18]
	Trachea	FPRL2	Innate immune response	[16–18]
	Lymph nodes	FPRL2	Innate immune response	[16–18]

**Table 2.** Formyl peptide receptor (FPR1, FPRL1, and FPRL2) representative ligands. The table summarizes the main differently derived formylated or non-formylated FPR ligands, indicating the origin, selectivity, and general intracellular signaling.

Classification	Ligand	Origin	Signaling	Selectivity	References
Formylated Bacterial Peptides	f-MLF	<i>E. coli</i>	Ca <sup>++</sup> mobilization, superoxide generation	FPR1	[14]
	f-MKNFKG	<i>Bacillus</i>	Ca <sup>++</sup> mobilization, superoxide generation	FPRL1	[31]
	f-MGFIS	<i>Streptococcus</i>	Ca <sup>++</sup> mobilization, superoxide generation	FPR1, FPRL1	[31]
	f-MAMKKL	<i>Salmonella</i>	Ca <sup>++</sup> mobilization, superoxide generation	FPR1	[31]
	f-MVMKFK	<i>Haemophilus</i>	Ca <sup>++</sup> mobilization, superoxide generation	FPR1, FPRL1	[31]
	f-MFIYCK	<i>Staphylococcus</i>	Ca <sup>++</sup> mobilization, superoxide generation	FPR1	[31]
	f-MKKIML	<i>Listeria</i>	Ca <sup>++</sup> mobilization, superoxide generation	FPR1, FPRL1	[31]
Formylated Mitochondria Peptides	f-MKKNLV	<i>Clostridium</i>	Ca <sup>++</sup> mobilization, superoxide generation	FPRL1	[31]
	f-MMYALF	Mitochondrion	Superoxide generation	FPRL1	[32]
	f-MLKIV	Mitochondrion	Ca <sup>++</sup> mobilization, ERK activation	FPRL1	[32]
	f-MYFINLTL	Mitochondrion	Ca <sup>++</sup> mobilization, ERK activation	FPRL1	[32]
	f-MFADRW	Mitochondrion	Ca <sup>++</sup> mobilization, ERKs activation	FPRL1	[32]
Microbe-Derived Non-Formylated Peptides	Mitocryptide-2	Mitochondrion	Ca <sup>++</sup> mobilization, ERK activation	FPRL1	[33]
	Hp(2-20)	<i>Helicobacter pylori</i>	Superoxide generation, cell proliferation, Akt and STAT3 activation, VEGFA secretion	FPRL1	[34]
	OC43 Coronavirus protein	OC43 Coronavirus	Unknown	Not clear	[35]
	229E Coronavirus protein	229E Coronavirus	Unknown	Not clear	[35]
	NL36 Coronavirus protein	NL36 Coronavirus	Unknown	Not clear	[35]
	spike protein	Ebola virus	Unknown	Not clear	[35]
	T20/DP178	HIV gp41	Ca <sup>++</sup> mobilization	FPR1	[20]
	T21/DP107	HIV gp41	Ca <sup>++</sup> mobilization	FPR1, FPRL1	[20]
	V3 peptide	HIV gp120	Ca <sup>++</sup> mobilization, CCR5 desensitization	FPRL1	[36]
	N36 peptide	HIV gp41	Ca <sup>++</sup> mobilization, chemokine receptorsn desensitization, NF-kB activation	FPRL1	[37]
	gG-2p20	Herpes simplex virus	Superoxide generation, NADPH oxidase activation, apoptosis	FPR1	[38]
	C5a HCV peptide	Hepatitis C virus	Ca <sup>++</sup> mobilization, degranulation, superoxide generation, MAPK activation	FPRL1	[39]
Host-Derived Molecules	Annexin 1	Host	ERK phosphorylation, NF-kB pathway	FPRL1	[40]
	Lipoxin-A4	Host	Ca <sup>++</sup> mobilization, ERKs, PI3K, Akt phosphorylation	FPRL1	[41]
	SAA	Host	Ca <sup>++</sup> mobilization, ERKs, JNK and p38MAPK activation, cytokine release, NF-kB and COX2 induction	FPRL1	[42]
	Aβ-42	host	PI3K/Akt pathway activation	FPRL1	[26]
	LL-37	host	Ca <sup>++</sup> mobilization, Bcl-xL expression, caspase-3 inhibition, MAPK and JAK/STAT signaling	FPRL1	[43]
Synthetic Peptides	WKYMVm	synthetic	Ca <sup>++</sup> mobilization, NADPH oxidase activation, ERK phosphorylation, MAPK and JNK activation, PKC activation	FPRL1	[44]

Table 2. Cont.

Classification	Ligand	Origin	Signaling	Selectivity	References
Synthetic Molecules	Quinazolinones	Synthetic	Ca <sup>++</sup> mobilization, ERK activation	FPRL1	[45]
	Benzimidazoles	Synthetic	Ca <sup>++</sup> mobilization	FPR1	[45]
	Pyrazolones	Synthetic	Ca <sup>++</sup> mobilization, desensitization of chemokine receptors	FPRL1	[45]
	Pyridazin-3(2H)-ones	Synthetic	Ca <sup>++</sup> mobilization	FPR1	[45]
	Chiral pyridazines	Synthetic	Ca <sup>++</sup> mobilization	FPRL1, FPRL1	[45]
	N-phenylureas	Synthetic	Ca <sup>++</sup> mobilization	FPRL1	[45]

ERK: extracellular signal-regulated kinase; Akt: protein kinase B; STAT3: signal transducer and activator of transcription 3; NADPH: nicotinamide adenine dinucleotide phosphate; VEGF: vascular endothelial growth factor; Aβ-42: β amyloid protein 42; JNK: c-Jun N-terminal kinase; PKC: protein kinase C; COX2: cyclooxygenase-2; PI3K: phosphoinositide 3-kinase; SAA: serum amyloid protein A; CCR5: C-C chemokine receptor 5; JAK: Janus kinase; MAPK: mitogen-activated protein kinase; NF-kB: nuclear factor κB.

Signal peptides at the N-terminal of the newly synthesized proteins are recognized by specific particles responsible for locating the proteins at the correct site. After translocation, signal peptides are removed by specific enzymes and the mature protein is released [56,57]. Prokaryotic and eukaryotic signal peptides present three highly conserved domains, containing the correct information for protein translocation and removal: an N-terminal region, starting with a methionine, a hydrophobic core, and a C-terminal region [58]. However, all prokaryotes start the protein synthesis with an N-formyl methionine [59], resulting in the fact that bacterial signal peptides are “N-formylated peptides”. Mitochondria, as bacterial ancestry [60], also initiate proteins synthesis with a formylated methionine, revealing that, besides bacteria, damaged host cells also release N-formylated peptides as damage-associated molecular patterns (DAMPs) [61].

These peptides thus represent a host danger signal, which induces innate immunity activation via specific pattern recognition receptors, corresponding to formyl peptide receptors—named according to their high affinity for N-formylated peptides.

#### 2.4. More Than N-Formylated Peptides: Other Ligands Detected by FPRL1

FPRs were originally discovered as receptors with high binding affinity for bacteria or mitochondria N-formylated peptides. In addition to N-formyl-methionine-leucyl-phenylalanine (fMLF), the prototype for N-formylated peptides [18,21], a variety of structurally different ligands have been shown to interact with formyl peptide receptors.

Compared to FPR1, FPRL1 exhibits a lower affinity for formylated peptides. On the contrary, FPRL1 shows the greatest ligand promiscuity, also detecting non-formylated peptides, synthetic molecules, and the eicosanoid Lipoxin A4 (LXA4) [20]. WKYMV is a synthetic, non-formylated peptide recognized by FPRL1. Figure 1 shows the interaction between FPRL1 and WKYMV, displaying the FPRL1 binding site. According to the nature of its ligand, FPRL1 modifies its conformation and consequently its biological function, eliciting a pro- or anti-inflammatory response. In addition, anti-inflammatory ligands may cause receptor homodimerization or heterodimerization with other FPRs, resulting in the activation of the pro-resolving pathway p38/MAPKAPK/Hsp27/IL10, and in the resolution of the inflammation [20,62,63]. The ability of FPRL1 to bind ligands, mediating opposite biological effects, makes it a potential target to control inflammation and inflammatory-associated diseases.

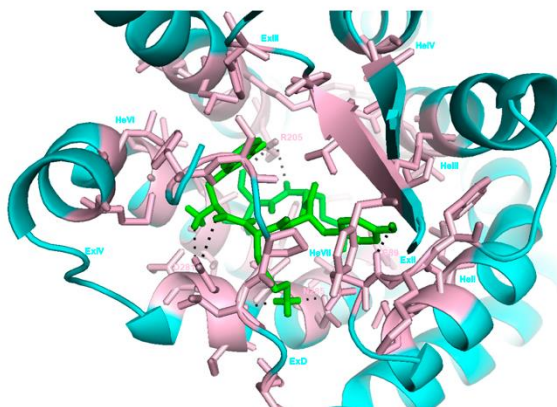


**Figure 1.** Schematic representation of the synthetic peptide WKYMV binding pocket for FPRL1. The receptor is shown in cartoon representation colored in cyan, while the ligand is shown in sticks colored in green. The amino acids of the binding site are represented in sticks colored in light pink. WKYMV forms hydrophobic interactions with the amino acids of the extracellular domain (ExD); II, III, IV, VI, VII transmembrane portions (He); II, III, IV extracellular portions (Ex); and hydrogen bonds with E89 (ExII), R205 (ExIII), D281, and N285 (ExIV). PyMOL Molecular Graphic System (Version 1.3 Shrodinger, LLC) was used to represent the WKYMV–FPRL1 interaction (PDBcode: 6LW5).

### 3. Formyl Peptide Receptors in *Helicobacter pylori* Chronic Infection

#### 3.1. *Helicobacter pylori* and Chronic Inflammatory Response

*Helicobacter pylori* is a Gram-negative bacterium colonizing the gastric mucosa of over 50% of the population worldwide [64]. The bacterium colonizes the stomach and infects gastric epithelial cells, promoting chronic inflammation, leading to chronic gastritis, which can eventually degenerate in peptic ulcer and then gastric carcinoma [65]. Several studies have reported the relationship between *H. pylori* infection and gastric cancer, classifying the bacterium as the primary cause of gastric carcinoma [66]. Our recent work demonstrates the capability of *H. pylori* to interfere also with biological processes outside the stomach, contributing to the development of neurodegenerative diseases, such as Alzheimer, or metabolic pathologies (type 2 diabetes, obesity, and cardiovascular diseases) [67]. Although the mechanisms responsible for the extra-gastric manifestations of *H. pylori* remain unclear, a plausible explanation may reside in the *H. pylori*-associated, low-grade inflammatory state. Therefore, the clinical outcome of *H. pylori* infection is related to the severity of the inflammatory response, influenced by both host characteristics and bacterial virulence factors [65].

*H. pylori* utilizes various virulence factors responsible for its pathogenicity by inducing different pathways, resulting in cytokine and chemokine release, as well as the production of oxygen/nitrogen species (ROS/RNS) and growth factors [68]. These factors—especially in chronic conditions—contribute to tissue damage and severe disease progression.

Lipopolysaccharide (LPS), peptidoglycan, and the cytotoxic-associated gene A (CagA) are the most studied *H. pylori* pathogenicity factors [68,69]. The gene *CagA* encodes the cytotoxic protein CagA, whose intracellular signaling results in the activation of inflammatory genes and in the modification of the cell scaffold, thus promoting neoplastic transformation [70]. LPS and peptidoglycan instead are directly involved in the bacterium's

adhesion to the gastric epithelium [64]. As these structures are unique to the pathogen, known as pathogen-associated molecular patterns (PAMPs), they are recognized by pattern recognition receptors (PRRs) displayed by eukaryotic cells. Specifically, Toll-like receptor 4 (TLR4) binds LPS, while peptidoglycan is recognized by gastric cells through nucleotide oligomerization domain 1 (NOD1) [68].

FPRs are one of the most relevant class of PRRs. They play an important role in *H. pylori* infection by interacting with Hp(2-20), an *H. pylori*-released, non-formylated peptide with the greatest affinity for formyl peptide receptor like-1. Hp(2-20) is a chemotactic factor [34], contributing to *Helicobacter pylori*-induced gastric inflammation [71,72].

### 3.2. *Helicobacter pylori* Hp(2-20) Modulated the Host Immune Response by Interacting with FPRL1

Hp(2-20) is a cecropin-like peptide released during *H. pylori* growth and possessing different functional characteristics. As an antimicrobial peptide (AMP), Hp(2-20) plays an important role in *H. pylori* gastric mucosa persistence by acting as bactericidal molecule [73], thus conferring an advantage over other microorganisms. Moreover, it orchestrates the host inflammatory response by interacting with FPRs [34]. When *H. pylori* colonizes the human stomach, the epithelial cells of the gastric mucosa represent the first component of the innate immune response to be encountered [74]. Hp(2-20) participates to activate the innate immune response by interacting with the FPRL1 expressed on epithelial gastric cells. In particular, the interaction between Hp(2-20) and FPRL1 favors *H. pylori* gastric mucosa inflammation [71] by initiating a cell signaling cascade, which leads to cytokine release, the recruitment of inflammatory cells, and stimulation of NADPH oxidase-dependent superoxide generation [75]. This bacterial peptide also stimulates gastric epithelial cell migration and proliferation, and increases the expression level of vascular endothelial growth factor (VEGF), whose role is to restore the gastric mucosa after induced injury [7,34]. These events, if contained, favor the host defense and the restoration of the homeostasis. However, in the case of *H. pylori* infection, the inflammatory response is sustained and exacerbated, thus resulting in the worsening of the clinical outcome due to the onset of severe gastric and extra-gastric diseases [67,76]. Interestingly, despite the massive inflammatory response, *Helicobacter pylori* has developed several strategies to manipulate the host immune system and persist within the gastric mucosa. *H. pylori* is able to both send and integrate signals from the gastric epithelium, allowing the host and bacteria to become linked in a dynamic equilibrium [77]. The long-term persistence of *H. pylori* promotes a permanent and low-grade inflammation, which is a risk factor for severe diseases, including cancer.

Given this scenario, Hp(2-20) has a critical role in the pathological processes associated with *H. pylori* infection by its interaction with FPRL1.

### 3.3. Hp(2-20) and FPRL1: Intracellular Signalling Cascade

In addition to G-protein coupled receptors, after ligand binding, FPRs undergo a conformational change that makes them able to interact with the heterotrimeric G protein. Upon activation, the G protein  $\alpha$  subunit exchanges guanosine diphosphate (GDP) with guanosine triphosphate (GTP) and dissociates from  $\beta$ - $\gamma$  subunits [78], leading to phospholipase C $\beta$  (PLC $\beta$ ) and phosphoinositide 3-kinase activation (PI3K $\gamma$ ) [22]. Both phospholipase C $\beta$  and phosphoinositide 3-kinase mediate signaling events associated with different cellular responses, such as chemotaxis, reactive oxygen species (ROS) generation, and degranulation.

Phospholipase C $\beta$  hydrolyzes phosphatidylinositol 4,5-bisphosphate (PIP2) in diacylglycerol (DAG)—which remains at the membrane level—and inositol trisphosphate (IP3). This latter moves to the endoplasmic reticulum, regulating Ca<sup>++</sup> release and increasing cytosolic Ca<sup>++</sup> levels. In addition, both of the second messengers activate protein kinase C (PKC), resulting in NADPH oxidase activation and ROS production [78].

Phosphoinositide 3-kinase, instead, mediates the conversion of phosphatidylinositol 4,5-bisphosphate (PIP2) in phosphatidylinositol 3,4,5-trisphosphate (PIP3), which in turn



activates protein kinase C (PKC). Furthermore, PI3K $\gamma$  activates protein kinase B (Akt) [79], directly involved in regulating the transcriptional activity of the nuclear factor  $\kappa$ B (NF- $\kappa$ B). Other intracellular effectors in the formyl peptide receptors signaling cascade include phospholipase A2 and D, mitogen-activated protein kinase (MAPK), extracellular signal-regulated kinase (ERK)1/2, c-Jun N-terminal kinase (JNK), and p38 [21,80,81].

The Hp(2-20)–FPRL1-induced signaling pathway promotes the activation of p42/44 MAPK (ERK), Akt, and signal transducer and activator of transcription (STAT) 3 [75,82], all mediators with a central role in the host defense against an injury. Akt and ERK induce the activation of the transcriptional nuclear factor  $\kappa$ B (NF- $\kappa$ B) [83,84], which plays a critical role in innate immunity as the primary regulator of inflammatory response by activating cytokine genes and the inflammasome [85]. Signal transducer and activator of transcription (STAT) 3 also has important immunomodulatory properties. However, chronic activation of STAT3, due to the *H. pylori* persistence, can degenerate in chronic inflammation and severe associated diseases [86]. Furthermore, several studies have shown the common involvement of the MAPK/ERK pathway in cancer progression [87]. Taken together, these traits make Hp(2-20) and formyl peptide receptor-like 1 critical players in *H. pylori* infection (Figure 2).

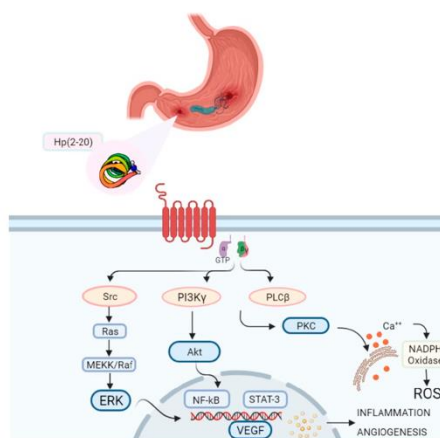


**Figure 2.** Schematic signalling pathway of Hp(2-20)-activated FPRL1. FPRL1 participates in the pathogenesis of *H. pylori* infection by interacting with Hp(2-20). During Hp(2-20) binding, the G protein  $\alpha$  subunit exchanges guanosine diphosphate (GDP) with guanosine triphosphate (GTP) and dissociates from  $\beta$ - $\gamma$  subunits. This activates various signal transduction events, resulting in oxidative stress, cell migration, inflammation, cell proliferation, and angiogenesis. These events, which are chronically induced, may lead to severe gastric diseases, including cancer. Abbreviations: Akt: protein kinase B; ERK: extracellular signal-regulated kinase; GTP: guanosine triphosphate; MEKK: mitogen-activated protein kinase kinase; NF- $\kappa$ B: nuclear factor  $\kappa$ B; PI3K $\gamma$ : phosphoinositide 3-kinase gamma; PLC $\beta$ : phospholipase C $\beta$ ; PKC: protein Kinase C; ROS: reactive oxygen species; STAT3: signal transducer and activator of transcription 3; VEGF: vascular endothelial growth factor.

Shortly, despite the role of Hp(2-20) in modulating the immune response against *H. pylori* infection, the chronic stimulation of FPRL1 induced by bacterium persistence

activates intracellular responses, resulting in exacerbation of the inflammatory process, thus contributing to the clinical outcome of the infection.

#### 4. Conclusions and Future Perspectives

The FPR family is one of the most important class of cell surface receptors, playing important roles in innate immunity and host defense by mediating key events during the inflammatory response. Nevertheless, detrimental effects can result from FPR activation. In recent years, several studies have demonstrated the link between FPR activation and the pathogenesis of inflammatory diseases, including cancer [13].

*Helicobacter pylori* infection represents the most frequent cause of gastric carcinoma. It colonizes and infects gastric epithelial cells by promoting chronic inflammation, leading to severe site-specific diseases [88]. In this context, FPRs—specifically FPRL1—play a critical role by interacting with the *H. pylori*-derived peptide Hp(2-20).

The activation of FPRL1 by Hp(2-20) triggers epithelial cell migration, proliferation, and angiogenesis. Thus, chronic stimulation of FPRL1 by Hp(2-20), resulting in persistent low grade inflammation, makes these functions harmful and Hp(2-20) a recognized risk factor, not only for *H. pylori*-associated gastric cancer [89], but also for other chronic inflammatory-related diseases [90].

Based on these considerations, FPR inhibition could represent a promising therapeutic strategy for treating various chronic inflammatory pathologies. Of particular interest is FPRL1, expressed by a variety of cells and tissues and able to bind a broad range of structurally different ligands, exerting pro- or anti-inflammatory actions. Thus, FPRL1 represents a potential target to inhibit inflammatory responses by using agonists with anti-inflammatory properties or antagonists.

This drew attention in searching novel natural molecules able to antagonize FPRL1 or elicit anti-inflammatory responses, paving the way for the discovery of new drugs for the treatment of inflammatory diseases.

Such an approach could also be extended to inflammatory disorders associated with viral infections. Our predictive studies (data not shown) indicate that FPRL1—showing an effective interaction with various coronavirus peptides—could also contribute to the coronavirus disease (COVID)-19 pathogenesis.

**Author Contributions:** Conceptualization, R.C. writing—original draft preparation, P.C.; writing—review and editing, C.M.; visualization, M.P. All authors have read and agreed to the published version of the manuscript.

**Funding:** This research received no external funding.

**Institutional Review Board Statement:** Not applicable.

**Informed Consent Statement:** Not applicable.

**Data Availability Statement:** Not applicable.

**Conflicts of Interest:** The authors declare no conflict of interest.

#### References

1. Yatim, K.M.; Lakkis, E.G. A brief journey through the immune system. *Clin. J. Am. Soc. Nephrol.* **2015**, *10*, 1274–1281. [\[CrossRef\]](#)
2. Mogensen, T.H. Pathogen recognition and inflammatory signaling in innate immune defenses. *Clin. Microbiol. Rev.* **2009**, *22*, 240–273. [\[CrossRef\]](#) [\[PubMed\]](#)
3. Basset, C.; Holton, J.; O'Mahony, R.; Roitt, I. Innate immunity and pathogen-host interaction. *Vaccine* **2003**, *21*, S12–S23. [\[CrossRef\]](#)
4. Marshall, J.S.; Warrington, R.; Watson, W.; Kim, H.L. An introduction to immunology and immunopathology. *Allergy Asthma Clin. Immunol.* **2018**, *14*, 1–10. [\[CrossRef\]](#) [\[PubMed\]](#)
5. Leoni, G.; Neumann, P.A.; Sumagin, R.; Denning, T.L.; Nusrat, A. Wound repair: Role of immune-epithelial interactions. *Mucosal Immunol.* **2015**, *8*, 959–968. [\[CrossRef\]](#)
6. Holmgren, J.; Czerkinsky, C. Mucosal immunity and vaccines. *Nat. Med.* **2005**, *11*, S45. [\[CrossRef\]](#)
7. Jeong, Y.S.; Bae, Y.S. Formyl peptide receptors in the mucosal immune system. *Exp. Mol. Med.* **2020**, *52*, 1694–1704. [\[CrossRef\]](#)
8. Medzhitov, R. Recognition of microorganisms and activation of the immune response. *Nature* **2007**, *449*, 819–826. [\[CrossRef\]](#)



9. Filep, J.G.; Sekheri, M.; El Kebir, D. Targeting formyl peptide receptors to facilitate the resolution of inflammation. *Eur. J. Pharmacol.* **2018**, *833*, 339–348. [\[CrossRef\]](#)
10. Barton, G.M. A calculated response: Control of inflammation by the innate immune system. *J. Clin. Investig.* **2008**, *118*, 413. [\[CrossRef\]](#)
11. Xiao, T.S. Innate immunity and inflammation. *Cell. Mol. Immunol.* **2017**, *14*, 1–3. [\[CrossRef\]](#)
12. Zhong, J.; Shi, G. Editorial: Regulation of Inflammation in Chronic Disease. *Front. Immunol.* **2019**, *10*, 737. [\[CrossRef\]](#)
13. Weiß, E.; Kretschmer, D. Formyl-Peptide Receptors in Infection, Inflammation, and Cancer. *Trends Immunol.* **2018**, *39*, 815–829. [\[CrossRef\]](#)
14. Ye, R.D.; Boulay, F.; Ji, M.W.; Dahlgren, C.; Gerard, C.; Parmentier, M.; Serhan, C.N.; Murphy, P.M. International union of basic and clinical pharmacology. LXXIII. Nomenclature for the formyl peptide receptor (FPR) family. *Pharmacol. Rev.* **2009**, *61*, 119–161. [\[CrossRef\]](#) [\[PubMed\]](#)
15. Kang, H.K.; Lee, H.-Y.; Kim, M.-K.; Park, K.S.; Park, Y.M.; Kwak, J.-Y.; Bae, Y.-S. The Synthetic Peptide Trp-Lys-Tyr-Met-Val-D-Met Inhibits Human Monocyte-Derived Dendritic Cell Maturation via Formyl Peptide Receptor and Formyl Peptide Receptor-Like 2. *J. Immunol.* **2005**, *175*, 685–692. [\[CrossRef\]](#) [\[PubMed\]](#)
16. Lee, H.Y.; Lee, M.; Bae, Y.-S. Formyl Peptide Receptors in Cellular Differentiation and Inflammatory Diseases. *J. Cell. Biochem.* **2017**, *118*, 1300–1307. [\[CrossRef\]](#) [\[PubMed\]](#)
17. Chen, K.; Bao, Z.; Gong, W.; Tang, P.; Yoshimura, T.; Wang, J.M. Regulation of inflammation by members of the formyl-peptide receptor family. *J. Autoimmun.* **2017**, *85*, 64–77. [\[CrossRef\]](#) [\[PubMed\]](#)
18. Migeotte, I.; Communi, D.; Parmentier, M. Formyl peptide receptors: A promiscuous subfamily of G protein-coupled receptors controlling immune responses. *Cytokine Growth Factor Rev.* **2006**, *17*, 501–519. [\[CrossRef\]](#)
19. He, H.-Q.; Ye, R. The Formyl Peptide Receptors: Diversity of Ligands and Mechanism for Recognition. *Molecules* **2017**, *22*, 455. [\[CrossRef\]](#)
20. Krepel, S.A.; Wang, J.M. Chemotactic Ligands that Activate G-Protein-Coupled Formylpeptide Receptors. *Int. J. Mol. Sci.* **2019**, *20*, 3426. [\[CrossRef\]](#)
21. Le, Y.; Murphy, P.M.; Wang, J.M. Formyl-peptide receptors revisited. *Trends Immunol.* **2002**, *23*, 541–548. [\[CrossRef\]](#)
22. Le, Y.; Oppenheim, J.J.; Wang, J.M. Pleiotropic roles of formyl peptide receptors. *Cytokine Growth Factor Rev.* **2001**, *12*, 91–105. [\[CrossRef\]](#)
23. Kim, S.D.; Kim, J.M.; Jo, S.H.; Lee, H.Y.; Lee, S.Y.; Shim, J.W.; Seo, S.-K.; Yun, J.; Bae, Y.-S. Functional Expression of Formyl Peptide Receptor Family in Human NK Cells. *J. Immunol.* **2009**, *183*, 5511–5517. [\[CrossRef\]](#) [\[PubMed\]](#)
24. Kim, M.K.; Min, D.S.; Park, Y.J.; Kim, J.H.; Ryu, S.H.; Bae, Y.S. Expression and functional role of formyl peptide receptor in human bone marrow-derived mesenchymal stem cells. *FEBS Lett.* **2007**, *581*, 1917–1922. [\[CrossRef\]](#)
25. Heo, S.C.; Kwon, Y.W.; Jang, I.H.; Jeong, G.O.; Yoon, J.W.; Kim, C.D.; Kwon, S.M.; Bae, Y.S.; Kim, J.H. WKYMVm-induced activation of formyl peptide receptor 2 stimulates ischemic neovasculation by promoting homing of endothelial colony-forming cells. *Stem Cells* **2014**, *32*, 779–790. [\[CrossRef\]](#) [\[PubMed\]](#)
26. Schröder, N.; Schaffrath, A.; Welter, J.A.; Putzka, T.; Griep, A.; Ziegler, P.; Brandt, E.; Samer, S.; Heneka, M.T.; Kaddatz, H.; et al. Inhibition of formyl peptide receptors improves the outcome in a mouse model of Alzheimer disease. *J. Neuroinflamm.* **2020**, *17*, 131. [\[CrossRef\]](#) [\[PubMed\]](#)
27. Yu, N.; Zhang, S.; Lu, J.; Li, Y.; Yi, X.; Tang, L.; Su, L.; Ding, Y. Serum amyloid A, an acute phase protein, stimulates proliferative and proinflammatory responses of keratinocytes. *Cell Prolif.* **2017**, *50*. [\[CrossRef\]](#)
28. VanCompernelle, S.E.; Clark, K.L.; Rummel, K.A.; Todd, S.C. Expression and Function of Formyl Peptide Receptors on Human Fibroblast Cells. *J. Immunol.* **2003**, *171*, 2050–2056. [\[CrossRef\]](#)
29. McCoy, R.; Haviland, D.L.; Molmenti, E.P.; Ziambaras, T.; Wetsel, R.A.; Perlmutter, D.H. N-formylpeptide and complement C5a receptors are expressed in liver cells and mediate hepatic acute phase gene regulation. *J. Exp. Med.* **1995**, *182*, 207–217. [\[CrossRef\]](#)
30. Chen, K.; Liu, M.; Liu, Y.; Yoshimura, T.; Shen, W.; Le, Y.; Durum, S.; Gong, W.; Wang, C.; Gao, J.L.; et al. Formylpeptide receptor-2 contributes to colonic epithelial homeostasis, inflammation, and tumorigenesis. *J. Clin. Investig.* **2013**, *123*, 1694–1704. [\[CrossRef\]](#)
31. Bufe, B.; Schumann, T.; Kappel, R.; Bogeski, I.; Kummerow, C.; Podgórska, M.; Smola, S.; Hoth, M.; Zufall, F. Recognition of bacterial signal peptides by mammalian formyl peptide receptors: A new mechanism for sensing pathogens. *J. Biol. Chem.* **2015**, *290*, 7369–7387. [\[CrossRef\]](#) [\[PubMed\]](#)
32. Wencelau, C.F.; Szasz, T.; McCarthy, C.G.; Baban, B.; NeSmith, E.; Webb, R.C. Mitochondrial N-formyl peptides cause airway contraction and lung neutrophil infiltration via formyl peptide receptor activation. *Pulm. Pharmacol. Ther.* **2016**, *37*, 49–56. [\[CrossRef\]](#) [\[PubMed\]](#)
33. Lind, S.; Gabl, M.; Holdfeldt, A.; Mårtensson, J.; Sundqvist, M.; Nishino, K.; Dahlgren, C.; Mukai, H.; Forsman, H. Identification of Residues Critical for FPR2 Activation by the Cryptic Peptide Mitocryptide-2 Originating from the Mitochondrial DNA-Encoded Cytochrome b. *J. Immunol.* **2019**, *202*, 2710–2719. [\[CrossRef\]](#) [\[PubMed\]](#)
34. de Paulis, A.; Prevete, N.; Rossi, F.W.; Rivellese, F.; Salerno, F.; Delfino, G.; Liccardo, B.; Avilla, E.; Montuori, N.; Mascolo, M.; et al. Helicobacter pylori Hp(2–20) Promotes Migration and Proliferation of Gastric Epithelial Cells by Interacting with Formyl Peptide Receptors In Vitro and Accelerates Gastric Mucosal Healing In Vivo. *J. Immunol.* **2009**, *183*, 3761–3769. [\[CrossRef\]](#) [\[PubMed\]](#)
35. Mills, J.S. Peptides derived from HIV-1, HIV-2, Ebola virus, SARS coronavirus and coronavirus 229E exhibit high affinity binding to the formyl peptide receptor. *Biochim. Biophys. Acta Mol. Basis Dis.* **2006**, *1762*, 693–703. [\[CrossRef\]](#)

36. Shen, W.; Proost, P.; Li, B.; Gong, W.; Le, Y.; Sargeant, R.; Murphy, P.M.; Van Damme, J.; Wang, J.M. Activation of the chemotactic peptide receptor FPRL1 in monocytes phosphorylates the chemokine receptor CCR5 and attenuates cell responses to selected chemokines. *Biochem. Biophys. Res. Commun.* **2000**, *272*, 276–283. [\[CrossRef\]](#)
37. Le, Y.; Jiang, S.; Hu, J.; Gong, W.; Su, S.; Dunlop, N.M.; Shen, W.; Li, B.; Wang, J.M. N36, a synthetic N-terminal heptad repeat domain of the HIV-1 envelope protein gp41, is an activator of human phagocytes. *Clin. Immunol.* **2000**, *96*, 236–242. [\[CrossRef\]](#)
38. Bellner, L.; Thorén, F.; Nygren, E.; Liljeqvist, J.-Å.; Karlsson, A.; Eriksson, K. A Proinflammatory Peptide from Herpes Simplex Virus Type 2 Glycoprotein G Affects Neutrophil, Monocyte, and NK Cell Functions. *J. Immunol.* **2005**, *174*, 2235–2241. [\[CrossRef\]](#)
39. Lin, Q.; Fang, D.; Hou, X.; Le, Y.; Fang, J.; Wen, F.; Gong, W.; Chen, K.; Wang, J.M.; Su, S.B. HCV Peptide (C5A), an Amphipathic  $\alpha$ -Helical Peptide of Hepatitis Virus C, Is an Activator of N-Formyl Peptide Receptor in Human Phagocytes. *J. Immunol.* **2011**, *186*, 2087–2094. [\[CrossRef\]](#)
40. Hebeda, C.B.; Sandri, S.; Benis, C.M.; de Paula-Silva, M.; Loiola, R.A.; Reutelingsperger, C.; Perretti, M.; Farsky, S.H.P. Annexin A1/Formyl Peptide Receptor Pathway Controls Uterine Receptivity to the Blastocyst. *Cells* **2020**, *9*, 1188. [\[CrossRef\]](#)
41. Guo, Z.; Hu, Q.; Xu, L.; Guo, Z.N.; Ou, Y.; He, Y.; Yin, C.; Sun, X.; Tang, J.; Zhang, J.H. Lipoxin A4 Reduces Inflammation Through Formyl Peptide Receptor 2/p38 MAPK Signaling Pathway in Subarachnoid Hemorrhage Rats. *Stroke* **2016**, *47*, 490–497. [\[CrossRef\]](#)
42. Hinrichs, B.H.; Matthews, J.D.; Siuda, D.; O’Leary, M.N.; Wolfarth, A.A.; Saeedi, B.J.; Nusrat, A.; Neish, A.S. Serum Amyloid A1 Is an Epithelial Prorestitutive Factor. *Am. J. Pathol.* **2018**, *188*, 937–949. [\[CrossRef\]](#)
43. Kim, S.-H.; Kim, Y.N.; Jang, Y.-S. Cutting Edge: LL-37-Mediated Formyl Peptide Receptor-2 Signaling in Follicular Dendritic Cells Contributes to B Cell Activation in Peyer’s Patch Germinal Centers. *J. Immunol.* **2016**, *198*, 629–633. [\[CrossRef\]](#)
44. Christophe, T.; Karlsson, A.; Dugave, C.; Rabiet, M.J.; Boulay, F.; Dahlgren, C. The Synthetic Peptide Trp-Lys-Tyr-Met-Val-Met-NH2 Specifically Activates Neutrophils through FPRL1/Lipoxin A4 Receptors and is an Agonist for the Orphan Monocyte-expressed Chemoattractant Receptor FPRL2. *J. Biol. Chem.* **2001**, *276*, 21585–21593. [\[CrossRef\]](#) [\[PubMed\]](#)
45. Schepetkin, I.A.; Khlebnikov, A.I.; Giovannoni, M.P.; Kirpotina, L.N.; Cilibrizzi, A.; Quinn, M.T. Development of Small Molecule Non-peptide Formyl Peptide Receptor (FPR) Ligands and Molecular Modeling of Their Recognition. *Curr. Med. Chem.* **2014**, *21*, 1478–1504. [\[CrossRef\]](#)
46. Cattaneo, F.; Parisi, M.; Fioretti, T.; Sarnataro, D.; Esposito, G.; Ammendola, R. Nuclear localization of Formyl-Peptide Receptor 2 in human cancer cells. *Arch. Biochem. Biophys.* **2016**, *603*, 10–19. [\[CrossRef\]](#) [\[PubMed\]](#)
47. Pierce, K.L.; Premont, R.T.; Lefkowitz, R.J. Seven-transmembrane receptors. *Nat. Rev. Mol. Cell Biol.* **2002**, *3*, 639–650. [\[CrossRef\]](#)
48. Wang, X.; Iyer, A.; Lyons, A.B.; Körner, H.; Wei, W. Emerging roles for G-protein coupled receptors in development and activation of macrophages. *Front. Immunol.* **2019**, *10*, 2031. [\[CrossRef\]](#) [\[PubMed\]](#)
49. Rosenbaum, D.M.; Rasmussen, S.G.F.; Kobilka, B.K. The structure and function of G-protein-coupled receptors. *Nature* **2009**, *459*, 356–363. [\[CrossRef\]](#)
50. Cattaneo, F.; Guerra, G.; Parisi, M.; De Marinis, M.; Tafuri, D.; Cinelli, M.; Ammendola, R. Cell-Surface Receptors Transactivation Mediated by G Protein-Coupled Receptors. *Int. J. Mol. Sci.* **2014**, *15*, 19700–19728. [\[CrossRef\]](#)
51. Sun, L.; Ye, R.D. Role of G protein-coupled receptors in inflammation. *Acta Pharmacol. Sin.* **2012**, *33*, 342–350. [\[CrossRef\]](#) [\[PubMed\]](#)
52. Gilder, A.S.; Wang, L.; Natali, L.; Karimi-Mostowfi, N.; Brifault, C.; Gonias, S.L. Pertussis toxin is a robust and selective inhibitor of high grade glioma cell migration and invasion. *PLoS ONE* **2016**, *11*, e0168418. [\[CrossRef\]](#) [\[PubMed\]](#)
53. Locht, C.; Coutte, L.; Mielcarek, N. The ins and outs of pertussis toxin. *FEBS J.* **2011**, *278*, 4668–4682. [\[CrossRef\]](#) [\[PubMed\]](#)
54. Zhuang, Y.; Liu, H.; Zhou, X.E.; Verma, R.K.; de Waal, P.W.; Jang, W.; Xu, T.H.; Wang, L.; Meng, X.; Zhao, G.; et al. Structure of formylpeptide receptor 2-Gi complex reveals insights into ligand recognition and signaling. *Nat. Commun.* **2020**, *11*, 1–12. [\[CrossRef\]](#)
55. Ivankov, D.N.; Payne, S.H.; Galperin, M.Y.; Bonissone, S.; Pevzner, P.A.; Frishman, D. How many signal peptides are there in bacteria? *Environ. Microbiol.* **2013**, *15*, 983–990. [\[CrossRef\]](#)
56. Bufer, B.; Zufall, F. The sensing of bacteria: Emerging principles for the detection of signal sequences by formyl peptide receptors. *Biomol. Concepts* **2016**, *7*, 205–214. [\[CrossRef\]](#)
57. Tjalsma, H.; Bolhuis, A.; Jongbloed, J.D.H.; Bron, S.; van Dijk, J.M. Signal Peptide-Dependent Protein Transport in *Bacillus subtilis*: A Genome-Based Survey of the Secretome. *Microbiol. Mol. Biol. Rev.* **2000**, *64*, 515–547. [\[CrossRef\]](#)
58. Von Heijne, G. Analysis of the distribution of charged residues in the N-terminal region of signal sequences: Implications for protein export in prokaryotic and eukaryotic cells. *EMBO J.* **1984**, *3*, 2315–2318. [\[CrossRef\]](#)
59. Piatkov, K.I.; Vu, T.T.M.; Hwang, C.-S.; Varshavsky, A. Formyl-methionine as a degradation signal at the N-termini of bacterial proteins. *Microb. Cell* **2015**, *2*, 376. [\[CrossRef\]](#)
60. Meyer, A.; Laverny, G.; Bernardi, L.; Charles, A.L.; Alsaleh, G.; Pottecher, J.; Sibilia, J.; Geny, B. Mitochondria: An organelle of bacterial origin controlling inflammation. *Front. Immunol.* **2018**, *9*, 536. [\[CrossRef\]](#)
61. Zhang, Q.; Raoof, M.; Chen, Y.; Sumi, Y.; Sursal, T.; Junger, W.; Brohi, K.; Itagaki, K.; Hauser, C.J. Circulating mitochondrial DAMPs cause inflammatory responses to injury. *Nature* **2010**, *464*, 104–107. [\[CrossRef\]](#) [\[PubMed\]](#)
62. Cooray, S.N.; Gobbetti, T.; Montero-Melendez, T.; McArthur, S.; Thompson, D.; Clark, A.J.L.; Flower, R.J.; Perretti, M. Ligand-specific conformational change of the G-protein-coupled receptor ALX/FPR2 determines proresolving functional responses. *Proc. Natl. Acad. Sci. USA* **2013**, *110*, 18232–18237. [\[CrossRef\]](#) [\[PubMed\]](#)

63. Raabe, C.A.; Gröper, J.; Rescher, U. Biased perspectives on formyl peptide receptors. *Biochim. Biophys. Acta Mol. Cell Res.* **2019**, *1866*, 305–316. [\[CrossRef\]](#) [\[PubMed\]](#)
64. Gottesmann, M.; Paraskevopoulou, V.; Mohammed, A.; Falcone, F.H.; Hensel, A. BabA and LPS inhibitors against *Helicobacter pylori*: Pectins and pectin-like rhamnogalacturonans as adhesion blockers. *Appl. Microbiol. Biotechnol.* **2020**, *104*, 351–363. [\[CrossRef\]](#)
65. Cuomo, P.; Papaiani, M.; Fulgione, A.; Guerra, F.; Capparelli, R.; Medaglia, C. An Innovative Approach to Control *H. pylori*-Induced Persistent Inflammation and Colonization. *Microorganisms* **2020**, *8*, 1214. [\[CrossRef\]](#) [\[PubMed\]](#)
66. Polk, D.B.; Peek, R.M. *Helicobacter pylori*: Gastric cancer and beyond. *Nat. Rev. Cancer* **2010**, *10*, 403–414. [\[CrossRef\]](#)
67. Cuomo, P.; Papaiani, M.; Sansone, C.; Iannelli, A.; Iannelli, D.; Medaglia, C.; Paris, D.; Motta, A.; Capparelli, R. An In Vitro Model to Investigate the Role of *Helicobacter pylori* in Type 2 Diabetes, Obesity, Alzheimer's Disease and Cardiometabolic Disease. *Int. J. Mol. Sci.* **2020**, *21*, 8369. [\[CrossRef\]](#)
68. Lamb, A.; Chen, L.F. Role of the *Helicobacter pylori*-Induced inflammatory response in the development of gastric cancer. *J. Cell. Biochem.* **2013**, *114*, 491–497. [\[CrossRef\]](#)
69. Jimenez-Soto, L.F.; Haas, R. The CagA toxin of *Helicobacter pylori*: Abundant production but relatively low amount translocated. *Sci. Rep.* **2016**, *6*, 1–7. [\[CrossRef\]](#)
70. Hatakeyama, M. Structure and function of *Helicobacter pylori* cagA, the first-identified bacterial protein involved in human cancer. *Proc. Jpn. Acad. Ser. B Phys. Biol. Sci.* **2017**, *93*, 196–219. [\[CrossRef\]](#)
71. Bylund, J.; Christophe, T.; Boulay, F.; Nyström, T.; Karlsson, A.; Dahlgren, C. Proinflammatory activity of a cecropin-like antibacterial peptide from *Helicobacter pylori*. *Antimicrob. Agents Chemother.* **2001**, *45*, 1700–1704. [\[CrossRef\]](#) [\[PubMed\]](#)
72. de Paulis, A.; Prevete, N.; Fiorentino, I.; Walls, A.F.; Curto, M.; Petraroli, A.; Castaldo, V.; Ceppa, P.; Fiocca, R.; Marone, G. Basophils Infiltrate Human Gastric Mucosa at Sites of *Helicobacter pylori* Infection, and Exhibit Chemotaxis in Response to *H. pylori*-derived Peptide Hp(2–20). *J. Immunol.* **2004**, *172*, 7734–7743. [\[CrossRef\]](#)
73. Capparelli, R.; De Chiara, F.; Nocerino, N.; Montella, R.C.; Iannaccone, M.; Fulgione, A.; Romanelli, A.; Avitabile, C.; Blaiotta, G.; Capuano, F. New perspectives for natural antimicrobial peptides: Application as antiinflammatory drugs in a murine model. *BMC Immunol.* **2012**, *13*, 61. [\[CrossRef\]](#) [\[PubMed\]](#)
74. Peek, R.M.; Fiske, C.; Wilson, K.T. Role of innate immunity in *Helicobacter pylori*-induced gastric malignancy. *Physiol. Rev.* **2010**, *90*, 831–858. [\[CrossRef\]](#) [\[PubMed\]](#)
75. Cattaneo, F.; Parisi, M.; Ammendola, R. Distinct Signaling Cascades Elicited by Different Formyl Peptide Receptor 2 (FPR2) Agonists. *Int. J. Mol. Sci.* **2013**, *14*, 7193–7230. [\[CrossRef\]](#) [\[PubMed\]](#)
76. Contaldi, F.; Capuano, F.; Fulgione, A.; Cigliano, R.A.; Sanseverino, W.; Iannelli, D.; Medaglia, C.; Capparelli, R. The hypothesis that *Helicobacter pylori* predisposes to Alzheimer's disease is biologically plausible. *Sci. Rep.* **2017**, *7*, 7817. [\[CrossRef\]](#)
77. Blaser, M.J.; Kirschner, D. The equilibria that allow bacterial persistence in human hosts. *Nature* **2007**, *449*, 843–849. [\[CrossRef\]](#)
78. Dorward, D.A.; Lucas, C.D.; Chapman, G.B.; Haslett, C.; Dhaliwal, K.; Rossi, A.G. The role of formylated peptides and formyl peptide receptor 1 in governing neutrophil function during acute inflammation. *Am. J. Pathol.* **2015**, *185*, 1172–1184. [\[CrossRef\]](#)
79. Zhang, L.; Wang, G.; Chen, X.; Xue, X.; Guo, Q.; Liu, M.; Zhao, J. Formyl peptide receptors promotes neural differentiation in mouse neural stem cells by ROS generation and regulation of PI3K/AKT signaling. *Sci. Rep.* **2017**, *7*, 1–16. [\[CrossRef\]](#)
80. Bae, Y.S.; Song, J.Y.; Kim, Y.; He, R.; Ye, R.D.; Kwak, J.Y.; Suh, P.G.; Ryu, S.H. Differential activation of formyl peptide receptor signaling by peptide ligands. *Mol. Pharmacol.* **2003**, *64*, 841–847. [\[CrossRef\]](#)
81. Cattaneo, F.; Russo, R.; Castaldo, M.; Chambery, A.; Zollo, C.; Esposito, G.; Pedone, P.V.; Ammendola, R. Phosphoproteomic analysis sheds light on intracellular signaling cascades triggered by Formyl-Peptide Receptor 2. *Sci. Rep.* **2019**, *9*, 1–16. [\[CrossRef\]](#)
82. Rossi, F.W.; Prevete, N.; Montuori, N.; Ragno, P.; Selleri, C.; Marone, G.; de Paulis, A. Hp(2–20) peptide of *Helicobacter pylori* and the innate immune receptors: Specific role(s) of the formyl peptide receptors. *Le Infezioni Medicina* **2012**, *20* (Suppl. S2), 19–25.
83. Bai, D.; Ueno, L.; Vogt, P.K. Akt-mediated regulation of NF- $\kappa$ B and the essentialness of NF- $\kappa$ B for the oncogenicity of PI3K and Akt. *Int. J. Cancer* **2009**, *125*, 2863–2870. [\[CrossRef\]](#)
84. Seo, J.H.; Lim, J.W.; Kim, H. Differential Role of ERK and p38 on NF- $\kappa$ B Activation in *Helicobacter pylori*-Infected Gastric Epithelial Cells. *J. Cancer Prev.* **2013**, *18*, 346–350. [\[CrossRef\]](#)
85. Liu, T.; Zhang, L.; Joo, D.; Sun, S.C. NF- $\kappa$ B signaling in inflammation. *Signal. Transduct. Target. Ther.* **2017**, *2*, 1–9. [\[CrossRef\]](#)
86. Kasembeli, M.; Bharadwaj, U.; Robinson, P.; Tweardy, D. Contribution of STAT3 to Inflammatory and Fibrotic Diseases and Prospects for its Targeting for Treatment. *Int. J. Mol. Sci.* **2018**, *19*, 2299. [\[CrossRef\]](#) [\[PubMed\]](#)
87. Reddy, K.B.; Nabha, S.M.; Atanaskova, N. Role of MAP kinase in tumor progression and invasion. *Cancer Metastasis Rev.* **2003**, *22*, 395–403. [\[CrossRef\]](#) [\[PubMed\]](#)
88. Crowe, S.E. *Helicobacter* infection, chronic inflammation, and the development of malignancy. *Curr. Opin. Gastroenterol.* **2005**, *21*, 32–38. [\[PubMed\]](#)
89. Hou, X.L.; Ji, C.D.; Tang, J.; Wang, Y.; Wang, Y.X.; Xiang, D.F.; Li, H.Q.; Liu, W.; Liu, W.W.; Wang, J.X.; et al. FPR2 promotes invasion and metastasis of gastric cancer cells and predicts the prognosis of patients. *Sci. Rep.* **2017**, *7*, 1–11. [\[CrossRef\]](#) [\[PubMed\]](#)
90. Capparelli, R.; Iannelli, D. Genetics of Host Protection against *Helicobacter pylori* Infections. *Int. J. Mol. Sci.* **2021**, *22*, 3192. [\[CrossRef\]](#)

## **CHAPTER 3**

***Marine biomolecules: a new challenge for biotechnological applications. The effects of the algal alkaloid Caulerpin in modulating Formyl peptide receptors expression in Helicobacter pylori infection***

### **3.1 Marine natural products**

Both seas and oceans occupy over 70% of the earth's surface and represent the place where life first began. About 80% of all animal species habit the marine environment, often living in extreme conditions. Most of marine organisms have adapted to such conditions producing unique substances, which possess important biological properties (Fenical, 1982; Kim, 2019). This feature, together with the recent advancement of science and technology in improving marine biotechnology, stimulated great interest in marine ecosystem research, as a sustainable and attractive source of molecules with significant benefits for human health (Rotter et al., 2021).

### **3.2 Green algae: source of bioactive secondary metabolites**

Secondary metabolites are natural products generally produced by plants, fungi, bacteria and marine organisms (Vaishnav and Demain, 2011). Among numerous marine life forms, green algae provide the most extensive library of structurally different and biologically active secondary metabolites, which have found biotechnological utilization in pharmaceutical, nutraceutical and cosmetics industry (Costa et al., 2010; Shah et al., 2020; Souza et al., 2020). A surprisingly wide range of terpenes, alkaloids, polyphenols and steroids have been identified in marine green algae (Shah et al., 2020). These compounds are not essential for the growth and development of the organism producing them (Vaishnav and Demain, 2011). Their synthesis is strongly influenced by both biotic and abiotic stresses (Said et al., 2011) and serve to survive interspecies competition; provide defensive mechanisms; and assist reproductive processes (Vaishnav and Demain, 2011), suggesting their critical role in the phenomenon of marine biological invasion. Thus, investigation of secondary metabolites might provide information for understanding the activity of the algal invasive species and their abundance and distribution. Moreover, it allows to develop strategies to prevent or reduce detrimental effects of non-indigenous species.

### 3.2.1 Caulerpin: green algal secondary metabolite

Nowadays, the introduction of non-indigenous or alien species is a serious global threat (Chan and Briski, 2017). It represents one of the most important causes of changes in biodiversity and ecosystem, showing detrimental ecological and socio-economic effects (Del Coco et al., 2018).

*Caulerpa cylindracea* is a green macroalga (Figure 1) native to the SouthWestern Australia, which has shown high invasive potential, with severe impact on the Mediterranean Sea (Del Coco et al., 2018; Máximo et al., 2018).

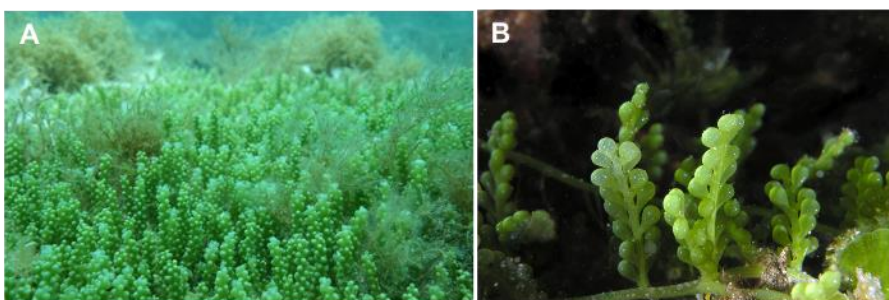


**Figure 1. (A)** *Caulerpa cylindracea* invading the Mediterranean Sea. **(B)** Zoom on the green alga.

Recent studies suggest that secondary metabolites derived from *Caulerpa cylindracea* exert significant antioxidant effects, explaining its invasive properties (Cavas and Yurdakoc, 2005). When two or more species compete for the same resources, they develop different strategies to prevail and survive to stress conditions (Choo et al., 2004). Algae respond to such conditions by producing a large amount of reactive oxygen species (ROS). However, uncontrolled production of ROS may become detrimental for the same species that produce them (Cavas and Yurdakoc, 2005), thus requiring antioxidant elements.

Caulerpin is one of the major *Caulerpa cylindracea* secondary metabolites, showing antioxidant properties. Therefore, it is directly involved in ensuring algal survival in a non-native habitat, contributing to replace native species, alter essential ecological processes and change the original community structure (Gorbi et al., 2014).



It is well known that antioxidants play key roles in preventing oxidative stress-induced diseases, suggesting the potential use of Caulerpin as therapeutic agents, further supported by recent demonstrations that Caulerpin possesses anti-inflammatory, antiviral, antibiotic and antitumoral properties (Vairappan, 2004; de Souza et al., 2009; Macedo et al., 2012; Mehra et al., 2019; Shah et al., 2020).

Given this scenario, the isolation of Caulerpin from the producing alga and the biotechnological and pharmaceutical exploitation, according to a recycling program, could contribute to reduce the impact of the invasion, favoring the recovery of beneficial substances for human health (Mollo et al., 2008). Finally, a combination of chemical and biological studies in a chemoecological approach might offer the opportunity to explore all factors affecting marine biological invasion and provide a promising biotechnological tool for the management of biological invasions (Mollo et al., 2008).

### **3.3 Biotechnological applications of Caulerpin as potential FPRs antagonist**

Formyl peptide receptors (FPRs) activation stimulates signal transduction pathways responsible for multiple functions, including cell migration and proliferation, reactive oxygen species generation and intracellular calcium release, which contribute to the inflammatory response associated with bacterial infections (Ye et al., 2009). In addition, activation of these signal pathways is responsible for biochemical responses which may promote severe tissue damages, contributing to chronic inflammatory diseases. Therefore, strategies inhibiting FPRs could represent a promising clinical approach.

In the effort to individuate novel relevant compounds able to inhibit the FPRs-signaling cascade, the library of molecules of the ICB-CNR (Pozzuoli, Na) was screened. Among the wide range of natural products available, Caulerpin seemed the most suitable. Criteria responsible for selecting Caulerpin as potential candidate were:

- the possibility to exploit undesired biomaterial, such as the invasive *Caulerpa cylindracea*, to obtain sustainable and bioactive chemicals and reduce detrimental effects of biological invasion.

- Anti-inflammatory and antioxidant properties.
- Low toxicity (de Souza et al., 2009).
- The attractive chemical structure (Figure 2).

Caulerpin is a bis-indole alkaloid characterized by two indole nuclei between an eight-member ring, which contains two carbonyl groups (Figure 2).

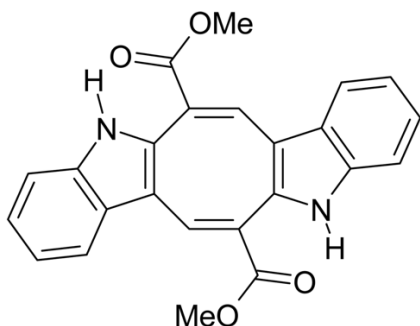


**Figure 2.** Chemical structure of Caulerpin.

Bis or tris-indole alkaloids are known to present unique properties which make them promising compounds for the development of new drugs (Gupta et al., 2007). Furthermore, indole derivatives are related to the metabolism of the amino acid tryptophane, whose rich peptides are recognized to be potent FPRs antagonists (Bae et al., 2004). Based on these considerations, Caulerpin was selected to be tested as potential antagonist of FPR2.



## References

- Bae, Y.S.; Lee, H.Y.; Jo, E.J.; Kim, J.I.; Kang, H.K.; Ye, R.D.; Kwak, J.Y.; Ryu, S.H. Identification of peptides that antagonize formyl peptide receptor-like 1-mediated signaling. *J Immunol.* **2004**; 173(1):607-14.
- Cavas, L.; Yurdakoc, K. A comparative study: assessment of the antioxidant system in the invasive green alga *Caulerpa racemosa* and some macrophytes from the Mediterranean. *J. Exp. Mar. Biol. Ecol.* **2005**; 321, 35–41.
- Chan, F.T.; Briski, E. An overview of recent research in marine biological invasions. *Mar Biol.* **2017**;164(6):121.
- Choo, K.; Snoeijs, P.; Pedersén, M. Oxidative stress tolerance in the filamentous green algae *Cladophora glomerata* and *Enteromorpha ahlneriana*. *J. Exp. Mar. Biol. Ecol.* **2004**; 298:111-123.
- Costa, L.S.; Fidelis, G.P.; Cordeiro, S.L.; Oliveira, R.M.; Sabry, D.A.; Câmara, R.B.G.; Nobre, L.T.D.B.; Costa, M.S.S.P.; Almeida-Lima, J.; Farias, E.H.C.; et al. Biological activities of sulfated polysaccharides from tropical seaweeds. *Biomed. Pharmacother.* **2010**, 64, 21–28.
- de Souza, É.T.; De Lira, D.P.; De Queiroz, A.C.; Da Silva, D.J.C.; De Aquino, A.B.; Campessato Mella, E.A.; Lorenzo, V.P.; De Miranda, G.E.C.; De Araújo-Júnior, J.X.; De Oliveira Chaves, M.C.; et al. The antinociceptive and anti-inflammatory activities of caulerpin, a bisindole alkaloid isolated from seaweeds of the genus *Caulerpa*. *Mar. Drugs.* **2009**; 7:689–704.
- Del Coco, L.; Felling, S.; Girelli, C.R.; Angilè, F.; Magliozzi, L.; Almada, F.; D'Aniello, B.; Mollo, E.; Terlizzi, A.; Fanizzi, F.P. <sup>1</sup>H NMR Spectroscopy and MVA to Evaluate the Effects of Caulerpin-Based Diet on *Diplodus sargus* Lipid Profiles. *Mar Drugs.* **2018**; 16(10):390.
- Fenical, W. Natural Products Chemistry in the Marine Environment. *Science.* **1982**; 215(4535):923.
- Gorbi, S.; Giuliani, M.E.; Pittura, L.; d'Errico, G.; Terlizzi, A.; Felling, S.; Grauso, L.; Mollo, E.; Cutignano, A.; Regoli, F. Could molecular effects of *Caulerpa racemosa* metabolites modulate the impact on fish populations of *Diplodus sargus*? *Mar Environ Res.* **2014**; 96:2-11.
- Gupta, L.; Talwar, A.; Chauhan, P.M. Bis and tris indole alkaloids from marine organisms: new leads for drug discovery. *Curr Med Chem.* **2007**;14(16):1789-803.
- Kim, S-K. Essential of Marine Biotechnology. *Springer, Cham.* **2019**; p. v.
- Macedo, N.R.P.V.; Ribeiro, M.S.; Villaça, R.C.; Ferreira, W.; Pinto, A.M.; Teixeira, V.L.; Cirne-Santos, C.; Paixão, I.C.N.P.; Giongo, V. Caulerpin as a potential antiviral drug against herpes simplex virus type 1. *Braz. J. Pharmacogn.* **2012**; 22:861–867.
- Máximo, P.; Ferreira, L.M.; Branco, P.; Lima, P.; Lourenço, A. Secondary Metabolites and Biological Activity of Invasive Macroalgae of Southern Europe. *Mar Drugs.* **2018**; 16(8):265.

- Mehra, R.; Bhushan, S.; Bast, F.; Singh, S. Marine macroalga *Caulerpa*: Role of its metabolites in modulating cancer signaling. *Mol. Biol. Rep.* **2019**; 46: 3545–3555.
- Mollo, E.; Gavagnin, M.; Carbone, M.; Castelluccio, F.; Pozzone, F.; Roussis, V.; Templado, J.; Ghiselin, M.T.; Cimino, G. Factors promoting marine invasions: a chemoecological approach. *Proc Natl Acad Sci U S A.* **2008**; 105(12):4582-6.
- Rotter, A.; Barbier, M.; Bertoni, F.; Bones, A.M.; Cancela, M.L.; Carlsoon, J.; Carvalho, M.F.; Ceglowska, M.; Chirivella-Martorell, J.; Dalay, M.C., et al. The Essentials of Marine Biotechnology. *Front. Mar. Sci.* **2021**; 8:629629.
- Said, S.A.; Fernandez, C.; Greff, S.; Torre, F.; Derridj, A.; Gauquelin, T.; Mevy, J.P. Inter-population variability of terpenoid composition in leaves of *Pistacia lentiscus* L. from Algeria: a chemoecological approach. *Molecules.* **2011**; 16(3):2646-57.
- Shah, S.A.A.; Hassan, S.S.U.; Bungau, S.; Si, Y.; Xu, H.; Rahman, M.H.; Behl, T.; Gitea, D.; Pavel, F.M.; Corb Aron, R.A., et al. Chemically Diverse and Biologically Active Secondary Metabolites from Marine Phylum chlorophyta. *Mar Drugs.* **2020**; 18(10):493.
- Souza, C.R.M.; Bezerra, W.P.; Souto, J.T. Marine Alkaloids with Anti-Inflammatory Activity: Current Knowledge and Future Perspectives. *Mar Drugs.* **2020**; 18(3):147.
- Vairappan, C.S. Antibacterial activity of major secondary metabolites found in four species of edible green macroalgae genus *Caulerpa*. *Asian J. Microbiol. Biotechnol. Environ. Sci.* **2004**; 6:197–201.
- Vaishnav, P.; Demain, A.L. Unexpected applications of secondary metabolites. *Biotechnol Adv.* **2011**; 29(2):223-9.
- Ye, R.D.; Boulay, F.; Wang, J.M.; Dahlgren, C.; Gerard, C.; Parmentier, M.; Serhan, C.N.; Murphy, P.M. International Union of Basic and Clinical Pharmacology. LXXIII. Nomenclature for the formyl peptide receptor (FPR) family. *Pharmacol Rev.* **2009**; 61(2):119-61.

## 3.4 Caulerpin Mitigates *Helicobacter pylori* - Induced Inflammation via Formyl Peptide Receptors



International Journal of  
Molecular Sciences



Article

### Caulerpin Mitigates *Helicobacter pylori*-Induced Inflammation via Formyl Peptide Receptors

Paola Cuomo <sup>1</sup>, Chiara Medaglia <sup>2</sup>, Ivana Allocca <sup>1</sup>, Angela Michela Immacolata Montone <sup>3</sup>, Fabrizia Guerra <sup>4</sup>, Serena Cabaro <sup>5</sup>, Ernesto Mollo <sup>6</sup>, Daniela Eletto <sup>7</sup>, Marina Papaiani <sup>1</sup> and Rosanna Capparelli <sup>8,\*</sup>

<sup>1</sup> Department of Agriculture, University of Naples Federico II, 80055 Naples, Italy; paola.cuomo@unina.it (P.C.); iv.allocca@gmail.com (I.A.); marina.papaiani@unina.it (M.P.)

<sup>2</sup> Department of Microbiology and Molecular Medicine, University of Geneva, Rue Michel-Servet 1, 1206 Geneva, Switzerland; chiara.medaglia@unige.ch

<sup>3</sup> Department of Food Inspection, Istituto Zooprofilattico Sperimentale del Mezzogiorno, 80055 Naples, Italy; angela.montone@izsmportici.it

<sup>4</sup> Department of Pharmacy, University of Naples Federico II, 80131 Naples, Italy; fabrizia.guerra@unina.it

<sup>5</sup> Department of Translational Medicine, University of Naples Federico II, 80131 Naples, Italy; serena.cabaro@unina.it

<sup>6</sup> National Research Council of Italy, Institute of Biomolecular Chemistry, 80078 Naples, Italy; emollo@icb.cnr.it

<sup>7</sup> Department of Pharmacy, University of Salerno, Via Giovanni Paolo II 132, 84084 Salerno, Italy; daeletto@unisa.it

<sup>8</sup> Task Force Microbioma, Department of Agriculture, University of Naples Federico II, 80055 Naples, Italy  
\* Correspondence: capparelli@unina.it



**Citation:** Cuomo, P.; Medaglia, C.; Allocca, I.; Montone, A.M.I.; Guerra, F.; Cabaro, S.; Mollo, E.; Eletto, D.; Papaiani, M.; Capparelli, R. Caulerpin Mitigates *Helicobacter pylori*-Induced Inflammation via Formyl Peptide Receptors. *Int. J. Mol. Sci.* **2021**, *22*, 13154. <https://doi.org/10.3390/ijms222313154>

Academic Editor: Monica Curro

Received: 20 October 2021

Accepted: 3 December 2021

Published: 5 December 2021

**Publisher's Note:** MDPI stays neutral with regard to jurisdictional claims in published maps and institutional affiliations.



**Copyright:** © 2021 by the authors. Licensee MDPI, Basel, Switzerland. This article is an open access article distributed under the terms and conditions of the Creative Commons Attribution (CC BY) license (<https://creativecommons.org/licenses/by/4.0/>).

**Abstract:** The identification of novel strategies to control *Helicobacter pylori* (Hp)-associated chronic inflammation is, at present, a considerable challenge. Here, we attempt to combat this issue by modulating the innate immune response, targeting formyl peptide receptors (FPRs), G-protein coupled receptors that play key roles in both the regulation and the resolution of the innate inflammatory response. Specifically, we investigated, in vitro, whether Caulerpin—a bis-indole alkaloid isolated from algae of the genus *Caulerpa*—could act as a molecular antagonist scaffold of FPRs. We showed that Caulerpin significantly reduces the immune response against Hp culture filtrate, by reverting the FPR2-related signaling cascade and thus counteracting the inflammatory reaction triggered by Hp peptide Hp(2–20). Our study suggests Caulerpin to be a promising therapeutic or adjuvant agent for the attenuation of inflammation triggered by Hp infection, as well as its related adverse clinical outcomes.

**Keywords:** *Helicobacter pylori*; formyl peptide receptors; inflammation; bis-indole structure

#### 1. Introduction

*Helicobacter pylori* (*H. pylori*) is a Gram-negative bacterium colonizing the gastric mucosa of over 50% of the humans worldwide [1]. Despite the fact that the infection is often asymptomatic, *H. pylori* represents one of the primary causes of gastric cancer, contributing to 75% of all gastric cancer cases [2,3]. While remaining a local pathogen, *H. pylori* may exert systemic effects and contribute to the occurrence of clinical extra-gastric manifestations. *H. pylori* infection, in fact, has been reported to increase the risk of iron deficiency anemia, as well as neurological, cardiovascular, dermatological and metabolic disorders [4–7]. The clinical outcomes of *H. pylori* infection depend on the complex relationship between host and bacterium [8,9]. The bacterium virulence, the host response, together with environmental factors contribute to the ability of *H. pylori* to colonize the harsh gastric environment over a long period, thus promoting long-term inflammation, a key feature for the development of severe gastric or extra-gastric diseases [10].

Inflammation is a defensive response triggered by the host innate immune system, in order to survive during an infection or an injury, favoring a return to homeostasis [11–13].

However, when prolonged, inflammation may cause more damage to the host than the pathogen [14], inducing intracellular metabolic changes and epigenetics modifications [15]. The immune system coordinates the inflammatory response through innate receptors, also known as pattern recognition receptors (PRRs), able to recognize highly conserved microbial structures [16].

Formyl peptide receptors (FPRs) are pattern recognition receptors (PRRs) belonging to the family of G<sub>i</sub>-protein coupled receptors, comprising FPR1, FPR2 and FPR3 [17,18]. Even though the nature of the evolutionary process responsible for FPRs' differentiation is poorly understood, it is clear that it originates from a common ancestor and that they acquire functional differences through gene duplication and natural selection [19]. As PRRs, FPRs trigger cellular defense mechanisms, by sensing pathogen associated molecular patterns (PAMPs) [20]. Consequently, they play a critical role in host defense as well as in the regulation of inflammatory processes by participating in the pathogenesis of inflammatory disorders [21,22]. FPRs can detect both bacteria and host mitochondria-derived formylated peptides. In addition, FPRs, and specifically FPR2, can respond to a large variety of structurally different ligands, including not-formylated peptides.

Hp(2–20) is a *H. pylori*-derived not-formylated peptide [23]. More specifically, it is a cecropin-like peptide [23] showing broad-spectrum antimicrobial properties, which provide a competitive advantage over other microorganisms, thus facilitating *H. pylori* persistence in gastric mucosa [24]. Furthermore, as an exogenous ligand of FPR2, Hp(2–20) possesses pro-inflammatory activities [25], by initiating a cell-signaling cascade resulting in chemiotaxis, cytokines release and NADPH oxidase-dependent superoxide generation [23,26]. Both the antimicrobial, and the pro-inflammatory activity of Hp(2–20), makes it a significant *H. pylori* virulence factor, contributing to the pathogenesis of *H. pylori* infection and related chronic diseases. Importantly, by functioning in a ligand-specific manner, Hp(2–20) has been recognized as one of the primary risk factor for the development and progression of *H. pylori*-associated gastric cancer [23,27]. Given this scenario, FPRs play an important role in the severity of *H. pylori* infection, thus representing a potential target to control *H. pylori*-induced chronic inflammation and the associated risks.

The recent return to traditional medicine and natural drugs has increased the interest in marine natural products with potential pharmacological activity. Moreover, the current problem of marine biological invasion and their resulting biological, economic and social impact [28] have prompted the investigation of the biological activities of the natural products present in some of the most invasive species. In particular, *Caulerpa cylindracea*, a green macroalga native to South Western Australia and invasive in the Mediterranean Sea, has been found to contain high levels of the bis-indole alkaloid Caulerpin (Cau), showing anti-inflammatory and antioxidant activity [29–31]. The indole nucleus is a promising scaffold for the discovery of new anti-inflammatory and antinociceptive drugs, as it provides suitable ligands for G-protein coupled receptors [32,33].

We investigated, for the first time, whether Cau could exert an anti-inflammatory role in the context of *H. pylori* infection. We found that Cau inhibits FPR2, thus reverting the Hp(2–20)-induced signaling cascade. Our findings suggest a prospective therapeutic application of Cau as an adjuvant to control *H. pylori*-associated chronic inflammation and to prevent its related adverse effects. Nevertheless, based on the key role of FPRs in inflammatory disorders and of indole nucleus as “privileged structure” in drug discovery, Cau could represent a potential competitive alternative to classical anti-inflammatory approaches by preventing long-term inflammatory damage.

## 2. Results

### 2.1. The Effect of Cau on Cell Viability

First, we evaluated the effect of Cau on the metabolic activity of AGS gastric adenocarcinoma epithelial cells, using an MTT (3-(4,5-dimethylthiazol-2-yl)-5-(2,4-diphenyltetrazolium bromide) solution) assay. AGS cells were cultured with different concentrations of Cau (spanning from 1.6  $\mu$ M to 405  $\mu$ M) for 24 h. As shown in Figure 1, Cau was not toxic up to

45  $\mu\text{M}$ , since cell viability was higher than 80% compared to the untreated control. More specifically, we determined  $\text{CC}_{50}$  and observed that the concentration of Cau that caused a 50% decrease of cell viability was 61.20  $\mu\text{M}$ .

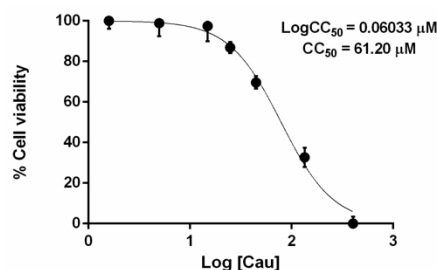


**Figure 1.** Effect of Cau on AGS cell viability. AGS cells were cultured with different concentrations of Cau for 24 h. Results were obtained by combining three independent experiments and represented as mean  $\pm$  SD compared to control cells (100% viability).

## 2.2. Cau Reverses the Pro-Inflammatory Action of Hp(2–20)

Then, we assessed the anti-inflammatory effects of Cau by RT-qPCR, determining whether it could affect the induction of pro-inflammatory cytokines in response to *Helicobacter pylori* culture filtrate (Hpcf) or Hp(2–20). AGS cells were pretreated for 30 min with Cau with or without Hpcf or the *H. pylori* released peptide Hp(2–20), as indicated in Figure 2. Results (Figure 2A) showed that Cau alone does not induce the expression of *IL-6*, *IL-8* and *TNF- $\alpha$*  pro-inflammatory cytokines genes. On the contrary, both Hpcf and Hp(2–20) stimulated the expression of *IL-6*, *IL-8* and *TNF- $\alpha$*  genes, with a higher expression level for Hpcf. Interestingly, cells pretreated with Cau and then cultured with Hpcf or Hp(2–20) displayed a reduced expression level of *IL-6*, *IL-8* and *TNF- $\alpha$* , compared to those not pretreated. Of note, the anti-inflammatory effect of Cau was stronger against Hp(2–20), rather than Hpcf. The data (Figure 2A,B) indicate that Cau exhibits in vitro anti-inflammatory properties. Further confirmation was provided by evaluating I $\kappa$ B- $\alpha$  phosphorylation (pI $\kappa$ B- $\alpha$ ) through Western Blot analysis (Figure 2B). Results showed that Hp(2–20) and Hpcf increased the expression of pI $\kappa$ B- $\alpha$  in AGS cells, and, consistent with the above data, pI $\kappa$ B- $\alpha$  was higher in cells stimulated with Hpcf than Hp(2–20). Conversely, Cau pretreated cells displayed a reduced expression of pI $\kappa$ B- $\alpha$ , compared to those that were untreated and not pretreated (Figure 2B). Notably, the pI $\kappa$ B- $\alpha$  downregulation was higher in Hp(2–20)-stimulated cells than in those stimulated with Hpcf (Figure 2B). The appreciable pro-resolving effect of Cau in presence of the FPRs agonist Hp(2–20), suggests that the anti-inflammatory action of Cau is due to a direct interaction with FPRs. Finally, the demonstrable capability of Cau in inhibiting the expression level of *IL-8* gene (Figure 2A)—widely recognized as chemoattractant cytokine or chemokine—supports the hypothesis that Cau may control chemotaxis and the oxidative burst [34] via FPRs.

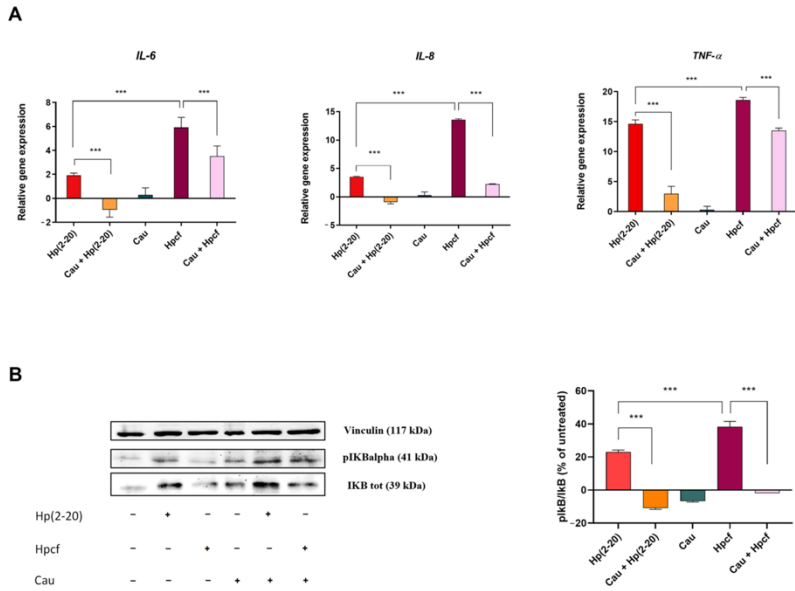


**Figure 2.** Cau significantly decreases the in vitro *H. pylori*-induced inflammatory response. **(A)** Relative gene expression of *IL-6*, *IL-8* and *TNF-α* was determined by quantitative real time PCR (qPCR), performed on RNA isolated from AGS cells cultured with Hp(2-20) 25  $\mu$ M or Hpcf for 2 h and cells pretreated with Cau 15  $\mu$ M and then cultured with Hp(2-20) 25  $\mu$ M or Hpcf for 2 h. All samples were normalized to GAPDH as the reference housekeeping gene. Furthermore, relative gene expression was normalized to basal activity (untreated control), in order to obtain relative fold expression. **(B)** Western Blot and densitometric analysis of the ratio pIκB-α/IκB-α, compared to control group. The analysis was performed on cell lysate prepared after stimulation with Hp(2-20) or Hpcf for 1 h with or without Cau pretreatment (30 min). Vinculin was used for normalization. Graphs report the results of at least three independent experiments, represented as means  $\pm$  SD. Statistical analysis was performed by GraphPad Prism software, using one-way ANOVA followed by Bonferroni post hoc correction. \*\*\*  $p < 0.0001$ .

### 2.3. The Effect of Cau on Hp(2-20)-Induced Chemotactic Signals

It has been reported that Hp(2-20) promotes the activation of chemotactic factors [35], thus triggering the FPRs downstream signaling pathway. Therefore, we investigated the effect of Cau on Hp(2-20)-induced chemotactic factors, by analyzing the expression profile of chemokine genes in AGS cells through RT-qPCR. As expected, Hp(2-20) induced a significant increase in chemotactic signals (Figure 3), while Cau reduced the expression of chemokine genes, similarly to the FPR2 antagonist WRW4, which we used as a positive control. Based on these findings, Cau, as well as WRW4, was found to inhibit FPR2 and the related signaling pathway. Furthermore, we performed an in vitro scratch assay. As expected, it confirmed the chemotactic activity of Hp(2-20) and interestingly, it revealed the capability of Cau to inhibit Hp(2-20)-induced cell migration (Supplementary Material, Figure S1), validating its potential role as an FPR2 antagonist.

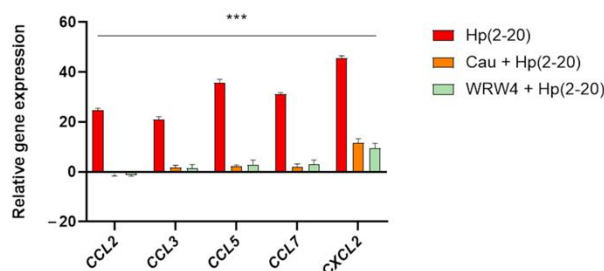


**Figure 3.** Cau attenuates Hp(2–20)-induced chemotactic signals. Relative genes expression of *CCL2*, *CCL3*, *CCL5*, *CLL7* and *CXCL2* was determined by quantitative real time PCR (qPCR), performed on RNA isolated from AGS cells cultured with Hp(2–20) 25  $\mu$ M for 2 h and cells pretreated with Cau 15  $\mu$ M or WRW4 10  $\mu$ M for 30 or 15 min, respectively, and then cultured with Hp(2–20) 25  $\mu$ M for 2 h. All samples were normalized to GAPDH as the reference housekeeping gene. Furthermore, relative gene expression was normalized to basal activity (untreated control), in order to obtain relative fold expression. Graphs report the results of at least three independent experiments, represented as means  $\pm$  SD. Statistical analysis was performed by GraphPad Prisma software, using one-way ANOVA followed by Bonferroni post hoc correction. \*\*\*  $p < 0.0001$  (Hp(2–20) vs. Cau + Hp(2–20) and Hp(2–20) vs. WRW4 + Hp(2–20)).

#### 2.4. Cau Prevents Hp(2–20)-Induced Inflammatory Response in Macrophages

Monocyte-derived macrophage recruitment is an important hallmark during inflammation [36]. According to different stimuli, macrophages change their polarization from M1 (classical activated macrophages) to M2 (alternatively activated macrophages) and vice versa, exhibiting either a pro-inflammatory or anti-inflammatory phenotype, respectively [37]. Previous results (Figures 2A and 3) demonstrated that Hp(2–20)-stimulated cells up-regulated the expression of *CCL2*, *CCL3* and *TNF- $\alpha$*  genes, which are known to induce the macrophage pro-inflammatory phenotype [38,39]. Therefore, we evaluated the production of IL-1 $\beta$  and TNF- $\alpha$ —pro-inflammatory cytokines released by classically activated monocyte-derived macrophages—in THP-1 macrophages, cultured with the conditioned medium from AGS cells stimulated with Hp(2–20) either treated with Cau or left untreated. The THP-1 macrophages were incubated with the AGS conditioned medium for up to 24 h and their medium was collected at different time points, in order to measure the concentration of IL-1 $\beta$  and TNF- $\alpha$  using an ELISA assay, which normalized to the concentration of IL-1 $\beta$  and TNF- $\alpha$  contained in the conditioned medium of AGS cells that were differently stimulated. Figure 4 shows a time-dependent increase in IL-1 $\beta$  and TNF- $\alpha$  cytokines in cells treated with the conditioned medium of AGS stimulated with Hp(2–20) alone, and a marked decrease in the cytokines of cells treated with the conditioned medium of AGS stimulated with Hp(2–20) pretreated with Cau, suggesting the potential role of Cau in affecting the macrophage state.



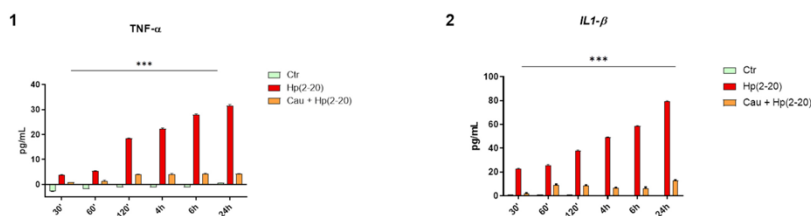


**Figure 4.** Cau prevents AGS-mediated macrophages activation. Cytokines: (1) TNF- $\alpha$  and (2) IL-1 $\beta$  were measured by performing ELISA in macrophages culture medium, collected at different times. Results are expressed as pg of cytokines secreted in mL of macrophages medium, differently treated: (1) conditioned medium of AGS cells cultured with Hp(2-20) 25  $\mu$ M for 24 h; (2) conditioned medium of AGS cells pretreated with Cau 15  $\mu$ M for 30 min and then cultured with Hp(2-20) 25  $\mu$ M for 24 h. Values were normalized to the concentration of the cytokines of the AGS conditioned medium and represent mean  $\pm$  SD of at least three independent experiments, each performed in triplicate. Statistical analysis was performed by GraphPad Prisma software, using one-way ANOVA test followed by Bonferroni post hoc correction. \*\*\*  $p < 0.0001$  (Ctr vs. Hp(2-20) and Hp(2-20) vs. Cau + Hp(2-20)).

#### 2.5. Cau Affects the Hp(2-20)-Induced ROS Production via Mitochondrial and NADPH Oxidase-Dependent Mechanisms

Reactive oxygen species (ROS) play a critical role as microbicidal agents, participating in the initiation, as well as the resolution of the inflammatory process. However, if left uncontrolled, oxidative stress may be one of the primary causes of chronic inflammation and chronic inflammation-associated diseases, including cancer. To determine whether Cau could affect Hp(2-20)-induced ROS production, AGS cells were pretreated with Cau and then stimulated with Hp(2-20), and intracellular ROS production was assessed. As shown in Figure 5, Hp(2-20) increased the ROS production compared to the untreated control, while Cau mitigated this effect. Interestingly, the Cau effect was comparable to the WRW4 response, suggesting that Cau reverses Hp(2-20)-stimulated ROS production by suppressing the FPR2 signaling cascade. Robust evidence has demonstrated that FPRs regulate oxidative burst via NADPH oxidase dependent ROS production [40]. Nevertheless, we also investigated the role of mitochondria in Hp(2-20)-induced ROS generation. Hp(2-20)-stimulated AGS cells were pretreated with rotenone (Rot), which inhibits the mitochondrial electron transport chain [41], causing a significant reduction in ROS production compared to cells stimulated with Hp(2-20) alone (Figure 6A). Rotenone reverted Hp(2-20)-induced ROS production similarly to WRW4. This suggests that mitochondria contribute to Hp(2-20)-induced ROS production. However, we observed that mitochondria-dependent ROS production upon Hp(2-20) stimulation was dose-dependent (Supplementary Material, Figure S3). This was further confirmed by examining the expression level of the mitochondrial antioxidant enzyme encoding gene *SOD2*, which was also found to be up-regulated in Hp(2-20) stimulated cells in a dose dependent manner (Supplementary Material, Figure S3) and importantly, it was found to be down-regulated in Cau pretreated cells (Figure 6B). Therefore, Cau hinders Hp(2-20)-induced ROS production acting on both mitochondria and NADPH oxidase via FPR2.



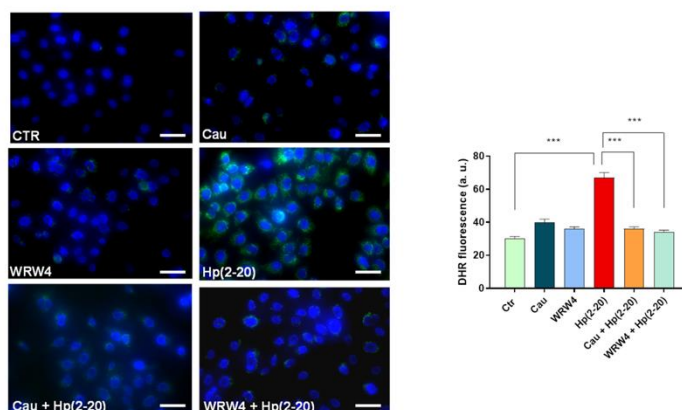


**Figure 5.** Cau moderates FPR2-mediated ROS production. DHR-loaded cells differently treated: (1) control cells; (2) Hp(2–20) 25  $\mu$ M for 1 h; (3) Cau 15  $\mu$ M for 1.5 h; (4) WRW4 10  $\mu$ M for 1.5 h; (5) Cau 15  $\mu$ M for 30 min and Hp(2–20) 25  $\mu$ M for 1 h; (6) WRW4 10  $\mu$ M for 15 min and Hp(2–20) 25  $\mu$ M for 1 h, observed with a fluorescence microscope (on the left, scale bar: 100  $\mu$ m) and quantification of the mean fluorescence of individual cells (on the right). Results are expressed as arbitrary units and represent the mean  $\pm$  SD calculated from three independent experiments, each performed in duplicate. Statistical analysis was performed by GraphPad Prisma software, using one-way ANOVA followed by Bonferroni post hoc correction. \*\*\*  $p < 0.0001$ .

The pro-oxidant effect of Hp(2–20) was verified by evaluating, using RT-qPCR, the expression of the *p53* gene, which plays a central role in protecting cells from genetic insult by sensing cellular redox status [42]. In agreement with this finding, our results showed increased levels of *p53* gene in Hp(2–20) stimulated cells and a significant decrease in Cau pretreated cells (Figure 6C). Interestingly, *p53* mRNA expression was found to decrease in a time-dependent manner in Hp(2–20) stimulated cells, with a marked decrease 6 h post stimulation (Figure 6C). Levels of *p53* are, in fact, tightly regulated in response to an excessive levels of oxidative stress [43], as induced by the concentration of Hp(2–20) used, indicated through reduced levels of SOD2 gene compared to Hp(2–20), of 100  $\mu$ M (Supplementary Material, Figure S3). This may explain why *p53* gene levels decrease after the strong induction measured 1 h after Hp(2–20) treatment.

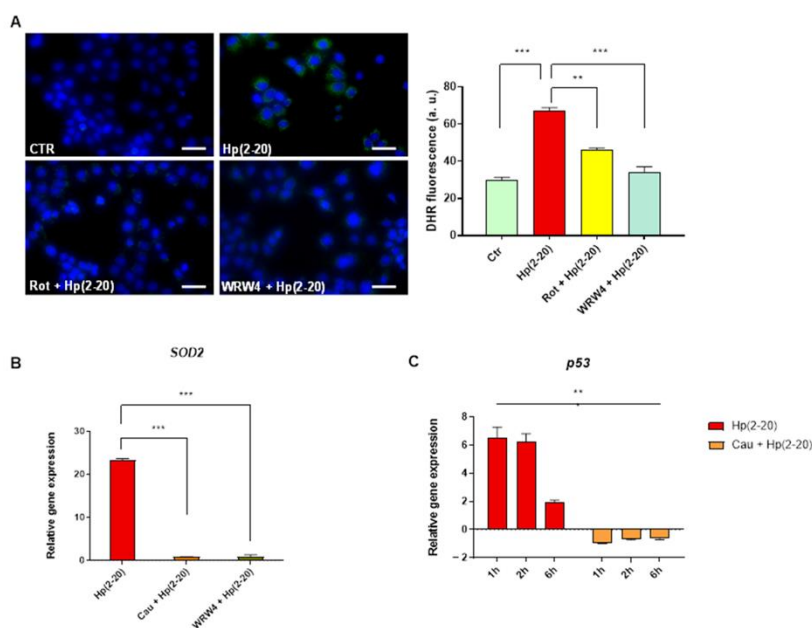


**Figure 6.** Cau reverses Hp(2-20)-induced ROS produced by mitochondria. (A) DHR-loaded cells differently treated: (1) control cells; (2) Hp(2-20) 100  $\mu$ M for 1 h; (3) Rotenone 0.5 mM for 15 min and Hp(2-20) 100  $\mu$ M for 1 h; (4) WRW4 10  $\mu$ M for 15 min and Hp(2-20) 100  $\mu$ M for 1 h, observed with a fluorescence microscope (on the left, scale bar: 100  $\mu$ m) and quantification of the mean fluorescence of individual cells (on the right). Results are expressed as arbitrary units and represent the average  $\pm$  SD calculated from three independent experiments each performed in duplicate. Statistical analysis was performed by GraphPad Prism software, using one-way ANOVA. \*\*  $p < 0.001$ ; \*\*\*  $p < 0.0001$ . (B) Relative gene expression of *SOD2* by quantitative real time PCR (qPCR) in cells treated with: (1) Hp(2-20) 25  $\mu$ M for 2 h; (2) Cau 15  $\mu$ M for 30 min and then Hp(2-20) 25  $\mu$ M for 2 h; (3) WRW4 10  $\mu$ M for 15 min and then Hp(2-20) 25  $\mu$ M for 2 h. (C) Relative gene expression of *p53* by quantitative real time PCR (qPCR) in cells treated with: (1) Hp(2-20) 25  $\mu$ M for 1 h; (2) Hp(2-20) 25  $\mu$ M for 2 h; (3) Hp(2-20) 25  $\mu$ M for 6 h; (4) Cau 15  $\mu$ M for 30 min and Hp(2-20) 25  $\mu$ M for 1 h; (5) Cau 15  $\mu$ M for 30 min and Hp(2-20) 25  $\mu$ M for 2 h; (6) Cau 15  $\mu$ M for 30 min and Hp(2-20) 25  $\mu$ M for 6 h. All samples were normalized to GAPDH as reference housekeeping gene. Furthermore, relative gene expression was normalized to basal activity (untreated control), in order to obtain relative fold expression. Graphs report the results of at least three independent experiments, represented as means  $\pm$  SD. Statistical analysis was performed by GraphPad Prism software, using one-way ANOVA followed by Bonferroni post hoc for multi-comparison (more than two groups) or student's t test for single-comparison (two groups). \*\*  $p < 0.001$ ; \*\*\*  $p < 0.0001$ .

### 2.6. Cau Acts as FPR2 Inhibitor

To confirm whether Cau acts on FPR2, inhibiting Hp(2–20) downstream signaling, we first examined *FPR2* gene expression in response to Cau by performing quantitative real time PCR (qPCR). Figure 7A shows a similar trend in mRNA levels of *FPR2* by WRW4 and Cau. Specifically, neither WRW4 nor Cau were found to activate FPR2. Interestingly, according to the classical receptor theory [44,45], they were found to up-regulate Hp(2–20)-induced *FPR2* gene expression over time, thus preventing FPR2 activation.

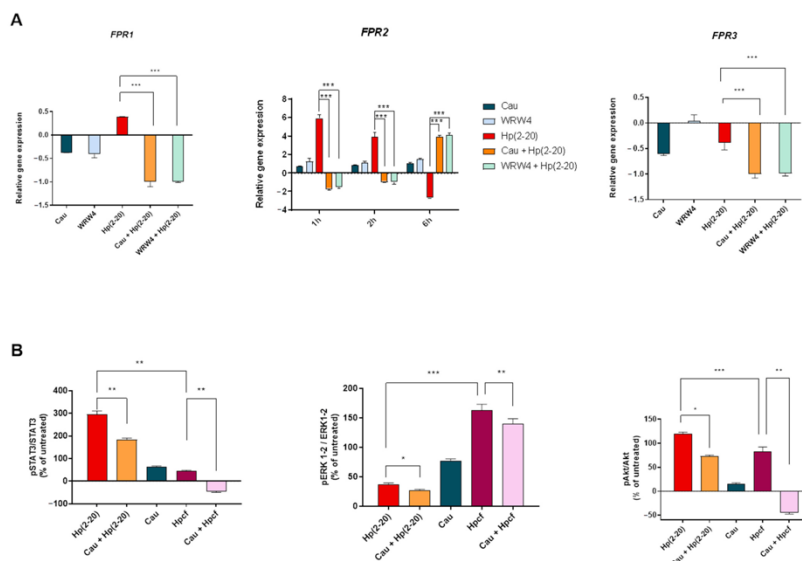


**Figure 7.** Cau inhibits FPR2 and its signaling cascade. (A) Relative gene expression of *FPR1*, *FPR2* and *FPR3* by quantitative real time PCR (qPCR) in cells treated with: (1) Cau 15  $\mu$ M for 2.5 h; (2) WRW4 10  $\mu$ M for 2.25 h; (3) Hp(2–20) 25  $\mu$ M for 2 h; (4) Cau 15  $\mu$ M for 30 min and then Hp(2–20) 25  $\mu$ M for 2 h; (5) WRW4 10  $\mu$ M for 15 min and then Hp(2–20) 25  $\mu$ M for 2 h. *FPR2* gene was further analyzed in cells treated as reported above, but incubated with Hp(2–20) for 1 or 6 h. All samples were normalized to GAPDH as reference housekeeping gene. Furthermore, relative gene expression was normalized to basal activity (untreated control), in order to obtain relative fold expression. (B) Densitometric analysis derived from Western Blot of the ratio pSTAT3/STAT3; pERK1-2/ERK1-2; pAkt/Akt, compared to control group. The analysis was performed on cell lysate prepared after stimulation with Hp(2–20) or Hpcf for 1 h; 15 or 5 min, respectively, either with or without Cau pretreatment (30 min). Vinculin was used for normalization. Graphs report the results of at least three independent experiments, represented as means  $\pm$  SD. Statistical analysis was performed by GraphPad Prism software, using one-way ANOVA followed by Bonferroni post hoc correction. \*  $p < 0.05$ ; \*\*  $p < 0.001$ ; \*\*\*  $p < 0.0001$ .

Furthermore, we also investigated the activity of Cau on FPR1 and FPR3. Our results showed a non-significant induction of FPR1 or FPR3 mRNA levels after 2 h of exposure to Hp(2–20) and consequently, a non-significant effect of both Cau and WRW4. These results suggest the specific action of Cau in inhibiting FPR2, the receptor showing higher affinity for Hp(2–20).

Next, we investigated the effect of Cau on the Hp(2–20)-induced signaling pathway. Upon Hp(2–20) binding, FPRs induced Akt, STAT3 and ERK1/2 phosphorylation [46]. Thus, we stimulated AGS cells—either with or without Cau pretreatment—with Hp(2–20) or Hpcf, and measured the STAT3, ERK1/2 and Akt phosphorylation by Western Blot analysis. As shown in Figure 7B, both Hp(2–20) and Hpcf-stimulated cells increased the STAT3, Akt and ERK1/2 phosphorylation compared to the control cells. Of note, ERK1/2 activation was higher in Hpcf-stimulated cells than in Hp(2–20)-stimulated cells, and, interestingly, ERK1/2 was found to be more phosphorylated in cells treated with Cau alone than in Hp(2–20)-stimulated cells (Figure 7B). This result is consistent with our idea to use Cau as a pro-resolving molecule, leading to gastric epithelium wound healing. Moreover, as expected, Cau pretreatment was found to reduce STAT3, Akt and ERK1/2 activation both in Hp(2–20) and Hpcf-stimulated cells (Figure 7B). However, Cau reduced ERK1/2 phosphorylation by only 10% and 30% in Hp(2–20) and Hpcf-stimulated cells, respectively. In addition, as well as ERK1/2, we observed a higher inhibition of Akt activation in Hpcf-stimulated cells rather than in Hp(2–20) ones. FPRs have been assumed to induce the transactivation of tyrosine kinase receptors (TKRs) via NADPH oxidase-dependent ROS production [18,46]. Previous results demonstrated the antioxidant effect of Cau by inhibiting FPR2 (Figure 5). However, it is well known that Cau is also able to scavenge free radicals in a receptor-independent manner [47]. Therefore, based on these findings, the major reduction of Akt and, to a lesser extent, ERK1/2 activation elicited by Cau in Hpcf-stimulated cells, may also be due to the effective antioxidant role of Cau, thus inhibiting TKRs interplay and the related signaling pathway.

#### 2.7. Cau-FPR2 Interaction: Predictive Computational Studies

Finally, predictive molecular modeling studies were performed to investigate the interaction between Cau and FPR2. As shown in Figure 8A, Cau fits well with FPR2 ligand binding domain, occupying a small area of the receptor binding pocket. In addition, a partial overlap between WKYMV (FPR2 agonist) and Cau was predicted (Figure 8B). Cau was found to form hydrophobic interactions with FPR2 amino acids involved in hydrophobic interactions with WKYMV (Figure 8C). Specifically, Cau interacts with the amino acids (Phe257, Asp281, Asn285 and Arg201, Arg205) showing a critical role in ligand binding and formation of hydrogen bonds for FPR2 [48]. Despite the limits of this predictive approach, these data provide further evidence of the direct binding of Cau with FPR2.

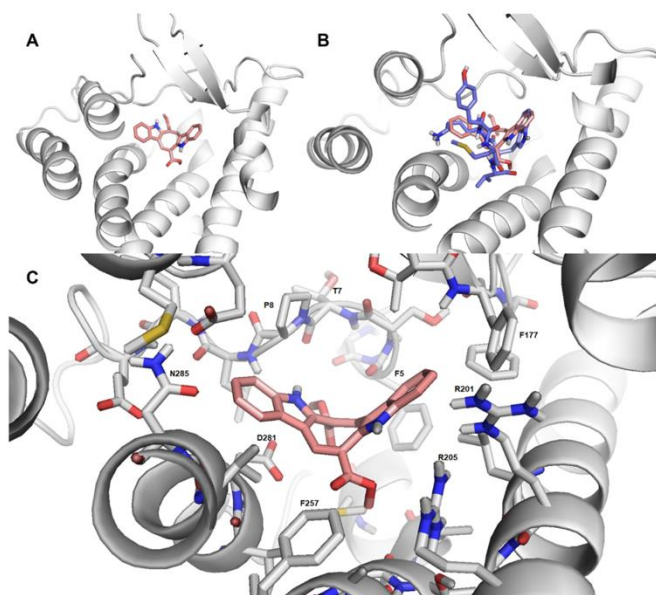


**Figure 8.** Cau interacts with FPR2, occupying its binding pocket. (A) Schematic representation of the complex FPR2-Cau. The receptor is represented in grey cartoon, while the ligand is shown in pink sticks. (B) Overall structure of the complex FPR2-Cau-WKYMV. The receptor is shown in grey cartoon, while the ligands are shown in pink or blue sticks, respectively. A partial overlap between Cau and WKYMV is shown. (C) Binding pocket of Cau in FPR2. The receptor is represented in grey cartoon, while the ligand is shown in pink sticks. The amino acids of the binding site are represented via grey sticks. Cau forms hydrophobic interaction with amino acids of the extracellular domain, I; II; III extracellular portion and VI transmembrane portion, which also constitute the WKYMV binding pocket.

### 2.8. Cau: A More Potent Anti-Inflammatory Molecule than Indomethacin

Indomethacin (Indo) is a member of the non-steroidal anti-inflammatory drugs (NSADs) class, used to treat inflammation and pain. Alongside the essential role of indomethacin in inhibiting prostaglandins synthesis, additional mechanisms could explain its potency. Both indomethacin and Cau possess the indole scaffold in their structure. More specifically, Cau presents an additional indole ring to indomethacin (Figure 9A). The structural similarity and the capability of indomethacin in suppressing formyl-peptides induced cell migration [49] led us to examine the potential interaction between indomethacin and FPRs. Indomethacin pretreatment, indeed, was found to modulate FPR2 induction triggered by Hp(2–20), as well as in cells pretreated with Cau (Figure 9B). These data provide evidence about the role of indomethacin on FPRs. We also observed a more potent anti-inflammatory effect for Cau than indomethacin. Figure 9C, shows a higher decrease in cytokines (MIP-1 $\beta$ , IL-8 and TNF- $\alpha$ ) by Cau than indomethacin in cells stimulated with Hpcf.

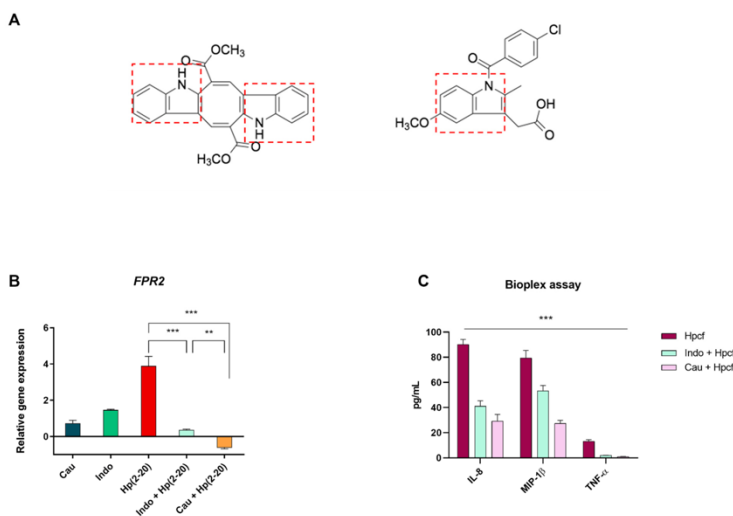


**Figure 9.** Cau possesses one additional indole nucleus to indomethacin and therefore major anti-inflammatory effects. (A) Molecular structure of Cau (on the left) is compared to indomethacin (on the right). Both Cau and indomethacin contain an indole scaffold, indicated with a red square. (B) Relative gene expression of *FPR2* by quantitative real time PCR (qPCR) in cells treated with: (1) Cau 15  $\mu$ M for 2.5 h; (2) WRW4 10  $\mu$ M for 2.25 h; (3) Hp(2-20) 25  $\mu$ M for 2 h; (4) Cau 15  $\mu$ M for 30 min and then Hp(2-20) 25  $\mu$ M for 2 h; (5) Indomethacin 100  $\mu$ g/mL for 30 min and then Hp(2-20) 25  $\mu$ M for 2 h; (6) Hpcf; (7) Indomethacin 100  $\mu$ g/mL for 30 min and then Hpcf for 2 h; (8) Cau 15  $\mu$ M for 30 min and then Hpcf for 2 h. All samples were normalized to GAPDH as the reference housekeeping gene. Furthermore, relative gene expression was normalized to basal activity (untreated control), in order to obtain relative fold expression. Graphs report the results of at least three independent experiments, represented as means  $\pm$  SD. (C) Cytokines TNF- $\alpha$ , IL-8 and MIP-1 $\beta$  were measured by Bio-plex assay in AGS cells culture medium. Results are expressed as pg of cytokines secreted in mL of cell medium, differently treated: (1) Hpcf for 24 h; (2) Cau 15  $\mu$ M for 30 min and then Hpcf for 24 h; (3) indomethacin 200  $\mu$ M for 30 min and then *H. pylori* culture supernatant for 24 h. Values were normalized to basal activity (CTR) and represent mean  $\pm$  SD of at least three independent experiments, each performed in triplicate. Statistical analysis was performed by GraphPad Prisma software, using one-way ANOVA followed by Bonferroni post hoc correction. \*\*  $p < 0.001$ ; \*\*\*  $p < 0.0001$ .

### 3. Discussion

*Helicobacter pylori* is one of the most common human-colonizing bacteria, and its resultant infection can promote chronic inflammation. It is usually acquired during early childhood [50], remaining asymptomatic for long time. The significant capability of the bacterium in evading the host immune system and developing strategies to resist the common antimicrobial therapy means *H. pylori* is able to persist for decades in the harsh gastric environment, establishing lifelong chronic inflammation, which leads to severe clinical outcomes [1,9]. Strategies to control chronic inflammation, by modulating the immune system, may represent a promising approach to improve *H. pylori* clinical outcomes and counteract chronic diseases.

In the present study, we focused our attention on FPRs, proposing FPRs as a novel target to ameliorate the detrimental effects derived from *H. pylori*-induced chronic inflammation. In particular, we investigated the potential capability of Cau to act as an attractive



target for FPRs, inhibiting Hp(2–20) signaling pathway. The choice to use Cau in this study was based on its particular chemical structure, characterized by two indole nuclei. Indole, in fact, has been considered the most privileged scaffold in drug discovery [51,52] because of its anti-inflammatory, anti-cancer, antioxidant, anti-diabetic, antimicrobial, antiviral and anti-hypertensive roles [32,51,53]. In addition, the presence of two indole nuclei makes Cau similar to W-rich peptides, such as WRW<sub>4</sub>, which was found to interact with FPR2, exerting antagonistic effects [54].

For the first time, our results show the potential capability of Cau in antagonizing FPR2, as well as WRW<sub>4</sub>. Cau was tested as a probable target for all FPRs. However, it was found to distinguish between the three FPRs, interacting selectively with FPR2. The unique characteristic of indole rings in transferring electrons and favoring amino acids receptor reaction makes them effective components of the molecule. Specifically, Cau was observed to occupy the FPR2 binding pocket, forming a hydrophobic environment that could contribute to the stabilization of the receptor interaction, potentially competing with other ligands. This view was supported by the finding that Cau limited Hp(2–20)-induced cellular responses, via the inhibiting oxidative burst, chemotaxis and pro-inflammatory cytokines release.

NF- $\kappa$ B is the most important mediator of the inflammatory response, regulating the transcriptional activity of pro-inflammatory genes [55–57]. Our data, distinctly indicate an important role for Cau in suppressing Hp(2–20)-induced NF- $\kappa$ B signaling in gastric epithelial cells, by inhibiting phosphorylation and the degradation of the NF- $\kappa$ B inhibitor protein I $\kappa$ B- $\alpha$ . In contrast, Cau was not found to be as effective within the context of different bacterial stimuli. In the case of Hpcf, in fact, Cau did not display a significant suppression of I $\kappa$ B- $\alpha$  phosphorylation compared to when Hp(2–20) was used. To further assess the regulation of NF- $\kappa$ B pathway, IL-8, IL-6 and TNF- $\alpha$  genes were selected to validate the above results. The potent pro-inflammatory cytokine, IL-8, plays a key role in initiating the chemotactic process and, together with IL-6 and TNF- $\alpha$ , is strongly associated with the *H. pylori*-related chronic inflammation [58,59]. Cau was found to reduce IL-8, IL-6 and TNF- $\alpha$  gene transcription, both in Hp(2–20) and Hpcf stimulated cells. However, consistent with the previous data, it showed a more important inhibitory activity in Hp(2–20)-stimulated cells, than in Hpcf-stimulated cells. Taken together, these data indicate the pivotal role of Cau in modulating the inflammatory response, by acting selectively on FPRs. The modulation of Hp(2–20)-induced pro-inflammatory signaling by Cau was also demonstrated in monocyte-derived macrophages. Given the key role of macrophages in the immune response, we monitored the effect of Cau on macrophages exposed to Hp(2–20)-stimulated AGS cells microenvironment, observing a decreased expression of the pro-inflammatory cytokines IL-1 $\beta$  and TNF- $\alpha$ , commonly secreted by M1 polarized macrophages [60]. This suggests the importance of Cau as an FPR2 target, in mitigating the inflammatory response and affecting the state of macrophage polarization. The activation of gastric epithelial FPRs by Hp(2–20), triggers different signaling pathways, including MAPK/ERK, PI3K/Akt and STAT3 [23,61], which modulate important biological functions associated with the immune response—specifically, cell migration, proliferation and differentiation [27,62,63]. However, they also play central roles in tumor growth [62,64]. This makes Hp(2–20) controversial. A group of researchers demonstrated that Hp(2–20) induces gastric mucosal healing by stimulating cell migration and proliferation [61,65]. However, in the context of *H. pylori* persistence, the chronic activation of FPR2 by Hp(2–20) may promote cancer development and progression [27,66]. In agreement with the literature, our study indicated the increased activation of STAT3, Akt and ERK1/2 in Hp(2–20)-stimulated gastric epithelial cells, while Cau was found to reduce this response. Interestingly, the suppression of the above-mentioned key signaling molecules was found more remarkable in Hpcf-stimulated cells, than in those cultured with Hp(2–20). Apart from the FPRs signaling pathway, *H. pylori* activates different host-signaling pathways, responsible for cell and tissue alterations. Recent studies have demonstrated the critical role of the tyrosine kinase receptor (TKR) signaling pathway in *H. pylori* infection [67], as it leads to chronic inflammation and tu-

morigenesis [68,69]. It is well accepted that NADPH-derived ROS are highly involved in activating the TKRs signaling pathway and that FPRs induce TKRs transactivation via NADPH-oxidase dependent ROS production [18,70]. Here, we observed an increase in ROS production in Hp(2-20)-cultured cells, due to FPR2 activation and the important effect of Cau in neutralizing ROS by inhibiting FPR2 downstream signaling, as well as WRW4. Additional data demonstrated increased ROS production in Hpcf-stimulated cells than in Hp(2-20)-stimulated cells (data not shown), which was only partially attributable to FPR2 activation. Hpcf, contains many other factors which might contribute to ROS generation, thus causing TKRs signaling pathway activation. Therefore, the demonstrated antioxidant capability of Cau caused by inhibiting the FPRs signaling pathway, as well as its reported role as a free radical scavenger [47], could explain the unexpected beneficial effect of Cau in reducing STAT3, Akt and ERK1/2 phosphorylation, by inhibiting TKRs signaling pathway activation. This finding supports the success of Cau in counteracting *H. pylori*-related inflammatory diseases.

ROS are an important hallmark of inflammation. Excessive ROS generation is directly involved in the pathogenesis of several inflammatory disorders, including neurodegeneration, cardiovascular diseases, atherosclerosis and cancer [71,72]. Many studies have reported the crucial role of oxidative stress in the progression of *H. pylori*-related gastric carcinogenesis [73]. Moreover, the role of oxidative stress in the pathogenesis of *H. pylori*-associated extra-gastric diseases cannot be discounted [10]. FPRs are known to regulate the oxidative burst via NADPH oxidase-dependent ROS production [40]. However, studies have reported crosstalk between ROS produced at the mitochondria and the cytosol level, which exacerbates oxidative stress [74]. In the present study, we validated the pro-oxidant role of Hp(2-20) via FPRs and demonstrated the role of mitochondria in enhancing the oxidative stress from Hp(2-20). Interestingly, Cau was found to reverse Hp(2-20)-induced ROS production, targeting both mitochondria and NADPH oxidase.

Finally, we compared Cau with indomethacin, a traditional anti-inflammatory drug containing one indole nucleus. Extraordinarily, our data revealed that indomethacin may modulate the expression of FPR2, thus elucidating its potential pharmacological effect, which is still poorly understood. Nevertheless, Cau displayed a greater inhibitory effect against FPR2 than indomethacin and, at the same time, a more effective anti-inflammatory role. These results highlight the association between FPRs and inflammatory conditions and the importance of indole as a scaffold for anti-inflammatory drugs, by targeting FPRs.

#### 4. Materials and Methods

##### 4.1. Cell Culture

Human gastric AGS cell line and human monocytic THP-1 cell line were obtained from the American Type Culture Collection (ATCC, Manassas, VA, USA, #CRL-1739 and #TIB-202, respectively). AGS cells were grown in Dulbecco's modification of Eagle's medium, high glucose (DMEM; Microtech, Naples, Italy) supplemented with 10% fetal bovine serum (FBS; Microtech, Naples, Italy), 1% penicillin/streptomycin (Gibco, Waltham, MA, USA) and 1% L-glutamine (Gibco, Waltham, MA, USA). THP-1 cells were grown in RPMI-1640 (Microtech, Naples, Italy) and supplemented with 10% fetal bovine serum (FBS; Microtech, Naples, Italy), 1% penicillin/streptomycin (Gibco, Waltham, MA, USA) and 1% L-glutamine (Gibco, Waltham, MA, USA). Both AGS and THP-1 cell lines were maintained in a humidified environment, containing 5% CO<sub>2</sub> at 37 °C. The THP-1 cells were induced to differentiate into macrophages through exposure to phorbol-12-myristate-13-acetate (PMA, 100 ng/mL; Sigma Aldrich, St. Louis, MO, USA) for 48 h. Cells were then washed twice, and culture medium was substituted with RPMI-1640 without PMA, followed by a resting period of 24 h.

##### 4.2. Helicobacter Pylori Culture Filtrate Production

*H. pylori* P12 strains, kindly provided by Dr. Marguerite Clyne (University College Dublin), were cultured on selective Columbia agar (Oxoid, Basingstoke, Hampshire, UK)



containing 7% (v/v) defibrinated horse blood (Oxoid, Basingstoke, Hampshire, UK) supplemented with an antibiotic mix (DENT or Skirrow, respectively, Oxoid, Basingstoke, Hampshire, UK). Bacteria plates were incubated for 3–4 days in a capnophilic atmosphere with 10% CO<sub>2</sub> at 37 °C. Once grown on the plate, bacteria were scraped using brain heart infusion (BHI Oxoid, Basingstoke, Hampshire, UK) and measured at optical density at 600 nm (OD<sub>600</sub>) considering 1 OD<sub>600</sub> =  $1 \times 10^8$  bacteria/mL. In order to prepare *H. pylori* broth growth,  $2 \times 10^7$  bacteria/mL were cultured in liquid DMEM (Euroclone, Milan, Italy), supplemented with 10% fetal bovine serum (FBS; Euroclone, Milan, Italy) and incubated in a capnophilic atmosphere with 10% CO<sub>2</sub> at 37 °C. After 24 h, bacterial suspension was centrifuged at 10,000 g for 10 min to remove bacteria and the supernatant was filtered by using a 0.22 µm filter (Euroclone, Milan, Italy). The obtained culture filtrate was stored at −80 °C until use.

#### 4.3. Cau Extraction and Purification

*Caulerpa cylindracea* was collected in Italy in the Gulf of Pozzuoli and exhaustively extracted with acetone at room temperature, as reported by Magliozzi et al. [75]. Briefly, the acetone extract was evaporated at a reduced pressure and the residual water was extracted with diethyl ether. The diethyl ether extract was first fractionated on Sephadex column (CHCl<sub>3</sub>/MeOH; 1:1) and the obtained fraction was further purified by silica-gel column chromatography (gradient of light petroleum ether/Et<sub>2</sub>O, as eluent) to produce pure Cau, identified by comparing <sup>1</sup>H- and <sup>13</sup>C-NMR spectroscopic data with the literature [76,77]. Size-exclusion chromatography was achieved using Sephadex LH-20 column, whereas silica-gel column chromatography was performed using Merck Kieselgel 60 powder. NMR data were recorded on a Bruker Avance-400 spectrometer using an inverse probe fitted with a gradient along the z axis.

#### 4.4. Cell Viability Assay

The effects of Cau on AGS cells were assessed by performing MTT assay. Briefly, AGS cells were seeded at a density of  $2 \times 10^3$  per well in a 96-well plate and incubated at 37 °C in a 5% CO<sub>2</sub> atmosphere overnight. After cell attachment, the medium was replaced with fresh medium containing different concentrations of Cau and cells were incubated for 24 h. Twenty µL of 3-(4,5-dimethylthiazol-2-yl)-5-(3,4-diphenyltetrazolium bromide) solution (MTT) were added to each well and cells were further incubated at 37 °C in a 5% CO<sub>2</sub> atmosphere for 3 h. Finally, the medium was removed, and the resultant formazan crystals were dissolved in 200 µL of DMSO. Absorbance was recorded at 570 nm using an EnVision 2102 multilabel reader (PerkinElmer, Waltham, MA, USA). Cell viability was calculated as the ratio between the mean absorbance of the sample and the mean absorbance of the untreated cells and expressed in percentage.

#### 4.5. In Vitro Scratch Assay

AGS cells migration was tested by performing in vitro scratch assay, as described by de Paulis et al. [61]. Briefly, confluent monolayers of cells were treated with mitomycin for 2 h (2 µg/mL) to inhibit cell growth. Monolayers were then scratched using a pipette tip, in order to create a gap. After scratching, medium and cell debris were removed, and cells were washed with a fresh medium and incubated for 12 h with Hp(2–20) with or without Cau pretreatment.

#### 4.6. RNA Extraction and Quantitative Real-Time PCR

AGS cells were seeded at a density of  $0.5 \times 10^6$  per well in 12-well plates to analyze the expression profiling of (1) cytokine and chemokine genes; (2) *FPRs* genes; (3) mitochondrial superoxide dismutase (*SOD2*) gene and (4) *p53* gene at different times post-inflammatory stimulus, represented by Hp(2–20) (synthesized by Innovagen, Lund, Sweden) or Hpcf, in the presence or absence of the Cau pretreatment. Total RNA was extracted from individual wells by PureLink<sup>®</sup> RNA Mini Kit (ThermoFisher Scientific, Waltham, MA, USA), according

to the manufacturer instructions. Genomic DNA was removed by digestion with DNase I, Amplification Grade (ThermoFisher Scientific). Extracted RNA was quantified and analyzed for purity, using Nanodrop-ND 1000 spectrophotometer (ThermoFisher Scientific) and finally reverse-transcribed using the high-capacity cDNA Reverse transcription kit (Applied Biosystem, Bedford, MA, USA). Gene transcript levels were measured using TaqMan PCR master 2× reagent or Power SYBR® Green PCR Master Mix (Applied Biosystem®) on a StepOne™ Real-Time PCR System (Applied Biosystem®), according to the standard-mode thermal cycling conditions, according to the manufacturer's protocol. The relative expression level of analyzed genes was determined using probes or primers reported in the Supplementary Material, Table S1. All samples were normalized to GAPDH as the reference housekeeping gene and the relative quantitative expression was determined using the  $2^{-\Delta\Delta C_t}$  method [78–80].

#### 4.7. Measurement of Cytokines Production in Macrophages

Opportunately differentiated THP-1 cells were seeded at a density of  $0.5 \times 10^6$  per well in 12-well plates and stimulated with AGS-conditioned medium for 24 h. AGS-conditioned medium was prepared by seeding  $2 \times 10^6$  cells per well in 6-well plates. After treatment with the pro-inflammatory stimulus Hp(2–20), preceded or not by Cau pre-treatment, the medium was collected and filtered by passage in a 0.22 µm filter (Sigma Aldrich). Supernatants of THP-1 cells were collected at different times post-stimulation with AGS-conditioned medium and stored at  $-80^\circ\text{C}$  until use. Secretion of IL-1β and TNF-α was detected by Human ELISA kit (Abcam, Waltham, MA, USA), according to the manufacturer instructions.

#### 4.8. Intracellular ROS Measurement

AGS cells were split at 80–90% of confluency, seeded ( $0.5 \times 10^6$ ) in 35 mm culture dishes, and incubated at  $37^\circ\text{C}$  in a 5%  $\text{CO}_2$  atmosphere overnight. After cell attachment, ROS detection assay was assayed using dihydrorhodamine 123 (DHR; Sigma Aldrich, Missouri, USA), as described by Cuomo et al. [81]. Briefly, cells were preloaded with 10 µM DHR for 20 min and treated as detailed in the figure legend. After treatments, DAPI (Thermo Fischer Scientific) was used as a nuclear counterstain, and cells were analyzed with a Zeiss Axioskop 2 Hal100 fluorescence microscope equipped with a digital camera (Nikon). The excitation and emission wavelengths were 488 and 515 nm, respectively. Images were digitally acquired with exposure times of 100–400 ms and processed for fluorescence determination with ImageJ software version 2.1.0/1.53c.

#### 4.9. Western Blotting for Protein Studies

AGS cells were split at 80–90% of confluency, seeded ( $2 \times 10^6$  per well) in 6-well plates and incubated at  $37^\circ\text{C}$  in a 5%  $\text{CO}_2$  atmosphere until cell attachment. Cells were serum-starved 12–16 h prior the stimulation, using serum-free DMEM containing 0.25% BSA and incubated at  $37^\circ\text{C}$  in a  $\text{CO}_2$  incubator. After treatments, cells were washed and harvested using RIPA buffer (50 mM Tris-HCl pH 8.8, 150 mM NaCl, 0.1% SDS, 0.5% NP-40, 0.5% DOC; protease and phosphatase inhibitor cocktail, Sigma-Aldrich), incubated for 20 min at  $4^\circ\text{C}$  and centrifugated at  $10,000 \times g$  for 15 min. Pellets were discarded and cell lysates were stored at  $-80^\circ\text{C}$  until use. Proteins (30 µg/lane, in Sample Buffer: 4× Laemmli Sample Buffer #1610747) were separated in 7.5–15% SDS-polyacrylamide gel and then transferred to a nitrocellulose membrane (Amersham™ Nitrocellulose Western blotting membranes 0.2µm) by electrotransfer. Briefly, filters were blocked for 1 h at room temperature in 5% (w/v) non-fat milk in Tris-buffered saline Tween-20 (TBST: 0.1% Tween, 150 mM NaCl, 10 mM Tris-HCl, pH 7.5) and probed with antibodies as reported in the Supplementary Material, Table S2. After several washings in TBST, membranes were incubated with the appropriate secondary antibodies (Supplementary Material, Table S2). Finally, immunoreactive proteins were visualized with enhanced chemiluminescence (Amersham International, Buckinghamshire, UK). The blots were stripped using a stripping buffer and

then re-probed to detect the total protein of interest. Each Western blot band was quantified using Image Lab software version 6.0 (Bio-Rad, Hercules, CA, USA).

#### 4.10. Cytokines Assay

AGS cells were split at 80–90% of confluency, seeded ( $2 \times 10^6$  per well) in 6-well plates and incubated at 37 °C in a 5% CO<sub>2</sub> atmosphere until cell attachment. Cells were serum-starved 12–16 h prior the stimulation, using serum-free DMEM containing 0.25% BSA and incubated at 37 °C in a CO<sub>2</sub> incubator. After 24 h of treatment, medium was collected and centrifugated at 10,000× *g* to remove debris and dead cells and analysed for the concentration of IL-8, G-CSF, TNF-α and MIP-1β, by using the Bioplex Multiplex human cytokine assay (Bio-Rad), as indicated by manufacturer's instructions. As a multiplexed assay, the Bioplex assay can simultaneously detect more analytes in a single sample [82].

#### 4.11. Molecular Modeling

To predict and characterize the potential interaction of Cau with FPR2, computational studies were assessed. A 3D structure model of FPR2 was downloaded from Protein Data Bank (RCSB PDB), using the crystal structure of the complex FPR2-WKYMVm (PDBcode: 6LW5) as a model. The WKYMV ligand was successively removed by PyMOL Molecular Graphic System (Version 1.3 Shrodinger, LLC, New York, NY, USA), obtaining the receptor pdb file. The initial 3D conformation of Cau was obtained from PubChem (ncbi library). The receptor and ligand were then adapted for docking with the AutoDock Tools. Docking analysis was carried out with AutoDock Vina (Trott and Olson, 2010), setting the grid box at 26 Å × 40 Å × 32 Å for the receptor. In conclusion, molecular details of Cau recognition by FPR2 were analyzed with PyMOL Molecular Graphic System (Version 1.3 Shrodinger, LLC).

#### 4.12. Statistical Analysis

Statistical analysis was performed using GraphPad Prism 8.0 software, San Diego, CA, USA. All data were compared using One-way ANOVA followed by Bonferroni's multiple comparisons test, in order to compare different groups. Experimental data are presented as mean ± SD of at least three independent experiments, each performed in triplicate. Lastly, *p* values < 0.05 were considered statistically significant.

### 5. Conclusions

In conclusion, the current study aimed to provide in vitro proofs on the role of FPRs in the pathogenesis of *H. pylori*-associated chronic inflammation, by interacting with the *H. pylori*-released peptide Hp(2–20). Concurrently, it demonstrated the impressive effects of Cau on health, by targeting FPR2, thus controlling the *H. pylori*-associated chronic inflammation and related disorders. Taken together, our results suggest the potential clinical application of Cau for the control of numerous inflammatory disorders, which are among the main health problems occurring today. Nevertheless, future studies are required to validate our in vitro findings in vivo.

**Supplementary Materials:** The following are available online at <https://www.mdpi.com/article/10.3390/ijms222313154/s1>.

**Author Contributions:** Conceptualization, R.C.; methodology, P.C.; validation, M.P.; formal analysis, P.C., I.A., S.C., F.G.; Caulerpin extraction, E.M.; data curation, A.M.J.M., D.E.; writing—original draft preparation, P.C.; writing—review and editing, C.M.; project administration, R.C. All authors have read and agreed to the published version of the manuscript.

**Funding:** This research received no external funding.

**Institutional Review Board Statement:** Not applicable.

**Informed Consent Statement:** Not applicable.

**Data Availability Statement:** The data presented in this study are available within the article.

**Conflicts of Interest:** The authors declare no conflict of interest.

## References

1. Tshibangu-Kabamba, E.; Yamaoka, Y. *Helicobacter pylori* infection and antibiotic resistance—From biology to clinical implications. *Nat. Rev. Gastroenterol. Hepatol.* **2021**, *18*, 613–629. [\[CrossRef\]](#)
2. Mentis, A.F.A.; Boziki, M.; Grigoriadis, N.; Papavassiliou, A.G. *Helicobacter pylori* infection and gastric cancer biology: Tempering a double-edged sword. *Cell. Mol. Life Sci.* **2019**, *76*, 2477–2486. [\[CrossRef\]](#) [\[PubMed\]](#)
3. White, J.R.; Winter, J.A.; Robinson, K. Differential inflammatory response to *Helicobacter pylori* infection: Etiology and clinical outcomes. *J. Inflamm. Res.* **2015**, *8*, 137–147. [\[CrossRef\]](#)
4. Charitos, I.A.; D'agostino, D.; Topi, S.; Bottalico, L.; Li, C.-F.; Yang, C.-C.; Chiang, N.-J. 40 Years of *Helicobacter pylori*: A Revolution in Biomedical Thought. *Gastroenterol. Insights* **2021**, *12*, 111–135. [\[CrossRef\]](#)
5. Durazzo, M.; Adriani, A.; Fagonee, S.; Saracco, G.M.; Pellicano, R. *Helicobacter pylori* and Respiratory Diseases: 2021 Update. *Microorganisms* **2021**, *9*, 2033. [\[CrossRef\]](#)
6. Mladenova, I. *Helicobacter pylori* and cardiovascular disease: Update 2019. *Minerva Cardioangiol.* **2019**, *67*, 425–432. [\[CrossRef\]](#) [\[PubMed\]](#)
7. Li, J.Z.; Li, J.Y.; Wu, T.F.; Xu, J.H.; Huang, C.Z.; Cheng, D.; Chen, Q.K.; Yu, T. *Helicobacter pylori* Infection Is Associated with Type 2 Diabetes, Not Type 1 Diabetes: An Updated Meta-Analysis. *Gastroenterol. Res. Pract.* **2017**, *2017*, 5715403. [\[CrossRef\]](#) [\[PubMed\]](#)
8. Mégraud, F.; Bessède, E.; Varon, C. *Helicobacter pylori* infection and gastric carcinoma. *Clin. Microbiol. Infect.* **2015**, *21*, 984–990. [\[CrossRef\]](#) [\[PubMed\]](#)
9. Wroblewski, L.E.; Peek, R.M., Jr.; Wilson, K.T. *Helicobacter pylori* and Gastric Cancer: Factors That Modulate Disease Risk. *Clin. Microbiol. Rev.* **2010**, *23*, 713–739. [\[CrossRef\]](#)
10. Cuomo, P.; Papaiani, M.; Sansone, C.; Iannelli, D.; Medaglia, C.; Paris, D.; Motta, A.; Capparelli, R. An In Vitro Model to Investigate the Role of *Helicobacter pylori* in Type 2 Diabetes, Obesity, Alzheimer's Disease and Cardiometabolic Disease. *Int. J. Mol. Sci.* **2020**, *21*, 8369. [\[CrossRef\]](#)
11. Furman, D.; Campisi, J.; Verdin, E.; Carrera-Bastos, P.; Targ, S.; Franceschi, C.; Ferrucci, L.; Gilroy, D.W.; Fasano, A.; Miller, G.W.; et al. Chronic inflammation in the etiology of disease across the life span. *Nat. Med.* **2019**, *25*, 1822–1832. [\[CrossRef\]](#)
12. Chen, L.; Deng, H.; Cui, H.; Fang, J.; Zuo, Z.; Deng, J.; Li, Y.; Wang, X.; Zhao, L. Inflammatory responses and inflammation-associated diseases in organs. *Oncotarget* **2017**, *9*, 7204–7218. [\[CrossRef\]](#) [\[PubMed\]](#)
13. Barton, G.M. A calculated response: Control of inflammation by the innate immune system. *J. Clin. Investig.* **2008**, *118*, 413–420. [\[CrossRef\]](#) [\[PubMed\]](#)
14. Nathan, C. Points of control in inflammation. *Nature* **2002**, *420*, 846–852. [\[CrossRef\]](#)
15. Van der Heijden, C.D.C.C.; Noz, M.P.; Joosten, L.A.B.; Netea, M.G.; Riksen, N.P.; Keating, S.T. Epigenetics and Trained Immunity. *Antioxid. Redox Signal.* **2018**, *29*, 1023–1040. [\[CrossRef\]](#) [\[PubMed\]](#)
16. Paludan, S.R.; Pradeu, T.; Masters, S.L.; Mogensen, T.H. Constitutive immune mechanisms: Mediators of host defence and immune regulation. *Nat. Rev. Immunol.* **2021**, *21*, 137–150. [\[CrossRef\]](#)
17. Raabe, C.A.; Gröper, J.; Rescher, U. Biased perspectives on formyl peptide receptors. *Biochim. Biophys. Acta-Mol. Cell Res.* **2019**, *1866*, 305–316. [\[CrossRef\]](#)
18. Cattaneo, F.; Russo, R.; Castaldo, M.; Chambery, A.; Zollo, C.; Esposito, G.; Pedone, P.V.; Ammendola, R. Phosphoproteomic analysis sheds light on intracellular signaling cascades triggered by Formyl-Peptide Receptor 2. *Sci. Rep.* **2019**, *9*, 17894. [\[CrossRef\]](#)
19. Muto, Y.; Guindon, S.; Umemura, T.; Kohidai, L.; Ueda, H. Adaptive evolution of formyl peptide receptors in mammals. *J. Mol. Evol.* **2015**, *80*, 130–141. [\[CrossRef\]](#) [\[PubMed\]](#)
20. Boillat, M.; Carleton, A.; Rodriguez, I. From immune to olfactory expression: Neofunctionalization of formyl peptide receptors. *Cell Tissue Res.* **2021**, *383*, 387–393. [\[CrossRef\]](#)
21. Wang, H.; Peng, X.; Ge, Y.; Zhang, S.; Wang, Z.; Fan, Y.; Huang, W.; Qiu, M.; Ye, R.D. A Ganoderma-Derived Compound Exerts Inhibitory Effect through Formyl Peptide Receptor 2. *Front. Pharmacol.* **2020**, *11*, 337. [\[CrossRef\]](#)
22. Liang, W.; Chen, K.; Gong, W.; Yoshimura, T.; Le, Y.; Wang, Y.; Wang, J.M. The Contribution of Chemoattractant GPCRs, Formylpeptide Receptors, to Inflammation and Cancer. *Front. Endocrinol.* **2020**, *11*, 17. [\[CrossRef\]](#)
23. Cattaneo, F.; Parisi, M.; Ammendola, R. Distinct Signaling Cascades Elicited by Different Formyl Peptide Receptor 2 (FPR2) Agonists. *Int. J. Mol. Sci.* **2013**, *14*, 7193–7230. [\[CrossRef\]](#)
24. Park, S.-C.; Kim, M.-H.; Hossain, M.A.; Shin, S.Y.; Kim, Y.; Stella, L.; Wade, J.D.; Park, Y.; Hahn, K.-S. Amphipathic  $\alpha$ -helical peptide, HP (2–20), and its analogues derived from *Helicobacter pylori*: Pore formation mechanism in various lipid compositions. *Biochim. Biophys. Acta (BBA)-Biomembr.* **2007**, *1778*, 229–241. [\[CrossRef\]](#)
25. Bylund, J.; Christophe, T.; Boulay, F.; Nyström, T.; Karlsson, A.; Dahlgren, C. Proinflammatory Activity of a Cecropin-Like Antibacterial Peptide from *Helicobacter pylori*. *Antimicrob. Agents Chemother.* **2001**, *45*, 1700–1704. [\[CrossRef\]](#)
26. Cuomo, P.; Papaiani, M.; Capparelli, R.; Medaglia, C. The Role of Formyl Peptide Receptors in Permanent and Low-Grade Inflammation: *Helicobacter pylori* Infection as a Model. *Int. J. Mol. Sci.* **2021**, *22*, 3706. [\[CrossRef\]](#) [\[PubMed\]](#)

27. Hou, X.-L.; Ji, C.-D.; Tang, J.; Wang, Y.-X.; Xiang, D.-F.; Li, H.-Q.; Liu, W.-W.; Wang, J.-X.; Yan, H.-Z.; Wang, Y.; et al. FPR2 promotes invasion and metastasis of gastric cancer cells and predicts the prognosis of patients. *Sci. Rep.* **2017**, *7*, 3153. [\[CrossRef\]](#) [\[PubMed\]](#)
28. Vitale, R.M.; D'Aniello, E.; Gorbis, S.; Martella, A.; Silvestri, C.; Giuliani, M.E.; Fellous, T.; Gentile, A.; Carbone, M.; Cutignano, A.; et al. Fishing for Targets of Alien Metabolites: A Novel Peroxisome Proliferator-Activated Receptor (PPAR) Agonist from a Marine Pest. *Mar. Drugs* **2018**, *16*, 431. [\[CrossRef\]](#)
29. Máximo, P.; Ferreira, L.M.; Branco, P.; Lima, P.; Lourenço, A. Secondary Metabolites and Biological Activity of Invasive Macroalgae of Southern Europe. *Mar. Drugs* **2018**, *8*, 265. [\[CrossRef\]](#)
30. Liu, Y.; Morgan, J.B.; Coothankandaswamy, V.; Liu, R.; Jekabsons, M.B.; Mahdi, F.; Nagle, D.G.; Zhou, Y.-D. The Caulerpa Pigment Caulerpin Inhibits HIF-1 Activation and Mitochondrial Respiration. *J. Nat. Prod.* **2009**, *72*, 2104–2109. [\[CrossRef\]](#) [\[PubMed\]](#)
31. Souza, C.R.M.; Bezerra, W.P.; Souto, J.T. Marine Alkaloids with Anti-Inflammatory Activity: Current Knowledge and Future Perspectives. *Mar. Drugs* **2020**, *18*, 147. [\[CrossRef\]](#)
32. De Sá Alves, F.R.; Barreiro, E.J.; Fraga, C.A. From nature to drug discovery: The indole scaffold as a “privileged structure”. *Mini Rev. Med. Chem.* **2009**, *9*, 782–793. [\[CrossRef\]](#)
33. Guerra, A.S.; Malta, D.J.; Laranjeira, L.P.; Maia, M.B.; Colaço, N.C.; de Lima, M.C.; Galdino, S.L.; da Rocha Pitta, I.; Gonçalves-Silva, T. Anti-inflammatory and antinociceptive activities of indole-imidazolidine derivatives. *Int. Immunopharmacol.* **2011**, *11*, 1816–1822. [\[CrossRef\]](#)
34. Moore, B.B.; Kunkel, S.L. Attracting Attention: Discovery of IL-8/CXCL8 and the Birth of the Chemokine Field. *J. Immunol.* **2019**, *202*, 3–4. [\[CrossRef\]](#)
35. De Paulis, A.; Prevete, N.; Fiorentino, I.; Walls, A.F.; Curto, M.; Petraroli, A.; Castaldo, V.; Ceppa, P.; Fiocca, R.; Marone, G. Basophils Infiltrate Human Gastric Mucosa at Sites of *Helicobacter pylori* Infection, and Exhibit Chemotaxis in Response to H. pylori-derived Peptide Hp(2–20). *J. Immunol.* **2004**, *172*, 7734–7743. [\[CrossRef\]](#) [\[PubMed\]](#)
36. Louwe, P.A.; Badiola Gomez, L.; Webster, H.; Perona-Wright, G.; Bain, C.C.; Forbes, S.J.; Jenkins, S.J. Recruited macrophages that colonize the post-inflammatory peritoneal niche convert into functionally divergent resident cells. *Nat. Commun.* **2021**, *12*, 1770. [\[CrossRef\]](#) [\[PubMed\]](#)
37. Orecchioni, M.; Ghosheh, Y.; Pramod, A.B.; Ley, K. Macrophage Polarization: Different Gene Signatures in M1(LPS+) vs. Classically and M2(LPS-) vs. Alternatively Activated Macrophages. *Front. Immunol.* **2019**, *10*, 1084. [\[CrossRef\]](#)
38. Ruytinx, P.; Proost, P.; Van Damme, J.; Struyf, S. Chemokine-Induced Macrophage Polarization in Inflammatory Conditions. *Front. Immunol.* **2018**, *9*, 1930. [\[CrossRef\]](#)
39. Gregory, J.L.; Morand, E.F.; McKeown, S.J.; Ralph, J.A.; Hall, P.; Yang, Y.H.; McColl, S.R.; Hickey, M.J. Macrophage Migration Inhibitory Factor Induces Macrophage Recruitment via CC Chemokine Ligand 2. *J. Immunol.* **2006**, *177*, 8072–8079. [\[CrossRef\]](#)
40. Ruytinx, P.; Proost, P.; Van Damme, J.; Struyf, S. Pro-Resolving FPR2 Agonists Regulate NADPH Oxidase-Dependent Phosphorylation of HSP27, OSR1, and MARCKS and Activation of the Respective Upstream Kinases. *Antioxidants* **2021**, *10*, 134. [\[CrossRef\]](#)
41. Heinz, S.; Freyberger, A.; Lawrenz, B.; Schladt, L.; Schmuck, G.; Ellinger-Ziegelbauer, H. Mechanistic Investigations of the Mitochondrial Complex I Inhibitor Rotenone in the Context of Pharmacological and Safety Evaluation. *Sci. Rep.* **2017**, *7*, 45465. [\[CrossRef\]](#)
42. Berkers, C.R.; Maddocks, O.D.; Cheung, E.C.; Mor, I.; Vousden, K.H. Metabolic regulation by p53 family members. *Cell Metab.* **2013**, *18*, 617–633. [\[CrossRef\]](#)
43. Liu, B.; Chen, Y.; Clair, D.K.S. ROS and p53: Versatile partnership. *Free Radic. Biol. Med.* **2008**, *44*, 1529–1535. [\[CrossRef\]](#) [\[PubMed\]](#)
44. Abbas, S.Y.; Nogueira, M.I.; Azmitia, E.C. Antagonist-induced increase in 5-HT1A-receptor expression in adult rat hippocampus and cortex. *Synapse* **2007**, *61*, 531–539. [\[CrossRef\]](#)
45. Toth, M.; Shenk, T. Antagonist-mediated down-regulation of 5-hydroxytryptamine type 2 receptor gene expression: Modulation of transcription. *Mol. Pharmacol.* **1994**, *45*, 1095–1100. [\[PubMed\]](#)
46. Annunziata, M.C.; Parisi, M.; Esposito, G.; Fabbrocini, G.; Ammendola, R.; Cattaneo, F. Phosphorylation Sites in Protein Kinases and Phosphatases Regulated by Formyl Peptide Receptor 2 Signaling. *Int. J. Mol. Sci.* **2020**, *21*, 3818. [\[CrossRef\]](#) [\[PubMed\]](#)
47. Estevão, M.S.; Carvalho, L.C.; Ferreira, L.M.; Fernandes, E.; Manuel, M.; Marques, B. Analysis of the antioxidant activity of an indole library: Cyclic voltammetry versus ROS scavenging activity. *Tetrahedron Lett.* **2011**, *52*, 101–106. [\[CrossRef\]](#)
48. Schepetkin, I.A.; Khlebnikov, A.I.; Giovannoni, M.P.; Kirpotina, L.N.; Cilibizzi, A.; Quinn, M.T. Development of small molecule non-peptide formyl peptide receptor (FPR) ligands and molecular modeling of their recognition. *Curr. Med. Chem.* **2014**, *21*, 1478–1504. [\[CrossRef\]](#) [\[PubMed\]](#)
49. Perianin, A.; Gaudry, M.; Marquetty, C.; Giroud, J.-P.; Hakim, J. Protective effect of indomethacin against chemotactic deactivation of human neutrophils induced by formylated peptide. *Biochem. Pharmacol.* **1988**, *37*, 1693–1698. [\[CrossRef\]](#)
50. Rajindrajith, S.; Devanarayana, N.M.; de Silva, H.J. *Helicobacter pylori* infection in children. *Saudi J. Gastroenterol.* **2009**, *15*, 86–94. [\[CrossRef\]](#)
51. Kumari, A.; Singh, R.K. Medicinal chemistry of indole derivatives: Current to future therapeutic perspectives. *Bioorg. Chem.* **2019**, *89*, 103021. [\[CrossRef\]](#)
52. Kumar, S. A brief review of the biological potential of indole derivatives. *Future J. Pharm. Sci.* **2020**, *6*, 121. [\[CrossRef\]](#)
53. Kaushik, N.K.; Kaushik, N.; Attri, P.; Kumar, N.; Kim, C.H.; Verma, A.K.; Choi, E.H. Biomedical Importance of Indoles. *Molecules* **2013**, *18*, 6620–6662. [\[CrossRef\]](#)



54. Bae, Y.-S.; Lee, H.Y.; Jo, E.J.; Kim, J.I.; Kang, H.-K.; Ye, R.D.; Kwak, J.-Y.; Ryu, S.H. Identification of Peptides That Antagonize Formyl Peptide Receptor-Like 1-Mediated Signaling. *J. Immunol.* **2004**, *173*, 607–614. [\[CrossRef\]](#)
55. Tak, P.P.; Firestein, G.S. NF- $\kappa$ B: A key role in inflammatory diseases. *J. Clin. Investig.* **2001**, *107*, 7–11. [\[CrossRef\]](#)
56. Liu, T.; Zhang, L.; Joo, D.; Sun, S.-C. NF- $\kappa$ B signaling in inflammation. *Signal Transduct. Target. Ther.* **2017**, *2*, 17023. [\[CrossRef\]](#) [\[PubMed\]](#)
57. Taniguchi, K.; Karin, M. NF- $\kappa$ B, inflammation, immunity and cancer: Coming of age. *Nat. Rev. Immunol.* **2018**, *18*, 309–324. [\[CrossRef\]](#) [\[PubMed\]](#)
58. Lin, Q.; Xu, H.; Chen, X.; Tang, G.; Gu, L.; Wang, Y. *Helicobacter pylori* cytotoxin-associated gene A activates tumor necrosis factor- $\alpha$  and interleukin-6 in gastric epithelial cells through P300/CBP-associated factor-mediated nuclear factor- $\kappa$ B p65 acetylation. *Mol. Med. Rep.* **2015**, *12*, 6337–6345. [\[CrossRef\]](#) [\[PubMed\]](#)
59. Devi, S.; Ansari, S.A.; Vadivelu, J.; Mégraud, F.; Tenguria, S.; Ahmed, N. *Helicobacter pylori* Antigen HP0986 (TieA) Interacts with Cultured Gastric Epithelial Cells and Induces IL8 Secretion via NF- $\kappa$ B Mediated Pathway. *Helicobacter* **2014**, *19*, 26–36. [\[CrossRef\]](#) [\[PubMed\]](#)
60. Atri, C.; Guerfali, F.Z.; Laouini, D. Role of Human Macrophage Polarization in Inflammation during Infectious Diseases. *Int. J. Mol. Sci.* **2018**, *19*, 1801. [\[CrossRef\]](#)
61. De Paulis, A.; Prevete, N.; Rossi, F.W.; Rivellese, F.; Salerno, F.; Delfino, G.; Liccardo, B.; Avilla, E.; Montuori, N.; Mascolo, M.; et al. *Helicobacter pylori* Hp(2–20) promotes migration and proliferation of gastric epithelial cells by interacting with formyl peptide receptors in vitro and accelerates gastric mucosal healing in vivo. *J. Immunol.* **2009**, *183*, 3761–3769. [\[CrossRef\]](#)
62. Kim, B.-H.; Yi, E.H.; Ye, S.-K. Signal transducer and activator of transcription 3 as a therapeutic target for cancer and the tumor microenvironment. *Arch. Pharmacol. Res.* **2016**, *39*, 1085–1099. [\[CrossRef\]](#) [\[PubMed\]](#)
63. Xie, X.; Yang, M.; Ding, Y.; Yu, L.; Chen, J. Formyl peptide receptor 2 expression predicts poor prognosis and promotes invasion and metastasis in epithelial ovarian cancer. *Oncol. Rep.* **2017**, *38*, 3297–3308. [\[CrossRef\]](#)
64. Jiang, N.; Dai, Q.; Su, X.; Fu, J.; Feng, X.; Peng, J. Role of PI3K/AKT pathway in cancer: The framework of malignant behavior. *Mol. Biol. Rep.* **2020**, *47*, 4587–4629. [\[CrossRef\]](#)
65. Wu, D. Signaling mechanisms for regulation of chemotaxis. *Cell Res.* **2005**, *15*, 52–56. [\[CrossRef\]](#) [\[PubMed\]](#)
66. Coffelt, S.B.; Tomchuck, S.L.; Zwezdaryk, K.J.; Danka, E.S.; Scandurro, A.B. Leucine Leucine-37 Uses Formyl Peptide Receptor-Like 1 to Activate Signal Transduction Pathways, Stimulate Oncogenic Gene Expression, and Enhance the Invasiveness of Ovarian Cancer Cells. *Mol. Cancer Res.* **2009**, *7*, 907–915. [\[CrossRef\]](#) [\[PubMed\]](#)
67. Leite, M.; Marques, M.S.; Melo, J.; Pinto, M.T.; Cavadas, B.; Aroso, M.; Gomez-Lazaro, M.; Seruca, R.; Figueiredo, C. *Helicobacter Pylori* Targets the EPHA2 Receptor Tyrosine Kinase in Gastric Cells Modulating Key Cellular Functions. *Cells* **2020**, *9*, 513. [\[CrossRef\]](#)
68. Page, T.H.; Smolinska, M.; Gillespie, J.; Urbaniak, A.M.; Foxwell, B.M. Tyrosine kinases and inflammatory signalling. *Curr. Mol. Med.* **2009**, *9*, 69–85. [\[CrossRef\]](#) [\[PubMed\]](#)
69. Gschwind, A.; Fischer, O.M.; Ullrich, A. The discovery of receptor tyrosine kinases: Targets for cancer therapy. *Nat. Rev. Cancer* **2004**, *4*, 361–370. [\[CrossRef\]](#)
70. Paletta-Silva, R.; Rocco-Machado, N.; Meyer-Fernandes, J.R. NADPH oxidase biology and the regulation of tyrosine kinase receptor signaling and cancer drug cytotoxicity. *Int. J. Mol. Sci.* **2013**, *14*, 3683–3704. [\[CrossRef\]](#) [\[PubMed\]](#)
71. Mittal, M.; Siddiqui, M.R.; Tran, K.; Reddy, S.P.; Malik, A.B. Reactive oxygen species in inflammation and tissue injury. *Antioxid. Redox Signal.* **2014**, *20*, 1126–1167. [\[CrossRef\]](#) [\[PubMed\]](#)
72. Dikalov, S. Crosstalk between mitochondria and NADPH oxidases. *Free Radic. Biol. Med.* **2011**, *51*, 1289–1301. [\[CrossRef\]](#)
73. Butcher, L.D.; den Hartog, G.; Ernst, P.B.; Crowe, S.E. Oxidative Stress Resulting From *Helicobacter pylori* Infection Contributes to Gastric Carcinogenesis. *Cell. Mol. Gastroenterol. Hepatol.* **2017**, *3*, 316–322. [\[CrossRef\]](#)
74. Fukai, T.; Ushio-Fukai, M. Cross-Talk between NADPH Oxidase and Mitochondria: Role in ROS Signaling and Angiogenesis. *Cells* **2020**, *9*, 1849. [\[CrossRef\]](#) [\[PubMed\]](#)
75. Magliozzi, L.; Maselli, V.; Almada, F.; Di Cosmo, A.; Mollo, E.; Polese, G. Effect of the algal alkaloid caulerpin on neuropeptide Y (NPY) expression in the central nervous system (CNS) of *Diplodus sargus*. *J. Comp. Physiol.* **2019**, *205*, 203–210. [\[CrossRef\]](#) [\[PubMed\]](#)
76. Chay, C.I.C.; Cansino, R.G.; Pinzón, C.I.E.; Torres-Ochoa, R.O.; Martínez, R. Synthesis and Anti-Tuberculosis Activity of the Marine Natural Product Caulerpin and Its Analogues. *Mar. Drugs* **2014**, *12*, 1757–1772. [\[CrossRef\]](#)
77. Maiti, B.C.; Thomson, R.H.; Mahendran, M. ChemInform Abstract: The structure of caulerpin, a pigment from caulerpa algae. *Chem. Informationsd.* **1978**, *9*, 32. [\[CrossRef\]](#)
78. Livak, K.J.; Schmittgen, T.D. Analysis of relative gene expression data using real-time quantitative PCR and the  $2^{-\Delta\Delta CT}$  Method. *Methods* **2001**, *25*, 402–408. [\[CrossRef\]](#) [\[PubMed\]](#)
79. Papaiani, M.; Paris, D.; Woo, S.L.; Fulgione, A.; Rigano, M.M.; Parrilli, E.; Tutino, M.L.; Marra, R.; Manganiello, G.; Casillo, A.; et al. Plant Dynamic Metabolic Response to Bacteriophage Treatment after *Xanthomonas campestris* pv. *campestris* Infection. *Front. Microbiol.* **2020**, *11*, 732. [\[CrossRef\]](#)
80. Fulgione, A.; Papaiani, M.; Cuomo, P.; Paris, D.; Romano, M.; Tuccillo, C.; Palomba, L.; Medaglia, C.; De Seta, M.; Esposito, N.; et al. Interaction between MyD88, TIRAP and IL1RL1 against *Helicobacter pylori* infection. *Sci. Rep.* **2020**, *10*, 15831. [\[CrossRef\]](#)

81. Cuomo, P.; Papaiani, M.; Fulgione, A.; Guerra, F.; Capparelli, R.; Medaglia, C. An Innovative Approach to Control, *H. pylori*-Induced Persistent Inflammation and Colonization. *Microorganisms* **2020**, *8*, 1214. [[CrossRef](#)] [[PubMed](#)]
82. Iannelli, D.; D'Apice, L.; Cottone, C.; Viscardi, M.; Scala, F.; Zoina, A.; Del Sorbo, G.; Spigno, P.; Capparelli, R. Simultaneous detection of cucumber mosaic virus, tomato mosaic virus and potato virus Y by flow cytometry. *J. Virol. Methods* **1997**, *69*, 137–145. [[CrossRef](#)]

GENE	PRIMER
<i>GAPDH</i> (Glyceraldehyde-3-Phosphate Dehydrogenase)	FW: 5'-CCTCTGACTTCAACAGCGACAC-3' RW: 5'-CACCACCCTGTTGCTGTAGCCA-3'
<i>TNF-α</i> (Tumor necrosis factor alpha)	FW: 5'-CCTGGTATGAGCCCATCTAT-3' RW: 5'-ACAGGGCAATGATCCCAAAGTA-3'
<i>IL8</i> (Interleukin 8)	FW: 5'-ACTTAGATGTCAGTGCATAAAGAC-3' RW: 5'-TTATGAATTCTCAGCCCTCTTCAA-3'
<i>IL6</i> (Interleukin 6)	FW: 5'-CCACTCACCTCTTCAGAACG-3' RW: 5'-CATCTTTGGAAGGTTCAAGTTG-3'
<i>SOD2</i> (Superoxide Dismutase 2)	FW: 5'-CTGATTGGACAAGCAGCAA-3' RW: 5'-CTGGACAAACCTCAGCCCTA-3'
<i>p53</i> (Tumor Protein 53)	FW: 5'-AGAGTCTATAGGCCACCCC-3' RW: 5'-GCTCGACGCTAGGATCTGAC-3'
	<b>PROBE</b>
<i>FPR1</i> (Formyl Peptide Receptor 1)	Hs04235426_s1
<i>FPR2</i> (Formyl Peptide Receptor 2)	Hs02759175_s1
<i>FPR3</i> (Formyl Peptide Receptor 3)	Hs00266666_s1
<i>GAPDH</i> (Glyceraldehyde-3-Phosphate Dehydrogenase)	Hs02786624_g1
<i>CCL2</i> (C-C Motif Chemokine Ligand 2)	Hs00234140_m1
<i>CCL3</i> (C-C Motif Chemokine Ligand 3)	Hs00234142_m1
<i>CCL5</i> (C-C Motif Chemokine Ligand 5)	Hs99999048_m1
<i>CCL7</i> (C-C Motif Chemokine Ligand 7)	Hs00171147_m1
<i>CXCL2</i> (C-X-C Motif Chemokine Ligand 2)	Hs00601975_m1

**Table S1. Primers and probes used for RT-qPCR.**

Primary Antibodies	Company	Dilution
Vinculin	Santa Cruz Biotechnology; mouse monoclonal antibody	1:10000
plkB-α (ser32/36) (phospho Inhibitor of Nuclear Factor Kappa B alpha)	Cell Signaling; rabbit monoclonal antibody	1:250
IκB-α (C-21) (Inhibitor of Nuclear Factor Kappa B)	Santa Cruz biotechnology; mouse monoclonal antibody	1:250
pERK1/2 (th202/tyr204) (phospho Extracellular signal-Regulated Kinases)	Cell Signaling; rabbit monoclonal antibody	1:1000
ERK1/2 (C-9); sc-514302 (Extracellular signal-Regulated Kinases)	Santa Cruz biotechnology; rabbit monoclonal antibody	1:1000
pAkt (ser473) (phospho protein kinase B)	Santa Cruz biotechnology; rabbit monoclonal antibody	1:500
Akt1 (Protein kinase B)	Millipore cat 07416 Lot 28745; mouse monoclonal antibody	1:500
pSTAT3 (tyr705) (phosphor Signal Transducer and Activator of Transcription 3)	Cell Signaling; rabbit monoclonal antibody	1:500
STAT3 (F-2); sc-8019 (Signal Transducer and Activator of Transcription 3)	Santa Cruz biotechnology	1:500
<b>Secondary Antibodies</b>	<b>Company</b>	<b>Dilution</b>
Goat Anti-Rabbit HRP	sc-2027 Santa Cruz Biotechnology	1:5000
Goat Anti-Mouse HRP	sc-2025 Santa Cruz Biotechnology	1:5000

**Table S2. Antibodies used for Western Blot analysis.**



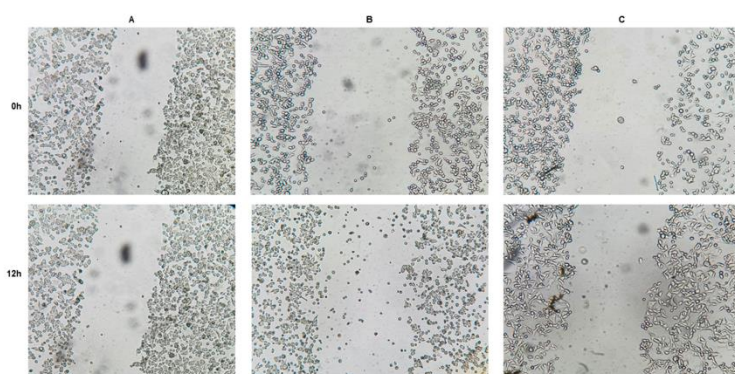


**Figure S1. Cau prevents Hp(2-20)-induced cell migration.** Cell migration by in vitro scratch assay was performed on AGS cells differently treated: (A) untreated; (B) Hp(2-20) 25  $\mu$ M; (C) Cau 15  $\mu$ M for 30 minutes and then Hp(2-20) 25  $\mu$ M. Cells were incubated for 12 hours and pictures were captured before and after cell incubation.

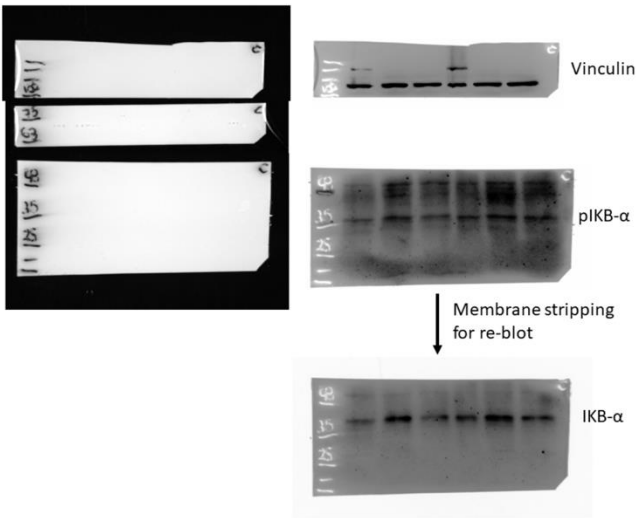
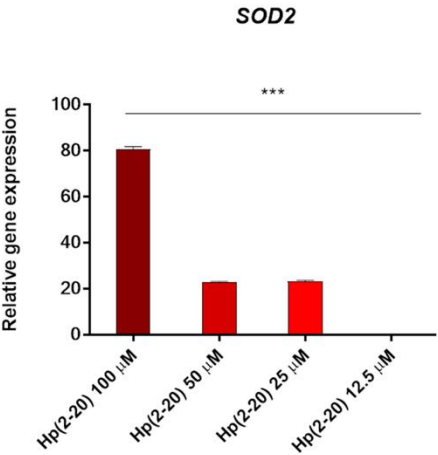


Figure S2. Uncropped and unadjusted Western Blot images corresponding to Figure 2B



*Figure S3. Hp(2-20) increases SOD2 gene in a dose-dependent manner.* Relative gene expression of *SOD2* by quantitative real-time PCR (qPCR) in cells treated with Hp(2-20) at different concentrations, as indicated. All samples were normalized to GAPDH as reference housekeeping gene. Furthermore, relative gene expression was normalized to basal activity (untreated control), in order to obtain relative fold expression. Graphs report the results of at least three independent experiments, represented as means  $\pm$  SD. Statistical analysis was performed by GraphPad Prisma software, using one-way ANOVA followed by Bonferroni post-hoc correction. \*\*\*  $p < 0.0001$ .

## **CHAPTER 4**

***Metabolomics: A footprinting  
metabolic approach to assess cell  
response to Caulerpin treatment in  
modulating Helicobacter pylori  
systemic effects***

## 4.1 Introduction

One of the most important discoveries of the last decades is that metabolism and immune system are closely connected. Both are tightly regulated and play vital roles in the maintenance of cell homeostasis (Hotamisligil, 2006). Dysregulation of any of these two systems may lead to chronic metabolic disorders, such as obesity, insulin resistance and type two diabetes, which represent a severe threat to the global population (Alwarawrah, 2018).

The immune system is essential for the organism's survival; it mounts an effective defensive response against pathogens, by inducing inflammation. *H. pylori* establishes a chronic infection, which leads to a persistent inflammatory state (Salama et al., 2013). Chronic inflammation is the main cause of metabolic disorders (Franceschi et al., 2014). Consequently, *H. pylori* represents a serious risk for human health, made worst since it is not a pathogen easy to eradicate (Jenks, 2002). In this context, the use of an anti-inflammatory agent makes possible to preserve the physiological integrity of gastric and extra-gastric functions of the host.

In the previous chapter § 3.4, we have demonstrated that Caulerpin could inhibit FPRs and consequently modulate both immune and metabolic functions of the host.

Metabolomics is an effective tool to analyze cell biochemical alterations. Cells can secrete enzymes and metabolites into the extracellular environment, which in turn can interact and modify the extracellular metabolic profile (Villas-Bôas et al., 2006). Here, we used the NMR-based footprinting metabolomics approach, to characterize *in vitro* systemic metabolic changes due to *H. pylori*-induced inflammation and investigate the capacity of Caulerpin to modulate them. We investigated whether *H. pylori* culture filtrate (Hpcf) promotes metabolic changes responsible for systemic effects, which could explain the possible pathogenic mechanism of systemic disorders associated with *H. pylori* inflammation, validating and implementing the results reported in Chapter 1. Furthermore, we compared metabolic changes in presence or absence of Caulerpin treatment, in order to define its beneficial anti-inflammatory effects.

## 4.2 Materials and methods

### 4.2.1 Cell culture

Human gastric AGS cell line (ATCC, Manassas, VA, USA, #CRL-1739) was maintained in Dulbecco's modification of Eagle's medium, high glucose (DMEM; Microtech, Naples, Italy), supplemented with 10% fetal bovine serum (FBS; Microtech, Naples, Italy), 1% penicillin/streptomycin (Gibco, Waltham, MA, USA) and 1% L-glutamine (Gibco, Waltham, MA, USA) in a humidified atmosphere at 37°C and 5% CO<sub>2</sub>.

### 4.2.2 *Helicobacter pylori* culture filtrate preparation

*H. pylori* culture filtrate was prepared as described in Chapter 3, § 3.4. In detail, *H. pylori* P12 strains, kindly provided by Dr. Marguerite Clyne (University College Dublin), were cultured on selective Columbia agar (Oxoid, Basingstoke, Hampshire, UK) containing 7% (v/v) defibrinated horse blood (Oxoid, Basingstoke, Hampshire, UK) supplemented with an antibiotic mix (DENT or Skirrow, respectively, Oxoid, Basingstoke, Hampshire, UK). Bacteria plates were incubated for 3–4 days in a capnophilic atmosphere with 10% CO<sub>2</sub> at 37°C. Once grown on the plate, bacteria were scraped using brain heart infusion (BHI Oxoid, Basingstoke, Hampshire, UK) and measured at optical density at 600 nm (OD600) considering 1 OD600 =  $1 \times 10^8$  bacteria/mL. In order to prepare *H. pylori* culture filtrate (Hpcf),  $2 \times 10^7$  bacteria/mL were cultured in liquid DMEM (Euroclone, Milan, Italy), supplemented with 10% fetal bovine serum (FBS; Euroclone, Milan, Italy) and incubated in a capnophilic atmosphere with 10% CO<sub>2</sub> at 37°C. After 24 h, bacterial suspension was centrifuged at 10,000 g for 10 min to remove bacteria and the supernatant was filtered by using a 0.22 µm filter (Euroclone, Milan, Italy). The obtained culture filtrate was stored at –80°C until use.

Chapter 4

### 4.2.3 Cell culture for footprint metabolite profiling by NMR analysis

AGS cells were split at 80-90% of confluence, seeded ( $2 \times 10^6$  per flask) in 16 T25 culture flasks (Nunc™, ThermoFischer, Waltham, MA, USA) to give four biological replicates at each condition [1) untreated cells; 2) cells stimulated with Hpcf for 2 hours; 3) cells treated with Caulerpin 15 µM for 2.5 hours; 4) cells pretreated with Caulerpin 15 µM for 30 minutes and then stimulated with Hpcf for

2 hours] and incubated at 37°C in a 5% CO<sub>2</sub> atmosphere overnight. After cell attachment, the medium was replaced, and cells were incubated as reported above for 2.5 hours. After this incubation period, growth medium was collected and centrifugated at 3000 x g for 10 minutes at 4°C, to remove cells and cell debris. Finally, it was stored at -80°C until NMR-based metabolomics analysis.

#### 4.2.4 NMR sample preparation

To achieve the NMR-based footprinting metabolomics analysis, growth media were rapidly defrosted and 630 µL of each fluid sample were pipetted into eppendorfs containing 70 µL of <sup>2</sup>H<sub>2</sub>O containing sodium 3-(trimethylsilyl)-2,2,3,3-tetradeuteropropionate (TSP) 0.1 mM and sodium azide 3 mM as antimicrobial agent, reaching 700 µL of total volume.

#### 4.2.5 NMR spectra acquisition

NMR spectra were recorded on a Bruker Avance III-600 MHz spectrometer (Bruker BioSpin GmbH, Rheinstetten, Germany), equipped with a TCI CryoProbe<sup>TM</sup> fitted with a gradient along the Z-axis, at a probe temperature of 300K (27°C). One-dimensional (<sup>1</sup>H-NMR) spectra were acquired by using the excitation sculpting sequence for water suppression (Hwang and Shaka, 1995). Two-dimensional (2D) homonuclear (<sup>1</sup>H-<sup>1</sup>H; TOCSY) spectra were acquired using MLEV-17 pulse sequence, incorporating the excitation sculpting sequence (Bax and Davis, 1985; Griesinger et al., 1988). The resonances of both 1D and homonuclear 2D spectra were referenced to internal sodium 3-(trimethylsilyl)-2,2,3,3-tetradeuteropropionate (0.1 mM; TSP) which was assumed to resonate at δ = 0.00 ppm. Two-dimensional heteronuclear (<sup>1</sup>H-<sup>13</sup>C; HSQC) spectra were recorded on the spectrometer operating at 150.90 MHz for <sup>13</sup>C, using pre-saturation for water suppression (Kay et al., 1992; Schleucher et al., 1994). HSQC resonances spectra were referenced to the lactate doublet (βCH<sub>3</sub>), assumed at 1.33 ppm for <sup>1</sup>H and 20.76 ppm for <sup>13</sup>C.

Chapter 4

#### 4.2.6 NMR data processing

To obtain cell supernatants datasets, the following spectral area were selected: 9.50-0.50 ppm. Each proton spectrum was automatically segmented into integrated regions (buckets) of 0.02 ppm, using the AMIX 3.6 package (Bruker Biospin, Germany). The

residual water resonance region (5.00-4.58 ppm) was excluded, and the binned regions were normalized to the total spectrum area. Multivariate statistical data analysis was applied to each dataset to differentiate culture medium profiles of Hpcf-stimulated cells and Caulerpin-treated cells, through NMR spectra, according to their different metabolic content. Selected statistical models were also created to elucidate Hpcf-induced metabolic changes, by comparing Hpcf alone and culture medium of Hpcf-stimulated cells. Each integrated dataset was reshaped as a matrix and imported into SIMCA-P 14 package (Umetrics, Umea, Sweden) where unsupervised PCA, supervised PLS-DA and OPLS-DA discriminant analyses were performed. PCA was first applied to check outliers and uncover initial trends within the dataset by investigating the systematic variation in the data matrix, in order to identify trends and clusters. Once assessed data homogeneity, PLS-DA or OPLS-DA discriminant analysis was employed to improve group discrimination. The performance of each elaborated model was evaluated via the parameters R<sup>2</sup> and Q<sup>2</sup>, respectively indicating the goodness of fit and the goodness of prediction. Selected isolated signals with  $|p_{corr}| \geq 0.7$ , VIP >1 (Variable Importance in the Projection) were then considered for univariate statistical analysis.

#### **4.2.7 Network Analysis**

Enrichment analysis on selected and more representative metabolites was applied using the 'diffusion' and 'pagerank' method computed by the FELLA package in R (Picart-Armada et al., 2017; Picart-Armada et al., 2018). Starting from the set of altered compounds, such analysis suggests affected reactions, enzymes, modules and pathways using label propagation in a knowledge model network based on Homo sapiens database in KEGG. The resulting network and subnetwork are visualized and exported in related plot and table with a threshold of  $p < 0.05$ .

#### **4.2.8 Statistical Analysis**

One-way analysis of variance (ANOVA) followed by Bonferroni post hoc correction was used to determine metabolites ~~statistically~~ significant among different groups. ~~p values < 0.05 were~~ Chapter 4 statistically significant.

### **4.3 Results and Discussion**



#### 4.3.1 *Helicobacter pylori* culture filtrate may promote a systemic metabolic reprogramming

Growth medium from AGS cells incubated or not with *H. pylori* culture filtrate (CTR and AGS+Hpcf, respectively) were analyzed by NMR-spectroscopy. In figure 1, footprint spectra of both CTR and AGS+HPCF classes are illustrated.

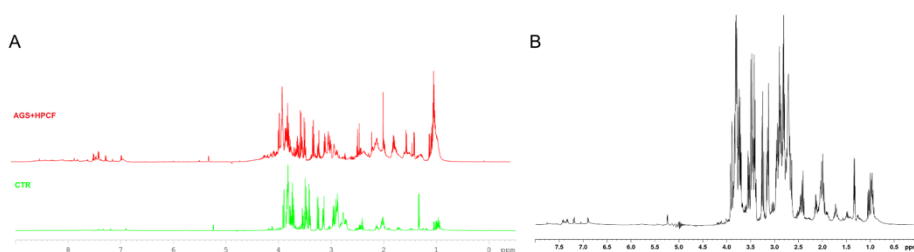
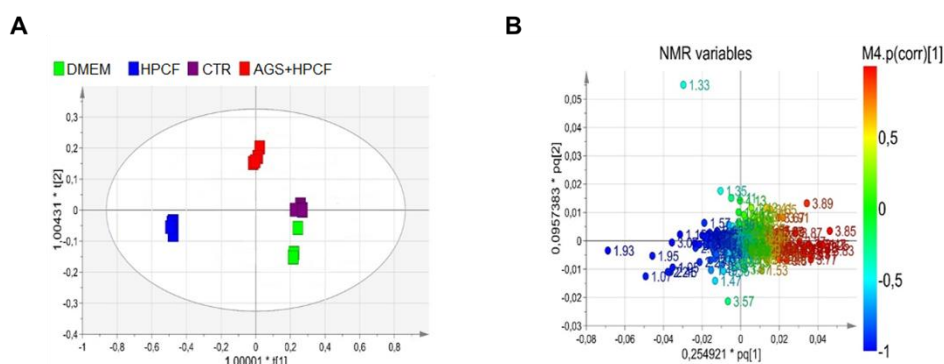


**Figure 1.** (A) Representative  $^1\text{H}$  NMR spectra of the growth medium from AGS cells incubated or not with *H. pylori* culture filtrate (red or green spectrum, respectively). (B) Representative  $^1\text{H}$  NMR spectrum of the medium used to grow both cells and *H. pylori*.

Noticeably, all components of DMEM medium (sugars, amino acids and vitamins), used for both *H. pylori* and cells growth, contribute to NMR spectra. In this context, because of the high levels of normal medium components, it is difficult to detect extracellular metabolic changes associated with *H. pylori* infection. Therefore, orthogonal projection to latent structures-discriminant analysis (OPLS-DA) was performed in order to select and highlight data variation, which is strictly related to cell condition, by comparing spectra from growth medium of AGS cells incubated or not with *H. pylori* culture filtrate (AGS+HPCF and CTR, respectively) with both the *H. pylori* culture filtrate (HPCF) and the medium used to grow both *H. pylori* and cells (DMEM). In this way, it was easier to examine metabolic differences connected with extracellular metabolic changes resulted from cell metabolites uptake or excretion, in presence of *H. pylori*, in spite of DMEM medium components.

A three component OPLS-DA model was built with parameters  $R^2=88\%$  and  $Q^2=69\%$  which represent how well the model fits data and the ability in predicting new data, respectively. The associated scores and loadings plots are reported in Figure 2A; 3A and 2B; 3B, respectively.

The  $t[1]$  component in Figure 2A clearly distinguishes the metabolic profile of CTR and DMEM classes (placed at  $t[1]$  positive coordinates) from the metabolic profile of the HPCF class (placed at  $t[1]$  negative coordinates), likely due to metabolic changes induced by *H. pylori*, which can produce or uptake essential metabolites, thus altering the metabolic content of its growth medium. Figure 2A also distinguishes the metabolic profile of HPCF and DMEM classes (placed at  $t[2]$  negative coordinates) from the metabolic profile of the AGS+HPCF class (placed at  $t[2]$  positive coordinates), likely due to metabolic differences attributable to *H. pylori* exposure. Finally, the  $t[3]$  component depicted in Figure 3A, clearly distinguishes the metabolic profile of AGS+HPCF and DMEM classes (placed at  $t[3]$  negative coordinates) from the profile of HPCF and CTR classes (placed at  $t[3]$  positive coordinates), likely due to the role of DMEM medium in metabolic alterations. The pattern of metabolites responsible for the separation among various classes is represented in figures 2B and 3B.



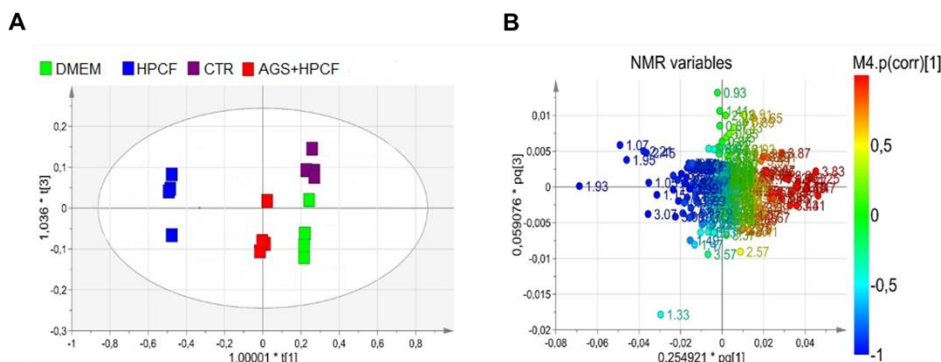


**Figure 3.** Orthogonal Projection to Latent Structure Discriminant Analysis (OPLS-DA) of medium samples. **(A)** Scores plot showing a distinct separation of CTR and HPCF classes (violet and blue squares, respectively) from DMEM and AGS+HPCF classes (green and red squares, respectively). **(B)** Loading plot indicating NMR variables (chemical shift) of metabolites responsible for between-classes separation, characterized by  $|p(corr)|$  value  $> 0.7$ .

*H. pylori* is known to be highly adapted parasite. To grow and survive, *H. pylori* requires low oxygen tension and specific growth factors. It can metabolize many amino acids as fast energy source (Nedenskov, 1994; Stark et al., 1997). As expected, results reported in Figure 4 show reduced levels of the amino acids: proline, valine, leucine, lysine, arginine, threonine, aspartate, and glutamate in *H. pylori* culture filtrate class (HPCF), compared to samples from the medium used to grow *H. pylori* without the bacterium (DMEM), and, consistently, increased levels of products derived from the amino acid anaerobic metabolism, such as: acetate, propionate and lactate. The amino acid ornithine, instead, was found upregulated in HPCF class compared to DMEM one (Figure 4). Ornithine is the product of the arginine hydrolysis, reaction responsible for urea production, which is fundamental for *H. pylori* infection. *H. pylori*, in fact, produces large amounts of the enzyme urease, which catalyzes the reaction of conversion of urea into ammonia, thus increasing gastric pH and favoring its survival and colonization (Olivera-Severo et al., 2017). Finally, HPCF class was found to downregulate glucose level, compared to DMEM class (Figure 4), providing a further explanation about increased levels of the metabolite lactate, as product of the anaerobic glucose metabolism (Chalk et al., 1994).

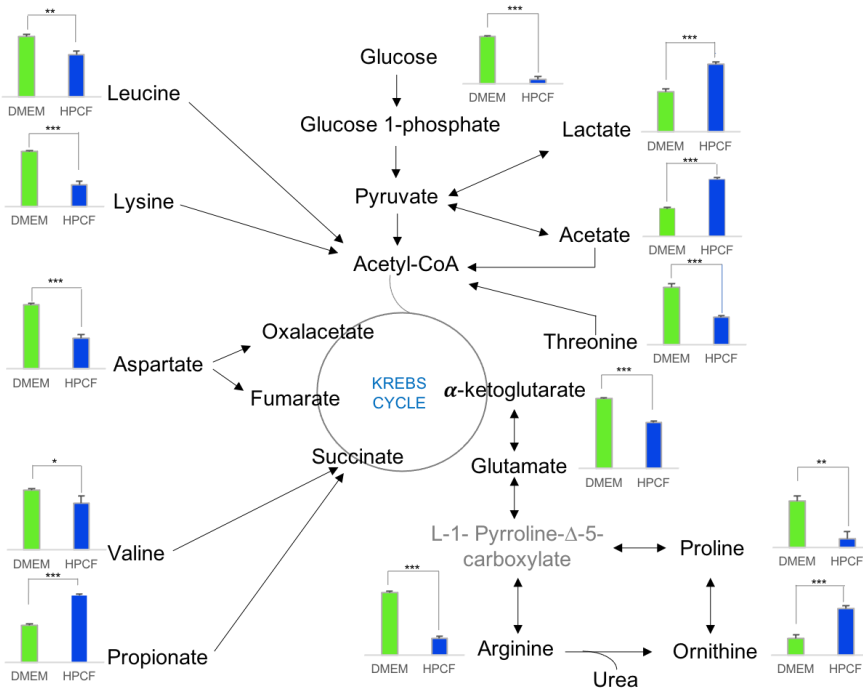


**Figure 4.** Schematic representation of the metabolite profile of growth medium from HPCF and DMEM samples. Bar graphs show means  $\pm$  SD. \*  $p < 0.05$ ; \*\*  $p < 0.001$ ; \*\*\*  $p < 0.0001$ .

Lactate is a clear metabolic signature of the inflammatory state (Certo et al., 2021). Usually, cells respond to stress conditions by metabolizing glucose into lactate. In line with this finding, higher levels of lactate were found in the growth medium from the AGS+HPCF class, compared to both HPCF and CTR classes (Figure 5), suggesting that Hpcf exposure promotes lactate secretion in the extracellular environment, which can lead to a metabolic reprogramming, enhancing fatty acid synthesis and exacerbating the inflammatory response (Pucino et al., 2019). Both inflammation and fatty acids are key contributors to chronic metabolic diseases (Wen et al., 2011). A large body of evidence suggested that elevation of circulating fatty acids is the major metabolic disorder leading to obesity and insulin resistance, which can cause type two diabetes (Boden, 2003; Fryk et al., 2021). These results support the hypothesis that *H. pylori* infection interferes with metabolic processes outside the stomach, predisposing to chronic systemic diseases, such as insulin resistance and type two diabetes. This conclusion was further

confirmed by the correlation analysis, which detected insulin secretion and type two diabetes mellitus as the main altered metabolic pathways (Figure 6).

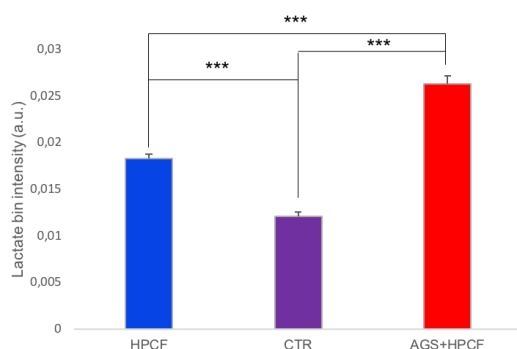


**Figure 5.** Expression level of lactate in the growth medium of AGS cells incubated or not with Hpcf (CTR and AGS+HPCF, respectively) or in the H. pylori culture filtrate (HPCF). Bar graphs show means  $\pm$  SD. \*\*\*  $p < 0.0001$ .

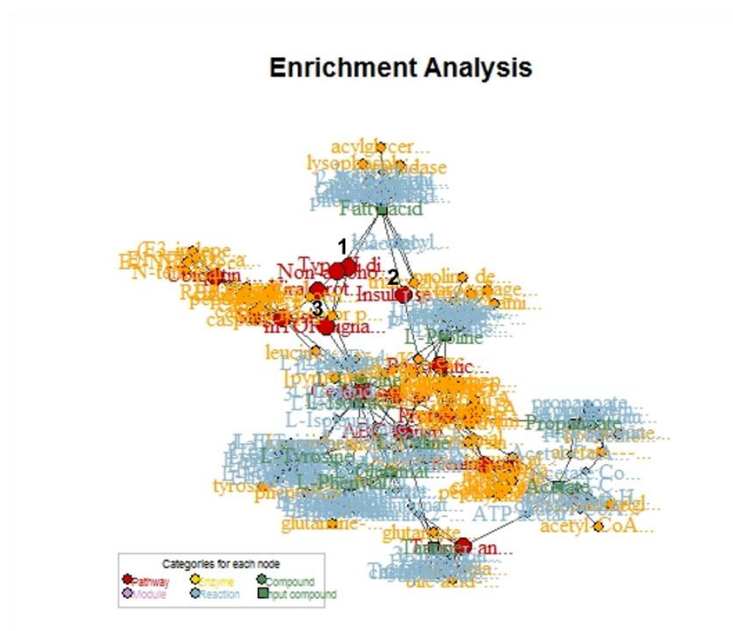


**Figure 6.** Connected network of metabolites differently expressed between growth medium from AGS cells incubated or not with Hpcf (CTR and AGS+HPCF). This image provides information on the pathways (red) in which metabolites are involved, their crosstalk and reactions and how metabolites reached the highlighted pathways. **(1)** Type 2 Diabetes; **(2)** insulin secretion and **(3)** mTOR signaling pathway are the major pathways responsible for class separation.

### 4.3.2 Caulerpin may recover the *H. pylori* culture filtrate-induced metabolic changes

To investigate the effects of Caulerpin in modulating the footprint metabolic changes induced by Hpcf, growth medium from AGS cells incubated in the absence or presence of Caulerpin treatment was analyzed by NMR-spectroscopy. More specifically, NMR analysis of growth medium from: 1) untreated cells (CTR); 2) Hpcf-stimulated cells (AGS+HPCF); 3) Caulerpin-treated cells (CAU) and 4) cells treated with Caulerpin and stimulated with Hpcf (CAU+HPCF) was performed and the resultant spectra (Figure 7) were examined by performing the OPLS-DA.

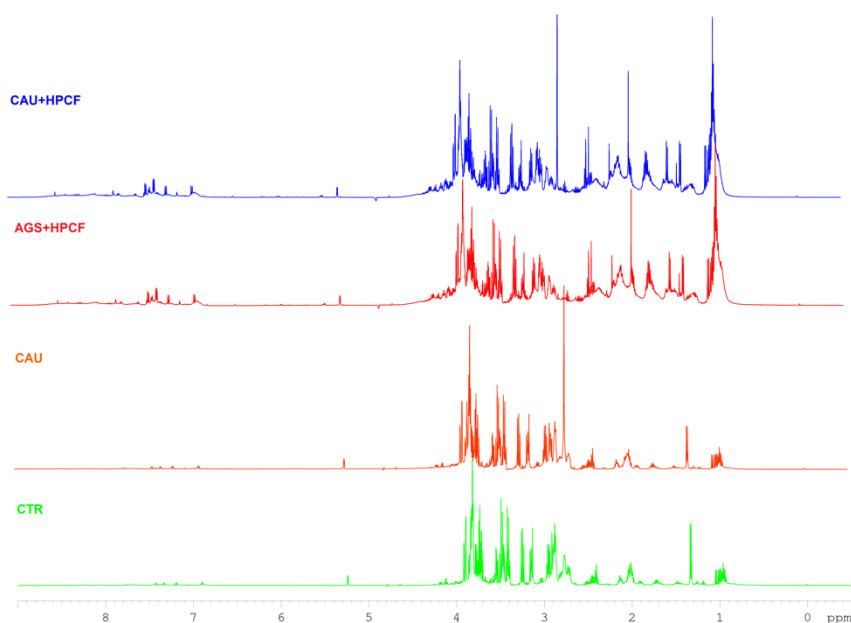


**Figure 7.** Representative <sup>1</sup>H NMR spectra of the growth medium from AGS cells incubated or not with *H. pylori* culture filtrate (red or green spectrum, respectively), treated with Caulerpin alone (orange spectrum) and incubated with *H. pylori* culture filtrate, but treated with Caulerpin (blue spectrum).

A strong OPLS-DA model was built with three predictive components with parameters  $R^2=93\%$  and  $Q^2=83\%$ , which represent how well the model fits data and the ability in predicting new data, respectively. The associated OPLS-DA scores and loadings plots are represented in Figure 8A; 9A and 8B; 9B, respectively. In figure 8A, scores plot shows a distinct separation

between CTR/CAU classes (placed at  $t[1]$  positive coordinates) and AGS+HPCF/CAU+HPCF classes (placed at  $t[1]$  negative coordinates), indicating that the  $t[1]$  component accounts for metabolic changes induced by Hpcf. In addition, Figure 7A clearly distinguishes the metabolic profile of CAU and CAU+HPCF classes (placed at  $t[2]$  negative coordinates) from the metabolic profile of CTR and AGS+HPCF classes (placed at  $t[2]$  positive coordinates), suggesting that  $t[2]$  component accounts for metabolic changes associated with Caulerpin treatment. Figure 8A, finally, provides more information about Caulerpin influence. It shows a cluster between CTR and CAU classes (placed at  $t[3]$  zero coordinates), and a clear separation between AGS+HPCF and CAU+HPCF classes (placed at  $t[3]$  negative coordinates and  $t[3]$  positive coordinates, respectively). This suggests that Caulerpin alone doesn't alter the cell footprint metabolic profile but promotes metabolic changes in presence of inflammatory stimuli. The pattern of metabolites responsible for the separation among four classes is represented in figures 8B and 9B.

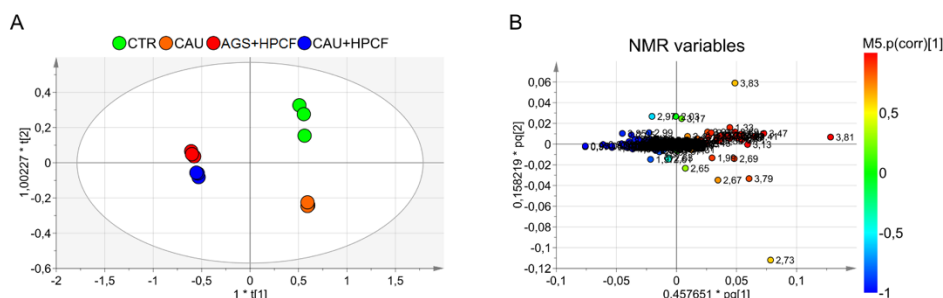
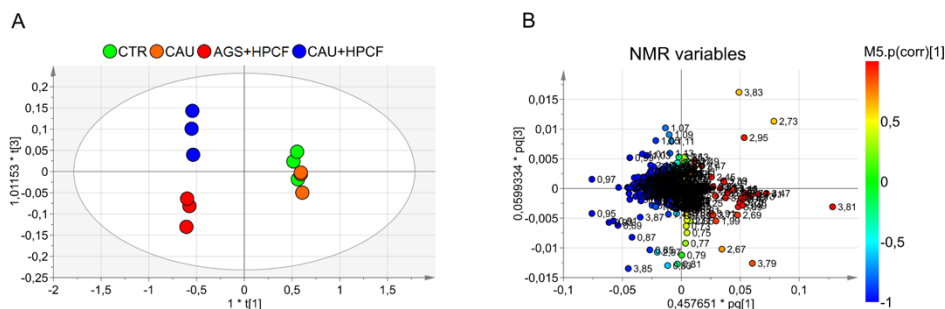


**Figure 8.** Orthogonal Projection to Latent Structure Discriminant Analysis (OPLS-DA) of growth medium samples. **(A)** Scores plot showing a distinct separation of CTR and CAU samples (green and orange circles, respectively) from AGS+HPCF and CAU+HPCF samples (red and blue circles, respectively) along the first component  $t[1]$ , and a distinct separation of CAU and CAU+HPCF samples (orange and blue circles, respectively) from CTR and AGS+HCF samples (green and red circles, respectively) along the second component  $t[2]$ . **(B)** Loading plot indicating NMR variables (chemical shift) of metabolites responsible for between-classes separation, characterized by  $|p(\text{corr})|$  value  $> 0.7$ .







inhibition (Penberthy, 2009; Ma et al., 2016). Nicotinamide has also been reported to contribute to the maintenance of the normal cellular metabolism through modulation of the mTOR pathway [which was found dysregulated in Hpcf stimulated cells (Figure 5)] and prevention of excessive lactate production (Maiese, 2020). Based on these evidences, nicotinamide might be useful in modulating and preventing metabolic disorders (Maiese, 2020). Therefore, reduced levels of nicotinate in the growth medium of cells stimulated with Hpcf but treated with Caulerpin indicate that in the presence of Caulerpin, cells use nicotinate for NAD<sup>+</sup> production, in order to temperate the Hpcf-induced inflammatory response and promote cell energy homeostasis, thus offering the opportunity to overcome *H. pylori*-associated systemic risks. In addition, reduced levels of two branched chain amino acids (BCAA, leucine and isoleucine) were found in the growth medium of cells incubated with Hpcf and treated with Caulerpin (CAU+HPCF), compared to those incubated with Hpcf and not treated with Caulerpin (AGS+HPCF) (Figure 10C). It is widely recognized that high extracellular levels of BCAA are directly associated with metabolic disorders (Adeva et al., 2012). Thus, taken together, obtained results suggest the contribution of *H. pylori* inflammation in metabolic diseases and the role of Caulerpin in modulating *H. pylori* detrimental effects by reducing the inflammatory response.

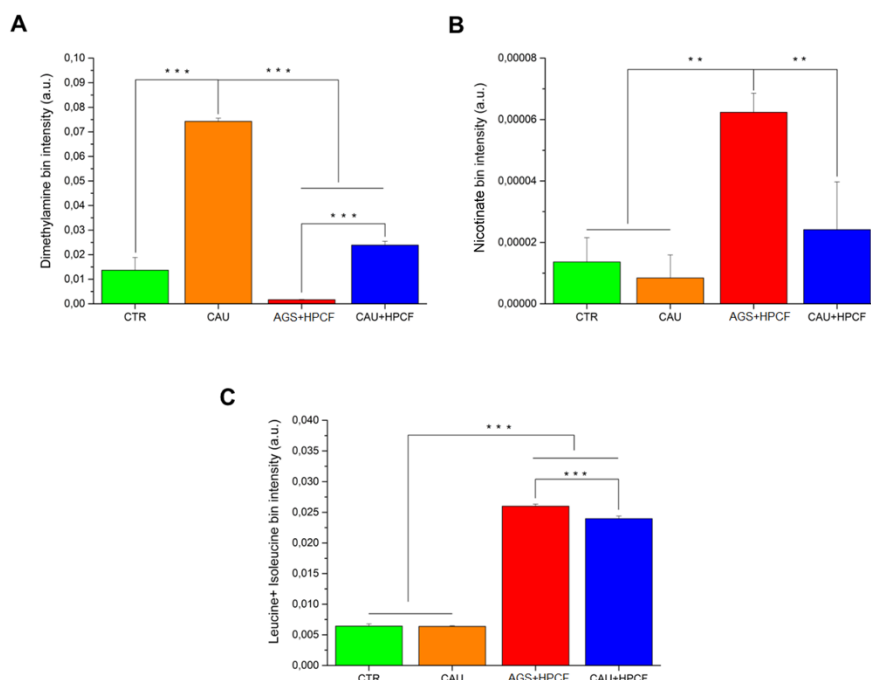


**Figure 10.** Expression level of: **(A)** dimethylamine; **(B)** nicotinate; **(C)** leucine and isoleucine in the growth medium of AGS cells incubated or not with Hpcf (CTR and AGS+HPCF, respectively), incubated with Hpcf and treated with Caulerpin (CAU+HPCF) and treated with Caulerpin alone (CAU). Bar graphs show means  $\pm$  SD. \*\* p < 0.001; \*\*\* p < 0.0001.

## 4.4 Conclusion

In conclusion, this study explored the cell growth medium metabolomics, in order to characterize systemic metabolic alterations due to *H. pylori*-induced inflammation. It showed that *H. pylori*-associated inflammation causes metabolite alteration and dysregulation of the following metabolic pathways: mTOR signaling pathway, insulin secretion and type two diabetes mellitus, suggesting the role of *H. pylori* infection and, in particular, of the resulting inflammation, in the pathogenesis of extra-gastric diseases. In addition, the present study investigated the efficacy of Caulerpin in modulating the inflammatory response associated with

*H. pylori* infection, showing its ability in recovering Hpcf-induced metabolic changes.

Our results suggest lactate as the main metabolite for predicting the risk of metabolic disorders occurring during *H. pylori* infection and nicotinate for evaluating the efficacy of Caulerpin in mitigating the *H. pylori*-induced inflammation and related clinical outcomes.

## References

- Adeva, M.M.; Calviño, J.; Souto, G.; Donapetry, C. Insulin resistance and the metabolism of branched-chain amino acids in humans. *Amino Acids*. **2012**; 43(1):171-81.
- Alwarawrah, Y.; Kiernan, K.; MacIver, N.J. Changes in Nutritional Status Impact Immune Cell Metabolism and Function. *Front Immunol*. **2018**; 9:1055.
- Bax, A.; Davis, D.G. MLEV-17-based two-dimensional homonuclear magnetization transfer spectroscopy. *J Magn Reson*. **1985**; 65(2):355.
- Boden, G. Effects of free fatty acids (FFA) on glucose metabolism: significance for insulin resistance and type 2 diabetes. *Exp Clin Endocrinol Diabetes*. **2003**; 111(3):121-4.
- Certo, M.; Tsai, C.H.; Pucino, V.; Ho, P.C.; Mauro, C. Lactate modulation of immune responses in inflammatory versus tumour microenvironments. *Nat Rev Immunol*. **2021**; 21(3):151-161.
- Chalk, P.A.; Roberts, A.D.; Blows, W.M. Metabolism of pyruvate and glucose by intact cells of *Helicobacter pylori* studied by <sup>13</sup>C NMR spectroscopy. *Microbiology*. **1994**; 140 (Pt 8):2085-92.
- Franceschi, F.; Zuccalà, G.; Roccarina, D.; Gasbarrini, A. Clinical effects of *Helicobacter pylori* outside the stomach. *Nat Rev Gastroenterol Hepatol*. **2014**; 11(4):234-42.
- Fryk, E.; Olausson, J.; Mossberg, K.; Strindberg, L.; Schmelz, M.; Brogren, H.; Gan, L.M.; Piazza, S.; Provenzani, A.; Becattini, B.; et al. Hyperinsulinemia and insulin resistance in the obese may develop as part of a homeostatic response to elevated free fatty acids: A mechanistic case-control and a population-based cohort study. *EBioMedicine*. **2021**; 65:103264.
- Griesinger, C.; Otting, G.; Wuethrich, K.; Ernst, R.R. Clean TOCSY for proton spin system identification in macromolecules. *J Am Chem Soc*. **1988**; 110(23):7870.
- Güven, K.C.; Percot, A.; Sezik, E. Alkaloids in marine algae. *Mar Drugs*. **2010**; 8(2):269-84.
- Hotamisligil, G.S. Inflammation and metabolic disorders. *Nature*. **2006**; 444(7121):860-7.
- Hwang, T.L.; Shaka, A.J. Water Suppression That Works. Excitation Sculpting Using Arbitrary Wave-Forms and Pulsed-Field Gradients. *J Magn Reso. Ser*. **1995**; 112(2):275.
- Jenks, P.J. Causes of failure of eradication of *Helicobacter pylori*. *BMJ*. **2002**; 325(7354):3-4.
- Kay, L.E.; Keifer, P.; Saarinen, T. Pure absorption gradient enhanced heteronuclear single quantum correlation spectroscopy with improved sensitivity. *J Am Chem Soc*. **1992**; 114(26):10663.
- Lucena, A.M.M.; Souza, C.R.M.; Jales, J.T.; Guedes, P.M.M.; de Miranda, G.E.C.; de Moura, A.M.A.; Araújo-Júnior, J.X.; Nascimento, G.J.; Scortecci, K.C.; Santos, B.V.O.; Souto, J.T. The Bisindole Alkaloid

- Caulerpin, from Seaweeds of the Genus *Caulerpa*, Attenuated Colon Damage in Murine Colitis Model. *Mar Drugs*. **2018**; 16(9):318.
- Ma, Y.; Bao, Y.; Wang, S.; Li, T.; Chang, X.; Yang, G.; Meng, X. Anti-Inflammation Effects and Potential Mechanism of Saikosaponins by Regulating Nicotinate and Nicotinamide Metabolism and Arachidonic Acid Metabolism. *Inflammation*. **2016**; 39(4):1453-61.
- Maiese, K. New Insights for nicotinamide: Metabolic disease, autophagy, and mTOR. *Front Biosci* (Landmark Ed). **2020**; 25:1925-1973.
- Nedenskov, P. Nutritional requirements for growth of *Helicobacter pylori*. *Appl Environ Microbiol*. **1994**; 60(9):3450-3.
- Olivera-Severo, D.; Uberti, A.F.; Marques, M.S.; Pinto, M.T.; Gomez-Lazaro, M.; Figueiredo, C.; Leite, M.; Carlini, C.R. A New Role for *Helicobacter pylori* Urease: Contributions to Angiogenesis. *Front Microbiol*. **2017**; 8:1883.
- Penberthy, W.T. Nicotinamide adenine dinucleotide biology and disease. *Current Pharmaceutical Design*. **2009**; 15:1-2.
- Picart-Armada, S.; Fernández-Albert, F.; Vinaixa, M.; Rodríguez, M.A.; Aivio, S.; Stracker, T.H.; Yanes, O.; Perera-Lluna, A. Null diffusion-based enrichment for metabolomics data. *PLoS One*. **2017**; 12(12):e0189012.
- Picart-Armada, S.; Fernández-Albert, F.; Vinaixa, M.; Yanes, O.; Perera-Lluna, A. FELLA: an R package to enrich metabolomics data. *BMC Bioinformatics*. **2018**; 19(1):538.
- Pucino, V.; Certo, M.; Bulusu, V.; Cucchi, D.; Goldmann, K.; Pontarini, E.; Haas, R.; Smith, J.; Headland, S.E.; Blighe, K., et al. Lactate Buildup at the Site of Chronic Inflammation Promotes Disease by Inducing CD4+ T Cell Metabolic Rewiring. *Cell Metab*. **2019**; 30(6):1055-1074.e8.
- Rodrigues, F.A.P.; Santos, A.D.D.C.; de Medeiros, P.H.Q.S.; Prata, M.M.G.; Santos, T.C.S.; da Silva, J.A.; Brito, G.A.C.; Dos Santos, A.A.; Silveira, E.R.; Lima, A.Â.M.; Havt, A. Gingerol suppresses sepsis-induced acute kidney injury by modulating methylsulfonylmethane and dimethylamine production. *Sci Rep*. **2018**; 8(1):12154.
- Salama, N.R.; Hartung, M.L.; Müller, A. Life in the human stomach: persistence strategies of the bacterial pathogen *Helicobacter pylori*. *Nat Rev Microbiol*. **2013**; 11(6):385-99.
- Schleucher, J.; Schwendinger, M.; Sattler, M.; Schmidt, P.; Schedletzky, O.; Glaser, S.J.; Sørensen, O.W.; Griesinger, C. A general enhancement scheme in heteronuclear multidimensional NMR employing pulsed field gradients. *J Biomol NMR*. **1994**; 4(2):301-6.
- Stark, R.M.; Suleiman, M.S.; Hassan, I.J.; Greenman, J.; Millar, M.R. Amino acid utilisation and deamination of glutamine and asparagine by *Helicobacter pylori*. *J Med Microbiol*. **1997**; 46(9):793-800.
- Villas-Bôas, S.G.; Noel, S.; Lane, G.A.; Attwood, G.; Cookson, A. Extracellular metabolomics: a metabolic footprinting approach to assess fiber degradation in complex media. *Anal Biochem*. **2006**; 349(2):297-305.

Wen, H.; Gris, D.; Lei, Y.; Jha, S.; Zhang, L.; Huang, M.T.; Brickey, W.J.; Ting, J.P. Fatty acid-induced NLRP3-ASC inflammasome activation interferes with insulin signaling. *Nat Immunol.* **2011**; 12(5):408-15.

**CONCLUDING**  
**REMARKS**

Caulerpin is a well-known and highly attractive anti-inflammatory molecule. Despite numerous pharmacological studies have demonstrated its effectiveness in modulating inflammation and subsequent tissue damages, the potential mechanism responsible for the anti-inflammatory action of this molecule has not been fully investigated.

The objective of this PhD thesis was to provide new insights into Caulerpin, which could: **i)** increase understanding of its mode of action and **ii)** support its use as potential adjuvant in the therapy against *H. pylori* infection.

As discussed in previous chapters, Caulerpin was suggested to modulate the inflammatory response associated with *H. pylori* infection through Formyl peptide receptor 2 inhibition (Figure 1). In addition, investigation of extracellular metabolic changes caused by Caulerpin on *H. pylori*-inflamed cells provided valuable data which confirmed the ability of Caulerpin in controlling the *H. pylori*-induced inflammation and the subsequent systemic clinical effects (metabolic diseases).

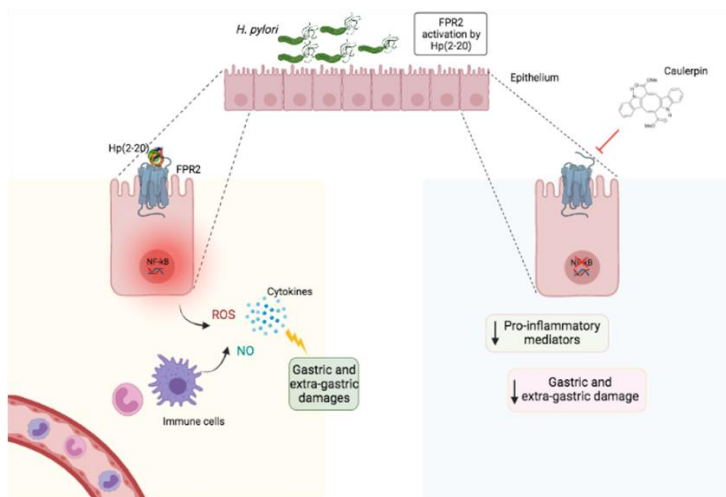


**Figure 1.** Schematic representation of this PhD thesis objective.

Nevertheless, this study presents some limitations. We addressed the therapeutical applicability of Caulerpin in reducing the *H. pylori*-associated inflammation, proving its effectiveness against Hpcf or Hp(2-20), but we did not investigate the efficacy of the molecule by infecting cells with *H. pylori* strains. Our preliminary data (not reported in the present study) confirmed the anti-inflammatory role



of Caulerpin when cells were infected with living bacterium. However, we still need to explore the potential antimicrobial effect of Caulerpin and evaluate its possible use against *H. pylori*-antibiotic resistant strains. Lastly, *in vivo* studies should be performed to further investigate the clinical potential of Caulerpin and determinate probable adverse effects.

In conclusion, this study paves the way for the possibility to use Caulerpin as anti-inflammatory agent, in combination on not with the common therapy against *H. pylori*-resistant strains, in order to reduce the risk to develop severe diseases.

Interestingly, such an approach could also be extended to sterile inflammatory diseases.

## **APPENDIX**

## Experience in foreign laboratory:

Internship at the Company Sequentia Biotech SL (Barcelona, Spain) from 20<sup>th</sup> September to 20<sup>th</sup> December 2021. The work was carried out under the supervision of Dr. Riccardo Aiese Cigliano.

## List of publications:

- D'Amato, M.; Paris, D.; Molino, A.; **Cuomo, P.**; Fulgione, A.; Sorrentino, N.; Palomba, L.; Maniscalco, M.; Motta, A. The Immune-Modulator Pidotimod Affects the Metabolic Profile of Exhaled Breath Condensate in Bronchiectatic Patients: A Metabolomics Pilot Study. *Front Pharmacol.* **2019**; 10:1115. doi: 10.3389/fphar.2019.01115.
- Papaiani, M.; **Cuomo, P.**; Fulgione, A.; Albanese, D.; Gallo, M.; Paris, D.; Motta, A.; Iannelli, D.; Capparelli, R. Bacteriophages Promote Metabolic Changes in Bacteria Biofilm. *Microorganisms.* **2020**; 8(4):480. doi: 10.3390/microorganisms8040480.
- **Cuomo, P.**; Papaiani, M.; Fulgione, A.; Guerra, F.; Capparelli, R.; Medaglia, C. An Innovative Approach to Control H. pylori-Induced Persistent Inflammation and Colonization. *Microorganisms.* **2020**; 8(8):1214. doi: 10.3390/microorganisms8081214.
- **Cuomo, P.**; Papaiani, M.; Sansone, C.; Iannelli, A.; Iannelli, D.; Medaglia, C.; Paris, D.; Motta, A.; Capparelli, R. An In Vitro Model to Investigate the Role of Helicobacter pylori in Type 2 Diabetes, Obesity, Alzheimer's Disease and Cardiometabolic Disease. *Int J Mol Sci.* **2020**; 21(21):8369. doi: 10.3390/ijms21218369.
- Fulgione, A.; Papaiani, M.; **Cuomo, P.**; Paris, D.; Romano, M.; Tuccillo, C.; Palomba, L.; Medaglia, C.; De Seta, M.; Esposito, N.; Motta, A.; Iannelli, A.; Iannelli, D.; Capparelli, R. Interaction between MyD88, TIRAP and IL1RL1 against Helicobacter pylori infection. *Sci Rep.* **2020**; 10(1):15831. doi: 10.1038/s41598-020-72974-9.
- Cavaliere, C.; Montone, A.M.I.; Aita, S.E.; Capparelli, R.; Cerrato, A.; **Cuomo, P.**; Laganà, A.; Montone, C.M.;

- Piovesana, S.; Capriotti, A.L. Production and Characterization of Medium-Sized and Short Antioxidant Peptides from Soy Flour-Simulated Gastrointestinal Hydrolysate. *Antioxidants* (Basel). **2021**; 10(5):734. doi: 10.3390/antiox10050734.
- Soria, L.R.; Gurung, S.; De Sabbata, G.; Perocheau, D.P.; De Angelis, A.; Bruno, G.; Polishchuk, E.; Paris, D.; **Cuomo, P.**; Motta, A.; Orford, M.; Khalil, Y.; Eaton, S.; Mills, P.B.; Waddington, S.N.; Settembre, C.; Muro, A.F.; Baruteau, J.; Brunetti-Pierri, N. Beclin-1-mediated activation of autophagy improves proximal and distal urea cycle disorders. *EMBO Mol Med.* **2021**; 13(2):e13158. doi: 10.15252/emmm.202013158.
  - **Cuomo, P.**; Papaiani, M.; Capparelli, R.; Medaglia, C. The Role of Formyl Peptide Receptors in Permanent and Low-Grade Inflammation: Helicobacter pylori Infection as a Model. *Int J Mol Sci.* **2021**; 22(7):3706. doi: 10.3390/ijms22073706.
  - **Cuomo, P.**; Medaglia, C.; Allocca, I.; Montone, A.M.I.; Guerra, F.; Cabaro, S.; Mollo, E.; Eletto, D.; Papaiani, M.; Capparelli, R. Caulerpin Mitigates Helicobacter pylori-Induced Inflammation via Formyl Peptide Receptors. *Int J Mol Sci.* **2021**; 22(23):13154. doi: 10.3390/ijms222313154.
  - Capparelli, R.; **Cuomo, P.**; Papaiani, M.; Pagano, C.; Montone, A.M.I.; Ricciardelli, A.; Iannelli, D. Bacteriophage-Resistant Salmonella rissen: An In Vitro Mitigated Inflammatory Response. *Viruses.* **2021**; 13(12):2468. doi: 10.3390/v13122468.



# The Immune-Modulator Pidotimod Affects the Metabolic Profile of Exhaled Breath Condensate in Bronchiectatic Patients: A Metabolomics Pilot Study

## OPEN ACCESS

**Edited by:** Ilidko Horvath, National Koranyi Institute of TB and Pulmonology, Hungary

**Reviewed by:** Nadia Mores, Catholic University of the Sacred Heart, Italy

**\*Correspondence:** Mauro Maniscalco [mauromaniscalco@hotmail.com](mailto:mauromaniscalco@hotmail.com)  
Andrea Motta [andrea.motta@icb.cnr.it](mailto:andrea.motta@icb.cnr.it)

<sup>†</sup>These authors have contributed equally to this work

<sup>‡</sup>These authors share senior authorship

**Specialty section:** This article was submitted to Respiratory Pharmacology, a section of the journal Frontiers in Pharmacology

**Received:** 10 April 2019

**Accepted:** 30 August 2019

**Published:** 03 October 2019

### Citation:

D'Amato M, Paris D, Molino A, Cuomo P, Fulgione A, Sorrentino N, Palomba L, Maniscalco M and Motta A (2019) The Immune-Modulator Pidotimod Affects the Metabolic Profile of Exhaled Breath Condensate in Bronchiectatic Patients: A Metabolomics Pilot Study. *Front. Pharmacol.* 10:1115. doi: 10.3389/fphar.2019.01115

<sup>1</sup> Division of Pneumology, Department of Respiratory Diseases, University of Naples Federico II, AORN dei Colli-Monaldi Hospital, Naples, Italy; <sup>2</sup> Institute of Biomolecular Chemistry, National Research Council, Pozzuoli, Italy; <sup>3</sup> Department of Agriculture, University of Naples Federico II, Portici, Italy; <sup>4</sup> Department of Biomolecular Sciences, University of Urbino Carlo Bo, Urbino, Italy; <sup>5</sup> Pulmonary Rehabilitation Unit, ICS Magerit SPA, IRCCS, Telesse Terme, Italy

**Introduction:** Pidotimod, a synthetic dipeptide molecule with biological and immunological activities, is used to reduce the number of exacerbations or pneumonitis in patients with inflammatory diseases.

In the present study, we investigated whether Pidotimod modifies the metabolomic pathways measured in the exhaled breath condensate (EBC) of non-cystic fibrosis bronchiectatic patients (NCFB).

**Materials and Methods:** We analyzed 40 adult patients affected by NCFB. They were randomly selected to receive Pidotimod 800 mg b/d for 21 consecutive days (3 weeks) per month for 6 months (20 patients, V<sub>1</sub> group) or no drug (20 patients, V<sub>0</sub> group), with a 1:1 criterion and then followed as outpatients.

**Results:** EBC samples were collected from all patients at baseline and after 6 months. They were investigated by combined nuclear magnetic resonance (NMR) spectroscopy and multivariate statistical analysis to uncover metabolic differences between EBC from NCFB patients before and after therapy with Pidotimod. Pulmonary function test and pulmonary exacerbations were analyzed at baseline and at the end of Pidotimod therapy. The EBC metabolites were all identified, and through statistical evaluation, we were able to discriminate the two samples' classes, with acetate, acetoin, lactate, and citrate as statistically significant discriminatory metabolites. The model was validated by using a blind set of 20 NCFB samples, not included in the primary analysis.

No differences were observed in PFT after 6 months. At the end of the study, there was a significant decrease of exacerbation rate in V<sub>1</sub> group as compared with V<sub>0</sub> group, with a substantial reduction of the number of mild or severe exacerbations ( $p < 0.001$ ).

**Discussion:** Pidotimod modifies the respiratory metabolic phenotype ("metabotype") of NCFB patients and reduces the number of exacerbations.

**Keywords:** biomarkers, bronchiectasis, disability, exhaled, metabolomics, NMR, outcome, rehabilitation

## INTRODUCTION

Bronchiectasis represents one of the most important healthcare problems due to the high mortality rate and the increased incidence worldwide (King et al., 2006). It is a pulmonary chronic inflammatory disease characterized by bronchial dilatation that can develop in response to many etiologies, like acquired conditions (infection, pulmonary fibrosis, recurrent, or chronic aspiration), as well as congenital conditions [cystic fibrosis (CF), primary ciliary dyskinesia (PCD)] (Chalmers et al., 2012), all leading to bronchus anomalies. Bronchiectasis is associated with chronic cough and sputum production, and, as a chronic lung disorder, it brings about poor quality of life and frequent exacerbations. The economic burden of this disease has been estimated to be similar to chronic obstructive pulmonary disease (COPD). It obviously increases with disease severity, hospitalizations, need for intensive care, and use of inhaled antibiotics (Goeminne et al., 2019). Therefore, there is a continuous search for a pharmacological therapy useful to improve patient conditions and reduce the economic burden (Kocurek and Jagana, 2019).

Pidotimod is a synthetic dipeptide molecule with biological and immunological activities on the adaptive and the innate immune responses, as suggested by *in vivo* and *in vitro* studies (Riboldi et al., 2009; Esposito et al., 2015). Pidotimod has been used to reduce exacerbations or pneumonitis in patients with chronic inflammatory disorders (Trabattoni et al., 2017).

In the last few years, metabolomics has become a leading tool in defining disease phenotype because it is able to correlate the metabolic dysregulation with the phenotype. Metabolomics is a useful tool to investigate airway diseases, their treatment, and follow-up as the respiratory tract offers a natural matrix (exhaled breath), which is easily collected as condensate (EBC) (Maniscalco et al., 2018a; Maniscalco et al., 2019). Nuclear magnetic resonance (NMR)-based metabolomics of EBC has progressively gained importance for quantitative determination of the metabolic response to several respiratory disorders (Paris et al., 2018). It unambiguously recognizes markers that separate adults with COPD from healthy subjects (de Laurentiis et al., 2008), unstable CF from stable CF (Montuschi et al., 2012), CF from PCD (Montuschi et al., 2014), and asthma from COPD (Maniscalco et al., 2018b). Furthermore, NMR-based metabolomics was able to demonstrate that the phenotype of obese asthmatic patients is fully different from that of patients independently affected by asthma or obesity (Maniscalco et al., 2017).

In the present study, we investigated the effects of the Pidotimod in non-cystic fibrosis bronchiectasis (NCFB) patients from EBC samples. By using NMR-based metabolomics, we aimed at uncovering the metabolites and related pathways affected by the immunostimulator, which may become useful indications of the immune response.

## MATERIALS AND METHODS

### Patients

All patients were recruited from the Respiratory Department of the Monaldi Hospital (Naples, Italy). We enrolled 40 adults

with proven and documented diagnosis of idiopathic or post-infectious bronchiectasis with HRCT affecting two or more lobes; history of at least 4 bronchial infections in the previous year characterized by fever and/or cough with increased sputum; stable pulmonary function with an FEV<sub>1</sub> ≥ 80% of predicted; no asthma or COPD, stable drug treatment in the 4 weeks prior to screening; and ability to read and complete questionnaires. A second set (the test group, not considered for the primary analysis) included 20 NCFB patients and was used as a control set to verify blindly the models' reliability. They were collected under similar clinical and experimental conditions. Pidotimod was taken at a dose of 800 mg b/d for 3 weeks a month for 6 consecutive months. From these patients, EBC was collected before Pidotimod administration and after 6 months from the first administration. The exacerbation was defined as worsening of two of the following signs or symptoms for at least two consecutive days, and requiring antibiotic treatment: dyspnea, wheezing, cough, amount of sputum, and sputum purulence with subsequent antibiotic treatment.

The local Ethical Committee approved the study, and an informed written consent was obtained from patients.

### Exhaled Breath Condensate Collection and Processing

All subjects were asked to refrain from food intake for 8 h before the test and from alcoholic drinks for 18 h before collecting the EBC, which they confirmed before sample collection. EBC was collected in random order and in the same room with a TURBO-DECCS condenser set at  $-5.0 \pm 1.0^\circ\text{C}$  (Medivac, Pilastrello, Parma, Italy, medivac.it). Briefly, all subjects were asked to breathe at tidal volume through the mouthpiece for 15 min while sitting comfortably and wearing a nose clip. They were instructed to seal their mouth around the mouthpiece, which was kept dry by periodically swallowing excess saliva. They were also asked to rinse their mouth thoroughly before and every 5 min during the test. We obtained, on average,  $2.0 \pm 0.3$  ml (mean  $\pm$  SD) of EBC from each subject. Volatile substances were removed by a gentle nitrogen gas flow for 3 min. EBC samples were immediately sealed in polypropylene tubes and stored first in dry ice and then at  $-80^\circ\text{C}$  until NMR acquisition (de Laurentiis et al., 2008).

The salivary contamination of the samples was tested by measuring their  $\alpha$ -amylase activity. The colorimetric reaction (Infinity Amylase Reagent, Sigma, Milan, Italy) is based on the hydrolysis of starch. The absorption was detected at 540 nm with a spectrophotometer (HP8453E Agilent Technologies Italia S.p.A., Cernusco sul Naviglio, Milan, Italy). The limit of detection was 0.078 U/ml. Saliva contamination was also checked with the 1D NMR spectra, in which contaminated spectra present signals from carbohydrates (which are absent in EBC spectra). Except for one sample from V<sub>0</sub> (untreated) class and two samples from V<sub>1</sub> (treated) group, which presented saliva contamination in both the amylase test and NMR spectra, the remaining samples (19 untreated and 18 treated) were uncontaminated. In fact, the intense saliva signals, originating from carbohydrates and resonating between 3.3 and 5.5 ppm (de Laurentiis et al., 2008),

were absent in the EBC spectra. Therefore, the samples analyzed were 19 untreated control patients, and 18 were Pidotimod-treated. Regarding the external test group used to verify the model, we considered all of the 20 samples as none of them was contaminated by saliva.

The room temperature remained constant ( $24^{\circ}\text{C} \pm 1.0^{\circ}\text{C}$ ) throughout the sampling period. Possible air contaminants in the collecting room were monitored with a dedicated sampling pump for air monitoring (Zambelli EGO PLUS TT; Zambelli, Milan, Italy), working at a flow rate of 8 l/min and tidal volume (500 ml) into the condenser, so as to simulate human breath. The pump was connected to the condenser outlet for 15 minutes, and special filters (3M Particulate Filters P100; 3M Italia, Milan, Italy; tested against particles approximately  $0.3 \mu\text{m}$  in size) for respiratory protection were applied to the one-way valve of the mouthpiece condenser used for the whole set of experiments. NMR spectra of condensed room air from the collecting device were devoid of signals, confirming the absence of air pollutants (data not shown).

To reduce the risk of contamination by inhaling hospital air, subjects were sampled after a 30-minute rest in the greenhouse of the Department of Respiratory Medicine, which was shown to be contaminant free as described above for the collecting room.

### NMR Sample Preparation

EBC samples were rapidly defrosted. To provide a field frequency lock, 70 ml of a  $^2\text{H}_2\text{O}$  solution (containing 0.1 mmol/l sodium TSP as a chemical-shift reference for  $^1\text{H}$  spectra and sodium azide, a bacteriostatic agent at 3 mmol/l) was added to 630 ml of EBC, reaching 700 ml of total volume.

### NMR Spectroscopy Measurements

All spectra were recorded on a 600-MHz Bruker AVANCE-III Spectrometer (Bruker BioSpin GmbH, Rheinstetten, Germany) equipped with a CryoProbe. 1D  $^1\text{H}$ -NMR spectra were collected at  $27^{\circ}\text{C}$  with the excitation sculpting pulse sequence to suppress the water resonance. We used a double-pulsed field gradient echo, with a soft square pulse of 4 ms at the water resonance frequency and gradient pulses of 1 ms each in duration, adding 128 transients of 64k complex points, with an acquisition time of 4 s/transient. Time-domain data were all zero-filled to 128k complex points, and before Fourier transformation, an exponential multiplication of 0.6 Hz was applied.

2D clean TOCSY spectra were recorded by using a standard pulse sequence and incorporating the excitation sculpting sequence for water suppression (Griesinger et al., 1988). In general, 320 equally spaced evolution-time period  $t_1$  values were acquired, averaging 4 transients of 2,048 points. Time-domain data matrices were all zero-filled to 4,096 points in both dimensions, and before Fourier transformation, a Lorentz-to-Gauss window with different parameters was applied for both  $t_1$  and  $t_2$  dimensions for all the experiments. The spectral positions of the lines ("resonances") in both homonuclear 1D and 2D spectra were referred to the spectral position of the signal originating from 0.10 mmol/l TSP, which was assumed to resonate at a  $\delta$  value of 0.00 ppm.

For the natural abundance of 2D  $^1\text{H}$ - $^{13}\text{C}$  HSQC spectra, we used an echo-antiecho phase-sensitive pulse sequence by using adiabatic pulses for decoupling (Kay et al., 1992). Hundred twenty-eight equally spaced evolution-time period  $t_1$  values were acquired, averaging 48 transients of 2,048 points and using GARP4 for decoupling. The final data matrix was zero-filled to 4,096 in both dimensions and apodized before Fourier transformation by a shifted cosine window function in  $t_2$  and in  $t_1$ . Linear prediction was also applied to extend the data to twice their length in  $t_1$ . The spectral positions of the "resonances" were referred to the lactate signal ( $\beta\text{CH}_3$ ), which was assumed to resonate at 1.33 ppm for  $^1\text{H}$  and 20.76 ppm for  $^{13}\text{C}$ .

### Statistical Analysis

Since there are no standardized methods for evaluating the power of the analysis for projection methods such as orthogonal projections to latent structures (OPLS) analysis, we consider our study a pilot study for which no *a priori* power analysis was possible. Since biomarkers and their concentration changes that could determine class separation were unknown before analysis, we used our results to backward evaluate the power of our analysis.

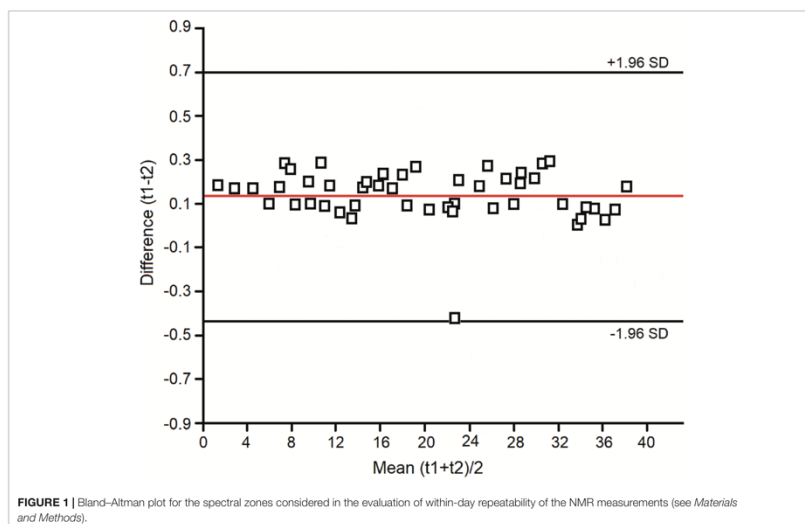
By varying the parameters  $1-\alpha$  from 95 to 99.9% and  $1-\beta$  from 80 to 99.9%, and using the accuracy percentages obtained for our validation tests for untreated/treated patients, for a  $1-\alpha$  value of 95% and a  $1-\beta$  value of 80%, we obtained a number of subjects corresponding to  $14 \pm 2$  for both classes, whereas for a  $1-\alpha$  value of 99.9% and a  $1-\beta$  value of 99.9%, we obtained a number of  $16 \pm 2$  for untreated/treated patients.

Here, we analyzed 19 untreated and 18 treated patients, corresponding to a number of enrolled subjects that is in line with the backward analysis. Typically, the  $1-\alpha$  value is 95%, and the  $1-\beta$  value is at least equal to 80%, whereas a value of 99.9% represents an extreme requirement. On the other hand, the permutation and the validation tests done within the OPLS Discriminant Analysis (OPLS-DA) have confirmed the existence and validity of the model and avoided the overfitting problem (see below).

Within-day, between-day, and technical repeatability, and detection limits were assessed as previously reported (Carraro et al., 2007; Montuschi et al., 2012; de Laurentis et al., 2013). Assessment of within-day repeatability of NMR spectra was according to Bland and Altman, and all spectral lines were considered. Two EBC samples were collected twice within the same day (at times 0 h and 12 h) from four untreated and four treated subjects. Each spectrum was subdivided in six equally corresponding regions, while the region 5.20–4.50 ppm, containing the residual water resonance, was excluded. All regions were integrated and normalized to the total spectrum area. We obtained 6 parameters (the integrated fractional regions) for each spectrum, which for 8 subjects amounted to 48 values. All values except one fell within the 2SD range, indicating a good within-day repeatability (Figure 1).

Between-day repeatability was expressed as ICC of the 4.4–0.4-ppm spectral region. The ICC was 0.99. Technical repeatability was assessed by repeating NMR spectroscopy on four different samples





(two from untreated and two from treated patients) four times consecutively. The ICC for the 4.4–0.4-ppm spectral region was 0.98. The measured detection limit was  $0.07 \pm 0.02 \mu\text{M}$  for phenylalanine signals (not shown), the lowest detectable concentration with respect to the internal TSP concentration standard.

We used multivariate analysis to discriminate signals/metabolites and identify hidden phenomena and trends in ensembles of spectra. Proton NMR spectra were automatically data reduced to 390 integral segments (“buckets”), each of 0.02 ppm, using the AMIX 3.6 software package (Bruker BioSpin GmbH, Rheinstetten, Germany), within the 0.10–8.60-ppm region. The residual water resonance region (5.20–4.50 ppm) was excluded, and each integrated region was normalized to the total spectrum area to avoid possible dilution effects on the signals.

The data format obtained (X matrix) was imported into SIMCA-P +14 package (Umetrics, Umeå, Sweden), and principal components analysis (PCA) and OPLS-DA were performed. PCA is an unsupervised technique that reduces dimensionality without *a priori* knowledge of sample categories, while OPLS-DA is a supervised technique and requires *a priori* knowledge of sample categories. Mean-centering was applied as data pre-treatment for PCA, while Pareto scaling was used prior to OPLS-DA. PCA was performed to reduce the dimensionality of the data and to reveal any clustering of the four study groups in an unsupervised manner. Once class homogeneity was assessed for each group, supervised OPLS-DA was applied, where a dummy variable Y matrix was used. Supervised regressions were

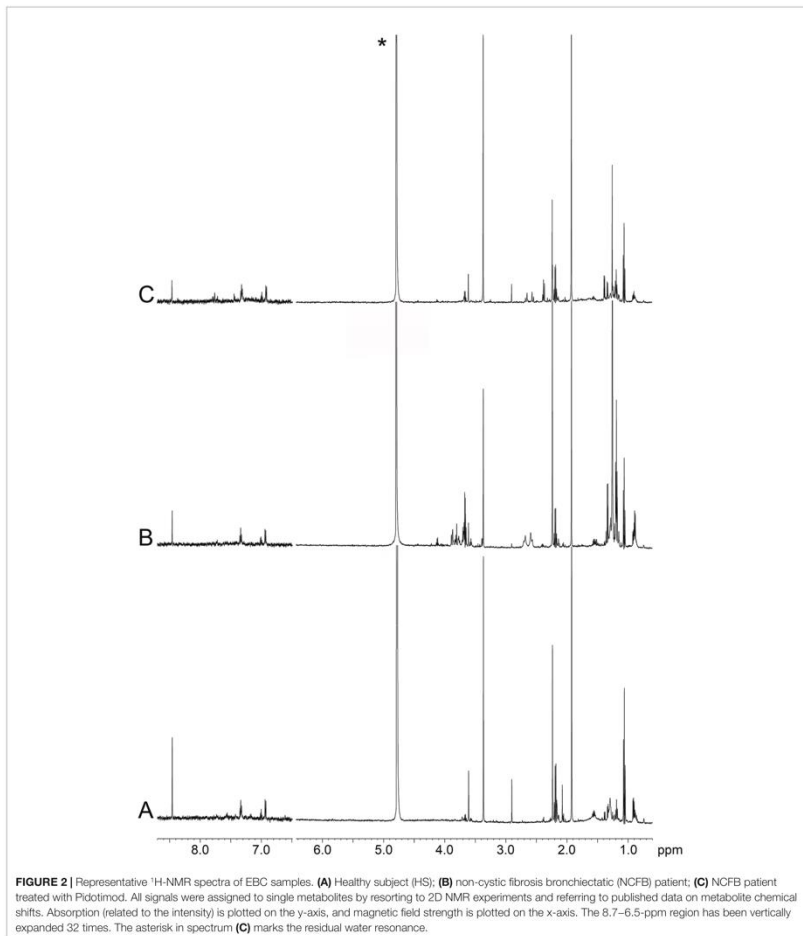
conducted comparing two groups at a time in order to generate predictive models. The model quality was evaluated by using the goodness-of-fit parameter ( $R^2$ ) and the goodness-of-prediction parameter ( $Q^2$ ). We actually tested both OPLS and orthogonal signal correction (OSC) routines together with the PLS-DA to verify data fitting and possible data over-fitting, which was excluded. The obtained OPLS models turned out to be improved in terms of both predictive and interpretive abilities.

Associated scores plots were used to visualize sample class distribution and highlight putative markers for classification. To check for model overfitting and data regression performance, each OPLS-DA model was validated by an internal iterative 7-round cross-validation, response to permutation test (800 repeats), and analysis of variance testing of cross-validated predictive residuals (CV-ANOVA). Statistical significance for selected metabolites and PFT was determined by parametric (Student’s t) or non-parametric (Wilcoxon) tests for paired data, according to the results of normality test performed to evaluate each distribution (Shapiro–Wilk test). Chi square was used for comparing proportions. For all tests, only  $p$  values  $< 0.05$  were considered as statistically significant.

## RESULTS

Figure 2 depicts representative NMR profiles (spectra) of EBC samples from a NCFB patient before (B) and after (C)





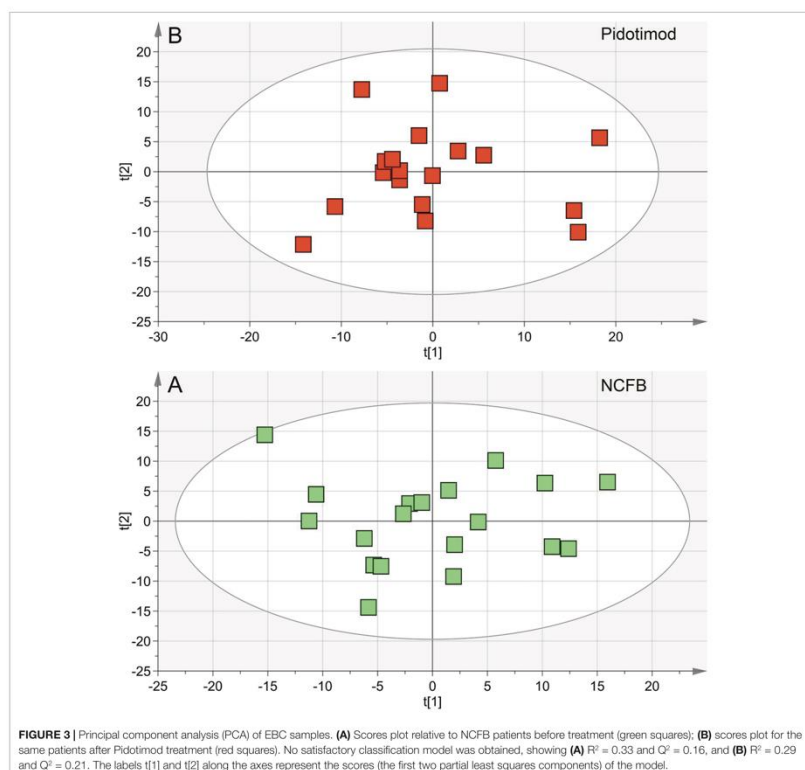
Pidotmod treatment. As a comparison, the spectrum of a healthy subject is also reported (A). Spectral lines were assigned to specific metabolites by resorting to 2D correlation experiments (not shown; see *Materials and Methods*) with the

aid of published chemical-shift data on metabolites, and sample spiking with corresponding standards. A qualitative evaluation of the spectra suggests that the Pidotmod treatment (**Figure 2C**) simplifies the EBC profile with respect to the untreated

NCFB (the group of the signals between 4.0 and 3.5 ppm, the group around 1.0 ppm as well as the intensity of some sharp singlets in spectrum B), becoming comparable to the healthy subject profile (spectrum 2A). However, some peculiarities are still present. For example, compared with the NCFB profile (2B), the treated NCFB (2C) maintains the citrate and lactate signals at 2.51 and 1.33 ppm, respectively, although reduced in intensity. This would indicate that the Pidotimod treatment affects the NCFB metabolic phenotype ("metabotype") generating a different metabotype that relates to (but is not the same than) the normal one. That is, Pidotimod administration does not heal from NCFB but improves the pathophysiological status (*vide infra*).

To obtain relevant biochemical information from NMR data, each spectrum was analyzed through multivariate statistical analysis, namely, PCA and OPLS-DA.

We first verified the homogeneity of all classes ( $V_0$  and  $V_1$  patients) and the presence of possible outliers by applying PCA before the application of supervised analysis. **Figure 3** reports the PCA scores plots obtained for the EBC samples collected from the NCFB before (3A, green squares) and after (3B, red squares) Pidotimod administration. No discernible patterns were identified, neither subgroups nor outliers, confirming that the classes are homogeneous. Therefore, all of the NMR spectra from the 19 untreated and the 18 treated samples were included in the statistical analysis. The model quality was evaluated by using the



goodness-of-fit parameter ( $R^2$ ) and the goodness-of-prediction parameter ( $Q^2$ ). For them, acceptable values must be  $\geq 0.5$ , with  $|R^2 - Q^2| < 0.2 - 0.3$ . For the depicted models, we obtained two principal components with  $R^2 = 0.33$  and  $Q^2 = 0.16$ , and  $R^2 = 0.29$  and  $Q^2 = 0.21$  for plots 3A and 3B, respectively, which is an indication of the absence of subgroups. The existence of probable outliers was also verified in the external test set of 20 NCFB patients. PCA analysis detected neither subgroups nor outliers, with quality parameters  $R^2 = 0.24$  and  $Q^2 = 0.19$ , confirming class homogeneity (not shown).

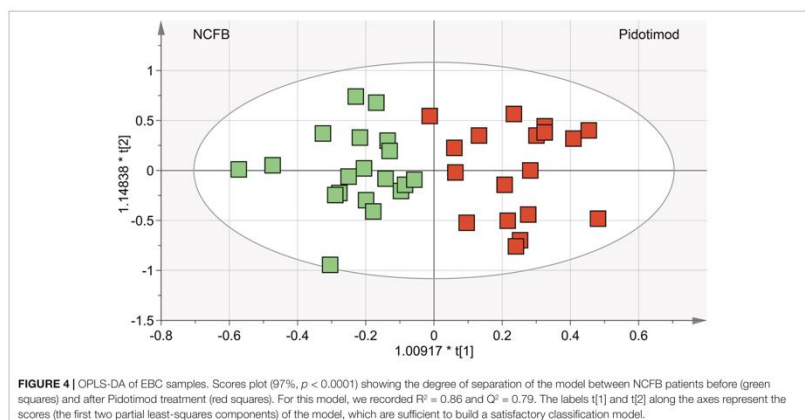
OPLS-DA was next performed, obtaining a strong regression model (97%,  $p < 0.0001$ ; **Figure 4**) between NCFB patients before (green squares) and after (red squares) Pidotimod administration. The resulting supervised model was tested by iteratively predicting the class membership of every sample, and the results were used to evaluate  $R^2$  and  $Q^2$ . For this model, we recorded  $R^2 = 0.86$  and  $Q^2 = 0.79$ . From the associated loadings plot (**Figure 5**), we identified the NMR signals (*i.e.*, the metabolites) responsible for the class separation. Namely, 3.37 ppm (methanol), 2.51 ppm (citrate), 2.23 ppm (acetone/acetoin), 2.19 and 1.07 ppm (propionate), 1.89 ppm (acetate), 1.37 ppm (acetoin), 1.33 ppm (lactate), 1.29 and 1.25 ppm (saturated fatty acids, SFA), and 1.19 ppm (ethanol). The signals on the left side (like 2.51 and 1.33 ppm) were more expressed in the NCFB  $V_0$  class, while those on the right side (like 1.89 and 1.37 ppm) were increased in the Pidotimod  $V_1$  class. In addition, the signals at 1.89, 1.25, and 1.19 ppm were more responsible for intra-class differences than for inter-class differences, because their contribution is larger along the orthogonal component than the parallel or predictive component.

The statistically significant metabolites are depicted in the Variable Importance in the Projection (VIP) plot (**Figure 6A**)

and in the corresponding S plot (**Figure 6B**). It is important to notice that when more than one chemical group belonging to the same metabolite is observed in the NMR spectrum, the corresponding buckets are all reported in the VIP plot. For example, the two vertical bars ("buckets") in the VIP at 1.33 and 4.11 ppm both originate from lactate, being the signals of the methyl and methine protons, respectively. Considering  $VIP > 1$  and  $p_{corr} > 0.5$ , we identified four statistically significant variables/metabolites: 2.51 ppm (citrate), 1.89 ppm (acetate), 1.37 ppm (acetoin), and 1.33 ppm (lactate), whose variations are reported in **Figure 7**. The four statistically relevant metabolites were then used for between-group classification. We confirmed the above model obtaining only a 4% reduction of the quality parameters (95%;  $R^2 = 0.81$ ;  $Q^2 = 0.72$ ;  $p < 0.0008$ ). In particular, acetate and acetoin concentration increased in  $V_1$  class (after Pidotimod administration), while citrate and lactate decreased. Therefore, these metabolites are relevant biomarkers with an important role in the physiological answer to Pidotimod treatment.

The performance of the OPLS-DA model was also evaluated using a sample set not included in the model calculation. Specifically, we tested an external data set of EBC samples obtained from 20 NCFB patients not included in the primary analysis and collected under similar experimental conditions. They were projected onto the corresponding statistical model, and the results are displayed in **Figure 8**. We obtained high-quality parameters ( $R^2 = 0.87$  and  $Q^2 = 0.85$ ) as all samples (blue-dotted green squares) are correctly located in the predicted NCFB area. The discriminating metabolites characterizing the NCFB-Pidotimod coincide with those found for the above calculated model.

To interpret the biological relevance of the data, using the MetaboAnalyst 4.0 platform (Chong et al., 2018), we examined



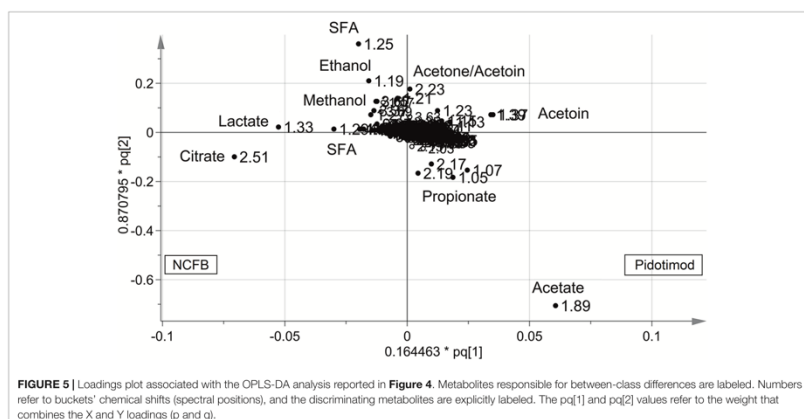


**FIGURE 5 |** Loadings plot associated with the OPLS-DA analysis reported in **Figure 4**. Metabolites responsible for between-class differences are labeled. Numbers refer to buckets' chemical shifts (spectral positions), and the discriminating metabolites are explicitly labeled. The  $pq[1]$  and  $pq[2]$  values refer to the weight that combines the X and Y loadings ( $p$  and  $q$ ).

the metabolic pathways in which the differently regulated metabolites are involved. The found pathways are depicted in **Figure 9**, which reports the impact of each pathway *versus*  $p$  values. Using the discriminating metabolites, we uncovered 12 metabolic pathways that appear to be significantly dysregulated upon treatment. From them, we extrapolated pyruvate ( $p = 1.00 \times 10^{-6}$ ; impact, 0.24), citrate ( $p = 9.77 \times 10^{-3}$ ; impact, 0.08), sulfur ( $p = 7.94 \times 10^{-5}$ ; impact, 0.065), and methane ( $p = 6.31 \times 10^{-4}$ ; impact, 0.06) metabolisms as the most probable. They might contain molecular species potentially relevant as biomarkers for specific pathophysiologic processes within the respiratory metabolome.

No difference was observed in FVC, and  $FEV_1$  in patients who had taken Pidotimod ( $FEV_1$  from  $2.4 \pm 0.9$  to  $2.8 \pm 0.6$  l and FVC from  $2.9 \pm 1.1$  to  $3.2 \pm 1.1$  l) as compared to controls ( $FEV_1$   $2.6 \pm 0.9$  to  $2.5 \pm 0.9$  l and FVC  $2.8 \pm 0.9$  to  $3.1 \pm 0.9$  l),  $p$  always  $> 0.05$ , although the number of exacerbations was significantly lower (7 in treated group vs. 20 in untreated group,  $p < 0.001$ ).

The untreated samples were also examined after 6 months ( $V_0$ ). The comparison of the NMR spectra and the (unsupervised) PCA and (supervised) OPLS-DA analyses did not show relevant changes. In particular, we verified the homogeneity of samples and the presence of possible outliers by applying PCA. The PCA scores plot achieved for the class including the control samples. In particular, at the 19 samples collected at  $V_0$ , we added 20 samples obtained after 6 months. Since none of the 20 selected NCFB patients presented saliva contamination, they were all included in the analysis and amounted to 39 samples. No discernible patterns, neither subgroups nor outliers were identified (**Figure 10**), confirming that they formed a homogeneous class, without notable differences in the metabolic profiles after 6 months. The

goodness-of-fit parameter ( $R^2$ ) and the goodness-of-prediction parameter ( $Q^2$ ). The quality parameters we obtained were  $R^2 = 0.27$  and  $Q^2 = 0.21$ , which are an indication of the absence of subgroups.

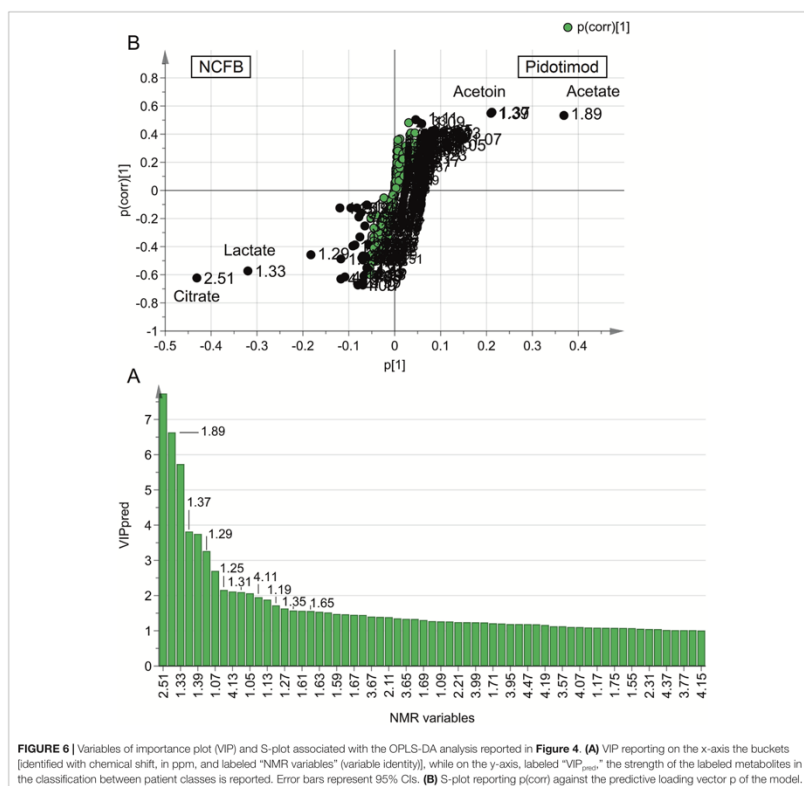
We next applied OPLS-DA obtaining no regression model (32%,  $p < 0.19$ ) between NCFB controls at 0 time and after 6 months. For this model, we recorded  $R^2 = 0.36$  and  $Q^2 = 0.29$ , confirming that no relevant metabolic differences were observed after 6 months in the controls.

We found no correlation between metabolomic data and spirometric results in the study group. Identically, no correlations were observed between metabolites and any of the anthropometric parameters (listed in **Table 1**).

## DISCUSSION

In our study, NMR-based metabolomics of EBC has shown that the immunomodulatory Pidotimod affects the respiratory metabolic phenotype ("metabotype") of NCFB patients. Pidotimod was administered according to clinical practice, at a dose of 800 mg/b/d for 3 weeks (21 days). At such dose, Pidotimod induces dendritic cells (DCs) maturation, up-regulates the expression of HLA-DR and of co-stimulatory molecules, stimulates DCs to release pro-inflammatory molecules driving T-cell proliferation and differentiation toward a Th1 phenotype, enhances natural killer (NK) cells functions, and promotes phagocytosis (Esposito et al., 2015), resulting in a significant upregulation of both innate and, possibly, adaptive immune responses (Trabattoni et al., 2017).

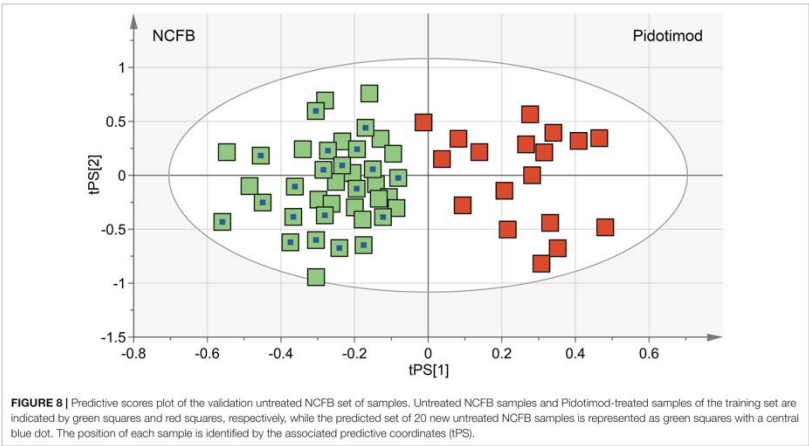
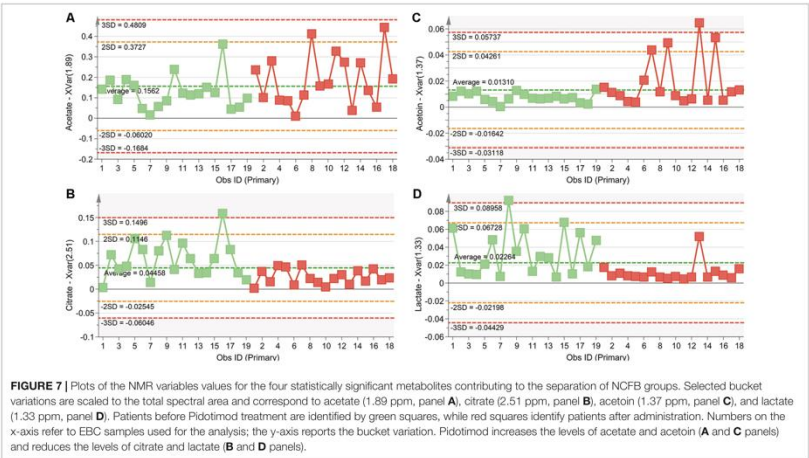
In our respiratory metabolic phenotype, the treatment altered the levels of methanol, citrate, acetone/acetoin, propionate, acetate, lactate, saturated fatty acids and ethanol, with citrate,



acetate, acetoin, and lactate being statistically significant. In particular, after treatment, acetate and acetoin increased while citrate and lactate decreased. Pathway topology analysis indicated (in order of impact percentage) pyruvate, citrate, sulfur, and methane metabolisms as the most probable pathways affected by Pidotimod.

Pyruvate is the end product of glycolysis, which finally enters the mitochondria where it sustains the citric acid cycle. Disorder in pyruvate metabolism is involved in several diseases, including COPD (Gray et al., 2014), in which removal of pyruvate dysmetabolism improved physical performance, which is an important therapeutic goal in COPD (Calvert et al., 2008). Under

aerobic conditions, pyruvate enters the tricarboxylic acid (TCA) cycle to produce also citrate. Consumption of exogenous citrate blocked growth and increased apoptosis in a mesothelioma cell line highly resistant to cisplatin (Zhang et al., 2009) and inhibited proliferation of A549 lung cancer cells *in vitro* and *in vivo* (Hanai et al., 2012). Such a potential antitumor function for citrate is attributed to an effect on immune response and signal transduction pathways (Ren et al., 2017). We found that, upon Pidotimod treatment, the level of citrate decreased together with lactate. Therefore, it is conceivable that the immunomodulator activates citrate consumption in bronchiectatic patients, as a part of the general immune response. It is suggested that citrate could



become a biomarker to monitor the response to the Pidotimod therapy *via* NMR-based metabolomics of EBC.

The lactate decrease in treated NCFB patients could have a direct link with reduced citrate level. In red blood cells incubated with deuterated citrate, *ca.* one-third of the lactate that could not be explained by glucose oxidation and 2,3-diphosphoglycerate consumption alone originates from citrate uptake and metabolism (D'Alessandro et al., 2017). Recent

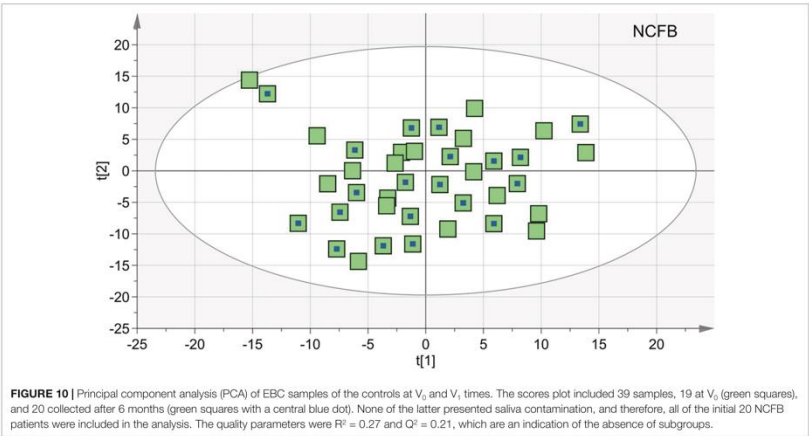
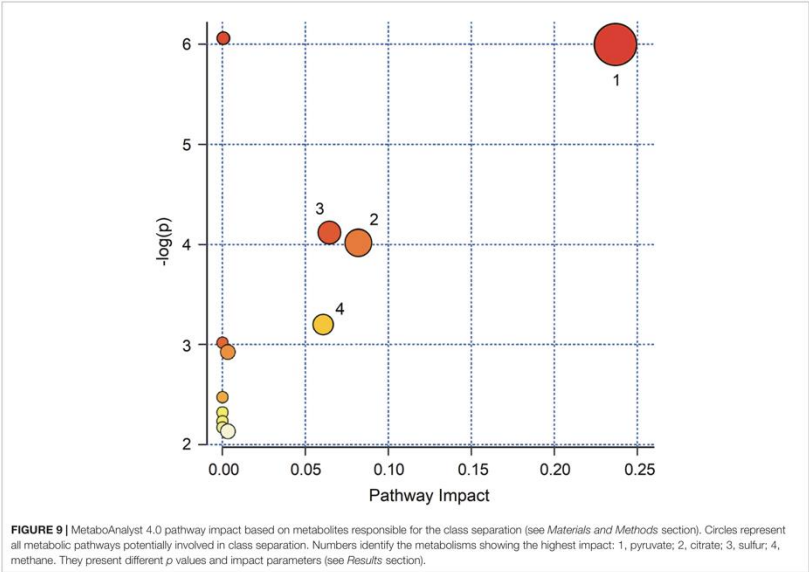




TABLE 1 | Patient characteristics\*.

Anthropometric data	Controls	Pidotimod	All	Validation set
n	19	18	37	20
Female gender	60%	70%	65%	68%
Age (years)	56 ± 12	57 ± 13	56.7 ± 16	55.9 ± 14
BMI (kg/m <sup>2</sup> )	25.3 ± 4.2	28.5 ± 4.8	27.5 ± 4.9	26.2 ± 4.7
FEV <sub>1</sub> pre-BD (l)	2.6 ± 0.9	2.4 ± 0.9	2.5 ± 0.9	2.4 ± 0.8
FVC pre-BD (l)	3.1 ± 0.9	2.9 ± 1.1	3.0 ± 1.0	3.0 ± 0.9
FEV <sub>1</sub> /FVC	84 ± 8.2	85 ± 8.0	85 ± 7.9	83 ± 8.3
SGRQ	45.8 ± 1.6	47.8 ± 1.8	46.8 ± 1.3	44.6 ± 1.9
Exacerbations in previous year	4 ± 2	4 ± 2	4 ± 2	4 ± 2

\*Data are expressed as numbers or means ± SDs. One-way ANOVA and unpaired *t* tests were used for comparing groups. Significance was defined as a *p* < 0.05. Mean ± standard deviation or percentage.

FEV<sub>1</sub> pre-BD, forced expiratory volume at 1 second pre-bronchodilator; FVC pre-BD, forced vital capacity pre-bronchodilator; SGRQ, San George Respiratory Questionnaire.

studies suggest that lactate can be a source of carbon for the citric acid cycle (Hui et al., 2017). As such, the parallel reduction of citrate and lactate in treated NCFB patients could be part of the immune activation brought about by Pidotimod, in which citrate and lactate are both involved *via* the citric acid cycle.

Sulfur-containing metabolites play an important role in maintaining and supporting immune functions by modulating the actions of oxidant stress in transcription factor activation (Grimble, 2006). For example, in animals under protein-deficient diet and showing inflammation after endotoxin injection, addition of methionine to the diet normalized tissue glutathione (GSH) content and upregulated lung neutrophils (Hunter and Grimble, 1994). Therefore, activation of the sulfur metabolism is part of the defense mechanism, which should favor a reduction of lung inflammation.

Methane metabolism is involved in the global carbon cycle, and, among the three types of known methanogenic pathways, the one converting acetate to methane [KEGG module M00357, [www.genome.jp/kegg/](http://www.genome.jp/kegg/) relates to the increased acetate found in treated NCFB patients. Methane metabolism is tightly connected with several metabolic cycles, including sulfur and pyruvate [KEGG map 00680, [www.genome.jp/kegg/](http://www.genome.jp/kegg/)]. It is also involved in the production of cellular energy, which suggests, together with the upregulation of the citric acid cycle, that the energy requirement is increased after treatment, recalling the improved exercise tolerance observed in COPD upon the upregulation of pyruvate metabolism (Calvert et al., 2008).

Acetate and acetoin increased after Pidotimod treatment. Acetate, a short-chain fatty acid, controls some proinflammatory mediators (Arpaia, 2014; Ishiguro et al., 2014) and drives leukocyte migration to inflammatory sites (Vinolo et al., 2011). Therefore, increased levels of acetate after Pidotimod administration responded to the drug immunomodulator activity.

Acetoin (3-hydroxy-2-butanone), which is detected in the breath of patients with cystic fibrosis, causes direct structural damage and likely interacts with the host immune system (Whiteson et al., 2014). It is the product of the detoxication process of acetaldehyde (Otsuka et al., 1996) but may also be a bacterial fermentation product produced by both pathogenic and non-pathogenic bacteria (Filipiak et al., 2012). The relative contribution of lung microbiome to the production of the

acetoin found in the EBC samples is still unknown. In addition, reactive carbonyls such as diacetyl (2,3-butanedione) are contained in tobacco and many food (including butter), and consumer products are detoxified by carbonyl reductases in the lung, in particular, dicarbonyl/l-xylulose reductase (DCXR), a multifunctional lysosomal enzyme expressed in the airway epithelium. The reactive  $\alpha$ -dicarbonyl group in diacetyl causes protein damage *in vitro*. DCXR metabolizes diacetyl to acetoin, its reduced product that lacks this  $\alpha$ -dicarbonyl group (Ebert et al., 2015). Therefore, acetoin increases linked to Pidotimod treatment might be explained by the requirement of limiting pulmonary inflammation by activating the detoxification process of diacetyl groups stimulated by Pidotimod.

We are aware that the present study has some limitations. First, it is a non-controlled study and relies on a restricted number of subjects; therefore, our data are preliminary, and this should be considered a pilot study. Further studies on the effectiveness of Pidotimod in the treatment of NCFB patients are needed to determine prospectively the relevance of the perturbed metabolic pathways. However, we confirmed that NMR-based metabolomics is a noninvasive approach for the evaluation of therapy in respiratory diseases, with important implications for follow-ups and personalized treatments.

The metabolic changes are not immediately visible in systemic variations, and therefore, a direct link between clinics and metabolomics may not be manifested. Lack of correlation of metabolic data with clinical parameters could be related to the use of a single biomatrix (EBC) in the understanding of a complex system, which is globally represented by the clinical parameters (Maniscalco and Motta, 2017). The fact that the clinical indications do not always refer to molecules with a MW < 2,000 Da may also support the absence of correlation. We are presently applying NMR-based pharmacometabolomics to multiple biofluids (serum, urine, EBC, and saliva) to obtain possible global parameters that could be compared with clinical parameters. By integrating the metabolomics profiles of different biofluids, we aim at better defining the pathways affected by immunomodulators.

Finally, the response to Pidotimod should have been better monitored by clinical parameters—for example, following the decrease of the pulmonary exacerbation occurrence. However,



although the clinical parameters are central, we believe that our analysis may be complementary in the assessment of the Pidotimod effects, and that the evolution of pulmonary exacerbations can be efficaciously monitored *via* molecular determinants and altered pathways.

Considering these limitations, our findings, obtained by using an unbiased methodology, unequivocally indicate that NCFB patients when treated with Pidotimod present specific metabolic alteration that might be useful to follow the treatment. This possibility adds strong relevance to the use of EBC- and NMR-based metabolomics to the clinics of respiratory pathologies. The described statistical model defines the change in "metabotype" obtained after Pidotimod treatment. This is very important since NMR profiling makes *no a priori* assumptions about EBC components that may be associated with a particular therapy. Furthermore, it analyzes the sample in a multiparametric way, identifying new and unsuspected links between processes and pathways perturbed in a disease state.

## REFERENCES

- Arpaia, N. (2014). Keeping peace with the microbiome: acetate dampens inflammatory cytokine production in intestinal epithelial cells. *Immunol. Cell Biol.* 92 (7), 561–562. doi: 10.1038/icb.2014.40
- Calvert, L. D., Shelley, R., Singh, S. J., Greenhaff, P. L., Bankart, J., Morgan, M. D., et al. (2008). Dichloroacetate enhances performance and reduces blood lactate during maximal cycle exercise in chronic obstructive pulmonary disease. *Am. J. Respir. Crit. Care Med.* 177 (10), 1090–1094. doi: 10.1164/rccm.200707-1032OC
- Carraro, S., Rezi, S., Reniero, F., Heberger, K., Giordano, G., Zancanato, S., et al. (2007). Metabolomics applied to exhaled breath condensate in childhood asthma. *Am. J. Respir. Crit. Care Med.* 175 (10), 986–990. doi: 10.1164/rccm.200606-7690C
- Chalmers, J. D., Smith, M. P., McHugh, B. J., Doherty, C., Govan, J. R., and Hill, A. T. (2012). Short- and long-term antibiotic treatment reduces airway and systemic inflammation in non-cystic fibrosis bronchiectasis. *Am. J. Respir. Crit. Care Med.* 186 (7), 657–665. doi: 10.1164/rccm.201203-0487OC
- Chong, J., Soufian, O., Li, C., Caraus, L. Li, S., Bourque, G., et al. (2018). *MetaboAnalyst 4.0*: towards more transparent and integrative metabolomics analysis. *Nucleic Acids Res.* 46 (W1), W486–W494. doi: 10.1093/nar/gky310
- D'Alessandro, A., Nemkov, T., Yoshida, T., Bordbar, A., Palsson, B. O., and Hansen, K. C. (2017). Citrate metabolism in red blood cells stored in additive solution-3. *Transfusion* 57 (2), 325–336. doi: 10.1111/trf.13892
- de Laurentiis, G., Paris, D., Melck, D., Maniscalco, M., Marsico, S., Corso, G., et al. (2008). Metabonomic analysis of exhaled breath condensate in adults by nuclear magnetic resonance spectroscopy. *Eur. Respir. J.* 32 (5), 1175–1183. doi: 10.1183/09031936.00072408
- de Laurentiis, G., Paris, D., Melck, D., Montuschi, P., Maniscalco, M., Bianco, A., et al. (2013). Separating smoking-related diseases using NMR-based metabolomics of exhaled breath condensate. *J. Proteome Res.* 12 (3), 1502–1511. doi: 10.1021/pr301171p
- Ebert, B., Kisiela, M., and Maser, E. (2015). Human DCXR—another 'moonlighting protein' involved in sugar metabolism, carbonyl detoxification, cell adhesion and male fertility? *Biol. Rev. Camb. Philos. Soc.* 90 (1), 254–278. doi: 10.1111/brev.12108
- Esposito, S., Garziano, M., Rainone, V., Trabattini, D., Biasin, M., Senatore, L., et al. (2015). Immunomodulatory activity of pidotimod administered with standard antibiotic therapy in children hospitalized for community-acquired pneumonia. *J. Transl. Med.* 13, 288. doi: 10.1186/s12967-015-0649-z
- Filiplak, W., Sponring, A., Baur, M. M., Ager, C., Filiplak, A., Wiesenhofer, H., et al. (2012). Characterization of volatile metabolites taken up by or released from *Streptococcus pneumoniae* and *Haemophilus influenzae* by using GC-MS. *Microbiology* 158 (Pt 12), 3044–3053. doi: 10.1099/mic.0.062687-0
- Goeminne, P. C., Hernandez, F., Diel, R., Filonenko, A., Hughes, R., Juelich, F., et al. (2019). The economic burden of bronchiectasis—known and unknown: a systematic review. *BMC Pulm. Med.* 19 (1), 54. doi: 10.1186/s12890-019-0818-6
- Gray, L. R., Tompkins, S. C., and Taylor, E. B. (2014). Regulation of pyruvate metabolism and human disease. *Cell Mol. Life Sci.* 71 (14), 2577–2604. doi: 10.1007/s00018-013-1539-2
- Griesinger, C., Otting, G., Wuethrich, K., and Ernst, R. R. (1988). Clean TOCSY for proton spin system identification in macromolecules. *J. Am. Chem. Soc.* 110 (23), 7870–7872. doi: 10.1021/ja00231a044
- Grimble, R. F. (2006). The effects of sulfur amino acid intake on immune function in humans. *J. Nutr.* 136 (6 Suppl), 1660S–1665S. doi: 10.1093/jn/136.6.1660S
- Hanai, J., Doro, N., Sasaki, A. T., Kobayashi, S., Cantley, L. C., Seth, P., et al. (2012). Inhibition of lung cancer growth: ATP citrate lyase knockdown and statin treatment leads to dual blockade of mitogen-activated protein kinase (MAPK) and phosphatidylinositol-3-kinase (PI3K)/AKT pathways. *J. Cell Physiol.* 227 (4), 1709–1720. doi: 10.1002/jcp.22895
- Hui, S., Ghergurovich, J. M., Morscher, R. J., Jiang, C., Teng, X., Lu, W., et al. (2017). Glucose feeds the TCA cycle via circulating lactate. *Nature* 551 (7678), 115–118. doi: 10.1038/nature24057
- Hunter, E. A., and Grimble, R. F. (1994). Cysteine and methionine supplementation modulate the effect of tumor necrosis factor alpha on protein synthesis, glutathione and zinc concentration of liver and lung in rats fed a low protein diet. *J. Nutr.* 124(12):2319–2328.
- Ishiguro, K., Ando, T., Maeda, O., Watanabe, O., and Goto, H. (2014). Suppressive action of acetate on interleukin-8 production via tubulin-alpha acetylation. *Immunol. Cell Biol.* 92 (7), 624–630. doi: 10.1038/icb.2014.31
- Kay, L. E., Keifer, P., and Saarinen, T. (1992). Pure absorption gradient enhanced heteronuclear single quantum correlation spectroscopy with improved sensitivity. *J. Am. Chem. Soc.* 114, 10663–10665. doi: 10.1021/ja00052a088
- King, P. T., Holdsworth, S. R., Freezer, N. J., Villanueva, E., and Holmes, P. W. (2006). Characterisation of the onset and presenting clinical features of adult bronchiectasis. *Respir. Med.* 100 (12), 2183–2189. doi: 10.1016/j.rmed.2006.03.012
- Kocurek, E. G., and Jagana, R. (2019). Noncystic fibrosis bronchiectasis management: opportunities and challenges. *Curr. Opin. Pulm. Med.* 25 (2), 192–200. doi: 10.1097/MCP.0000000000000562
- Maniscalco, M., and Motta, A. (2017). Biomarkers in allergic asthma: Which matrix should we use? *Clin. Exp. Allergy* 47 (8), 1097–1098. doi: 10.1111/cea.12978
- Maniscalco, M., Paris, D., Melck, D. J., D'Amato, M., Zedda, A., Sofia, M., et al. (2017). Coexistence of obesity and asthma determines a distinct respiratory metabolic phenotype. *J. Allergy Clin. Immunol.* 139 (5), 1536–1547 e1535. doi: 10.1016/j.jaci.2016.08.038
- Maniscalco, M., Cutignano, A., Paris, D., Melck, D. J., Molino, A., Fuschillo, S., et al. (2018a). Metabolomics of exhaled breath condensate by nuclear magnetic

## DATA AVAILABILITY STATEMENT

The raw data supporting the conclusions of this manuscript will be made available by the authors, without undue reservation, to any qualified researcher.

## ETHICS STATEMENT

Protocol n. 5/18 OSS Maugeri IRCCS, Telesse (BN). Committee of the Scientific Institute Pascale, Naples, Italy (23 May 2018).

## AUTHOR CONTRIBUTIONS

MD, AMol, MM, and AMot ideated the study, enrolled patients, and discussed the study. DP, PC, AF, NS, and LP acquired the data and followed patients. DP, PC, and AMot performed statistical analysis. MD, AMol, MM, and AMot coordinated and discussed the study.

- resonance spectroscopy and mass spectrometry: a methodological approach. *Curr. Med. Chem.* doi: 10.2174/092986732566181008122749
- Maniscalco, M., Paris, D., Melck, D. J., Molino, A., Carone, M., Ruggeri, P., et al. (2018b). Differential diagnosis between newly diagnosed asthma and COPD using exhaled breath condensate metabolomics: a pilot study. *Eur. Respir. J.* 51 (3). doi: 10.1183/13993003.01825-2017
- Maniscalco, M., Fuschillo, S., Paris, D., Cutignano, A., Sanduzzi, A., and Motta, A. (2019). Clinical metabolomics of exhaled breath condensate in chronic respiratory diseases. *Adv. Clin. Chem.* 88, 121–149. doi: 10.1016/bs.acc.2018.10.002
- Montuschi, P., Paris, D., Melck, D., Lucidi, V., Ciabattini, G., Raia, V., et al. (2012). NMR spectroscopy metabolomic profiling of exhaled breath condensate in patients with stable and unstable cystic fibrosis. *Thorax* 67 (3), 222–228. doi: 10.1136/thoraxjnl-2011-200072
- Montuschi, P., Paris, D., Montella, S., Melck, D., Mirra, V., Santini, G., et al. (2014). Nuclear magnetic resonance-based metabolomics discriminates primary ciliary dyskinesia from cystic fibrosis. *Am. J. Respir. Crit. Care Med.* 190 (2), 229–233. doi: 10.1164/rccm.201402-0249LE
- Otsuka, M., Mine, T., Ohuchi, K., and Ohmori, S. (1996). A detoxication route for acetaldehyde: metabolism of diacetyl, acetoin, and 2,3-butanediol in liver homogenate and perfused liver of rats. *J. Biochem.* 119 (2), 246–251. doi: 10.1093/oxfordjournals.jbchem.a021230
- Paris, D., Maniscalco, M., and Motta, A. (2018). Nuclear magnetic resonance-based metabolomics in respiratory medicine. *Eur. Respir. J.* 52 (4). doi: 10.1183/13993003.01107-2018
- Ren, J. G., Seth, P., Ye, H., Guo, K., Hanai, J. I., Husain, Z., et al. (2017). Citrate Suppresses tumor growth in multiple models through inhibition of glycolysis, the tricarboxylic acid cycle and the IGF-1R pathway. *Sci. Rep.* 7 (1), 4537. doi: 10.1038/s41598-017-04626-4
- Riboldi, P., Gerosa, M., and Meroni, P. L. (2009). Pidotimod: a reappraisal. *Int. J. Immunopathol. Pharmacol.* 22 (2), 255–262. doi: 10.1177/039463200902200201
- Trabattoni, D., Clerici, M., Centanni, S., Mantero, M., Garziano, M., and Blasi, F. (2017). Immunomodulatory effects of pidotimod in adults with community-acquired pneumonia undergoing standard antibiotic therapy. *Pulm. Pharmacol. Ther.* 44, 24–29. doi: 10.1016/j.pupt.2017.03.005
- Vinolo, M. A., Rodrigues, H. G., Hatanaka, E., Sato, F. T., Sampaio, S. C., and Curi, R. (2011). Suppressive effect of short-chain fatty acids on production of proinflammatory mediators by neutrophils. *J. Nutr. Biochem.* 22 (9), 849–855. doi: 10.1016/j.jnutbio.2010.07.009
- Whiteson, K. L., Meinardi, S., Lim, Y. W., Schmieder, R., Maughan, H., Quinn, R., et al. (2014). Breath gas metabolites and bacterial metagenomes from cystic fibrosis airways indicate active pH neutral 2,3-butanedione fermentation. *ISME J.* 8 (6), 1247–1258. doi: 10.1038/ismej.2013.229
- Zhang, X., Varin, E., Allouche, S., Lu, Y., Poulain, L., and Icard, P. (2009). Effect of citrate on malignant pleural mesothelioma cells: a synergistic effect with cisplatin. *Anticancer Res.* 29 (4), 1249–1254.

**Conflict of Interest:** The authors declare that the research was conducted in the absence of any commercial or financial relationships that could be construed as a potential conflict of interest.

The reviewer NM declared a past co-authorship with one of the authors to the handling editor.

Copyright © 2019 D'Amato, Paris, Molino, Cuomo, Fulgione, Sorrentino, Palomba, Maniscalco and Motta. This is an open-access article distributed under the terms of the Creative Commons Attribution License (CC BY). The use, distribution or reproduction in other forums is permitted, provided the original author(s) and the copyright owner(s) are credited and that the original publication in this journal is cited, in accordance with accepted academic practice. No use, distribution or reproduction is permitted which does not comply with these terms.



## Brief Report

# Bacteriophages Promote Metabolic Changes in Bacteria Biofilm

Marina Papaiani <sup>1,†</sup> , Paola Cuomo <sup>1,†</sup>, Andrea Fulgione <sup>1,2</sup> , Donatella Albanese <sup>3</sup> ,  
Monica Gallo <sup>4</sup>, Debora Paris <sup>5</sup>, Andrea Motta <sup>5,\*</sup>, Domenico Iannelli <sup>1</sup> and  
Rosanna Capparelli <sup>1,\*</sup>

<sup>1</sup> Department of Agricultural Sciences, University of Naples Federico II, 80055 Portici, Naples, Italy; marina.papaiani@unina.it (M.P.); paola.cuomo@unina.it (P.C.); andrea.fulgione@unina.it (A.F.); iannelli@unina.it (D.I.)

<sup>2</sup> Istituto Zooprofilattico Sperimentale del Mezzogiorno (IZSM), 80055 Portici, Naples, Italy

<sup>3</sup> Department of Industrial Engineering University of Salerno, 84084 Fisciano, Italy; dalbanese@unisa.it

<sup>4</sup> Department of Molecular Medicine and Medical Biotechnology, University of Naples Federico II, 80131 Naples, Italy; monica.gallo@unina.it

<sup>5</sup> Institute of Biomolecular Chemistry, National Research Council, 80078 Pozzuoli, Naples, Italy; dparis@icb.cnr.it

\* Correspondence: andrea.motta@icb.cnr.it (A.M.); capparel@unina.it (R.C.)

† These authors also contributed equally to this work.

Received: 6 February 2020; Accepted: 27 March 2020; Published: 28 March 2020



**Abstract:** Bacterial biofilm provides bacteria with resistance and protection against conventional antimicrobial agents and the host immune system. Bacteriophages are known to move across the biofilm to make it permeable to antimicrobials. Mineral hydroxyapatite (HA) can improve the lytic activity of bacteriophages, and, together with eicosanoic acid (C20:0), can destroy the biofilm structure. Here, we demonstrate the efficacy of the combined use of phage, HA and C20:0 against *Xanthomonas campestris* pv *campestris* (Xcc) biofilm. We used nuclear magnetic resonance (NMR)-based metabolomics to investigate the molecular determinants related to the lytic action, aiming at identifying the metabolic pathways dysregulated by phage treatment. Furthermore, we identified specific markers (amino acids, lactate and galactomannan) which are involved in the control of biofilm stability. Our data show that Xccp1, alone or in combination with HA and C20:0, interferes with the metabolic pathways involved in biofilm formation. The approach described here might be extended to other biofilm-producing bacteria.

**Keywords:** bacteriophages; biofilm; NMR; metabolomics

## 1. Introduction

The concern about bacterial resistance to antibiotics and microbial biofilm production is rapidly increasing. The latest data collected by the European Centre for Disease Prevention and Control highlight a persistent increase of antibiotic-resistant bacteria in the clinical area, as well as in the food industry and agriculture [1].

Biofilm production is the response of bacteria to adverse environmental conditions [2], such as the presence of antibiotics, or the need to establish a chronic colonization [3–5]. The creation of a (thick) biofilm represents a physical barrier to antibiotics, and structural modifications can also develop in membrane composition and in the antibiotics' targets [6,7]. At present, microbial biofilm production represents a major economic and clinical problem, and its prevention and treatment are therefore a major concern.

Bacteriophages (phages) are viruses infecting bacteria, and in contrast to many antibiotics [8], phages can selectively lyse bacteria protected by the biofilm [9–11]. In addition, phages are species-specific, and therefore can be used to target pathogenic bacteria without disturbing non-harmful commensal bacteria [12]. At present, the use of phages to control pathogens in the food industry and agriculture is rather limited [13]. Moreover, since antibiotics have lost much of their power against bacteria, phage therapy may acquire a major role in combating resistant bacterial strains. Consequently, understanding the molecular determinants of phage–host interactions appears to be an essential step for a safe application of the therapy [14]. Recently, metabolomics analysis has suggested that the molecular response to phage infection is specific, as the molecular interactions taking place depend upon the phage and host bacterial strain [15,16]. Metabolomics is the systematic identification and quantification of all metabolites (i.e., the metabolome) in a biological matrix. Metabolomics is particularly effective to investigate how phages act against bacteria during infection [14,15]. Currently, nuclear magnetic resonance (NMR)-based metabolomics is widely used to define alteration of metabolic profiles, unambiguously recognizing biomarkers that characterize different systems biology states.

In this paper, by using NMR-based metabolomics, we investigated the molecular determinants related to the action of the phage against the *Xanthomonas campestris* pv. *campestris* (Xcc) biofilm. Xcc is a Gram-negative bacterium distinguished into several pathovars with specific host range. Xcc is the causal agent of crucifer (including broccoli, cabbage, cauliflower, radish, etc.) black rot disease, causing yield loss in agricultural production world-wide [17]. As with many phytopathogenic bacteria, Xcc produces a range of factors that help the bacterium to parasitize the host [18]. The exopolysaccharides can obstruct the xylem vessels, causing tissue necrosis and leaf wilting [19]. In particular, we aimed at characterizing the metabolic pathways dysregulated by phage treatment, which could become the possible targets, as well as providing an indication of the efficacy of the treatment. Previous studies have demonstrated that hydroxyapatite (HA) enhances the activity of phages. The low degree of crystallinity and the presence of carbonate ions in the crystal structure make HA extremely reactive in biological systems and particularly suitable to interact and transport bacteriophages [20]. The eicosanoic acid (C20:0) weakens the bacterial biofilm structure [21–23], and phage Xccp1 can control Xcc infection in plants (submitted by Papaïanni). Here, we demonstrated that the simultaneous use of HA, C20:0 and Xccp1 destroys the Xcc biofilm structure, identifying specific biomarkers involved in the control of biofilm stability.

## 2. Material and Methods

### 2.1. Isolation and Growth of Xcc Phages

Ten grams of rhizospheric soil from *Brassica oleracea* plants with black rot symptoms (characteristic of Xcc infection) were suspended in 15 mL of nutrient broth (Sigma Aldrich, Milan, Italy) and shaken for 30 min at 24 °C. Soil sediment was removed by centrifugation (5000 rpm for 10 min), and individual supernatants (15 mL) were transferred into sterile flasks. Forty milliliters of  $10^6$  colony-forming units (CFU) per mL of Xcc bacteria in exponential growth phase were added to each flask. Flasks were incubated overnight at 24 °C. Cultures were treated with chloroform, clarified by centrifugation, and filtered through Millipore 0.22 µm-pore-size membrane filters (MF-Millipore, Darmstadt, Germany). Filtrates were tested for the presence of Xcc-specific phages as described [20].

### 2.2. Eicosanoic Acid Activity against Biofilm

The eicosanoic acid (C20:0) activity was tested by the crystal violet staining test [24]. Individual wells of a polystyrene 96 flat-well plate (Falcon) were spotted with 200 µL of Xcc bacteria ( $10^6$  colony-forming units per mL). To facilitate bacterial attachment, the plates were incubated for 72 h at 24 °C without shaking. C20:0 was then added (60 µg/mL, 120 µg/mL, or 240 µg/mL per well), and again incubated for 8 h. After treatment, planktonic cells were gently removed, and the wells washed three times with water. For NMR studies, C20:0 was used at the lowest concentration.

### 2.3. Preparation of Supernatants for Metabolic Analysis

To facilitate biofilm formation, the Xcc bacterial suspension was distributed in Erlenmeyer flasks (50 mL/flask) and incubated for 72 h at 24 °C under a static condition. Next, 5 mL of phages ( $10^8$  plaque forming-units (PFU)/mL), acid (30 µg/mL) or Xccφ1+HA+C20:0 ( $10^8$  PFU/mL, 5 mg/mL and 30 µg/mL respectively) were added to each flask. After 3 h incubation at 24 °C, the cultures were collected, centrifuged (13,000 rpm for 20 min) and the supernatants stored at +4 °C for NMR analysis.

### 2.4. NMR Spectroscopy

NMR spectra were recorded on a Bruker Avance III-600 MHz spectrometer (Bruker BioSpin GmbH, Rheinstetten, Germany), equipped with a TCI CryoProbe™ fitted with a gradient along the Z-axis, at a probe temperature of 27 °C. One-dimensional (1D) proton spectra were acquired at 600 MHz by using the excitation sculpting sequence [25]. Two-dimensional (2D) total correlation spectroscopy (TOCSY) spectra [26,27] were acquired using the MLEV-17 a broadband decoupling cycle from Malcolm Levitt and incorporating the excitation sculpting sequence for water suppression. Spectra were referenced to internal 0.1 mM sodium 3-(trimethylsilyl)-2,2,3,3-tetradeuteriopropionate (TSP), assumed to resonate at  $\delta = 0.00$  ppm. Two-dimensional  $^1\text{H}$ - $^{13}\text{C}$  heteronuclear single-quantum coherence (HSQC) spectra were recorded at 150.90 MHz for  $^{13}\text{C}$  using pre-saturation for water suppression [28]. HSQC spectra were referenced to the  $\alpha$ -glucose doublet resonating at 5.24 ppm for  $^1\text{H}$  and 93.10 ppm for  $^{13}\text{C}$ .

### 2.5. Multivariate Data Analysis

The 0.50–9.50 ppm spectral region of each spectrum was automatically binned into 0.02 ppm width regions (buckets) and integrated using the AMIX 3.9.7 package (Bruker Biospin GmbH, Rheinstetten, Germany). The residual water resonance (4.40–5.60 ppm) was removed from the analyzed spectral area, and the integrated sections were normalized to the total spectrum area. To discriminate samples according to their metabolic variations, NMR profiles were studied using the Soft Independent Modeling of Class Analogy (SIMCA)14 package (Umetrics, Umeå, Sweden). Principal component analysis (PCA) and Orthogonal Projection to Latent Structures Discriminant Analysis (OPLS-DA) [29] were performed. PCA was used to reduce data dimensionality and to evaluate class homogeneity, highlighting possible clustering in an unsupervised manner. Once class homogeneity was assessed for each group, supervised OPLS-DA was applied. The quality of all PCA and OPLS-DA models was evaluated using the  $R^2$  and  $Q^2$  parameters, which represent the goodness-of-fit and the goodness-of-prediction, measuring how well the model fits the data, and how well the model predicts new data, respectively. For  $R^2$  and  $Q^2$ , acceptable values must have been  $\geq 0.5$ , with  $|R^2 - Q^2| < 0.2$ – $0.3$ . Normality test and ANOVA test with Bonferroni correction were performed with the OriginPro 9.1 software package (Origin Lab Corporation, Northampton, MA, USA).

### 2.6. Pathway Analysis

Pathway topology and biomarker analysis were carried out using Metaboanalyst 4.0 [30]. Metabolites were selected by evaluating both variable importance in projection (VIP) values  $> 1$  in class discrimination and correlation values  $|\text{pq}[\text{corr}]| > 0.7$ .

## 3. Results

### 3.1. Phage Xccφ1, Hydroxyapatite, and Eicosanoic Acid Modulate Xcc Biofilm

In bacterial infections, hydroxyapatite (HA) nanocrystals help in bacteriophage delivery and are reported to improve some of the bacteriophage biological properties [20]. In addition, although not bactericidal, C20:0 could be able to modify the microbial biofilm structure by altering the permeability of the cell [21,22,31,32].

It has been reported that C20:0 does not show a significant decrease in biofilm formation, especially at low concentration [33]. However, inhibition has been reported to be dose-dependent [34–36]. Transmission electron microscopy (TEM) examination identified Xccφ1 as a member of the Myoviridae family because of the contractile, long and relatively thick tail, with a central core separated from the head by the neck (Figure 1).

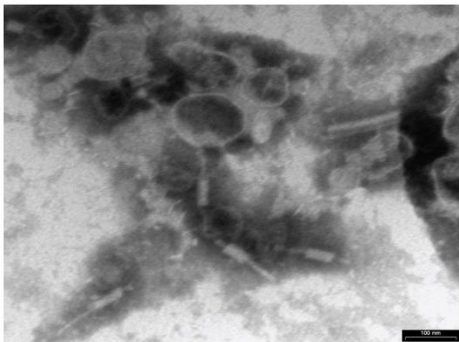


**Figure 1.** Phage Xccφ1 structure as observed by transmission electron microscopy (TEM). The scale bar represents 100 nm.

The action of HA on the biofilm was also tested. From crystal violet measurements, we found that HA has no effect on Xcc biofilm (Papaiani et al., manuscript in preparation) and exerts its enhancing action [20] (building the phage and improving its lytic activity) only in the presence of the phage. The C20:0 was approximately equally active at 60 µg/mL, 120 µg/mL and 240 µg/mL—all reducing the amount of biofilm by ca. 80%. In Figure 2 the anti-biofilm effect is reported as a percentage of the residual biofilm after treatment in comparison with untreated bacteria. In the following, C20:0 was always used at the lowest active concentration of 60 µg/mL.

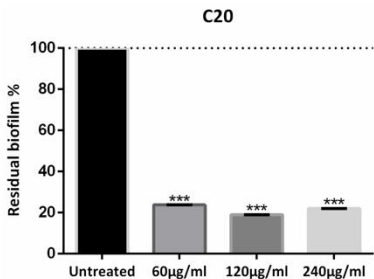


**Figure 2.** Eicosanoic acid (C20:0) activity on Xcc biofilm formation. Data are expressed as percent of residual biofilm. Each value indicates mean ± SD of three independent experiments. The *t* test was used to compare the absorbance of treated and untreated samples. \*\*\* *p* < 0.001.



### 3.2. NMR Analysis: Class Discrimination

The stability of the *Xcc* biofilm upon treatment with *Xcc*φ1, HA, C20:0, *Xcc*φ1+C20:0 and *Xcc*φ1+HA+C20 was analyzed by NMR-based metabolomics. We considered 10 samples for *Xcc*, *Xcc*φ1, C20:0, and *Xcc*φ1+HA+C20, while for HA and *Xcc*φ1+C20:0, we analyzed six samples for each class, which amounted to 52 samples. All classes were tested by unsupervised PCA- to verify the presence of possible subgroups and/or outliers; none were detected, confirming that the classes are homogeneous. For all classes, we obtained as quality parameters  $0.19 < R^2 < 0.20$  and  $0.15 < Q^2 < 0.22$ , with  $0.61 < p < 0.82$ , which was an indication that no subgroups could be identified in the sample set. Therefore, all 52 samples (and the NMR spectra) were included in the analysis.

We next applied supervised OPLS-DA to uncover metabolic differences between classes. In the scores plot of Figure 3A, the  $t[1]$  dimension identifies two groups. At negative values, we found *Xcc*φ1, *Xcc*φ1+C20:0, and *Xcc*φ1+HA+C20:0 classes, while the *Xcc*, HA, and C20:0 classes were located at positive values. For such a model, we obtained good quality parameters ( $R^2 = 0.68$ ;  $Q^2 = 0.75$ ;  $p = 2.310 \times 10^{-20}$ ), indicating that this was statistically significant. In particular, the scores plot data indicate that the first component highlights the effects of the phage (all treatments with phage are at negative values, while those without phage are at positive values), while the second one the effects of the C20:0 and HA on the biofilm [20].

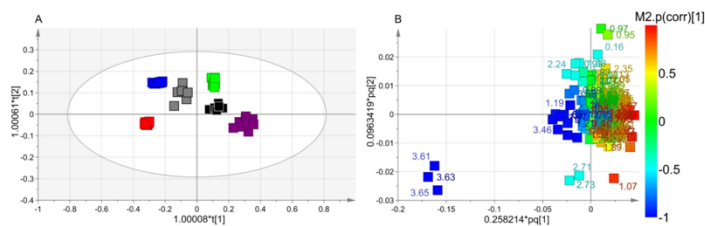


**Figure 3.** Orthogonal Projection to Latent Structure Discriminant Analysis (OPLS-DA) of *Xcc* biofilm treatment. (A) Scores plot showing the separation between *Xcc* (green squares), hydroxyapatite (HA) (black squares), *Xcc*φ1+C20:0 (gray squares), C20:0 (purple squares), *Xcc*φ1 (blue squares) and *Xcc*φ1+HA+C20:0 (red squares). (B) Loadings plot reporting the nuclear magnetic resonance (NMR) variables corresponding to metabolites responsible for class separation, displaying  $|p(\text{corr})| > 0.7$ .

The discriminating metabolites were identified in the associated loadings plot of Figure 3B, in which the numbers identify the NMR chemical shifts of the buckets. In particular, we considered those presenting statistical significance with variable importance in projection (VIP) values greater than 1 in class discrimination, and correlation values  $|p(\text{corr})|$  greater than 0.7. With respect to the untreated biofilm, *Xcc*φ1 induced the production of ethanol, galactomannan and glutamate and downregulated 2-aminoadipate, arginine, betaine, glycine, 3-methylhistidine, isobutyrate, isoleucine, lactate, leucine, lysine, methionine, phenylalanine, propionate, pyroglutamate, saturated fatty acids (SFAs), tyrosine and valine. With respect to *Xcc* biofilm, C20:0 presented an upregulation of arginine, dimethylamine, isobutyrate, lysine, 3-methylhistidine, pyroglutamate and tyrosine and downregulation of 2-aminoadipate, betaine, glutamate, glycine, isoleucine, leucine, methionine, phenylalanine, SFAs and valine. In comparison with *Xcc* biofilm, HA brought about an increase of dimethylamine, isobutyrate, lysine, 3-methylhistidine, and tyrosine, with a parallel reduction of betaine, glutamine, glycine, leucine, phenylalanine, and valine. *Xcc*φ1+C20:0 amplified ethanol, galactomannan and glutamate; and reduces arginine, glycine, 3-methylhistidine, isobutyrate, lactate, leucine, lysine, methionine, phenylalanine, propionate, SFAs, tyrosine and valine. Compared to *Xcc* biofilm, the *Xcc*φ1+HA+C20:0 class showed an increase of ethanol, dimethylamine, galactomannan

and SFAs and a decrease of 2-aminoadipate, betaine, glutamate, glycine, isobutyrate, lactate, leucine, lysine, methionine, phenylalanine, propionate, pyroglutamate and valine.

Interestingly, in the phage groups (Xcc $\phi$ 1, Xcc $\phi$ 1+C20:0 and Xcc $\phi$ 1+HA+C20:0), the dysregulated metabolites showed the same trend, with an increasing tendency towards the Xcc $\phi$ 1+HA+C20:0 class.

### 3.3. Pathway Analysis

NMR signals with VIP > 1 and  $|p(\text{corr})| > 0.7$  were used to identify the main metabolic pathways dysregulated between sample classes. Among the found pathways, the statistically significant examples were phenylalanine metabolism (labeled 1 in Figure 4; impact: 0.22); alanine, aspartate and glutamate metabolism (2; impact: 0.18); arginine and proline metabolism (3; impact: 0.17); glycine, serine and threonine metabolism (4; impact: 0.12); and glutathione metabolism (5; impact: 0.11).

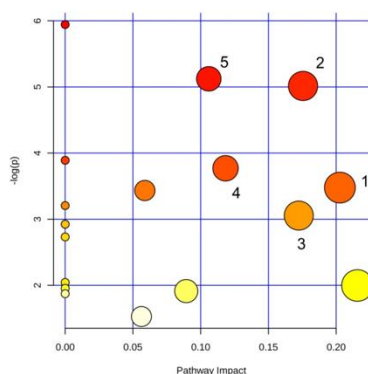


**Figure 4.** Pathway analysis based on most relevant metabolites identified by OPLS-DA. Pathways are identified as follows: 1, glycine, serine and threonine metabolism; 2, arginine biosynthesis; 3, glutamate and glutamine metabolism; 4, arginine and proline metabolism; 5, glutathione metabolism.

## 4. Discussion

In the present study, by using NMR-based metabolomics, we investigated the metabolic changes brought about by HA, C20:0, Xcc $\phi$ 1, Xcc $\phi$ 1+C20:0, and Xcc $\phi$ 1+HA+C20:0 on the Xcc biofilm. The scores plot of Figure 3A can be interpreted as follows. The Xcc $\phi$ 1, Xcc $\phi$ 1+C20:0 and Xcc $\phi$ 1+HA+C20:0 classes are placed at negative coordinates of the horizontal axis (the first component  $t[1]$ ), while Xcc, HA, and C20:0 classes are located at positive  $t[1]$ . Such a behavior derives from the presence/absence of phage, which drives the discrimination. The vertical component  $t[2]$  accounts for the separation between the Xcc $\phi$ 1+HA+C20:0 placed at  $t[2]$  negative coordinates in comparison with Xcc $\phi$ 1 and Xcc $\phi$ 1+C20:0 placed at  $t[2]$  positive coordinates. Such a separation can be ascribed to the presence/absence of C20:0 and HA, although a synergistic action cannot be excluded (Papaiani et al.; manuscript in preparation).

The pathway analysis identified the following dysregulated metabolic pathways involving amino acids: glycine, serine and threonine metabolism; arginine biosynthesis; glutamate and glutamine metabolism; arginine and proline metabolism; and glutathione metabolism (Figure 4). Interestingly, the amino acid metabolism is involved in the formation and maturation of the bacterial biofilm [37], and is an important energy source since it feeds the Tricarboxylic Acid Cycle (TCA).

In particular, with respect to Xcc, the C20:0 class, which does not include the phage, displays high levels of arginine, lysine, 3-methylhistidine, pyroglutamate and tyrosine; and low levels of glutamate,



glycine, isoleucine, leucine, methionine, phenylalanine and valine. HA increases dimethylamine, isobutyrate, lysine, 3-methylhistidine, and tyrosine, with a parallel reduction of betaine, glutamine, glycine, leucine, phenylalanine, and valine. Xcc $\phi$ 1 shows higher glutamate, and lower arginine, glycine, 3-methylhistidine, isoleucine, leucine, lysine, methionine, phenylalanine, pyroglutamate, tyrosine and valine. Compared to Xcc, Xcc $\phi$ 1+C20:0 amplifies ethanol, galactomannan and glutamate; and reduces arginine, glycine, 3-methylhistidine, isobutyrate, lactate, leucine, lysine, methionine, phenylalanine, propionate, SFAs, tyrosine and valine. Finally, the Xcc $\phi$ 1+HA+C20:0 class is characterized by a decrease of glutamate, glycine, isobutyrate, lactate, leucine, lysine, methionine, phenylalanine, pyroglutamate and valine. Even though all classes affect the film, the metabolic responses involve amino acids at different levels, implying that the lytic action is exerted in different way. For example, although the C20:0 and HA do not exert a bactericidal action, they modify the microbial biofilm structure by altering the permeability of the constituent cells [21,22,31,32], and the deep dysregulation of the amino acid metabolism suggests that the biofilm cells somehow “counteract” the lytic action of both C20:0 and HA by activating/deactivating specific amino acids. On the other hand, the comparison between the effects originating from the Xcc $\phi$ 1, Xcc $\phi$ 1+C20:0 and Xcc $\phi$ 1+HA+C20:0 treatment indicates a similar trend in all classes, showing an increasing efficacy in the lytic action for Xcc $\phi$ 1+HA+C20:0. This could be due to the possible synergistic action present in Xcc $\phi$ 1+HA+C20:0 (Papaiani et al., manuscript in preparation), whose effects on the metabolome remains to be investigated.

The pattern of lactate is also interesting. We described here a mature (72 h old) biofilm, potentially marked by reduced levels of oxygen—a condition promoting anaerobic glycolysis and the inhibition of the TCA cycle [38]. With respect to Xcc, lactate was downregulated at comparable levels in both Xcc $\phi$ 1, Xcc $\phi$ 1+C20:0 and Xcc $\phi$ 1+HA+C20:0 classes. Lactate contributes to biofilm production [39], and added to minimal medium, it favors bacterial cell adherence to surfaces and biofilm formation [40]. Therefore, as observed, the lytic action of Xcc $\phi$ 1, Xcc $\phi$ 1+C20:0 and Xcc $\phi$ 1+HA+C20:0 requires reduced levels of lactate [8,41].

High levels of SFAs are observed in the classes treated with phage. Since bacteria in the biofilm state increase their membrane stability and rigidity by incorporating exogenous fatty acids into the membrane [42], the observed SFAs increase could reflect the cell lysis caused by the phage and the subsequent release of SFAs in the exogenous environment (the supernatant).

The phage classes also show high levels of galactomannan. It has been reported that xanthan and galactomannan synergistically increase the biofilm viscosity of *X. campestris* [43]. Although xanthan was not detected, galactomannan increased drastically with phage, while it remained unchanged in the C20:0 and HA classes. Galactomannan gel is unstable since loses up to 50% of its water by syneresis [44]. Thus, the absence of xanthan and the high level of galactomannan suggest that the phage reduces the viscosity of the biofilm through the production of galactomannan.

Taken together, the above results highlight the ability of the phage to dysregulate the amino acids' metabolic pathways responsible for the formation and maturation of the bacterial biofilm, to reduce the lactate that favors biofilm production, and to upregulate the production of galactomannan that weakens the biofilm.

In conclusion, we have described here the action of Xcc $\phi$ 1, Xcc $\phi$ 1+C20:0 and Xcc $\phi$ 1-HA-C20:0 against Xcc bacterial biofilm identifying specific metabolic pathways that are dysregulated by the lytic action. Our data demonstrate that Xcc $\phi$ 1 alone or combined with HA and C20:0 interferes with the metabolic pathways involved in biofilm formation. The altered pathways may become the possible targets for the treatment of bacterial biofilm, as well as providing an indication of the efficacy of the treatment. The approach might be extended to the study of other biofilm-producing bacteria, such as *Escherichia coli* and *Pseudomonas aeruginosa*, in which Pf4 bacteriophage (filamentous bacteriophage) inhibits the metabolic activity of *Aspergillus fumigatus* biofilms [45], and NMR-based metabolomics could be reliably used to understand how phages act on the host metabolism.

**Author Contributions:** R.C. conceived the work; M.P., P.C. and D.P. performed the experiments; M.P., P.C., A.F., D.P., D.A. M.G. and A.M. analyzed the data; and A.M., D.I. and R.C. wrote the manuscript. All authors have read and agreed to the published version of the manuscript.

**Funding:** This research received no external funding.

**Conflicts of Interest:** The authors declare no competing financial interest.

## References

1. European Antimicrobial Resistance Surveillance Network (EARS-Net). Available online: <https://www.ecdc.europa.eu/en/about-us/partnerships-and-networks/disease-and-laboratory-networks/ears-net> (accessed on 27 March 2020).
2. Hall-Stoodley, L.; Costerton, J.W.; Stoodley, P. Bacterial biofilms: From the natural environment to infectious diseases. *Nat. Rev. Microbiol.* **2004**, *2*, 95–108. [CrossRef] [PubMed]
3. Costerton, J.W.; Stewart, P.S.; Greenberg, E.P. Bacterial biofilms: A common cause of persistent infections. *Science* **1999**, *284*, 1318–1322. [CrossRef]
4. Stewart, P.S.; Costerton, J.W. Antibiotic resistance of bacteria in biofilms. *Lancet* **2001**, *358*, 135–138. [CrossRef]
5. Burmølle, M.; Thomsen, T.R.; Fazli, M.; Dige, I.; Christensen, L.; Homøe, P.; Tvede, M.; Nyvad, B.; Tolker-Nielsen, T.; Givskov, M.; et al. Biofilms in chronic infections—A matter of opportunity—Monospecies biofilms in multispecies infections. *FEMS Immunol. Med. Microbiol.* **2010**, *59*, 324–336. [CrossRef] [PubMed]
6. Boudjemaa, R.; Cabriel, C.; Dubois-Brissonnet, F.; Bourg, N.; Dupuis, G.; Gruss, A.; Lévêque-Fort, S.; Briandet, R.; Fontaine-Aupart, M.-P.; Steenkeste, K. Impact of bacterial membrane fatty acid composition on the failure of daptomycin to kill staphylococcus aureus. *Antimicrob. Agents Chemother.* **2018**, *62*. [CrossRef]
7. Craft, K.M.; Nguyen, J.M.; Berg, L.J.; Townsend, S.D. Methicillin-resistant: Staphylococcus aureus (MRSA): Antibiotic-resistance and the biofilm phenotype. *Medchemcomm* **2019**, *10*, 1231–1241. [CrossRef]
8. Kortright, K.E.; Chan, B.K.; Koff, J.L.; Turner, P.E. Phage Therapy: A Renewed Approach to Combat Antibiotic-Resistant Bacteria. *Cell Host Microbe* **2019**, *25*, 219–232. [CrossRef]
9. Roy, B.; Ackermann, H.W.; Pandian, S.; Picard, G.; Goulet, J. Biological inactivation of adhering *Listeria monocytogenes* by listeriophages and a quaternary ammonium compound. *Appl. Environ. Microbiol.* **1993**, *59*, 2914–2917. [CrossRef]
10. Doolittle, M.M.; Cooney, J.J.; Caldwell, D.E. Tracing the interaction of bacteriophage with bacterial biofilms using fluorescent and chromogenic probes. *J. Ind. Microbiol.* **1996**, *16*, 331–341. [CrossRef]
11. Hughes, K.A.; Sutherland, I.W.; Jones, M.V. Biofilm susceptibility to bacteriophage attack: The role of phage-borne polysaccharide depolymerase. *Microbiology* **1998**, *144*, 3039–3047. [CrossRef]
12. Hanlon, G.W. Bacteriophages: An appraisal of their role in the treatment of bacterial infections. *Int. J. Antimicrob. Agents* **2007**, *30*, 118–128. [CrossRef] [PubMed]
13. Moye, Z.D.; Woolston, J.; Sulakvelidze, A. Bacteriophage applications for food production and processing. *Viruses* **2018**, *10*. [CrossRef] [PubMed]
14. Zhao, X.; Shen, M.; Jiang, X.; Shen, W.; Zhong, Q.; Yang, Y.; Tan, Y.; Agnello, M.; He, X.; Hu, F.; et al. Transcriptomic and metabolomics profiling of phage-host interactions between phage PaP1 and *Pseudomonas aeruginosa*. *Front. Microbiol.* **2017**, *8*. [CrossRef] [PubMed]
15. De Smet, J.; Zimmermann, M.; Kogadeeva, M.; Ceysens, P.J.; Vermaelen, W.; Blasdel, B.; Jang, H.B.; Sauer, U.; Lavigne, R. High coverage metabolomics analysis reveals phage-specific alterations to *Pseudomonas aeruginosa* physiology during infection. *ISME J.* **2016**, *10*, 1823–1835. [CrossRef] [PubMed]
16. Fernández, L.; Gutiérrez, D.; Rodríguez, A.; García, P. Application of Bacteriophages in the Agro-Food Sector: A Long Way Toward Approval. *Front. Cell. Infect. Microbiol.* **2018**, *8*, 296. [CrossRef]
17. Qian, W.; Jia, Y.; Ren, S.-X.; He, Y.-Q.; Feng, J.-X.; Lu, L.-F.; Sun, Q.; Ying, G.; Tang, D.-J.; Tang, H.; et al. Comparative and functional genomic analyses of the pathogenicity of phytopathogen *Xanthomonas campestris* pv. *campestris*. *Genome Res.* **2005**, *15*, 757–767. [CrossRef]
18. Dow, J.M.; Daniels, M.J. Pathogenicity determinants and global regulation of pathogenicity of *Xanthomonas campestris* pv. *campestris*. *Curr. Top. Microbiol. Immunol.* **1994**, *192*, 29–41.
19. Liao, C.-T.; Chiang, Y.-C.; Hsiao, Y.-M. Functional characterization and proteomic analysis of *lolA* in *Xanthomonas campestris* pv. *campestris*. *BMC Microbiol.* **2019**, *19*, 20. [CrossRef]

20. Fulgione, A.; Ianniello, F.; Papaiani, M.; Contaldi, F.; Sgamma, T.; Giannini, C.; Pastore, S.; Velotta, R.; Ventura, B.D.; Roveri, N.; et al. Biomimetic hydroxyapatite nanocrystals are an active carrier for *Salmonella* bacteriophages. *Int. J. Nanomed.* **2019**, *14*, 2219–2232. [\[CrossRef\]](#)
21. Papa, R.; Selan, L.; Parrilli, E.; Tilotta, M.; Sannino, F.; Feller, G.; Tutino, M.L.; Artini, M. Anti-Biofilm Activities from Marine Cold Adapted Bacteria Against *Staphylococci* and *Pseudomonas aeruginosa*. *Front. Microbiol.* **2015**, *6*, 1333. [\[CrossRef\]](#)
22. Papa, R.; Parrilli, E.; Sannino, F.; Barbato, G.; Tutino, M.L.; Artini, M.; Selan, L. Anti-biofilm activity of the Antarctic marine bacterium *Pseudoalteromonas haloplanktis* TAC125. *Res. Microbiol.* **2013**, *164*, 450–456. [\[CrossRef\]](#) [\[PubMed\]](#)
23. Casillo, A.; Casillo, A.; Parrilli, E.; Filomena, S.; Lindner, B.; Lanzetta, R.; Parrilli, M.; Tutino, M.L.; Corsaro, M.M. Structural Investigation of the Oligosaccharide Portion Isolated from the Lipooligosaccharide of the Permafrost Psychrophile *Psychrobacter arcticus* 273-4. *Mar. Drugs* **2015**, *13*, 4539–4555. [\[CrossRef\]](#) [\[PubMed\]](#)
24. Papaiani, M.; Contaldi, F.; Fulgione, A.; Woo, S.L.; Casillo, A.; Corsaro, M.M.; Parrilli, E.; Marcolungo, L.; Rossato, M.; Delledonne, M.; et al. Role of phage  $\phi$ 1 in two strains of *Salmonella* Rissen, sensitive and resistant to phage  $\phi$ 1. *BMC Microbiol.* **2018**, *18*, 208. [\[CrossRef\]](#) [\[PubMed\]](#)
25. Hwang, T.L.; Shaka, A.J. Water Suppression That Works. Excitation Sculpting Using Arbitrary Wave-Forms and Pulsed-Field Gradients. *J. Magn. Reson. Ser. A* **1995**, *112*, 275–279. [\[CrossRef\]](#)
26. Bax, A.; Davis, D.G. MLEV-17-based two-dimensional homonuclear magnetization transfer spectroscopy. *J. Magn. Reson.* **1985**, *65*, 355–360. [\[CrossRef\]](#)
27. Griesinger, C.; Otting, G.; Wuethrich, K.; Ernst, R.R. Clean TOCSY for proton spin system identification in macromolecules. *J. Am. Chem. Soc.* **1988**, *110*, 7870–7872. [\[CrossRef\]](#)
28. Schleucher, J.; Schwendinger, M.; Sattler, M.; Schmidt, P.; Schedletsky, O.; Glaser, S.J.; Sørensen, O.W.; Griesinger, C. A general enhancement scheme in heteronuclear multidimensional NMR employing pulsed field gradients. *J. Biomol. NMR* **1994**, *4*, 301–306. [\[CrossRef\]](#)
29. Trygg, J.; Wold, S. Orthogonal projections to latent structures (O-PLS). *J. Chemom.* **2002**, *16*, 119–128. [\[CrossRef\]](#)
30. Chong, J.; Soufan, O.; Li, C.; Caraus, I.; Li, S.; Bourque, G.; Wishart, D.S.; Xia, J. MetaboAnalyst 4.0: Towards more transparent and integrative metabolomics analysis. *Nucleic Acids Res.* **2018**, *46*, W486–W494. [\[CrossRef\]](#)
31. Walton, J.T.; Hill, D.J.; Protheroe, R.G.; Nevill, A.; Gibson, H. Investigation into the effect of detergents on disinfectant susceptibility of attached *Escherichia coli* and *Listeria monocytogenes*. *J. Appl. Microbiol.* **2008**, *105*, 309–315. [\[CrossRef\]](#)
32. Casillo, A.; Papa, R.; Ricciardelli, A.; Sannino, F.; Ziaco, M.; Tilotta, M.; Selan, L.; Marino, G.; Corsaro, M.M.; Tutino, M.L.; et al. Anti-Biofilm Activity of a Long-Chain Fatty Aldehyde from Antarctic *Pseudoalteromonas* haloplanktis TAC125 against *Staphylococcus epidermidis* Biofilm. *Front. Cell. Infect. Microbiol.* **2017**, *7*, 46. [\[CrossRef\]](#) [\[PubMed\]](#)
33. Lee, J.H.; Kim, Y.G.; Park, J.G.; Lee, J. Supercritical fluid extracts of *Moringa oleifera* and their unsaturated fatty acid components inhibit biofilm formation by *Staphylococcus aureus*. *Food Control* **2017**, *80*, 74–82. [\[CrossRef\]](#)
34. Yoon, B.K.; Jackman, J.A.; Valle-González, E.R.; Cho, N.J. Antibacterial free fatty acids and monoglycerides: Biological activities, experimental testing, and therapeutic applications. *Int. J. Mol. Sci.* **2018**, *19*. [\[CrossRef\]](#) [\[PubMed\]](#)
35. Bravo-Santano, N.; Ellis, J.K.; Calle, Y.; Keun, H.C.; Behrends, V.; Letek, M. Intracellular *staphylococcus aureus* elicits the production of host very long-chain saturated fatty acids with antimicrobial activity. *Metabolites* **2019**, *9*. [\[CrossRef\]](#)
36. Lade, H.; Park, J.H.; Chung, S.H.; Kim, H.I.; Kim, J.-M.; Joo, H.-S.; Kim, J.-S. Biofilm Formation by *Staphylococcus aureus* Clinical Isolates is Differentially Affected by Glucose and Sodium Chloride Supplemented Culture Media. *J. Clin. Med.* **2019**, *8*, 1853. [\[CrossRef\]](#)
37. Wong, H.S.; Maker, G.L.; Trengove, R.D.; O’Handley, R.M. Gas chromatography-mass spectrometry-based metabolite profiling of *Salmonella enterica* serovar typhimurium differentiates between biofilm and planktonic phenotypes. *Appl. Environ. Microbiol.* **2015**, *81*, 2660–2666. [\[CrossRef\]](#)

38. Santi, L.; Beys-Da-Silva, W.O.; Berger, M.; Calzolari, D.; Guimarães, J.A.; Moresco, J.J.; Yates, J.R. Proteomic profile of *Cryptococcus neoformans* biofilm reveals changes in metabolic processes. *J. Proteome Res.* **2014**, *13*, 1545–1559. [\[CrossRef\]](#)
39. Goodwine, J.; Gil, J.; Doiron, A.; Valdes, J.; Solis, M.; Higa, A.; Davis, S.; Sauer, K. Pyruvate-depleting conditions induce biofilm dispersion and enhance the efficacy of antibiotics in killing biofilms in vitro and in vivo. *Sci. Rep.* **2019**, *9*, 3763. [\[CrossRef\]](#)
40. Ene, I.V.; Heilmann, C.J.; Sorgo, A.G.; Walker, L.A.; de Koster, C.G.; Munro, C.A.; Klis, F.M.; Brown, A.J.P. Carbon source-induced reprogramming of the cell wall proteome and secretome modulates the adherence and drug resistance of the fungal pathogen *Candida albicans*. *Proteomics* **2012**, *12*, 3164–3179. [\[CrossRef\]](#)
41. Lee, J.H.; Okuno, Y.; Cavagnero, S. Sensitivity enhancement in solution NMR: Emerging ideas and new frontiers. *J. Magn. Reson.* **2014**, *241*, 18–31. [\[CrossRef\]](#)
42. Dubois-Brissonnet, E.; Trotier, E.; Briandet, R. The biofilm lifestyle involves an increase in bacterial membrane saturated fatty acids. *Front. Microbiol.* **2016**, *7*. [\[CrossRef\]](#) [\[PubMed\]](#)
43. Flemming, H.C.; Wingender, J. Relevance of microbial extracellular polymeric substances (EPSs) - Part I: Structural and ecological aspects. *Water Sci. Technol.* **2001**, *43*, 1–8. [\[CrossRef\]](#)
44. Dea, I.C.M.; Morris, E.R.; Rees, D.A.; Welsh, E.J.; Barnes, H.A.; Price, J. Associations of like and unlike polysaccharides: Mechanism and specificity in galactomannans, interacting bacterial polysaccharides, and related systems. *Carbohydr. Res.* **1977**, *57*, 249–272. [\[CrossRef\]](#)
45. Penner, J.C.; Ferreira, J.A.G.; Secor, P.R.; Sweere, J.M.; Birukova, M.K.; Joubert, L.-M.; Haagenen, J.A.J.; Garcia, O.; Malkovskiy, A.V.; Kaber, G.; et al. Pf4 bacteriophage produced by *Pseudomonas aeruginosa* inhibits *Aspergillus fumigatus* metabolism via iron sequestration. *Microbiology* **2016**, *162*, 1583–1594. [\[CrossRef\]](#) [\[PubMed\]](#)



© 2020 by the authors. Licensee MDPI, Basel, Switzerland. This article is an open access article distributed under the terms and conditions of the Creative Commons Attribution (CC BY) license (<http://creativecommons.org/licenses/by/4.0/>).



## Article

# An Innovative Approach to Control *H. pylori*-Induced Persistent Inflammation and Colonization

Paola Cuomo <sup>1,†</sup>, Marina Papaiani <sup>1,†</sup>, Andrea Fulgione <sup>2</sup>, Fabrizia Guerra <sup>3</sup>,  
Rosanna Capparelli <sup>1,\*</sup> and Chiara Medaglia <sup>4</sup>

<sup>1</sup> Department of Agricultural Sciences, University of Naples Federico II, 80055 Portici, Naples, Italy; paola.cuomo@unina.it (P.C.); marina.papaiani@unina.it (M.P.)

<sup>2</sup> Istituto Zooprofilattico Sperimentale del Mezzogiorno (IZSM), 80055 Portici, Naples, Italy; andrea.fulgione@unina.it

<sup>3</sup> Department of Pharmacy, University of Naples Federico II, 80131 Naples, Italy; fabrizia.guerra@unina.it

<sup>4</sup> Department of Microbiology and Molecular Medicine, University of Geneva Medical School, 1211 Geneva, Switzerland; chiara.medaglia@unige.ch

\* Correspondence: capparel@unina.it

† These authors contributed equally to this work.

Received: 27 July 2020; Accepted: 8 August 2020; Published: 10 August 2020



**Abstract:** *Helicobacter pylori* (*H. pylori*) is a Gram-negative bacterium which colonizes the human stomach. The ability of *H. pylori* to evade the host defense system and the emergence of antibiotic resistant strains result in bacteria persistence and chronic inflammation, which leads to both severe gastric and extra-gastric diseases. Consequently, innovative approaches able to overcome *H. pylori* clinical outcomes are needed. In this work, we develop a novel non-toxic therapy based on the synergistic action of *H. pylori* phage and lactoferrin adsorbed on hydroxyapatite nanoparticles, which effectively impairs bacteria colonization and minimizes the damage of the host pro-inflammatory response.

**Keywords:** *Helicobacter pylori*; bacteriophages; inflammation

## 1. Introduction

*Helicobacter pylori* (*Hp*) is a Gram-negative bacterium able to induce chronic infections in humans. It colonizes the gastric mucosa of over 50% of the population worldwide. *Hp* infects gastric epithelial cells and promotes chronic inflammation, leading to chronic gastritis, which can eventually degenerate in peptic ulcer and gastric carcinoma [1–3]. *Hp* also interferes with biological processes outside the stomach, causing extra-gastric diseases such as cardiovascular, neurological and metabolic diseases [4,5]. Our recent works suggest *Hp*-induced persistent inflammation as the key factor responsible for the pathogenicity of extra-gastric diseases (Papaiani et al., manuscript in preparation; Fulgione et al., under submission). Therefore, the clinical outcome of *Hp* infection is determined by the severity of local and systemic inflammatory response, which is regulated by both host and pathogen factors, rather than by the bacterial infection itself. More specifically, *Hp* virulence factors and their ability to evade the host immune system, especially in immunocompromised individuals, trigger an uncontrolled inflammatory response. Furthermore, the *Hp* genetic plasticity and the inappropriate use of antibiotics favor the spread of antibiotic resistant strains, which are difficult and sometimes impossible to treat [6].

Given this scenario, therapeutic treatments for *Hp* infection able to overcome the antimicrobial resistance and mitigate the inflammatory response represent a valid alternative to common antibiotic therapies. Phages are considered a promising substitute for traditional antibiotics, thanks to their unique characteristics such as host specificity and narrow spectrum of activity resulting in no alteration

of gut microbiota, exponential reproduction, and safety [7,8]. Indeed, phages are significantly better tolerated than antibiotics, as they replicate only in the target bacterium but cannot infect mammalian cells or interfere with their molecular mechanisms [9]. Moreover, the ability of phages to inhibit the inflammatory response favors the success of phage therapy [10,11], whose applicability to *Hp* infection is still poorly studied. Of note, bacteria also develop resistance to phages, but it is incomparably easier to develop new phages than new antibiotics [12]. The application of phages to treat bacterial infections involving different body sites is widely documented. The majority of these studies report the beneficial effects of phage administration for topical treatment of localized skin bacterial infections in wounds, burns, and trophic ulcers, including diabetic foot ulcers [13].

Despite its numerous advantages, the applicability of phage therapy to *Hp* infection is hindered by the harsh physiological conditions of the gastric environment. Specifically, the acidity of the gastric juice together with the digestive enzymes dramatically alter both the biological and structural components of phages, thus reducing their proliferation and concentration at the site of the infection [14,15]. The high sensitivity of phages to an acidic environment [16] can be overcome by natural coating, which protects phage particles from the gastric acidic environment, thus enhancing their stability without affecting the phage's infection ability. Natural coating thus represents an effective strategy to extend the applicability of phage therapy to gastric infections.

For many years, due to the development of medical nanotechnologies, nanoparticles have been studied and applied in the pharmaceutical field as drug delivery, in order to improve drug pharmacokinetic and pharmacodynamic [17,18]. Hydroxyapatite (HA)  $\text{Ca}_{10}(\text{PO}_4)_6\text{OH}_2$  is an inorganic material that is present as a natural component of human teeth and bones. Biocompatibility and biological inertia, as well as nanotechnology development [19], make HA the scaffold of choice for drug delivery [20].

Recent studies have shown the significant contribution of HA when complexed with bacteriophages. In particular, the complex phage-HA reduces the high susceptibility of phages to the acid gastric environment and increases its stability, resistance, and lytic activity [21,22].

In addition to phage therapy, another valid approach could be represented by the use of antimicrobial molecules such as the lactoferrin, whose activity against *Hp* infection has been widely investigated [23]. Lactoferrin (LF) is a mammalian glycoprotein present in milk and other mucosal secretions [24,25]. Due to its location, LF can be considered as a first-line mucosal defense peptide, which contributes to host protection against invading pathogens. Similar to phages, LF can act both on the bacteria (direct microbicidal and microbiostatic action) or can modulate the inflammatory response (indirect action). Moreover, it has been shown that, when complexed with HA, LF biological properties are increased [26].

In the present study, we evaluated the antimicrobial activity of a lytic bacteriophage specific to (*Hp*  $\phi$ ) alone or combined with LF adsorbed on HA nanoparticles (*Hp*  $\phi$  + LF-HA) against *Hp* infection. Interestingly, we demonstrated the synergistic action of phage and lactoferrin in reducing *Hp*-induced inflammation, in addition to *Hp* colonization.

## 2. Materials and Methods

### 2.1. Bacteria

Bacteria used in this study were isolated from human gastric biopsies, kindly provided by the gastroenterology department of "Ospedale Evangelico Villa Betania", Naples. The *Hp* species was confirmed by PCR assay of the specific pathogen gene *glmM* [27]. Bacteria were grown in Brain Heart Infusion broth (BHI; Oxoid, Thermo Fisher Scientific, Waltham, MA, USA), supplemented with horse serum 10% at 37 °C and 5%  $\text{CO}_2$  until they reached the exponential growth phase ( $\text{OD}_{600}$ : 0.6 to 0.8). Then, they were harvested by centrifugation ( $8 \times 10^3$  g for 10 min), washed with saline solution (0.15 M NaCl) and resuspended in BHI broth or saline solution ( $10^6$ – $10^8$  CFU/mL).



## 2.2. Phage Isolation

Samples from different patients were grown in BHI broth supplemented with horse serum 10% at 37 °C and 5% CO<sub>2</sub>. When cultures reached the exponential growth phase (OD<sub>600</sub>: 1.5 to 1.8), bacteria were washed with BHI broth supplemented with horse serum 10% and incubated again for 4 h at 37 °C. The supernatants were filtered through a 0.45 µm membrane and screened for the presence of phages by the spot test [28]. Supernatants, which resulted positive in the spot test, were tested five times again by performing the plaque-forming assay [21]. Individual plaques were expanded in BHI broth supplemented with horse serum 10% (2 mL) containing the sensitive bacterial host (10<sup>6</sup> CFU). Phage purification was carried out as described previously [29].

## 2.3. Adsorption Rate, Latent Period, and Phage Burst Size

The adopted procedures were those described previously [30]. Briefly, to measure the adsorption rate, 1 mL phage Hp φ (1.5 × 10<sup>3</sup> PFU/mL) and 1 mL Hp (5 × 10<sup>8</sup> CFU/mL) were mixed and the number of free phage particles was determined after treatment with chloroform (200 µL). To determine the latent period and burst size, Hp bacteria (5 × 10<sup>8</sup> CFU/mL) were incubated with phage Hp φ (3 × 10<sup>3</sup> PFU/mL) for 5 min, washed with cold BHI broth to remove free phage particles, and then resuspended in fresh medium. The cell suspension was periodically titrated for newly produced phage on Hp lawn [31].

## 2.4. Complex Hp Phage, Lactoferrin, and Hydroxyapatite Nanoparticles (Hp φ +LF-HA)

The Hp φ +LF-HA complex was prepared by mixing the LF-HA previously described (Fulgione et al., 2016) with 1 mL of Hp φ (10<sup>8</sup> PFU/mL) and incubated—under shaking condition—at room temperature for different times (0, 30', 90', 180', 300' and 24 h). After the different incubation all the samples were centrifuged, the pellet was suspended in distillate water, and the supernatant stored. The concentration of the active phage particles in the pellet was evaluated by the double layer assay (DLA) method [28]. Specifically, after an overnight incubation the phage particles were calculated. The samples that displayed the highest activity with the lower concentration were selected as optimal incubation time. Concurrently, the supernatant was tested for detecting the amount of phage tied to the LF-HA. Briefly, the supernatant was spotted (three spots of 10 µL) on the soft agar overlay. After overnight incubation, the titer was determined as reported by Papaïanni et al. [28].

## 2.5. Measurement of Cell Viability

### 2.5.1. MTT Assay

Analysis of cell viability was performed using the CellTiter 96® Aqueous One Solution Cell Proliferation Assay system (MTS assay) (Promega, Madison, WI, USA) (Carrieri et al., 2017). Human Caucasian gastric adenocarcinoma (AGS) cells, grown in DMEM medium (Gibco, Scotland) supplemented with 10% fetal bovine serum (FBS), penicillin (100 IU/mL), and streptomycin (100 µg/mL) (all from Gibco, Paisley, Scotland), were seeded in a 96-well plate (2500 cells/well) and incubated at 37 °C, in a humidified atmosphere with 5% CO<sub>2</sub>. After cells adhesion, they were treated with (1) Hp phage (Hp φ; 10<sup>6</sup> PFU/mL); (2) lactoferrin adsorbed on hydroxyapatite nanoparticles (LF-HA; 200–600 µg/mL); (3) the complex Hp φ +LF-HA described above. Twenty µL of CellTiter 96® Aqueous One Solution reagent was added to each well, according to the manufacturer's instructions. Absorbance was recorded at 490 nm after 2 h using an EnVision 2102 multilabel reader (PerkinElmer, Waltham, MA, USA).

### 2.5.2. Trypan Blue Test

Analysis of cell viability was performed by plating AGS cells (10<sup>6</sup> cells/well) in 6-well plates and letting them adhere in DMEM supplemented with 10% FBS, penicillin (100 IU/mL), and streptomycin

(100 µg/mL). After adhesion cells were washed three times with phosphate buffer saline (PBS; Gibco, Thermo Fisher Scientific, Waltham, MA, USA) and then treated with (1) *Hp* phage ( $Hp \varphi$ ;  $10^5$  PFU/mL or  $10^6$  PFU/mL); (2) lactoferrin adsorbed on hydroxyapatite nanoparticles (LF-HA; 200–600 µg/mL); (3) the complex *Hp*  $\varphi$  + LF-HA described above, for 24–48–72 h. At each time point, cells were washed three times with PBS and then 1.5 mL of 1% trypsin was added in each well. After incubation at 37 °C for 3 min, 3 mL of culture medium were added to each well and the whole mixture was transferred into a test tube for centrifugation and centrifuged for 3 min at 1000 g. The supernatant being aspirated and discarded, the cell pellet was resuspended with 1 mL of culture medium and 10 µL of resuspended cells were mixed with 10 µL of Trypan blue, which is able to color the necrotic cells. The percentage of viability was calculated as reported:  $N^\circ \text{ viable cells} / N^\circ \text{ nonviable cells} + \text{viable cells} \times 100$ .

#### 2.5.3. NO<sub>2</sub> Measurements

The accumulation of NO<sub>2</sub> in culture media was determined using Griess Reagent Kit for Nitrite Determination (Molecular Probes, Boyds, MA, USA), following the manufacturer's instructions [32].

#### 2.6. SEM Image

Water suspensions of the samples *Hp*  $\varphi$  + LF-HA complex—previously centrifuged at 13,000 rpm for 15 min—were deposited on 5 × 5 mm silicon chips and the solvent was evaporated under vacuum at 30 °C. The silicon supports were mounted on 13 mm SEM aluminum stubs and sputtered with a nanometric conductive layer of Au/Pd alloy using a Desk V TSC coating system (Denton Vacuum, Moorestown, NJ, USA). SEM micrographs were recorded with a Field Emission Gun Scanning Electron Microscope (FEGSEM) Nova NanoSem 450 (FEI/ Thermo Fisher Scientific, Waltham, MA, USA) under high vacuum conditions.

#### 2.7. *Helicobacter Pylori* Culture, Gastric Cell Infection

AGS cells were distributed in a 24-well plate ( $10^5$ /well) and allowed to adhere (37 °C, 5% CO<sub>2</sub>) in DMEM supplemented with 10% FBS, penicillin (100 IU/mL), and streptomycin (100 µg/mL). Wells were washed with DMEM to remove non-adherent cells. Cells were fed with 1 mL DMEM supplemented with 10% FBS and infected or not with *Helicobacter pylori* ( $10^4$  CFU/well). The plates were centrifuged (1000 rpm, 10 min) to facilitate cell contact, and then incubated for 24 h at 37 °C in 5% CO<sub>2</sub>. Cells infected with *Hp* were washed and treated with *Hp*  $\varphi$  ( $10^6$  PFU/well) for 3 or 24 h at 37 °C in 5% CO<sub>2</sub>.

#### 2.8. Quantitative Gene Expression Analysis

Total RNA was extracted following the Tryzol reagent protocol (Invitrogen, Thermo Fisher Scientific, Waltham, MA, USA). Gene transcript levels were measured using Power SYBR® Green PCR Master Mix (Applied Biosystems®, Thermo Fisher Scientific, Waltham, MA, USA) on a QuantStudio™ 3 Real-Time PCR System (Applied Biosystems®, Thermo Fisher Scientific, Waltham, MA, USA) [33]. QuantStudio Design & Analysis Software v1.1 (Applied Biosystems Thermo Fisher Scientific, Waltham, MA, USA) was used for the analysis of gene expression. All samples were normalized to GAPDH as reference housekeeping gene. The relative quantitative expression was calculated using the 2<sup>−ΔΔCT</sup> method [34].

#### 2.9. ROS Detection Assay

ROS formation was assayed using dihydrorhodamine 123 (DHR) as described by Palomba et al. [35]. Briefly, AGS cells infected with *H. pylori*, loaded with DHR (10 µM for 20 min), were treated for 1 h with (1) *Hp* phage (*Hp*  $\varphi$ ;  $10^6$  PFU/mL); (2) lactoferrin adsorbed on hydroxyapatite nanoparticles (LF-HA; 200–600 µg/mL); (3) the complex *Hp*  $\varphi$  + LF-HA described above, and analysed with a Leica DMI6000 fluorescence microscope equipped with a Leica DFC320 cooled digital CCD camera (Leica Microsystems). The excitation and emission wavelengths were 488 and 515 nm,



respectively. Images were collected with exposure times of 100–400 ms, digitally acquired, and processed for fluorescence determination at the single cell level with Metamorph Imaging Software (Leica MetaMorph © AF, Wetzlar, Germany). Mean fluorescence values were determined by averaging the fluorescence values of at least 50 cells/treatment.

3. Results

3.1. Phage Isolation

Following the treatment of the positive *Hp* isolated from different patients, several phage particles were yielded. The phage displaying the largest host range was designated *Hp*  $\phi$  (Table 1). After the purification and the starvation *Hp*  $\phi$  was further characterized based on the adsorption rate ( $1.89 \times 10^9$  mL/min), latent period (45 min), and burst size (80 PFU) (Figure 1A). The phage lytic activity, analyzed by MOI test, was independent of *Hp* concentration (Figure 1B).

**Table 1.** Phage host range determination on different samples from the gastroenterology department of “Ospedale Evangelico Villa Betania” Naples.

<i>Hp</i> Samples	<i>Hp</i> $\phi$
Patient 1	-
Patient 2	+
Patient 3	+
Patient 4	+
Patient 5	+
Patient 6	+
Patient 7	+
Patient 8	+
Patient 9	+
Patient 10	+
Patient 11	+
Patient 12	+
Patient 13	+
Patient 14	+
Patient 15	-
Patient 16	-
Patient 17	+
Patient 18	+
Patient 19	+
Patient 20	-
Patient 21	-
Patient 22	+
Patient 23	+
Patient 24	+
Patient 25	+
Patient 26	+
Patient 27	+
Patient 28	+

-, negative lysis result; +, positive lysis result.

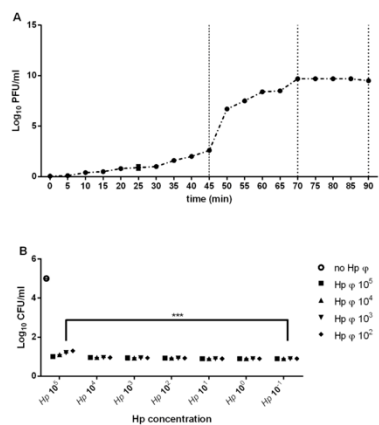


**Figure 1.** Phage characterization. (A) One step growth curve of phage. (B) Representation of phage activity on *Hp* growth. The figure illustrates the bacterial plate counts (CFU/mL) after the activity of the phage. Each value is the mean  $\pm$  SD of three independent experiments. \*\*\*  $p < 0.001$ . Statistical analysis was performed with Student's *t*-test. Values are expressed as the mean  $\pm$  SD from three independent experiments with three replicates for each data point.

### 3.2. *Hp* $\phi$ +LF-HA Complex

The combination ratio of *Hp*  $\phi$  and HA-LF (*Hp*  $\phi$  +LF-HA) was determined for the following experiments. In particular, the optimization of the treatment with *Hp*  $\phi$  and HA-LF complex was carried out by testing different concentrations of *Hp*  $\phi$  incubated with HA-LF (data not shown). The optimal combination ratio was further characterized using the SEM microscopy analysis in order to validate the bounds of the phage with LF-HA. Previous studies have characterized the lactoferrin adsorbed onto the HA nanocrystal [23]; Figure 2 shows the phage bounds into the pores of the nanocrystal HA particles and lactoferrin.

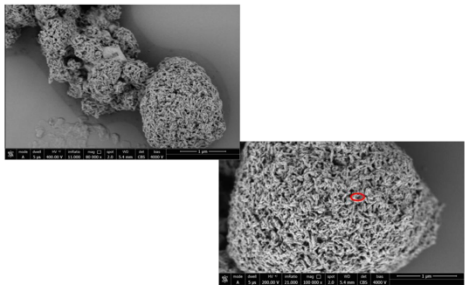


**Figure 2.** SEM image of the complex *Hp*  $\phi$  + LF-HA. The phage's capsid is represented as the light point (red square) on the HA nanocrystal.

3.3. Cytotoxic Activities of the Phage *Hp*  $\phi$

The isolated *Hp*  $\phi$  tested on human gastric cancer cell lines AGS alone or combined with LF-HA displayed non-cytotoxic activity. AGS cells remained vital for up to 72 h upon the treatments (Figure 3A). These results were confirmed by the Trypan Blue test, showing the treatment with the phage alone or combined with LF-HA does not induce the necrosis of the cells (Figure 3B). Compared to the cells treated with *Hp*, the phage alone or combined with LF-HA reduced  $\text{NO}_2$  production (Figure 3C). In particular, the complex showed the highest reduction of  $\text{NO}_2$  production.

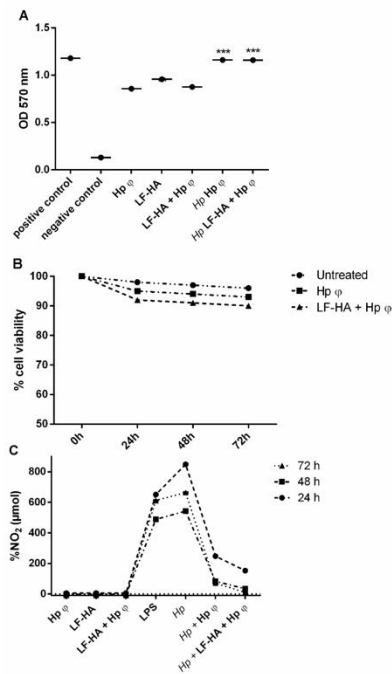


**Figure 3.** Cytotoxic assays. (A) MTT assay for cell viability. The experiment was performed in untreated AGS cells; cells treated with 50% ethanol; phage alone; *Hp* and phage; *Hp* and the complex *Hp*  $\phi$  + LF-HA. (B) Trypan blue test was performed at 72 h of treatment with 24 h time point. (C) % of  $\text{NO}_2$  levels in the culture medium. The measurements, obtained by Griess assay, were carried out in: Untreated AGS cells; cells treated with LPS (10  $\mu\text{g}/\text{mL}$ ); cells treated with *Hp*; cells treated with phage alone or combined with LF-HA; cells treated with *Hp* and phage alone or combined with LF-HA. \*\*\*  $p < 0.001$ . Statistical analysis was performed with Student's *t*-test. Values are the mean  $\pm$  SD from three independent experiments with three replicates for each data point.

### 3.4. In Vitro Infection of AGS Cells with *Helicobacter pylori* and Treatment with Hp $\phi$ +LF-HA

AGS human gastric cells were infected with *Hp* and incubated simultaneously with the phage; or treated for 24 h with the bacteria and then incubated for 3 h with Hp  $\phi$  alone or combined with LF-HA. The experiment was carried out in order to understand not only the efficacy of the phage, but the potential application as therapy; for this reason, the lytic activity was analyzed simultaneously or after the infection with *Hp*. The results displayed that the phage exerts antimicrobial activity also when administered when the infection is ongoing (Figure 4). Moreover, we explored the efficacy of the phage combined with LF adsorbed on synthetic hydroxyapatite nanoparticles, administered at 24 h post-infection. The complex displayed a four-fold enhanced antimicrobial activity compared to the phage alone (Figure 4).

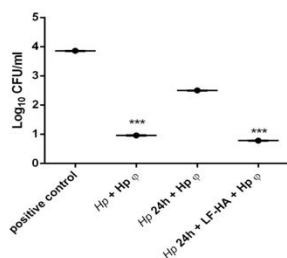


**Figure 4.** Modulation of antimicrobial effects against *Helicobacter pylori* on AGS cells. Antimicrobial activity of different treatments against *Hp* ( $10^6$  CFU/mL). Results are presented as mean value  $\pm$  SD and are representative of three independent experiments, each performed in triplicate. \*\*\*  $p$  value  $< 0.001$ .

In particular, Hp  $\phi$  used for extracellular bacteria reduced the colony counts of *Hp* not only when added simultaneously with the bacterium, but also when it was added 24 h after infection. When in complex with LF-HA, the phage activity can be correlated to the phage co-treatment. This result suggested that when the phage was in complex its activity was stabilized and increased over time. Hp  $\phi$  +LF-HA performed better also in terms of anti-inflammatory activity, inducing lower levels of *TNF- $\alpha$*  and *IFN- $\beta$*  genes (Figure 5)

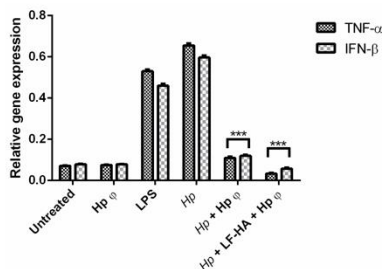


**Figure 5.** Expression profiling of AGS cell cytokine genes by quantitative real time PCR (qPCR). Cells were collected after 24 h of *Hp* infection and the different treatments. Statistical analysis was performed with Student's  $t$ -tests. \*\*\*  $p < 0.001$ .

### 3.5. ROS Detection Assay

Fluorescence microscope examination identified ROS overproduction in AGS cells infected with *Hp*, compared to control cells and a reduced production of ROS in cells treated with *Hp* phage, compared to *Hp* infected cells (Figure 6). A stronger reduction of ROS production was detected in cells treated with the complex *Hp*  $\phi$  + LF-HA compared to cells treated with *Hp*  $\phi$  (Figure 6A). In Figure 6B, results are reported as quantification of fluorescence of individual cells. To validate the ROS analysis the quantification of SOD1 production was carried out (Figure 6C). The relative gene expression confirms the decrease of ROS production when the AGS cells were treated with *Hp*  $\phi$  + LF-HA more than the cell treated with *Hp*  $\phi$  alone.

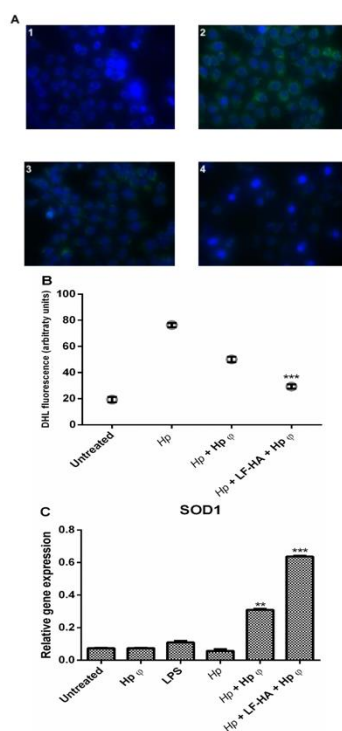


**Figure 6.** Effect of *Hp*  $\phi$  + LF-HA on ROS production. (A) DHR-loaded cells differently treated (1 untreated cell; 2 *Hp*; 3 *Hp* + *Hp*  $\phi$ ; 4 *Hp* + LF-HA + *Hp*  $\phi$ ), observed with a Leica DMI6000 fluorescence microscope equipped with Metamorph Imaging Software (Leica MetaMorph® AE, Wetzlar, Germany). (B) Quantification of the mean fluorescence of individual cells. Results are expressed as arbitrary units and represent the means  $\pm$  SD calculated from three to five separate experiments, each performed in duplicate. (C) Relative gene expression of *SOD1*. Statistical analysis was performed with Student's *t*-tests. \*\*  $p < 0.01$ ; \*\*\*  $p < 0.001$ .

#### 4. Discussion

The long-term *Hp* infection, and the associated chronic inflammation are the main risk factors for gastric cancer and extra-gastric diseases, which have an important social and economic impact worldwide, as they affect more than 50% of the population. Consequently, the treatment of *Hp* infection is essential for the management of more severe secondary pathologies. The recent and ever increasing problem of antibiotic resistance has determined the failure of the conventional treatment (proton pump inhibitors combined with clarithromycin and amoxicillin or metronidazole) against *Hp* infection [36,37]. Encouraging data are reported for the single three in one formulation, of metronidazole and tetracycline combined with bismute subcitrate potassium, which is able to eradicate *H. pylori*–clarithromycin resistant strains [38]. However, the urgent need of treatments able to substitute for common antibiotics makes the identification of innovative therapies necessary.

In previous studies, we showed the effective antimicrobial role of LF adsorbed on hydroxyapatite nanoparticles in *Hp* infection [23]. LF is an iron-binding protein able to chelate iron, inhibiting bacteria growth, and thus displaying bacteriostatic properties. In addition, lactoferrin binds to the outer membrane of Gram-negative bacteria, promoting the release of lipopolysaccharide (LPS) and cell lysis, thus also acting as a bactericidal [39,40].

In the present study, for the first time, we explored the role of *Hp* specific lytic phage (*Hp*  $\phi$ ) alone or combined with lactoferrin adsorbed on hydroxyapatite nanoparticles (*Hp*  $\phi$  +LF-HA) in counteracting *Hp* infection. We prove that LF-HA significantly increases *Hp*  $\phi$  activity. Our study suggests that phages complexed with lactoferrin are a powerful biological tool, able to specifically kill *Hp* without toxic effect on the host cells [41], thus representing a good therapeutic strategy in *Hp* infection. Moreover, the use of hydroxyapatite as carrier, able to improve the biological properties of both *Hp*  $\phi$  and LF [21,33], further supports our data. The efficacy of the above-described treatments was tested by using an in vitro model of *Hp* infection. In AGS cells infected with *Hp* for 24 h we found five-fold enhanced antimicrobial activity of the complex *Hp*  $\phi$  +LF-HA compared to *Hp*  $\phi$  (Figure 4). In fact, the complex *Hp*  $\phi$  +LF-HA administered after the infection was observed to maintain the bacterial load at the same level measured in cells infected with *Hp* and simultaneously treated with *Hp*  $\phi$  (Figure 4). These data indicate that LF-HA potentiates the antimicrobial activity of *Hp*  $\phi$ .

We next investigated the anti-inflammatory activity of *Hp*  $\phi$  alone or combined with LF-HA. Inflammation plays a key role in *Hp* infection by establishing serious tissue damages if not contained [42]. Both phage and lactoferrin have been recognized as modulators of inflammation, by attenuating the activation of the transcription factor NF- $\kappa$ B and in turn the release of pro-inflammatory cytokines [26,43]. The reduction of pro-inflammatory cytokines can be related to the LPS-binding properties of LF and phage, preventing LPS interaction with Toll-like receptor 4 (TLR4).

Based on this finding, we evaluated the expression level of gene encoding for TNF- $\alpha$  and IFN- $\beta$ , the main cytokines produced by LPS-stimulated TLR4 activation [44,45]. Cells treated with *Hp*  $\phi$  +LF-HA showed reduced TNF- $\alpha$  and IFN- $\beta$  gene expression, compared to cells treated with *Hp*  $\phi$  alone (Figure 5). Interestingly, we observed that the expression level of TNF- $\alpha$  and IFN- $\beta$  genes was lower in *Hp*  $\phi$  +LF-HA treated cells than in untreated ones (Figure 5).

A further confirmation of the role of phage and lactoferrin in modulating the inflammatory response was obtained by evaluating their capability of a negative regulation of *H. pylori*-induced reactive oxygen and nitrogen species (ROS and RNS) formation. In the presence of *H. pylori*, gastric epithelial cells produce ROS and RNS, an important hallmark of inflammation, which can lead to macromolecule damage, thus resulting in detrimental effects for the host cells rather than the microbial ones [46,47]. In the presence of *Hp*  $\phi$ , we detected a mitigated accumulation of ROS in infected AGS cells (Figure 6A,B). On the other hand, *Hp*  $\phi$  + LF-HA treatment considerably reduced ROS accumulation, compared to both *Hp*  $\phi$  treated and untreated cells (Figure 6A,B). Similar data were also obtained for the reactive nitrogen specie NO<sub>2</sub> (Figure 3C). In addition, we examined the expression levels of the *SOD1* gene, encoding for the antioxidant SOD1 enzyme, involved in neutralizing ROS and RNS [48]. An increased level of *SOD1* gene was found in *Hp*  $\phi$  +LF-HA treated cells (Figure 6C),

suggesting that the complex Hp  $\phi$  +LF-HA protects epithelial cells against the *H. pylori*-induced oxidative stress, by up-regulating the expression of antioxidant species [49].

## 5. Conclusions

In conclusion, this study describes the synergistic action of Hp  $\phi$  and LF-HA against *H. pylori*, and their capability to act as direct or indirect antimicrobial agents by reducing the bacterial colonization and the associated inflammation. However, some limitations should be noted. One of the major advantages of a combined therapy, both safety-wise and cost-wise, consists in reducing the doses of the single treatments. We addressed the potential therapeutic applicability of the complex Hp  $\phi$  +LF-HA, proving its effectiveness when administered upon the onset of the infection, but we did not determine the minimal effective combined doses of Hp  $\phi$  and LF-HA. We also still need to determine the genetic barrier to bacterial resistance against the complex Hp  $\phi$  +LF-HA. Lastly, additional in vivo studies should be performed in order to further investigate the efficacy and the clinical potential of the combined therapy. Nonetheless our findings suggest the complex Hp  $\phi$  +LF-HA as an innovative therapeutic approach for *Hp* infection. Importantly, this work may pave the way for a novel class of combined antibacterial therapies designed to fight a wide range of gastric infections.

**Author Contributions:** Conceptualization, R.C. and C.M.; methodology, P.C.; validation M.P.; data curation, A.F. and F.G.; writing—original draft preparation, P.C. and M.P.; writing—review and editing, C.M.; project administration, R.C. All authors have read and agreed to the published version of the manuscript.

**Funding:** This research received no external funding.

**Conflicts of Interest:** The authors declare no conflict of interest.

## References

- Schneider, S.; Carra, G.; Sahin, U.; Hoy, B.; Rieder, G.; Wessler, S. Complex cellular responses of *Helicobacter pylori*-colonized gastric adenocarcinoma cells. *Infect. Immun.* **2011**, *79*, 2362–2371. [\[CrossRef\]](#)
- Magalhães, A.; Marcos-Pinto, R.; Nairn, A.V.; dela Rosa, M.; Ferreira, R.M.; Junqueira-Neto, S.; Freitas, D.; Gomes, J.; Oliveira, P.; Santos, M.R.; et al. *Helicobacter pylori* chronic infection and mucosal inflammation switches the human gastric glycosylation pathways. *Biochim. Biophys. Acta Mol. Basis Dis.* **2015**, *1852*, 1928–1939. [\[CrossRef\]](#)
- Camilo, V.; Sugiyama, T.; Touati, E. Pathogenesis of *Helicobacter pylori* infection. *Helicobacter* **2017**, *22*, e12405. [\[CrossRef\]](#)
- Gravina, A.G.; Zagari, R.M.; De Musis, C.; Romano, L.; Loguercio, C.; Romano, M. *Helicobacter pylori* and extragastric diseases: A review. *World J. Gastroenterol.* **2018**, *24*, 3204–3221. [\[CrossRef\]](#)
- Contaldi, F.; Capuano, F.; Fulgione, A.; Aiese Cigliano, R.; Sanseverino, W.; Iannelli, D.; Medaglia, C.; Capparelli, R. The hypothesis that *Helicobacter pylori* predisposes to Alzheimer's disease is biologically plausible. *Sci. Rep.* **2017**, *7*, 7817. [\[CrossRef\]](#)
- Munita, J.M.; Arias, C.A. Mechanisms of Antibiotic Resistance. *World J. Gastroenterol.* **2018**, *24*, 3204.
- Romero-Calle, D.; Guimarães Benevides, R.; Góes-Neto, A.; Billington, C. Bacteriophages as Alternatives to Antibiotics in Clinical Care. *Antibiotics* **2019**, *8*, 138. [\[CrossRef\]](#)
- Capparelli, R.; Nocerino, N.; Lanzetta, R.; Silipo, A.; Amoresano, A.; Giangrande, C.; Becker, K.; Blaiotta, G.; Evidente, A.; Cimmino, A.; et al. Bacteriophage-Resistant *Staphylococcus aureus* Mutant Confers Broad Immunity against Staphylococcal Infection in Mice. *PLoS ONE* **2010**, *5*, e11720. [\[CrossRef\]](#)
- Principi, N.; Silvestri, E.; Esposito, S. Advantages and Limitations of Bacteriophages for the Treatment of Bacterial Infections. *Front. Pharmacol.* **2019**, *10*, 513. [\[CrossRef\]](#)
- Krut, O.; Bekeredjian-Ding, I. Contribution of the Immune Response to Phage Therapy. *J. Immunol.* **2018**, *200*, 3037–3044. [\[CrossRef\]](#)
- Górski, A.; Dąbrowska, K.; Międzybrodzki, R.; Weber-Dąbrowska, B.; Łusiak-Szelachowska, M.; Jorczyk-Matysiak, E.; Borysowski, J. Phages and immunomodulation. *Future Microbiol.* **2017**, *12*, 905–914. [\[CrossRef\]](#)



12. Labrie, S.J.; Samson, J.E.; Moineau, S. Bacteriophage resistance mechanisms. *Nat. Rev. Microbiol.* **2010**, *8*, 317–327. [\[CrossRef\]](#)
13. Morozova, V.V.; Vlassov, V.V.; Tikunova, N.V. Applications of Bacteriophages in the Treatment of Localized Infections in Humans. *Front. Microbiol.* **2018**, *9*, 1696. [\[CrossRef\]](#)
14. Nobrega, E.L.; Costa, A.R.; Santos, J.F.; Siliakus, M.F.; Van Lent, J.W.M.; Kengen, S.W.M.; Azeredo, J.; Kluskens, L.D. Genetically manipulated phages with improved pH resistance for oral administration in veterinary medicine. *Sci. Rep.* **2016**, *6*. [\[CrossRef\]](#)
15. Vinner, G.K.; Rezaie-Yazdi, Z.; Leppanen, M.; Stapley, A.G.F.; Leaper, M.C.; Malik, D.J. Microencapsulation of *Salmonella*-specific bacteriophage  $\phi$ 1 using spray-drying in a pH-responsive formulation and direct compression tableting of powders into a solid oral dosage form. *Pharmaceuticals* **2019**, *12*, 43. [\[CrossRef\]](#)
16. Dąbrowska, K. Phage therapy: What factors shape phage pharmacokinetics and bioavailability? Systematic and critical review. *Med. Res. Rev.* **2019**, *39*, med.21572. [\[CrossRef\]](#)
17. De Jong, W.H.; Born, P.J.A. Drug delivery and nanoparticles: Applications and hazards. *Int. J. Nanomed.* **2008**, *3*, 133–149. [\[CrossRef\]](#)
18. Devalapally, H.; Chaklam, A.; Amiji, M.M. Role of nanotechnology in pharmaceutical product development. *J. Pharm. Sci.* **2007**, *96*, 2547–2565. [\[CrossRef\]](#)
19. Ghiasi, B.; Sefidbakht, Y.; Rezaei, M. Hydroxyapatite for biomedicine and drug delivery. In *Advanced Structured Materials*; Springer: Berlin/Heidelberg, Germany, 2019; Volume 104, pp. 85–120.
20. Li, T.T.; Ling, L.; Lin, M.C.; Jiang, Q.; Lin, Q.; Lin, J.H.; Lou, C.W. Properties and mechanism of hydroxyapatite coating prepared by electrodeposition on a braid for biodegradable bone scaffolds. *Nanomaterials* **2019**, *9*, 679. [\[CrossRef\]](#)
21. Fulgione, A.; Ianniello, F.; Papaiani, M.; Contaldi, F.; Sgamma, T.; Giannini, C.; Pastore, S.; Velotta, R.; Della Ventura, B.; Roveri, N.; et al. Biomimetic hydroxyapatite nanocrystals are an active carrier for *Salmonella* bacteriophages. *Int. J. Nanomed.* **2019**, *14*, 2219–2232. [\[CrossRef\]](#)
22. Papaiani, M.; Cuomo, P.; Fulgione, A.; Albanese, D.; Gallo, M.; Paris, D.; Motta, A.; Iannelli, D.; Capparelli, R. Bacteriophages Promote Metabolic Changes in Bacteria Biofilm. *Microorganisms* **2020**, *8*, 480. [\[CrossRef\]](#)
23. Fulgione, A.; Nocerino, N.; Iannaccone, M.; Roperto, S.; Capuano, F.; Roveri, N.; Lelli, M.; Crasto, A.; Calogero, A.; Pilloni, A.P.; et al. Lactoferrin Adsorbed onto Biomimetic Hydroxyapatite Nanocrystals Controlling—In Vivo—The *Helicobacter pylori* Infection. *PLoS ONE* **2016**, *11*, e0158646. [\[CrossRef\]](#)
24. Okuda, M.; Nakazawa, T.; Yamauchi, K.; Miyashiro, E.; Koizumi, R.; Booka, M.; Teraguchi, S.; Tamura, Y.; Yoshikawa, N.; Adachi, Y.; et al. Bovine lactoferrin is effective to suppress *Helicobacter pylori* colonization in the human stomach: A randomized, double-blind, placebo-controlled study. *J. Infect. Chemother.* **2005**, *11*, 265–269. [\[CrossRef\]](#)
25. Drago-Serrano, M.E.; Campos-Rodriguez, R.; Carrero, J.C.; Delagarza, M. Lactoferrin: Balancing ups and downs of inflammation due to microbial infections. *Int. J. Mol. Sci.* **2017**, *18*, 501. [\[CrossRef\]](#)
26. Kruzel, M.L.; Zimecki, M.; Actor, J.K. Lactoferrin in a Context of Inflammation-Induced Pathology. *Front. Immunol.* **2017**, *8*, 1438. [\[CrossRef\]](#)
27. Tomasini, M.L.; Zanussi, S.; Sozzi, M.; Tedeschi, R.; Basaglia, G.; De Paoli, P. Heterogeneity of cag genotypes in *Helicobacter pylori* isolates from human biopsy specimens. *J. Clin. Microbiol.* **2003**, *41*, 976–980. [\[CrossRef\]](#)
28. Papaiani, M.; Contaldi, F.; Fulgione, A.; Woo, S.L.; Casillo, A.; Corsaro, M.M.; Parrilli, E.; Marcolungo, L.; Rossato, M.; Delledonne, M.; et al. Role of phage  $\phi$ 1 in two strains of *Salmonella* Rissen, sensitive and resistant to phage  $\phi$ 1. *BMC Microbiol.* **2018**, *18*, 208. [\[CrossRef\]](#)
29. Sambrook, J.; Fritsch, E.F.; Maniatis, T. *Molecular Cloning: A Laboratory Manual*; Cold Spring Harbor Laboratory Press: Cold Spring Harbor, NY, USA, 1989.
30. Capparelli, R.; Parlato, M.; Borriello, G.; Salvatore, P.; Iannelli, D. Experimental Phage Therapy against *Staphylococcus aureus* in Mice. *Antimicrob. Agents Chemother.* **2007**, *51*, 2765–2773. [\[CrossRef\]](#)
31. Papaiani, M.; Paris, D.; Woo, S.L.; Fulgione, A.; Rigano, M.M.; Parrilli, E.; Tutino, M.L.; Marra, R.; Manganiello, G.; Casillo, A.; et al. Plant dynamic metabolic response to bacteriophage treatment after *Xanthomonas campestris* pv. *campestris* infection. *Front. Microbiol.* **2020**, *11*, 732. [\[CrossRef\]](#)
32. Carrieri, R.; Manco, R.; Sapio, D.; Iannaccone, M.; Fulgione, A.; Papaiani, M.; de Falco, B.; Grauso, L.; Tarantino, P.; Ianniello, F.; et al. Structural data and immunomodulatory properties of a water-soluble heteroglycan extracted from the mycelium of an Italian isolate of *Ganoderma lucidum*. *Nat. Prod. Res.* **2017**, *31*, 2119–2125. [\[CrossRef\]](#)



33. Papaiani, M.; Ricciardelli, A.; Fulgione, A.; d'Errico, G.; Zoina, A.; Lorito, M.; Woo, S.L.; Vinale, F.; Capparelli, R. Antibiofilm Activity of a Trichoderma Metabolite against *Xanthomonas campestris* pv. *campestris*, Alone and in Association with a Phage. *Microorganisms* **2020**, *8*, 620. [\[CrossRef\]](#)
34. Livak, K.J.; Schmittgen, T.D. Analysis of Relative Gene Expression Data Using Real-Time Quantitative PCR and the 2- $\Delta\Delta$ CT Method. *Methods* **2001**, *25*, 402–408. [\[CrossRef\]](#)
35. Palomba, L.; Silvestri, C.; Imperatore, R.; Morello, G.; Piscitelli, F.; Martella, A.; Cristino, L.; Di Marzo, V. Negative regulation of leptin-induced reactive oxygen species (ROS) formation by cannabinoid CB1 receptor activation in hypothalamic neurons. *J. Biol. Chem.* **2015**, *290*, 13669–13677. [\[CrossRef\]](#)
36. Papastergiou, V.; Georgopoulos, S.D.; Karatapanis, S. Treatment of *Helicobacter pylori* infection: Meeting the challenge of antimicrobial resistance. *World J. Gastroenterol.* **2014**, *20*, 9898–9911. [\[CrossRef\]](#)
37. Goderska, K.; Agudo Pena, S.; Alarcon, T. *Helicobacter pylori* treatment: Antibiotics or probiotics. *Appl. Microbiol. Biotechnol.* **2018**, *102*. [\[CrossRef\]](#)
38. Pellicano, R.; Ribaldone, D.G.; Caviglia, G.P. Strategies for *Helicobacter pylori* eradication in the year 2020. *Saudi J. Gastroenterol.* **2020**, *26*, 63–65.
39. Orsi, N. The antimicrobial activity of lactoferrin: Current status and perspectives. *BioMetals* **2004**, *17*, 189–196. [\[CrossRef\]](#)
40. Iafisco, M.; Di Foggia, M.; Bonora, S.; Prat, M.; Roveri, N. Adsorption and spectroscopic characterization of lactoferrin on hydroxyapatite nanocrystals. *Dalt. Trans.* **2011**, *40*, 820–827. [\[CrossRef\]](#)
41. Salmund, G.P.C.; Fineran, P.C. A century of the phage: Past, present and future. *Nat. Rev. Microbiol.* **2015**, *13*, 777–786. [\[CrossRef\]](#)
42. Lamb, A.; Chen, L.F. Role of the *Helicobacter pylori*-Induced inflammatory response in the development of gastric cancer. *J. Cell. Biochem.* **2013**, *114*, 491–497. [\[CrossRef\]](#)
43. Górski, A.; Jonczyk-Matysiak, E.; Lusiak-Szelachowska, M.; Miedzybrodzki, R.; Weber-Dabrowska, B.; Borysowski, J. The potential of phage therapy in sepsis. *Front. Immunol.* **2017**, *8*, 1783. [\[CrossRef\]](#)
44. Soares, J.B.; Pimentel-Nunes, P.; Roncon-Albuquerque, R., Jr.; Leite-Moreira, A. The role of lipopolysaccharide/toll-like receptor 4 signaling in chronic liver diseases. *Hepatol. Int.* **2010**, *4*, 659–672. [\[CrossRef\]](#)
45. Yokota, S.I.; Pimentel-Nunes, P.; Roncon-Albuquerque, R.; Leite-Moreira, A. *Helicobacter pylori* lipopolysaccharides upregulate toll-like receptor 4 expression and proliferation of gastric epithelial cells via the MEK1/2-ERK1/2 mitogen-activated protein kinase pathway. *Infect. Immun.* **2010**, *78*, 468–476. [\[CrossRef\]](#)
46. Butcher, L.D.; den Hartog, G.; Ernst, P.B.; Crowe, S.E. Oxidative Stress Resulting From *Helicobacter pylori* Infection Contributes to Gastric Carcinogenesis. *CMGH* **2017**, *3*, 316–322. [\[CrossRef\]](#)
47. Ding, S.Z.; Minohara, Y.; Xue, J.F.; Wang, J.; Reyes, V.E.; Patel, J.; Dirden-Kramer, B.; Boldogh, I.; Ernst, P.B.; Crowe, S.E. *Helicobacter pylori* infection induces oxidative stress and programmed cell death in human gastric epithelial cells. *Infect. Immun.* **2007**, *75*, 4030–4039. [\[CrossRef\]](#)
48. Wang, Y.; Branicky, R.; Noë, A.; Hekimi, S. Superoxide dismutases: Dual roles in controlling ROS damage and regulating ROS signaling. *J. Cell Biol.* **2018**, *217*, 1915–1928. [\[CrossRef\]](#)
49. Kruzel, M.L.; Actor, J.K.; Zimecki, M.; Wise, J.; Ploszaj, P.; Mirza, S.; Kruzel, M.; Hwang, S.A.; Ba, X.; Boldogh, I. Novel recombinant human lactoferrin: Differential activation of oxidative stress related gene expression. *J. Biotechnol.* **2013**, *168*, 666–675. [\[CrossRef\]](#)



© 2020 by the authors. Licensee MDPI, Basel, Switzerland. This article is an open access article distributed under the terms and conditions of the Creative Commons Attribution (CC BY) license (<http://creativecommons.org/licenses/by/4.0/>).



OPEN

# Interaction between *MyD88*, *TIRAP* and *IL1RL1* against *Helicobacter pylori* infection

Andrea Fulgione<sup>1,2,11</sup>, Marina Papaiani<sup>1,11</sup>, Paola Cuomo<sup>3</sup>, Debora Paris<sup>3</sup>, Marco Romano<sup>4</sup>, Concetta Tuccillo<sup>4</sup>, Letizia Palomba<sup>5</sup>, Chiara Medaglia<sup>6</sup>, Massimiliano De Seta<sup>7</sup>, Nicolino Esposito<sup>7</sup>, Andrea Motta<sup>3</sup>, Antonio Iannelli<sup>8,9,10</sup>, Domenico Iannelli<sup>12</sup> & Rosanna Capparelli<sup>11,11</sup>

The Toll-interleukin 1 receptor superfamily includes the genes interleukin 1 receptor-like 1 (*IL1RL1*), Toll like receptors (*TLRs*), myeloid differentiation primary-response 88 (*MyD88*), and *MyD88* adaptor-like (*TIRAP*). This study describes the interaction between *MyD88*, *TIRAP* and *IL1RL1* against *Helicobacter pylori* infection. Cases and controls were genotyped at the polymorphic sites *MyD88* rs6853, *TIRAP* rs8177374 and *IL1RL1* rs11123923. The results show that specific combinations of *IL1RL1-TIRAP* (AA-CT; P:  $2.8 \times 10^{-17}$ ) and *MyD88-TIRAP-IL1RL1* (AA-CT-AA; P:  $1.4 \times 10^{-8}$ )—but not *MyD88* alone—act synergistically against *Helicobacter pylori*. Nuclear magnetic resonance (NMR) clearly discriminates cases from controls by highlighting significantly different expression levels of several metabolites (tyrosine, tryptophan, phenylalanine, branched-chain amino acids, short chain fatty acids, glucose, sucrose, urea, etc.). NMR also identifies the following dysregulated metabolic pathways associated to *Helicobacter pylori* infection: phenylalanine and tyrosine metabolism, pterine biosynthesis, starch and sucrose metabolism, and galactose metabolism. Furthermore, NMR discriminates between the cases heterozygous at the *IL1RL1* locus from those homozygous at the same locus. Heterozygous patients are characterized by high levels of lactate, and *IL1RL1*—both associated with anti-inflammatory activity—and low levels of the pro-inflammatory molecules IL-1 $\beta$ , TNF- $\alpha$ , COX-2, and IL-6.

*Helicobacter pylori* (*H. pylori*) is a Gram-negative, microaerophilic bacterium that colonizes the human stomach, and in most instances causes chronic gastritis. Though about half of the world population is infected with *H. pylori*, only <1% of infected patients develop peptic ulcer, gastric cancer, or lymphoma<sup>1</sup>. The virulence of the bacterium is in fact dependent upon several factors, especially its potential to produce toxins<sup>2</sup>, and the different routes of infection: vertical transmission (from parents to child) curbs pathogen virulence, while horizontal transmission (from one individual to another unrelated) breaks up the reduced virulence accumulated by the pathogen in the course of the co-evolution with the previous host<sup>3</sup>.

Notably, there is evidence that *H. pylori* might be associated with extra gastric diseases—Alzheimer's disease<sup>4</sup>, coronary heart disease<sup>5</sup>, atherosclerosis<sup>6</sup>—and, at the same time, might protect against other diseases: asthma

<sup>1</sup>Department of Agriculture Sciences, University of Naples "Federico II", Via Università, 100, 80055 Portici, Naples, Italy. <sup>2</sup>Istituto Zooprofilattico Sperimentale del Mezzogiorno, Via Salute, 2, 80055 Portici, Naples, Italy. <sup>3</sup>Institute of Biomolecular Chemistry, National Research Council, Via Campi Flegrei, 34, 80078 Pozzuoli, Naples, Italy. <sup>4</sup>Hepatogastroenterology Unit, Department of Precision Medicine, University of Campania "Luigi Vanvitelli", via Pansini, 5, 80131 Naples, Italy. <sup>5</sup>Department of Biomolecular Sciences, University of Urbino "Carlo Bo", Via Santa Chiara, 27, 61029 Urbino, Italy. <sup>6</sup>Department of Microbiology and Molecular Medicine, University of Geneva Medical School, Rue du Général-Dufour, 24, 1211 Genève 4, Switzerland. <sup>7</sup>Fondazione Evangelica Betania, Via Argine, 604, 80147 Naples, Italy. <sup>8</sup>Université Côte D'Azur, Campus Valrose, Batiment L, Avenue de Valrose, 28, 06108 Nice CEDEX 2, France. <sup>9</sup>Centre Hospitalier Universitaire de Nice - Digestive Surgery and Liver Transplantation Unit, Archet 2 Hospital, Route Saint-Antoine de Ginestière 151, CS 23079, 06202 Nice CEDEX 3, France. <sup>10</sup>Inserm, U1065, Team 8 "Hepatic Complications of Obesity and Alcohol", Route Saint Antoine de Ginestière 151, BP 2 3194, 06204 Nice CEDEX 3, France. <sup>11</sup>These authors contributed equally: Andrea Fulgione, Marina Papaiani and Rosanna Capparelli. <sup>12</sup>email: domenico.iannelli1935@gmail.com

and allergy<sup>6</sup>, esophageal adenocarcinoma, Barrett's esophagus, and gastroesophageal reflux<sup>7</sup>. Further, pathogen eradication with antibiotics can alter the gut microbiome and foster obesity or type 2 diabetes<sup>8</sup>. These findings indicate the importance of knowing risks and advantages associated with *H. pylori* eradication.

The members of the Toll-interleukin 1 receptor (TIR) superfamily are all characterized by the presence of the TIR domain. The superfamily includes interleukin 1 receptor-like 1 (*IL1RL1*) (also known as ST2), the Toll like receptors (*TLRs*), the adaptor molecule myeloid differentiation primary-response protein 88 (*MyD88*) and the *MyD88* adaptor-like *TIRAP* (also known as *MAL*). *TLRs* recognize pathogen associated molecular patterns (PAMPs), with *H. pylori* being recognized by several *TLRs*<sup>9</sup>. Following ligand binding, *TLRs* dimerize, go through a conformation change and—via their TIR domain—engage the adaptor proteins *MyD88* and *TIRAP*, which trigger a signal cascade leading to NF- $\kappa$ B activation and production of cytokines<sup>10</sup>. While the majority of the TIR family members activate NF- $\kappa$ B, *IL1RL1* inhibits NF- $\kappa$ B activation, as demonstrated by *IL1RL1*-deficient mouse macrophages, which produce higher levels of pro-inflammatory cytokines when challenged with lipopolysaccharides (LPS)<sup>11</sup>. *IL1RL1* exerts its inhibitory activity sequestering the adaptor molecules *MyD88* and *TIRAP* through the TIR domain<sup>11</sup>.

It is rare for genes to act alone. In most cases they form networks, highly flexible and adaptable<sup>12</sup>. The present study shows that *MyD88*, *TIRAP* and *IL1RL1*—all members of the same pathway<sup>13</sup> and the first two physically associated<sup>14</sup>—confer resistance against *H. pylori* infection acting in concert. While *MyD88* alone is unable to confer resistance, specific combinations of *MyD88* and *TIRAP* and of *MyD88*, *TIRAP* and *IL1RL1* act synergistically against *H. pylori*. The phenomenon of gene interaction is generally referred to as epistasis. Since this term has more than one meaning<sup>15</sup>, here we prefer using the unambiguous expression “gene interaction”.

Nuclear magnetic resonance (NMR)-based metabolomics is commonly used to identify metabolic pathways and to discriminate between specific metabolic phenotypes<sup>16,17</sup>. Here, NMR uncovers a potential crosstalk between metabolites and genes, and specific host pathways dysregulated by *H. pylori*.

## Results

**Interactions between *MyD88*, *TIRAP*, and *IL1RL1*.** *MyD88* and *TIRAP* interact against *H. pylori* infection<sup>18</sup>. We searched for potential proteins interacting with the *MyD88* and *TIRAP* proteins using the STRING database (<https://string-db.org>). The confidence level and maximum number of interacting proteins were set at the 0.4 and 5, respectively.

STRING database provided evidence that *IL1RL1* interacts with both *MyD88* and *TIRAP* (Fig. 1a). This conclusion is validated by current literature<sup>11,19</sup>. The samples (cases and controls) from an earlier study<sup>18</sup> were therefore used to test whether *IL1RL1* is associated with *H. pylori* infection, along with *MyD88* and *TIRAP*.

The *IL1RL1* SNP rs 11123923 was chosen to study since unique to have a rare allele frequency > 1%<sup>20</sup> out of the 159 *IL1RL1* SNPs identified by sequencing 45 cases and as many control samples (Supplementary Table S1).

The genes *MyD88*, *TIRAP*, and *IL1RL1* were first tested individually for association with *H. pylori* infection. *TIRAP* (OR: 0.50; *P*:  $3.7 \times 10^{-6}$ ) and *IL1RL1* (OR: 0.59; *P*:  $1.2 \times 10^{-4}$ )—but not *MyD88* (OR: 0.98; *P*: 0.95)—were associated with resistance to *H. pylori* infection (Table 1).

The study displayed additional interactions: between the genotypes *TIRAP*(CT)/*MyD88*(AG) vs *TIRAP*(CC)/*MyD88*(AA) (OR: 0.20; *P*:  $9.8 \times 10^{-9}$ ); *IL1RL1*(AA)/*MyD88*(AA) vs *IL1RL1*(CC)/*MyD88*(AA) (OR: 0.25; *P*:  $5.9 \times 10^{-9}$ ); *IL1RL1*(AA)/*TIRAP*(CT) vs *IL1RL1*(CC)/*TIRAP*(CC) (OR: 0.10; *P*:  $2.8 \times 10^{-17}$ ); *IL1RL1*(AA)/*MyD88*(AA)/*TIRAP*(CT) vs *IL1RL1*(CC)/*MyD88*(AA)/*TIRAP*(CC) (OR: 0.14; *P*:  $1.4 \times 10^{-6}$ ) (Table 2).

Finally, reduced expression levels of four inflammatory mediators (IL-6, COX2, TNF- $\alpha$ , and IL-1 $\beta$ ) were detected in patients with the *H. pylori*-resistant genotypes *IL1RL1*(AA)/*TIRAP*(CC); *IL1RL1*(AA)/*MyD88*(AA); and *IL1RL1*(AA)/*MyD88*(AA)/*TIRAP*(CT) vs *IL1RL1*(CC)/*MyD88*(AA)/*TIRAP*(CC) (Fig. 1b–d).

To the best of our knowledge, the present study is the first to describe the role of *MyD88*, *TIRAP*, and *IL1RL1* in the context of host resistance to *H. pylori* infection. A previous study by the same authors describes the interaction between *MyD88* and *TIRAP* and concludes that *MyD88* alone does not confer resistance to *H. pylori*, while the two genes do interact when in the double heterozygous combination (AG/CT; OR: 0.14; *P*:  $5.9 \times 10^{-13}$ )<sup>18</sup>. This result—confirmed in the present study (OR: 0.2; *P*:  $9.8 \times 10^{-9}$ )—is the unique detail linking the two studies.

**Nuclear magnetic resonance (NMR) analysis: cases versus controls.** Binding of IL-33 to its receptor *IL1RL1* may alter glucose and lipid metabolism<sup>21,22</sup>. Patients with type 2 diabetes or hypertriglyceridemia were therefore excluded. Thus, metabolome analysis was limited to blood samples from 59 cases and 17 controls. Representative proton spectra are shown in Supplementary Fig. S1.

Resonances were assigned to metabolites by comparing 2D NMR data with literature and/or online databases. Unsupervised PCA models excluded the presence of outliers (data not shown). OPLS-DA (VIP value > 1; correlation loading values [*p*(corr)] > 0.5) and a regression model with one predictive and one orthogonal component (goodness of fit:  $R^2 = 51\%$ ; power in prediction:  $Q^2 = 37\%$ ; significance for CV-ANOVA:  $P = 0.000001$ ) clearly differentiated cases (red squares) from controls (green squares) (Fig. 2a).

The scores plot of Fig. 2a shows a clear group separation along the predictive component between controls at negative values, and a dense cluster of cases placed mainly along t' positive values. The second orthogonal component instead describes the variation within each group. The associated loadings plot describes the NMR variables responsible for group separation (Fig. 2b).

The control group is characterized by high levels of tyrosine, tryptophan, phenylalanine, branched-chain amino acids (BCAA) (valine, leucine and isoleucine), 3-hydroxybutyrate, short chain fatty acids (SCFAs) and methyl-histidine, while the case group displays high levels of glucose, glucose-1-phosphate, sucrose, urea,

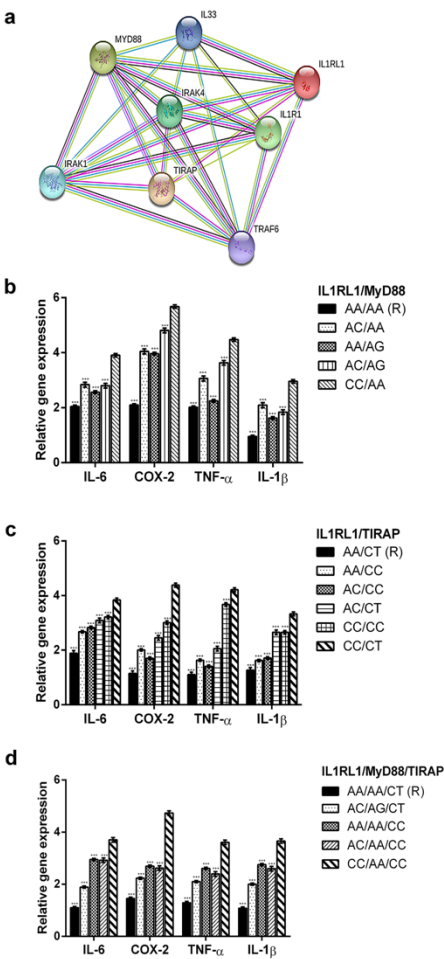


**Figure 1.** (a) MyD88, TIRAP and IL1RL1 interaction according to the STRING program; (b–d) Expression levels of IL-6, COX-2, TNF-α and IL-1β in patients with different combinations of IL1RL1, MyD88 and TIRAP. Each value represents the mean ± SD of 6 samples tested in triplicate.

Genes	Status	Number of individuals in each genotype			Total	HWE (P)	Allelic frequency		OR (CI) <sup>a</sup>	P value
		AA	AC	CC			Co	Ra		
IL1RL1	Cases	138	258	102	498	0.86 (0.35)	0.54	0.46	AA vs AC: 0.59 (0.46–0.77)	1.2 × 10 <sup>−4</sup>
	Controls	297	333	72	702	2.31 (0.12)	0.66	0.34		
MyD88	Cases	312	186	0	498	26.26 (3 × 10 <sup>−7</sup> )	0.81	0.19	AG vs AA 0.98 (0.77–1.25)	0.95
	Controls	421	254	27	702	2.24 (0.13)	0.78	0.22		
TIRAP	Cases	421	77	0	498	3.5 (0.061)	0.92	0.08	CT vs CC 0.50 (0.37–0.67)	3.7 × 10 <sup>−6</sup>
	Controls	508	184	10	702	2.15 (0.14)	0.85	0.15		

**Table 1.** Association between *IL1RL1* rs11123923, *MyD88* rs6853 and *TIRAP* rs8177374 polymorphic sites and *H. pylori* infection. Co common allele (*IL1RL1*: A; *MyD88*: A; *TIRAP*: C), Ra rare allele (*IL1RL1*: C; *MyD88*: G; *TIRAP*: T). <sup>a</sup> CI (confidence intervals) and P values were calculated with the Fisher's exact test.

Interactions	OR <sup>a</sup>	P value
<b>Allelic interactions</b>		
<i>IL1RL1</i> (AA vs AC)	0.59	1.2 × 10 <sup>−4</sup>
<i>MyD88</i> (AG vs AA)	0.98	0.95
<i>TIRAP</i> (CT vs CC)	0.50	3.7 × 10 <sup>−6</sup>
<b>Intergenic interactions</b>		
<i>IL1RL1</i> (AA)/ <i>MyD88</i> (AA) vs <i>IL1RL1</i> (CC)/ <i>MyD88</i> (AA)	0.25	5.9 × 10 <sup>−8</sup>
<i>IL1RL1</i> (AA)/ <i>MyD88</i> (AG) vs <i>IL1RL1</i> (CC)/ <i>MyD88</i> (AA)	0.32	2.5 × 10 <sup>−5</sup>
<i>TIRAP</i> (CC)/ <i>MyD88</i> (AG) vs <i>TIRAP</i> (CC)/ <i>MyD88</i> (AA)	1.30	5.4 × 10 <sup>−2</sup>
<i>TIRAP</i> (CT)/ <i>MyD88</i> (AG) vs <i>TIRAP</i> (CC)/ <i>MyD88</i> (AA)	0.20	9.8 × 10 <sup>−9</sup>
<i>IL1RL1</i> (AA)/ <i>TIRAP</i> (CT) vs <i>IL1RL1</i> (CC)/ <i>TIRAP</i> (CC)	0.10	2.8 × 10 <sup>−17</sup>
<i>IL1RL1</i> (AA)/ <i>TIRAP</i> (CC) vs <i>IL1RL1</i> (CC)/ <i>TIRAP</i> (CC)	0.61	2.2 × 10 <sup>−2</sup>
<i>IL1RL1</i> (AA)/ <i>MyD88</i> (AA)/ <i>TIRAP</i> (CC) vs <i>IL1RL1</i> (CC)/ <i>MyD88</i> (AA)/ <i>TIRAP</i> (CC)	0.48	1.4 × 10 <sup>−3</sup>
<i>IL1RL1</i> (AA)/ <i>MyD88</i> (AA)/ <i>TIRAP</i> (CT) vs <i>IL1RL1</i> (CC)/ <i>MyD88</i> (AA)/ <i>TIRAP</i> (CC)	0.14	1.4 × 10 <sup>−8</sup>

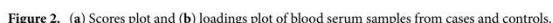
**Table 2.** Interaction between the *IL1RL1* rs11123923, *MyD88* rs6853 and *TIRAP* rs8177374 polymorphic sites and *H. pylori* infection. OR odds ratio estimated by Fisher's exact test; vs, withinlocus comparisons; /, between loci interactions.

glycolipids, and niacinamide. In particular, except for glucose-1-phosphate, sucrose, and niacinamide, all the discriminating metabolites were statistically significant (Figs. 3 and 4).

Further, pathway topology and biomarker analysis identified as significantly dysregulated the following metabolic pathways of phenylalanine, and tyrosine ( $P=1.05 \times 10^{-3}$ ; impact 0.22), pterine biosynthesis ( $P=3.63 \times 10^{-2}$ ; impact 0.16), starch and sucrose ( $P=1.23 \times 10^{-3}$ ; impact 0.15), and galactose metabolism ( $P=2.57 \times 10^{-3}$ ; impact 0.05) (Fig. 5).

Two differences are particularly relevant. First, the high level of urea displayed by the cases (Fig. 4) presumably reflects the increased need of urea by *H. pylori* for amino acid synthesis<sup>23</sup> and neutralization of the nitrogen excess accumulated by deamination of amino acids<sup>24</sup>. Second, *H. pylori* infection and high glucose levels (Fig. 3)—acting synergistically<sup>25</sup>—cause oxidative stress,  $\beta$ -cell dysfunction, and altered insulin secretion<sup>25</sup>. Finally, it has been suggested that impaired folate metabolism caused by *H. pylori* infection may affect cognitive functions<sup>26,27</sup>. Thus, the presence of pterines (a substrate for folate production) detected among cases in this study supports the hypothesis that *H. pylori* may predispose to Alzheimer's disease<sup>4</sup>.

**Nuclear magnetic resonance (NMR) analysis of cases.** Next aim was to identify potential metabolic differences between cases. This analysis was limited to the most representative class of cases (those homozygous at the *MYD88* and *TIRAP*, and heterozygous at the *IL1RL1* locus). For this purpose, it was built a regression model with two predictive components ( $R^2$  and  $Q^2$ ). The resulting scores plot differentiated heterozygous cases (*IL1RL1A/C*; n:14) from those homozygous (*IL1RL1A/A* (n:4) or *IL1RL1C/C* (n:6) (Fig. 6a)). The scores plot displays a main discrimination along the first predictive component between the heterozygous cases (red squares, located at t' positive coordinates) and both the homozygous AA (blue squares) and CC (black squares)



In particular, variables 4.12, 4.20, 1.32 (all originating from lactate) and 5.74–5.78 (from urea) are more intense in the corresponding AC group, which is placed at positive coordinates of the  $t^1$  axis (first component) in the scores plot. On the opposite, the same metabolites resulted less expressed in the AA and the CC groups, which are all placed at the opposite side of the  $t^1$  axis, namely negative values of the first component. The variables

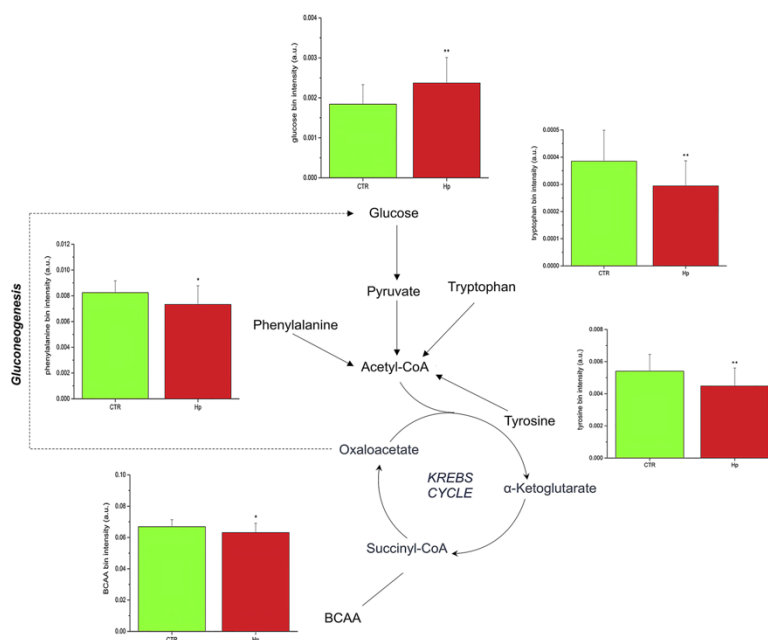


**Figure 3.** Expression levels and metabolic pathways of metabolites connected with Krebs cycle, glycolysis and gluconeogenesis.

5.24–5.22, and from 3.70 to 3.90 (Fig. 6b)—all corresponding to glucose resonances—are highly expressed in the CC group, placed at the corresponding superimposed quarter in the scores plot (Fig. 6a). Finally, variables 4.00, 6.92, 7.76, 7.86 from histidine resonances indicate the higher expression of this metabolite in the AA class. Signals with VIP value > 1 and correlation loading values  $|p(\text{corr})| > 0.5$  were selected as most relevant in the model discrimination. The corresponding bin quantification of the statistically significant metabolites glucose, and lactate are reported in Fig. 6c,d.

Finally, AC cases display low levels of IL-6, COX-2, TNF- $\alpha$ , IL-1 $\beta$ , and instead high level of IL1RL1, compared to homozygous cases (Fig. 7a,b).

### Discussion

There is growing evidence that genes rarely work alone<sup>28,29</sup>. More frequently, proteins tend to assemble into a complex, known as “cluster”, or “gene network”<sup>30</sup>. A gene cluster occurs more frequently between genes that physically interact or are members of the same biochemical pathway<sup>28,31</sup>. To detect the interaction between *MyD88* and *TIRAP* against *H. pylori* infection<sup>18</sup>, we built up on the notion that the *MyD88* and *TIRAP* proteins co-immune precipitate<sup>14</sup>. Here, to detect a potential third partner of *MyD88* and *TIRAP*, we used as probe the notion that *IL1RL1*, *MyD88*, and *TIRAP* are members of the same biochemical pathway<sup>13</sup>. The propensity of these genes to interact was then confirmed by the STRING tool (Fig. 1a).

Bateson defined epistasis as the phenomenon of a gene altering the phenotype of another gene<sup>32</sup>. Later, Fisher used the same term to describe two or more genes interacting non-additively<sup>33</sup>. The gene interactions described in this study conform to the statistical definition of Fisher as well as to that functional of Bateson. When tested individually, *TIRAP* (OR: 0.50;  $P$ :  $3.7 \times 10^{-6}$ ) and *IL1RL1* (OR: 0.59;  $P$ :  $1.2 \times 10^{-4}$ )—but not *MyD88* (OR: 0.98;  $P$ : 0.95)—confer resistance to *H. pylori* infection (Table 1). However, specific combinations of *MyD88* and *TIRAP* confer protection (OR: 0.20;  $P$ :  $9.8 \times 10^{-7}$ ) (Table 2). Robust interactions have also been observed between specific

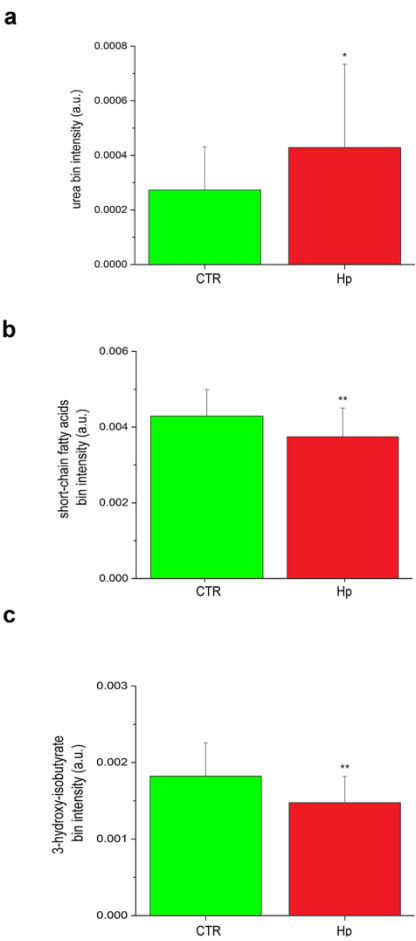


**Figure 4.** Expression levels of: (a) Urea, (b) Short chain fatty acids and (c) 3-Hydroxybutyrate detected in patients and controls.



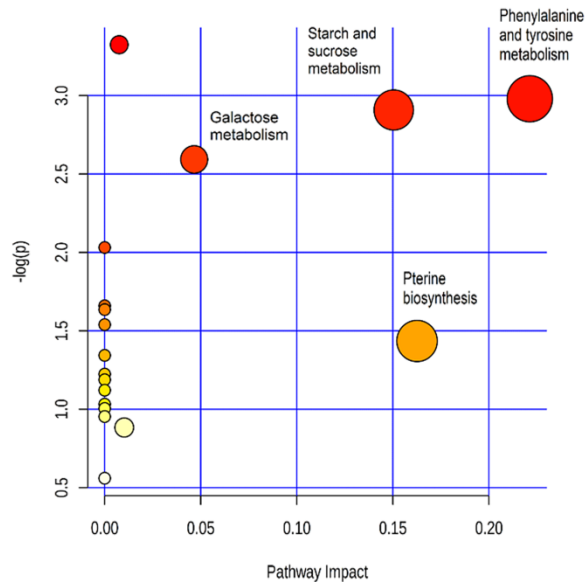


**Figure 5.** Impact and P value ( $-\log(p)$ ) of most representative metabolic pathways.

combinations of *IL1RL1* and *TIRAP* (OR: 0.10;  $P: 2.8 \times 10^{-17}$ ) and between *IL1RL1*, *MyD88* and *TIRAP* (OR: 0.14;  $P: 1.4 \times 10^{-8}$ ) (Table 2).

The marked differences noticed between metabolic profiles of cases and controls demand comments and plausible interpretations. BCAAs are present at low levels in cases. Pathway analysis shows that these molecules can generate glucose via gluconeogenesis (Fig. 3). Their reduced levels in patients may thus be explained assuming that BCAAs are depleted to secure the increased request of glucose associated with the response to *H. pylori* infection (Fig. 3). The high impact of the phenylalanine/tyrosine (impact 0.22;  $P = 1.05 \times 10^{-3}$ ) and starch/sucrose (impact 0.15;  $P = 1.23 \times 10^{-3}$ ) pathways concur with the proposed explanation (Fig. 5).

Major metabolic differences between cases and controls also involve inflammation. Patients infected with *H. pylori* show an excess of glucose (Fig. 3) and low levels of the ketone body 3-hydroxybutyrate and SCFAs (Fig. 4); the latter two molecules both inhibit NLRP3 activation<sup>34</sup>. This setting suggests that part of the excess of glucose might be converted to palmitate, which suppresses AMP-activated protein kinase, leading to ROS production and activation of the NLRP3 inflammasome<sup>35,36</sup>. In this context it seems plausible suggesting that the ketone body 3-hydroxybutyrate and SCFAs might be mobilized to counteract NLRP3 activation<sup>37,38</sup>. The proposed interpretation convincingly explains the reduced levels of SCFAs and 3-hydroxybutyrate.

Members of the TIR superfamily start the immune response by activating transcription of NF- $\kappa$ B and secretion of pro-inflammatory cytokines<sup>39</sup>. However, to prevent detrimental effects, inflammation needs to be tempered. This key function is assumed by *IL1RL1*. While almost all members of the TIR superfamily induce a TH1 (pro-inflammatory) response, *IL1RL1* (though member of the same family) inhibits the adaptors MyD88 and TIRAP and activates a TH2 (anti-inflammatory) response<sup>39</sup>, characterized by production of regulatory T cells (Treg), activation of the glucose transport gene *GLUT1*, that enhances glucose uptake and production of lactate<sup>40–42</sup>. In turn, lactate contributes to curb inflammation<sup>43</sup> by reducing the levels of the pro-inflammatory cytokines IL-1 $\beta$ , TNF- $\alpha$ , and IL-6<sup>44</sup>, while *H. pylori* senses lactate through the chemottractant receptor TtpC<sup>45</sup>.

The above data on the anti-inflammatory role of *IL1RL1* well support our suggestion that heterozygosity at the locus *IL1RL1* is associated with reduced inflammation in *H. pylori*-infected patients. This conclusion is based on several independent lines of evidence: a regression model with two predictive components clearly separate

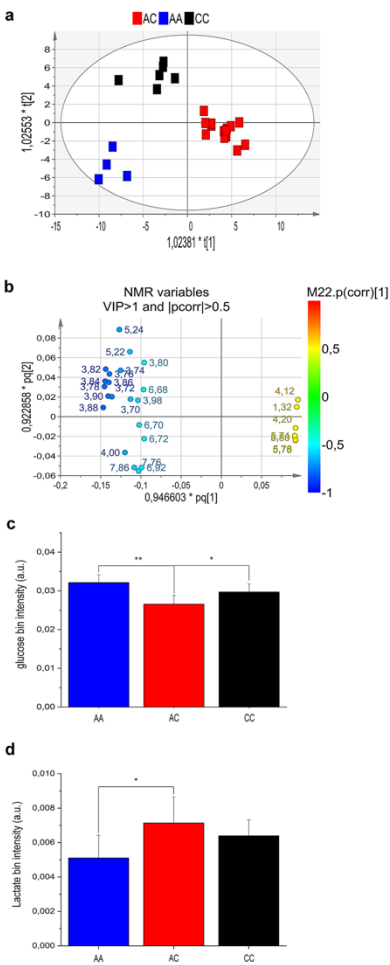


**Figure 6.** (a) Scores plot, (b) loadings plot, (c) glucose and (d) lactate levels of blood serum samples from patients homozygous at the MyD88 and TIRAP loci, but differing at the IL1RL1 locus.

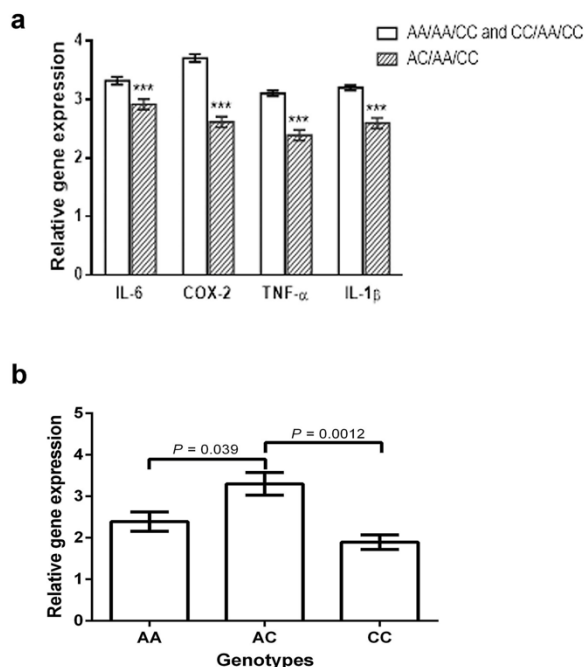


**Figure 7.** Expression levels of (a) IL-6, COX-2, TNF-α and IL-1β and (b) IL1RL1 in patients homozygous at the MyD88 and TIRAP loci, but differing at the IL1RL1 locus.

patients heterozygous at the *IL1RL1* locus (AC) from those homozygous (CC or AA) at the same locus (Fig. 6a;  $R^2 = 43$ ;  $Q^2 = 5\%$ ).

The results of the OPLS-DA analysis ( $R^2 = 43$ ;  $Q^2 = 5\%$ ) were confirmed by the independent procedure of probability calculus, which established that the probability that the patients in Fig. 6a cluster together by chance is  $1.8 \times 10^{-12}$  (see “Methods” section). This result shows the under-appreciated opportunity offered by metabolomics to reach solid conclusions enrolling a limited number of patients.

The AC patients are characterized by high levels of lactate (Fig. 6d), and IL1RL1 (Fig. 7b) (both associated with anti-inflammatory activity; see above)—and low levels of the pro-inflammatory molecules IL-1β, TNF-α, COX-2, and IL-6 (Fig. 7a). It is also cogent noting that the anti-inflammatory activity associated with the *IL1RL1*-AC genotype prescinds from the genotypes at the *MyD88* and *TIRAP* loci (Table 1).

*MyD88*, *TIRAP*, and *IL1RL1* well describe the elegant flexibility characterizing gene clusters. The majority of the TIR family members induce inflammation<sup>24</sup>. However, since an excess of inflammation is detrimental, the family includes *IL1RL1*, that curbs inflammation sequestering the pro-inflammatory adaptors *MyD88* and *TIRAP*<sup>29</sup>. Thus, to gain adaptability, gene clusters include members exerting opposite functions and network genetics engages Mendelian genetics. *IL1RL1*, independent from *MyD88* and *TIRAP* (Table 2), can finely control inflammation through the advantage of heterozygotes (the phenomenon describing the higher fitness of the heterozygous genotype compared to both homozygous genotypes), the dominant force maintaining genetic variation in the populations<sup>36,47</sup> and common diseases variants<sup>48</sup>.

A lateral result from this study, is that several metabolic pathways dysregulated by *H. pylori*—tyrosine, starch/sucrose and pterines metabolisms (Fig. 5)—have recently been reported to be dysregulated also in patients with

Alzheimer's disease<sup>49–52</sup>. These findings support the hypothesis that *H. pylori* may predispose to Alzheimer's disease<sup>5</sup>.

In summary, compared to single locus association studies, analysis of gene clusters extends results to several loci, increases the statistical power, and uncovers novel information about metabolic pathways associated with diseases<sup>43</sup>. Further, our data show that the combined analysis of genes and metabolites leads to results (such as patients subtyping on the basis of their inflammation levels), that the gene approach alone does not reach.

This study, which highlights a crosstalk between genes—in particular SNPs—and metabolites, could represent the basis for developing personal and specific therapeutic treatments. By this way, the proposed approach could be considered as “new alternative” to the well-known antimicrobial peptides, in the case of resistant strains such as *Staphylococcus epidermidis*<sup>54</sup> or, to the specific immunomodulatory methods for coeliac disease<sup>55</sup>.

Whether *IL1RL1* and lactate might represent clinically useful biomarkers of the inflammation remains to be investigated.

## Methods

**Cases and controls.** Cases and controls are the same used in the previous study (at least those still available)<sup>18</sup>. Patients with dysmetabolic diseases (type 2 diabetes or obesity) were excluded. Cases (498) were positive by the bacteriological, hematoxylin–eosin, and PCR tests for *H. pylori*. Controls (702) were participants negative to the above tests and, to exclude past infection, to the *H. pylori*-specific IgG antibody test (Abcam, Cambridge, UK; code ab108736)<sup>18</sup>.

The study has been approved by the Ethics Committee of Villa Betanina Hospital, and carried out in accordance with relevant guidelines and regulations (Declaration of Helsinki). In addition, the informed consent has been obtained from all participants.

**Genotyping.** Probes and TaqMan genotyping master mix were from Applied Biosystems (Life Technologies, Monza, Italy). Probes were specific for the following polymorphic sites (SNPs): *IL1RL1* rs11123923, *MyD88* rs6853 and *TIRAP* rs8177374. The PCR program was as described<sup>18</sup>. To confirm genotyping accuracy, PCR products representing 10% of the sample population were sequenced. ORs and 95% confidence intervals were calculated by Fisher's exact test using the statistical package GraphPad Prism version 5 (GraphPad, La Jolla, CA, USA).

**Quantitative real-time PCR.** RNA samples were reverse transcribed with the High-Capacity cDNA Reverse Transcription Kit (Applied Biosystem, Thermo Fisher Scientific Inc, Milan, Italy). Real-time PCR of *IL-6*, *COX-2*, *TNF-α* and *IL-1β* was carried out as described<sup>18</sup>. The expression level of *IL1RL1* was measured using the TaqMan Gene Expression Assay (Hs00249384\_m1; Life Technologies, Monza, Italy), and TaqMan PCR master 2X reagent (Applied Biosystem, Thermo Fisher Scientific Inc., Milan, Italy). The Applied Biosystem iCycler was used according to the manufacturer's instructions. PCR reactions were carried out in triplicate; expression values were calculated according to  $2^{-\Delta\Delta C_T}$  method and normalized against human glyceraldehydes-3-phosphate dehydrogenase (GAPDH) levels. As “calibrator”, we used a negative (control) sample.

The statistical analysis was carried out according to the two-way ANOVA using the statistical package GraphPad Prism version 5 (GraphPad, La Jolla, CA, USA).

**Protein network analysis.** *IL1RL1* was identified as third partner of *MyD88* and *TIRAP* using the STRING database (<https://string-db.org>). The level of confidence and the maximum number of interacting proteins were set at 0.4 and 5, respectively.

**Metabolites extraction.** Metabolites were extracted from blood samples (59 cases and 17 controls) as described<sup>46</sup>. Briefly, 2.5 mL of chloroform: methanol: dd H<sub>2</sub>O (1:1:1.3) mixture were added to 500 µL of individual blood samples and rapidly centrifuged (410 rpm; 20 min at 4 °C). The upper polar phase was collected and vacuum -dried at 30 °C using the rotational vacuum concentrator (model RVC 2-18 CD plus; Martin Christ Gefrier Trocknungsanlagen GmbH, Osterode am Harz, Germany).

Dried samples were suspended in 630 µL of phosphate buffer saline (PBS) plus 70 µL of deuterated solvent (containing 0.1 mM sodium 3-trimethylsilyl [2,2,3,3-<sup>2</sup>H<sub>4</sub>] propionate (TSP) as a chemical shift reference for <sup>1</sup>H spectra). Deuterated solvent was added to obtain a field-frequency lock. The final individual sample volume was 700 µL. All reagents were from Sigma-Aldrich S.r.l. Milan, Italy.

**NMR spectroscopy.** NMR spectra were recorded on a Bruker Avance III–600 MHz spectrometer (Bruker BioSpin GmbH, Rheinstetten, Germany) equipped with a TCI CryoProbe<sup>+</sup>, fitted with a gradient along the Z-axis, at a probe temperature of 300 K (27 °C).

Profile analysis and metabolites identification were determined from one- (1D), and two-dimensional (2D) spectra.

For further details, see Supplementary Methods.

**Multivariate data analysis.** The 0.60–9.40 ppm spectral area of blood aqueous extracts underwent bucketing, and each region of 0.02-ppm width was integrated by using the AMIX 3.9.15 software (Bruker Biospin GmbH, Rheinstetten, Germany). For further details, see Supplementary Methods.

**Principal component analysis (PCA) and orthogonal projection to latent structures discriminant analysis (OPLS-DA).** PCA<sup>57</sup> and OPLS-DA<sup>58</sup> were carried out with the SIMCA P+14 package (Umetrics, Umeå, Sweden). Data trends and the presence of possible outliers were evaluated by PCA, while OPLS-DA was used to better define clustering and metabolic variation. For further details, see Supplementary Methods.

The results of the OPLS-DA analysis were confirmed by the independent procedure of the probability calculus. The probability that the 4 patients AA cluster together by chance is  $(0.33)^4 = 10^{-2}$ ; that the 6 patients CC cluster together by chance is  $(0.33)^6 = 10^{-3}$ ; the probability that the 14 patients AC cluster together by chance is  $(0.33)^{14} = 1.8 \times 10^{-7}$ . The probability that the three events occur concurrently by chance is  $10^{-2} \times 10^{-3} \times 1.8 \times 10^{-7} = 1.8 \times 10^{-12}$ .

**Pathway analysis.** Pathway topology and biomarker analysis of discriminating metabolites were carried out by using MetaboAnalyst 4.0.<sup>59</sup> For further details, see Supplementary Methods.

#### Data availability

The authors declare that all the data supporting the findings of this study are included in this paper and its Supplementary Information files, and also are available from the corresponding author upon reasonable request.

Received: 7 May 2020; Accepted: 7 September 2020

Published online: 28 September 2020

#### References

- Kodaman, N. *et al.* Human and *Helicobacter pylori* coevolution shapes the risk of gastric disease. *Proc. Natl. Acad. Sci.* **111**, 1455–1460 (2014).
- Dundon, W. G., de Bernard, M. & Montecucco, C. Virulence factors of *Helicobacter pylori*. *Int. J. Med. Microbiol.* **290**, 647–658 (2001).
- Contaldi, F. *et al.* The hypothesis that *Helicobacter pylori* predisposes to Alzheimer's disease is biologically plausible. *Sci. Rep.* **7**, 7817 (2017).
- Zuin, M. *et al.* Coronary artery disease and *Helicobacter pylori* infection: Should we consider eradication therapy as cardiovascular prevention strategy? *Int. J. Cardiol.* **223**, 711–712 (2016).
- Nasif, W. A., Mukhtar, M. H., Nour Eldein, M. M. & Ashgar, S. S. Oxidative DNA damage and oxidized low density lipoprotein in Type II diabetes mellitus among patients with *Helicobacter pylori* infection. *Diabetol. Metab. Syndr.* **8**, 34 (2016).
- Blaser, M. J., Chen, Y. & Reibman, J. Does *Helicobacter pylori* protect against asthma and allergy? *Gut* **57**, 561–567 (2008).
- Anderson, L. A. *et al.* Relationship between *Helicobacter pylori* infection and gastric atrophy and the stages of the oesophageal inflammation, metaplasia, adenocarcinoma sequence: results from the FINBAR case-control study. *Gut* **57**, 734–739 (2008).
- Moreno-Indias, I., Cardona, F., Tinahones, F. J. & Queipo-Ortuño, M. I. Impact of the gut microbiota on the development of obesity and type 2 diabetes mellitus. *Front. Microbiol.* **5**, 190 (2014).
- Hu, Y., Liu, J.-P., Zhu, Y. & Lu, N.-H. The importance of toll-like receptors in NF- $\kappa$ B signaling pathway activation by *Helicobacter pylori* infection and the regulators of this response. *Helicobacter* **21**, 428–440 (2016).
- Akira, S. & Takeda, K. Toll-like receptor signalling. *Nat. Rev. Immunol.* **4**, 499–511 (2004).
- Brint, E. K. *et al.* ST2 is an inhibitor of interleukin 1 receptor and Toll-like receptor 4 signaling and maintains endotoxin tolerance. *Nat. Immunol.* **5**, 373–379 (2004).
- Breen, M. S., Kemena, C., Vlasov, P. K., Notredame, C. & Kondrashov, F. A. Epistasis as the primary factor in molecular evolution. *Nature* **490**, 535–538 (2012).
- Savenije, O. E. *et al.* Association of IL33-IL-1 receptor-like 1 (IL1RL1) pathway polymorphisms with wheezing phenotypes and asthma in childhood. *J. Allergy Clin. Immunol.* **134**, 170–177 (2014).
- Valkov, E. *et al.* Crystal structure of Toll-like receptor adaptor MAL/TIRAP reveals the molecular basis for signal transduction and disease protection. *Proc. Natl. Acad. Sci. U.S.A.* **108**, 14879–14884 (2011).
- Cordell, H. J. Epistasis: what it means, what it doesn't mean, and statistical methods to detect it in humans. *Hum. Mol. Genet.* **11**, 2463–2468 (2002).
- Wishart, D. S. NMR metabolomics: a look ahead. *J. Magn. Reson.* **306**, 155–161 (2019).
- Paris, D., Maniscalco, M. & Motta, A. Nuclear magnetic resonance-based metabolomics in respiratory medicine. *Eur. Respir. J.* **52**, 1801107 (2018).
- Fulgione, A. *et al.* Epistatic interaction between *MyD88* and *TIRAP* against *Helicobacter pylori*. *FEBS Lett.* **590**, 2127–2137 (2016).
- Bastith, S., Manavalan, B., Govindaraj, R. G. & Choi, S. In silico approach to inhibition of signaling pathways of Toll-like receptors 2 and 4 by ST2L. *PLoS ONE* **6**, e23989 (2011).
- Clarke, G. M. *et al.* Basic statistical analysis in genetic case-control studies. *Nat. Protoc.* **6**, 121–133 (2011).
- Niemela, S. *et al.* Could *Helicobacter pylori* infection increase the risk of coronary heart disease by modifying serum lipid concentrations? *Heart* **75**, 573–575 (1996).
- Buzás, G. M. Metabolic consequences of *Helicobacter pylori* infection and eradication. *World J. Gastroenterol.* **20**, 5226 (2014).
- Williams, C. L., Preston, T., Hossack, M., Slater, C. & McColl, K. E. *Helicobacter pylori* utilises urea for amino acid synthesis. *FEMS Immunol. Med. Microbiol.* **13**, 87–94 (1996).
- Hazell, S. L. & Mendz, G. L. How *Helicobacter pylori* works: an overview of the metabolism of *Helicobacter pylori*. *Helicobacter* **2**, 1–12 (1997).
- Mendz, G. L., Hazell, S. L. & Burns, B. P. Glucose utilization and lactate production by *Helicobacter pylori*. *J. Gen. Microbiol.* **139**, 3023–3028 (1993).
- Kountouras, J., Gavalas, E., Boziki, M. & Zavos, C. *Helicobacter pylori* may be involved in cognitive impairment and dementia development through induction of atrophic gastritis, vitamin B-12-folate deficiency, and hyperhomocysteinemia sequence [1]. *Am. J. Clin. Nutr.* **86**, 805–806 (2007).
- Berrett, A. N., Gale, S. D., Erickson, L. D., Brown, B. L. & Hedges, D. W. Folate and inflammatory markers moderate the association between *Helicobacter pylori* exposure and cognitive function in US adults. *Helicobacter* **21**, 471–480 (2016).
- Wu, X. *et al.* Bladder cancer predisposition: a multigenic approach to DNA-repair and cell-cycle-control genes. *Am. J. Hum. Genet.* **78**, 464–479 (2006).
- Gaiteri, C., Ding, Y., French, B., Tseng, G. C. & Sibille, E. Beyond modules and hubs: the potential of gene coexpression networks for investigating molecular mechanisms of complex brain disorders. *Genes Brain Behav.* **13**, 13–24 (2014).
- Segrè, D., DeLana, A., Church, G. M. & Kishony, R. Modular epistasis in yeast metabolism. *Nat. Genet.* **37**, 77–83 (2005).

31. Collins, S. R. *et al.* Functional dissection of protein complexes involved in yeast chromosome biology using a genetic interaction map. *Nature* **446**, 806–810 (2007).
32. Bateson, W., Mendel, G. & Mendel, G. *Mendel's Principles Of Heredity* by W. Bateson (University Press, Cambridge, 1909). <https://doi.org/10.5962/bhl.title.44575>.
33. Petronis, A. Epigenetics as a unifying principle in the aetiology of complex traits and diseases. *Nature* **465**, 721–727 (2010).
34. Youm, Y.-H. *et al.* The ketone metabolite  $\beta$ -hydroxybutyrate blocks NLRP3 inflammasome-mediated inflammatory disease. *Nat. Med.* **21**, 263–269 (2015).
35. Wen, H. *et al.* Fatty acid-induced NLRP3-ASC inflammasome activation interferes with insulin signaling. *Nat. Immunol.* **12**, 408–415 (2011).
36. Swanson, K. V., Deng, M. & Ting, J. P.-Y. The NLRP3 inflammasome: molecular activation and regulation to therapeutics. *Nat. Rev. Immunol.* **19**, 477–489 (2019).
37. Shimazu, T. *et al.* Suppression of oxidative stress by  $\beta$ -hydroxybutyrate, an endogenous histone deacetylase inhibitor. *Science* (80-) **339**, 211–214 (2013).
38. Luster, A. D., Alon, R. & von Andrian, U. H. Immune cell migration in inflammation: present and future therapeutic targets. *Nat. Immunol.* **6**, 1182–1190 (2005).
39. Kawai, T. & Akira, S. The role of pattern-recognition receptors in innate immunity: update on Toll-like receptors. *Nat. Immunol.* **11**, 373–384 (2010).
40. Kim, S. T. *et al.* The  $\alpha\beta$  T cell receptor is an anisotropic mechanosensor. *J. Biol. Chem.* **284**, 31028–31037 (2009).
41. Saitakis, M. *et al.* Different TCR-induced T lymphocyte responses are potentiated by stiffness with variable sensitivity. *Elife* **6**, e23190 (2017).
42. Rossy, J., Laufer, J. M. & Legler, D. F. Role of mechanotransduction and tension in T cell function. *Front. Immunol.* **9**, 2638 (2018).
43. Schaffer, K. & Taylor, C. T. The impact of hypoxia on bacterial infection. *FEBS J.* **282**, 2260–2266 (2015).
44. Ratter, J. M. *et al.* In vitro and in vivo effects of lactate on metabolism and cytokine production of human primary PBMCs and monocytes. *Front. Immunol.* **9**, 2564 (2018).
45. Machuca, M. A. *et al.* *Helicobacter pylori* chemoreceptor TipC mediates chemotaxis to lactate. *Sci. Rep.* **7**, 14089 (2017).
46. Crow, J. F., Muller, D., Dobzhansky, S. and overdominance. *J. Hered.* **20**, 351–380 (1987).
47. Haldane, J. B. S. A mathematical theory of natural selection. Part VIII. Metastable populations. *Math. Proc. Camb. Philos. Soc.* **27**, 137–142 (1931).
48. Kimura, M. Rules for testing stability of a selective polymorphism. *Proc. Natl. Acad. Sci.* **42**, 336–340 (1956).
49. Liu, T. F., Vachharajani, V. T., Yoza, B. K. & McCall, C. E. NAD<sup>+</sup>-dependent sirtuin 1 and 6 proteins coordinate a switch from glucose to fatty acid oxidation during the acute inflammatory response. *J. Biol. Chem.* **287**, 25758–25769 (2012).
50. Joseph, S. B., Castriello, A., Laffitte, B. A., Mangelsdorf, D. J. & Tontonoz, P. Reciprocal regulation of inflammation and lipid metabolism by liver X receptors. *Nat. Med.* **9**, 213–219 (2003).
51. Sparks Stein, P. *et al.* Serum antibodies to periodontal pathogens are a risk factor for Alzheimer's disease. *Alzheimers Dement.* **8**, 196–203 (2012).
52. Chen, J. *et al.* Gene expression analysis reveals the dysregulation of immune and metabolic pathways in Alzheimer's disease. *Oncotarget* **7**, 72469–72474 (2016).
53. Li, Y. & Agarwal, P. A pathway-based view of human diseases and disease relationships. *PLoS ONE* **4**, e4346 (2009).
54. Capparelli, R. *et al.* New perspectives for natural antimicrobial peptides: Application as anti-inflammatory drugs in a murine model. *BMC Immunol.* **13**, 61 (2012).
55. Rossi, M. *et al.* Intravenous or intranasal administration of gliadin is able to down-regulate the specific immune response in mice. *Scand. J. Immunol.* **50**, 177–182 (1999).
56. McHugh, C. *et al.* Rapid, reproducible, quantifiable NMR metabolomics: methanol and methanol: chloroform precipitation for removal of macromolecules in serum and whole blood. *Metabolites* **8**, 93 (2018).
57. Eriksson, L., Byrne, T., Johansson, E., Trygg, J. & Vikström, C. *Multi- and Megavariate Data Analysis: Basic Principles and Applications* (Umetrics Academy, Umea, 2013).
58. Trygg, J. & Wold, S. Orthogonal projections to latent structures (O-PLS). *J. Chemom.* **16**, 119–128 (2002).
59. Chong, J. *et al.* MetaboAnalyst 4.0: towards more transparent and integrative metabolomics analysis. *Nucleic Acids Res.* **46**, W486–W494 (2018).

#### Author contributions

A.F., M.P., P.C., D.P., C.T. and L.P. performed the experiments; A.F., M.R., A.M., C.M., M.D.S., N.E., A.I., D.I. and R.C. analysed the data, R.C., D.I. and A.F. conceived the work; and D.I. and R.C. wrote the manuscript. All authors reviewed the manuscript.

#### Competing interests

The authors declare no competing interests.


#### Additional information

**Supplementary information** is available for this paper at <https://doi.org/10.1038/s41598-020-72974-9>.

**Correspondence** and requests for materials should be addressed to D.I.

**Reprints and permissions information** is available at [www.nature.com/reprints](http://www.nature.com/reprints).

**Publisher's note** Springer Nature remains neutral with regard to jurisdictional claims in published maps and institutional affiliations.

 **Open Access** This article is licensed under a Creative Commons Attribution 4.0 International License, which permits use, sharing, adaptation, distribution and reproduction in any medium or format, as long as you give appropriate credit to the original author(s) and the source, provide a link to the Creative Commons licence, and indicate if changes were made. The images or other third party material in this article are included in the article's Creative Commons licence, unless indicated otherwise in a credit line to the material. If material is not included in the article's Creative Commons licence and your intended use is not permitted by statutory regulation or exceeds the permitted use, you will need to obtain permission directly from the copyright holder. To view a copy of this licence, visit <http://creativecommons.org/licenses/by/4.0/>.

© The Author(s) 2020



## Article

# Production and Characterization of Medium-Sized and Short Antioxidant Peptides from Soy Flour-Simulated Gastrointestinal Hydrolysate

Chiara Cavaliere <sup>1</sup>, Angela Michela Immacolata Montone <sup>2,3</sup>, Sara Elsa Aita <sup>1</sup>, Rosanna Capparelli <sup>4</sup>, Andrea Cerrato <sup>1</sup>, Paola Cuomo <sup>4</sup>, Aldo Laganà <sup>1,5</sup>, Carmela Maria Montone <sup>1,\*</sup>, Susy Piovesana <sup>1</sup> and Anna Laura Capriotti <sup>1</sup>

- <sup>1</sup> Department of Chemistry, Università di Roma "La Sapienza", Piazzale Aldo Moro 5, 00185 Rome, Italy; chiara.cavaliere@uniroma1.it (C.C.); saraelsa.aita@uniroma1.it (S.E.A.); andrea.cerrato@uniroma1.it (A.C.); aldo.lagana@uniroma1.it (A.L.); susy.piovesana@uniroma1.it (S.P.); annalaura.capriotti@uniroma1.it (A.L.C.)
- <sup>2</sup> Istituto Zooprofilattico Sperimentale del Mezzogiorno, Via Salute 2, Portici, 80055 Naples, Italy; angela.montone@izsmportici.it
- <sup>3</sup> Department of Industrial Engineering, Università degli Studi di Salerno, Via Giovanni Paolo II 132, 84084 Fisciano, Italy
- <sup>4</sup> Department of Agriculture Sciences, University of Naples "Federico II", Via Università 100, Portici, 80055 Naples, Italy; capparel@unina.it (R.C.); paola.cuomo@unina.it (P.C.)
- <sup>5</sup> CNR NANOTEC, Campus Ecotekne, University of Salento, Via Monteroni, 73100 Lecce, Italy
- \* Correspondence: carmelamaria.montone@uniroma1.it



**Citation:** Cavaliere, C.; Montone, A.M.I.; Aita, S.E.; Capparelli, R.; Cerrato, A.; Cuomo, P.; Laganà, A.; Montone, C.M.; Piovesana, S.; Capriotti, A.L. Production and Characterization of Medium-Sized and Short Antioxidant Peptides from Soy Flour-Simulated Gastrointestinal Hydrolysate. *Antioxidants* **2021**, *10*, 734. <https://doi.org/10.3390/antiox10050734>

Academic Editor: Simone Carradori

Received: 1 April 2021  
Accepted: 30 April 2021  
Published: 6 May 2021

**Publisher's Note:** MDPI stays neutral with regard to jurisdictional claims in published maps and institutional affiliations.



**Copyright:** © 2021 by the authors. Licensee MDPI, Basel, Switzerland. This article is an open access article distributed under the terms and conditions of the Creative Commons Attribution (CC BY) license (<https://creativecommons.org/licenses/by/4.0/>).

**Abstract:** Soybeans (*Glycine max*) are an excellent source of dietary proteins and peptides with potential biological activities, such as antihypertensive, anti-cholesterol, and antioxidant activity; moreover, they could prevent cancer. Also, soy contains all the essential amino acids for nutrition; therefore, it represents an alternative to animal proteins. The goal of this paper was the comprehensive characterization of medium-sized and short peptides (two to four amino acids) obtained from simulated gastrointestinal digestion. Two different analytical approaches were employed for peptide characterization, namely a common peptidomic analysis for medium-sized peptides and a suspect screening analysis for short peptides, employing an inclusion list of exact *m/z* values of all possible amino acid combinations. Moreover, fractionation by preparative reversed-phase liquid chromatography was employed to simplify the starting protein hydrolysate. Six fractions were collected and tested for antioxidative activity by an innovative antioxidant assay on human gastric adenocarcinoma AGS cell lines. The two most active fractions (2 and 3) were then characterized by a peptidomic approach and database search, as well as by a suspect screening approach, in order to identify potential antioxidant amino acid sequences. Some of the peptides identified in these two fractions have been already reported in the literature for their antioxidant activity.

**Keywords:** antioxidative activity; bioactive peptides; peptidomics; mass spectrometry; soybean

## 1. Introduction

In the last few decades, the opportunity to prevent, alleviate, or even treat some diseases by assuming functional food or bioactive compounds obtained from food is gaining increasing interest for both researchers and consumers. Therefore, in this field, efforts are aimed at the discovery of new bioactive compounds and new physiological functions of known compounds, as well as the identification of the most suitable and sustainable foods to extract these valuable substances at the industrial level.

It is known that certain amino acid sequences can have one or more biological functions; for this reason, many studies are focused on the identification of bioactive peptides, which can be naturally present in food or can be obtained from the parent protein in which they are encrypted [1,2]. These bioactive peptides are generally 2–20 amino acids long,



even if some bioactivities have been attributed to longer sequences (up to 43 amino acids, as in lunasin).

Bioactive peptides can be released from the parent protein during food processing (such as ripening, fermentation, and cooking), storage, or gastrointestinal digestion [2,3]. For research and industrial applications, several methodological approaches are available to obtain potential bioactive peptides encrypted in proteins, including chemical, physical, and biological ones. Among these, treatment with enzymes is the most suitable one for preserving functional and nutritional values of protein hydrolysate [4]. Nonetheless, the high cost, as well as production of bitter-tasting hydrolysates, are some of the main drawbacks in the employment of enzymes. To better simulate the physiological conditions in which peptides are formed from proteins, human digestive enzymes, which are found in the stomach, intestines, and pancreas (e.g., pepsin, trypsin, chymotrypsin, and pancreatin) can be used [5].

Since dietary proteins represent a cheap and valuable source of bioactive peptides, several foods of both animal and plant origin [2,6,7] have been investigated for this aim, including milk [3,8–10], meat, fish [11,12], egg, cereals, and soybean [1,3,7,13].

Soybean (*Glycine max*) has been cultivated for five millennia in Asian countries where, together with its derived products (e.g., soy milk, miso, tofu, etc.), it represents an important source of proteins (ca. 40% of the content) and peptides. Since the last century, soybean cultivation has become widespread in western countries, too [4]. Soy proteins contain all the essential amino acids, and therefore they represent a valid alternative to food of animal origin; furthermore, several biological functions and bioactivities have been attributed to their derived peptides [13], such as cancer and cardiovascular disease prevention, antihypertensive activity [14], hypocholesterolemic effect, and antioxidant properties [1,4,7,15,16]. In particular, the antioxidant activity, i.e., the defense against the free radical damage [17], could be useful in contrasting several pathologies, as well as in nutraceutical and cosmetics applications.

In the present work, we wanted to exploit the antioxidative activity of soybean peptides. Generally, antioxidant sequences are 3–6 amino acid long [6], which are easily metabolized and absorbed in the gastrointestinal tract. Therefore, we focused our attention on short and medium-sized peptides obtained by simulated gastrointestinal digestion of soy protein extracts. First, the soy hydrolysate was separated into six fractions, which were tested for antioxidative activity using an innovative, intracellular reactive oxygen species (ROS) detection assay; in this way, cytotoxic fractions were identified and discarded. Then the peptides, contained in two fractions showing the highest antioxidative properties, were identified using two different strategies for medium-sized and short peptides, respectively. Medium-sized peptides were analyzed by a shotgun proteomic approach, using nano-ultra-high-performance liquid chromatography coupled to tandem mass spectrometry (nanoUHPLC-MS/MS), with identification based on a database search using Proteome Discover software. For short peptides (2–4 amino acid long), the analysis was carried out by UHPLC-MS/MS, following the suspect screening strategy, and their identification was assisted by Compound Discoverer software. Indeed, short peptides have not been fully elucidated in soy yet, mainly because their identification is challenging and cannot be obtained using conventional proteomics approaches and informatics tools. Among the identified peptides, seven were already validated for antioxidative activity and are reported in a public database of food bioactive peptides.

## 2. Materials and Methods

### 2.1. Materials

All chemicals, reagents, and organic solvents of the highest grade available were purchased from Sigma-Aldrich (St. Louis, MO, USA) unless otherwise stated. Trifluoroacetic acid (TFA) was supplied by Romil Ltd. (Cambridge, UK). Ultrapure water was prepared by an Arium 611 VF system from Sartorius (Göttingen, Germany). Mass grade solvents used for medium-sized peptides were purchased from VWR International (Milan, Italy).



Optima LC-MS grade water and acetonitrile (ACN), used for short peptide analysis, were purchased from Thermo Fisher Scientific (Waltham, MA, USA).

## 2.2. Protein Extraction

Soy flour samples were purchased in a local market. An aliquot of 2.7 g of soy flour was extracted with 15 mL of a cold buffer consisting of 6 mol L<sup>-1</sup> urea, 10 mmol L<sup>-1</sup> Tris (hydroxymethyl) aminomethane hydrochloride (Tris-HCl, pH 8), 75 mmol L<sup>-1</sup> NaCl. The sample was vortexed for 50 min, then centrifuged at 9400× g at 4 °C for 30 min. All protein samples were quantified by the bicinchoninic acid (BCA) assay using bovine serum albumin (BSA) as standard, and stored at −80 °C until digestion.

## Protein Digestion

A simulated *in vitro* gastrointestinal digestion was performed as previously described [18], with some modifications. The pH of the protein extract was adjusted to 2.0 with 1 mol L<sup>-1</sup> HCl to mimic the stomach environment, then pepsin was used in an enzyme-to-protein ratio of 1:20. The solution was incubated at 37 °C for 1 h under static conditions. Then, the pH was adjusted to 7.5 with 1 mol L<sup>-1</sup> NaOH to stop pepsin digestion and create the best environment for pancreatin hydrolysis; pancreatin was added with an enzyme-to-protein ratio of 1:10. After 2 h, α-chymotrypsin was added with an enzyme-to-protein ratio of 1:20. The solution was incubated overnight at 37 °C. Enzymatic hydrolysis was stopped by decreasing the pH to 2.0 with TFA. The volume of the digested extract was reduced to 30 µL by an IKA RV 8 rotary evaporator (IKA-Werke GmbH & Co. KG, Staufen, Germany) for subsequent analyses.

## 2.3. Purification of Antioxidant Peptides from Soybeans

The hydrolyzed peptides were purified by preparative liquid chromatography (LC) using the Xbridge BEH C18 OBD Prep, 19 mm id × 250 mm column (particle size = 5 µm; Waters, Milford, MA, USA) as previously described [19,20], with some modifications. The chromatographic system was a Shimadzu Prominence LC-20A, including a CBM-20A controller, two LC-20 AP preparative pumps, and a DGU-20A3R inline degasser. An SPD-20A UV detector with a preparative cell (0.5 mm) was used. The FRC-10A (Shimadzu, Kyoto, Japan) auto-collector was employed. Data acquisition was performed by LabSolution software version 5.53 (Shimadzu, Kyoto, Japan). The detector was set at 214 nm.

Chromatography was operated at a flow-rate of 17 mL min<sup>-1</sup>, using H<sub>2</sub>O with 10 mmol L<sup>-1</sup> ammonium formate at pH 10 as phase A, and methanol/H<sub>2</sub>O (90/10, v/v), with 10 mmol L<sup>-1</sup> ammonium formate, pH 10 as phase B. The chromatographic gradient was as follows: B was increased from 0% to 50% in 20 min, then B was brought to 95% in 4 min and kept constant for 6 min. The column was equilibrated at starting condition for 6 min. Six fractions were collected every 5 min (as shown in Figure 1). Each peptide fraction was evaporated with a rotary evaporator and stored at −80 °C for subsequent analysis.

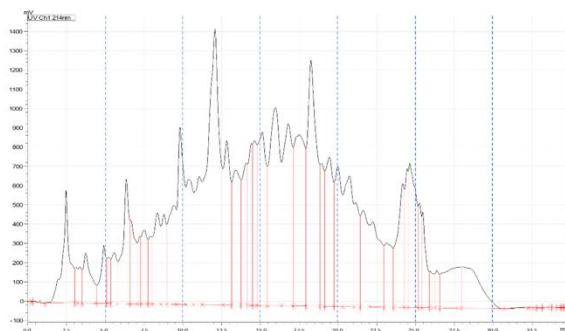


**Figure 1.** LC-UV chromatogram of hydrolyzed soybean extracts showing the applied fractionation.

## 2.4. Bioactivity Assays

### 2.4.1. Cell Culture

Human gastric adenocarcinoma cell line AGS (ATCC CRL-1739) was grown in DMEM-F12 medium, supplemented with 10% fetal bovine serum (FBS), 1% glutamine, and 1% penicillin + streptomycin (all from Microtech, Vero Beach, FL, USA) and cultured in T-75 flasks in a humidified incubator containing 5% CO<sub>2</sub> at 37 °C.

### 2.4.2. Intracellular Reactive Oxygen Species Measurement

AGS cells were split at 80–90% of confluency, seeded ( $0.5 \times 10^6$ ) in 35 mm culture dishes, and incubated at 37 °C in a 5% CO<sub>2</sub> atmosphere overnight. After cell attachment, ROS detection assay was assayed using dihydrorhodamine 123 (DHR, Sigma Aldrich, St. Louis, MO, USA), as described by Cuomo et al. [21]. Briefly, cells were loaded with DHR ( $10 \mu\text{mol L}^{-1}$  for 20 min), and were treated with (1)  $1 \text{ mmol L}^{-1}$  H<sub>2</sub>O<sub>2</sub> for 30 min; (2)  $1 \text{ mg mL}^{-1}$  soybean peptide fractions for 1 h, and (3)  $1 \text{ mg mL}^{-1}$  soybean peptide fractions for 1 h and  $1 \text{ mmol L}^{-1}$  H<sub>2</sub>O<sub>2</sub> for 30 min. After treatments, DAPI (Thermo Fischer Scientific, Waltham, MA, USA) was used as a nuclear counterstain, and cells were analyzed with a Zeiss Axioskop 2 Hal100 fluorescence microscope equipped with a digital camera (Nikon, Tokyo, Japan). The excitation and emission wavelengths were 488 and 515 nm, respectively. Images were digitally acquired with exposure times of 100–400 ms, and processed for fluorescence determination with ImageJ software. The fluorescence signal of the intracellular ROS was normalized on the DAPI fluorescence signal.

## 2.5. Analysis of Medium-Sized Peptides by nanoUHPLC-MS/MS

The chromatographic system was an Ultimate 3000 nanoUHPLC (Thermo Scientific, Bremen, Germany) coupled to an Orbitrap Elite mass spectrometer (Thermo Scientific). Pierce LTQ Velos ESI Positive Ion Calibration Solution (Thermo Fisher Scientific) was used to calibrate the instrument once a week, and the mass accuracy was <1.5 ppm.

Medium-sized peptides were analyzed as described in a previous work [22], with some modifications. A  $10 \mu\text{L}$  sample was injected and preconcentrated on a  $\mu$ -precolumn ( $300 \mu\text{m id} \times 5 \text{ mm}$ , Acclaim PepMap 100 C18, particle size  $5 \mu\text{m}$ , pore size  $100 \text{ \AA}$ ; Thermo Fisher Scientific) at a  $10 \mu\text{L min}^{-1}$  flow-rate of H<sub>2</sub>O/ACN 99:1 (*v/v*) containing 0.1% (*v/v*) TFA. Then the peptide mixture was separated on an EASY-Spray column (Thermo Fisher Scientific,  $75 \mu\text{m id} \times 15 \text{ cm}$ , PepMap C18,  $3 \mu\text{m}$  particles,  $100 \text{ \AA}$  pore size) operated at  $300 \text{ nL min}^{-1}$  and 35 °C.

The mobile phase was constituted by (1) H<sub>2</sub>O and (2) ACN, both with 0.1% formic acid. The chromatographic gradient, referred to as B, was 1% for 5 min, 1–5% in 2 min,

5–35% in 90 min, and 35–90% in 3 min. Finally, the column was rinsed at 90% B for 10 min and equilibrated at 1% B for 19 min.

Full-scan mass spectra were acquired in the 300–2000  $m/z$  range at 30,000 resolution (full width at half maximum, FWHM, at  $m/z$  400). Tandem mass spectra were acquired at 15,000 resolution (FWHM, at  $m/z$  400) in the top 10 data-dependent acquisition (DDA) mode, with the rejection of singly charged ions and unassigned charge states. Precursor ions were fragmented by higher-energy collisional dissociation (HCD), with 35% normalized collision energy (NCE) and a 2  $m/z$  isolation window. Dynamic exclusion was enabled with a repeat count of 1 and a repeat duration of 30 s, with an exclusion duration of 20 s. For each sample, three technical replicates were performed. Raw data files were acquired by Xcalibur software (version 2.2, Thermo Fisher Scientific).

#### 2.6. Analysis of Short Peptides by UHPLC-MS/MS

The short peptides were analyzed by reverse-phase (RP) chromatography, using the Vanquish H UHPLC system coupled to an Q Exactive mass spectrometer (Thermo Fisher Scientific, Bremen, Germany) and a heated electrospray source (ESI) [23]. The instrument was calibrated every 48 h using a Pierce LTQ Velos ESI Positive Ion Calibration Solution (Thermo Fisher Scientific); mass accuracy was <1 ppm. The peptide mixtures were separated on a Kinetex XB-C18 chromatographic column (2.1 mm id  $\times$  100 mm, particle size 2.6  $\mu$ m; Phenomenex, Torrance, CA, USA) kept at 40 °C. The mobile phase consisted of (1) H<sub>2</sub>O and (2) ACN, both containing 0.1% TFA ( $v/v$ ); the flow-rate was 0.4 mL  $\text{min}^{-1}$ . The gradient, referred to as B, was 1% for 2 min, 1–35% in 20 min, and 35–99% in 3 min. Finally, B was maintained at 99% for 3 min and then lowered again to 1%. The MS acquisition was performed in positive ionization mode in the range  $m/z$  150–750 with a resolution (FWHM,  $m/z$  200) of 70,000, while MS/MS spectra were recorded in top 5 DDA mode, using 35% NCE for HCD and a resolution of 35,000 (FWHM,  $m/z$  200). For the DDA (4980 unique masses), an inclusion list with exact  $m/z$  values for individually charged precursor ions was used. The inclusion lists were prepared using MatLab R2018, as previously described [24].

For each sample, three technical replicates were carried out. Raw data files were acquired by Xcalibur software (version 2.2 SP1.48; Thermo Fisher Scientific).

#### 2.7. Peptide Identification

##### 2.7.1. Medium-Sized Peptide Identification

The raw files of the digested fractions were submitted to the Proteome Discoverer software (version 1.3; Thermo Scientific) with the Mascot search engine (v.2.3; Matrix Science, London, UK) for the identification of peptides/proteins.

The research was performed against the proteome of *Glycine max* (Soybean) downloaded from Uniprot (<http://www.uniprot.org/> accessed on 11 January 2020, 85022 sequences). Nonspecific digestion was chosen, and neither fixed nor variable changes were set. The mass tolerances for the precursor and the product ions were set at 10 ppm and 0.05 Da, respectively. A decoy function was used for false discovery rate calculation, which was set at 1%.

##### 2.7.2. Short Peptide Identification

The identification of short peptides in fractionated gastrointestinal digests was performed following a data processing workflow implemented on Compound Discoverer (v. 3.1, Thermo Fisher Scientific, Bremen, Germany) [25]. The masses were extracted from the raw files based on customized parameters, aligning the signals, removing empty or missing MS/MS spectrum signals, and using short lists of complete peptides to match a possible composition. Manual validation of MS/MS spectra was also aided by the Compound Class Assessment Tool, which allowed to automatically match typical product ions from amino acids at the N-terminus, C-terminus, and in the middle of the sequence, and assign them to 20 classes of compounds (one for each natural amino acid). Provisional identification

of short peptides was obtained according to diagnostic fragmentation spectra, aided by mMass, which allows for *in silico* fragmentation of peptides [26].

### 3. Results and Discussion

#### 3.1. Sample Preparation

##### 3.1.1. Extraction

Three different extraction protocols were tested in terms of protein recovery, also aiming to minimize interference content in the extract. Furthermore, the total time required for sample preparation was also considered for a possible industrial scale-up of the process. Experimental details of protocols I and II are reported in Appendix A, whereas protocol III was selected for this work, and is reported in the experimental section. Briefly, protocol I [27] was based on the use of an extraction buffer containing sodium dodecyl sulfate (SDS), whereas glass beads and a buffer containing sodium deoxycholate (SDC) were used in protocol II [28] to enhance the lysis of cell walls. For protocol III, a buffer containing urea was used.

A BCA assay was employed to evaluate the protein extraction recovery of the three protocols, and results are shown in Figure 2. Protocol I gave the worst extraction efficiency, and was the most time-consuming; therefore, it is not suitable for a possible industrial scale-up. Protocol II gave the best result; however, the employment of glass beads does not allow us to extract large flour samples. Protocol III provided similar results and was the fastest, and for these reasons was selected.

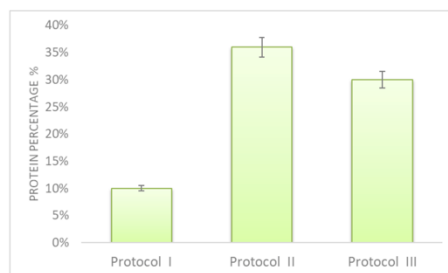


**Figure 2.** Protein recovery percentage obtained by applying three different extraction protocols. Evaluation was carried out by BCA assay, using BSA as a standard.

In protocol III, the employment of urea allows us to not only denature proteins but also to solubilize and extract them, as urea is a mild chaotropic agent. Moreover, all the other buffer constituents were compatible with the following analysis steps.

##### 3.1.2. Gastrointestinal Digestion

In the gut, endogenous proteases, such as pepsin, trypsin, and chymotrypsin, hydrolyze proteins into peptides, which will be further processed by peptidases in the intestinal tract [29]. Therefore, to reproduce gastrointestinal digestion, a sequence of different enzymes is generally used, mainly pepsin, trypsin, chymotrypsin, and papain [17].

To obtain putative bioactive peptides from soy by simulated gastrointestinal digestion, different enzymes were employed, mainly alcalase [16,30,31]; however, other proteases, also in combination, were used as well, including bromelain, papain, pepsin, flavourzyme, neutrase, protomax, and transglutaminase [4].

In this work, we sequentially used pepsin, papain, and chymotrypsin. During hydrolysis, temperature, pH, and enzyme-to-substrate ratio were carefully checked to obtain reproducible results (data not shown).

### 3.2. Soybean-Derived, Hydrolyzed Peptides in Oxidative Stress In Vitro

Recently, the antioxidant role of soybean, and specifically of peptides derived from hydrolysed soybean proteins, has been reported [15,32,33]. ROS are molecules physiologically produced during cell metabolism, participating in cell proliferation and survival. Nevertheless, external stimuli, i.e., environmental factors, xenobiotics, and microbial infection, may contribute to ROS accumulation, causing an imbalance between their production and removal by cellular antioxidant systems [34]. This can result in oxidative stress, leading to cell damage.

Using a DHR cell-permeable fluorogenic probe, which is useful to detect ROS production, the ability of bioactive soybean peptides was investigated to prevent ROS formation in  $H_2O_2$  stimulated cells. Among the six peptide fractions, we tested the antioxidant activity of fractions 2 and 3. The remaining fractions were excluded because of their cytotoxic effect (data not shown). Indeed, the choice of using a gastric cell line was determined by the need for evaluating the potential cytotoxic effect of the derived peptide fractions, justifying its potential use as functional food. As shown in Figure 3, the cells pre-treated with both fractions 2 and 3 displayed reduced ROS levels compared to  $H_2O_2$ -treated cells. Interestingly, compared to fraction 3, fraction 2 exhibited a higher protective effect against oxidative stress induced by  $H_2O_2$ , almost returning the cells to the control group. These results suggest that soybean peptides have important antioxidant activities, with particular attention to peptides contained in fraction 2.

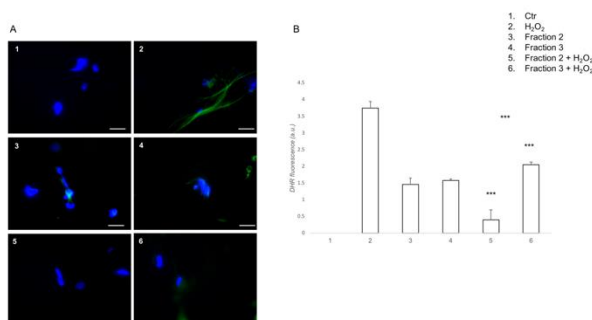


**Figure 3.** Soybean peptides prevents  $H_2O_2$ -induced, intracellular ROS formation. (A) DHR-loaded cells were pre-treated for 1 h with peptide fractions 2 or 3 ( $1 \text{ mg mL}^{-1}$ ), then incubated for further 30 min with  $H_2O_2$  ( $1 \text{ mmol L}^{-1}$ ), and finally observed and analyzed with a fluorescence microscope (scale bar:  $100 \text{ }\mu\text{m}$ ); (B) Quantification of the mean fluorescence of individual cells. Results are expressed as arbitrary units and represent the average  $\pm$  SD calculated from three independent experiments, each performed in duplicate. Statistical analysis was performed with ANOVA followed by Bonferroni's test. \*\*\*  $p < 0.001$ , comparing 5 with 2 or 6 and 6 with 2.

Compared to classical assays used to evaluate the antioxidant activity of soy hydrolysates, such as 2,2-diphenyl-1-picrylhydrazyl (DPPH) [16], oxygen radical absorbance capacity (ORAC) [31], lipid peroxidation inhibitory activity [30], and the employment of an intracellular ROS measurement allowed also to recognize the cytotoxic effect of some fractions.

### 3.3. Identification of Peptides in Fractions with High Antioxidative Activity

The antioxidant function of soy peptides has been attributed to multiple mechanisms, including hydrogen donation, scavenging of hydroxyl radicals, transition-metal ion chela-

tion, and active-oxygen quenching; therefore, it is widely accepted that there is a synergistic effect [4]. Nonetheless, it is still interesting to characterize the most bioactive species, also to better investigate the amino acid sequences responsible for the antioxidative activity. Therefore, the peptides contained in the two most active fractions, namely 2 and 3, were fully characterized and searched in BIOPEP-UWM database for confirmation.

### 3.3.1. Analysis of Short Peptides

The identification of short peptides is challenging for several reasons, as already reported [24]. Briefly, the main issues consist of the low possibility of identifying short sequences (<5 amino acids) by a proteomic database search [35], also due to the high occurrence of isobaric peptides and the scarce ionization efficiency of short peptides, which mainly form monoprotonated molecules in positive ESI. Moreover, scarce fragmentation data can be obtained. Therefore, a previously developed, specific method was employed for short peptide identification. Following a HRMS-based suspect screening approach, a list containing the exact masses of precursors relative to all the possible combinations of the 20 natural amino acids (from two to four, resulting in 168,400 unique combinations) was used.

A total of 132 unique amino acid sequences were identified in fractions 2 and 3. However, under the operating conditions, it was not possible to discriminate the isobaric leucine and isoleucine by tandem mass spectra; therefore, the occurrence of the two amino acids within the identified sequence was retained as equally probable (see Table S1 of Supplementary Materials). Consequently, 203 possible sequences were searched in BIOPEP-UWM database [36], where, on a total of 4216 food bioactive peptides, there are 689 validated sequences for antioxidative activity.

Table 1 reports the short peptides identified in fractions 2 and 3 of the soybean hydrolysate and matching antioxidative sequences reported in BIOPEP-UWM database. The sequences IR and LK, obtained from ovotransferrin protein, showed radical-scavenging activity by ORAC assay [37]. The dipeptide AW was obtained from the marine bivalve *Macra veneriformis*, and it showed hydroxyl, DPPH, and superoxide radical scavenging activities [38]. The dipeptide EL from casein positively responded to SOSA and DPPH assays [39]. The two last sequences, LH and ADF, were identified in soybean [40] and one of its derived products [41], respectively, and both were tested for antioxidative activity against the peroxidation of linoleic acid.

**Table 1.** Short peptides matching with BIOPEP-UWM sequences validated for antioxidative activity. Peak areas are average values of all the replicates.

Sequence	Peak Area Fraction 2 ( $\times 10^6$ )	Peak Area Fraction 3 ( $\times 10^6$ )	Peptide Source
Ile-Arg (IR)	13	815	Egg white ovotransferrin [37]
Leu-Lys (LK)	692	0.4	Egg white ovotransferrin [37]
Ala-Trp (AW)	1	332	Marine bivalve [38]
Glu-Leu (EL)	261	2	Milk casein [39]
Leu-His (LH)	2	92	Soybean [40]
Ala-Asp-Phe (ADF)	124	0.9	Okara [41]

Most of the other identified di-, tri-, and tetrapeptides are reported in the BIOPEP-UWM database with some biological functions, and the dipeptidyl peptidase IV inhibitor and ACE inhibitor are the most frequently occurring.

The list of the identified short sequences was also submitted to PeptideRanker [42], a server for the prediction of bioactive peptides based on a novel N-to-1 neural network, which assigns a generic bioactivity probability rank. Although 0.5 is the threshold value for labeling a peptide as bioactive, a 0.8 threshold is suggested to reduce false-positive



predictions. The rank assignment of the 203 short unique amino acid sequences is reported in Table S2 of the Supplementary Materials: 32 and 15 short peptides had a rank above 0.5 and 0.8, respectively. The latter included 10 dipeptides, 3 tripeptides, and 2 tetrapeptides. Of the six antioxidant peptides found in BIOPEP-UWM, only AW and ADF had a high rank, namely 0.9669 and 0.8062, respectively.

Concerning the amino acid composition of bioactive peptides, the presence of hydrophobic amino acid residues, such as W, F, P, G, K, I, and V, at both the N-terminus and C-terminus, are relevant for peptide antioxidative activity, as well as H and R at the C-terminus position [43]. In particular, the presence of H has been associated with metal-ion chelator, active-oxygen quencher, and hydroxyl radical scavenger properties [4,7]. Another contribution to the antioxidative activity (by free radical quenching) is provided by the excess electrons of the negatively charged residues E and D. Also, the relative positions of these amino acids can determine or enhance their activity [44].

All the bioactive short peptides reported in Table 1 present at least one of these characteristic residues. Moreover, all the identified sequences of our soybean hydrolysate with a prediction rank >0.8 assigned by PeptideRanker contain at least one of these amino acids.

### 3.3.2. Analysis of Medium-Sized Peptides

As expected, most of the medium-sized peptides are derived from glycinin, which is the major seed storage protein of soybean,  $\beta$ -conglycinin, and their isoforms and subunits. Indeed, these two proteins account for up to 80–90% of the total soy protein content. The peptide identification in fractions 2 and 3 are reported in Tables S3 and S4 of the Supplementary Materials, respectively.

Table 2 shows the only medium-sized peptide, identified in fraction 3, that matched with a validated antioxidant sequence in the BIOPEP-UWM database.

**Table 2.** Medium-sized peptide identified in fraction 3 that matched with a BIOPEP-UWM sequence validated for antioxidative activity.

Sequence	Peptide Source	PeptideRanker Score
VNPESQQGSPR	Soy [17]	0.155249

PeptideRanker was used to predict the general bioactivity of the medium-sized peptides as well. The peptide reported in Table 2 obtained a very low prediction score. In general, among the 136 sequences identified in fraction 2, 33 and 19 peptides had bioactivity prediction scores >0.5 and >0.8, respectively (see Table S5 in Supplementary Materials). Concerning fraction 3, only 3 and 1 sequences out of a total of 66 presented a score >0.5 and >0.8, respectively (see Table S6 of Supplementary Materials).

### 3.3.3. Further Considerations on Identified Peptides

The characteristics of peptides identified in the two active fractions were further analyzed by their grand average of hydropathy (GRAVY) index score, which is usually used to estimate the hydrophobicity or hydrophilicity of a protein. The resulting index, ranging between −2 and +2, will be positive for hydrophobic amino acid sequences. Figure 4A,B reports the GRAVY value distributions for short and medium-sized peptides. As is known, medium-sized peptides are more hydrophilic than short peptides.



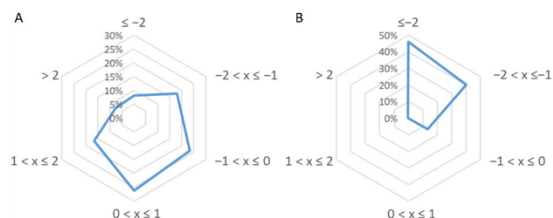


**Figure 4.** Gravy index score distribution for (A) short peptides and (B) medium-sized peptides identified in fractions 2 and 3 of soybean hydrolysate.

Generally, antioxidant peptides, besides containing the amino acids reported above, have a low molecular mass and a GRAVY score ranging between  $-0.5$  and  $+0.5$  [45]. About 50% of the short peptides identified in our research also meet the last criterion, as can be seen in Figure 4A. Regarding medium-size peptides, this requisite is possessed only by a small percentage (Figure 4B).

#### 4. Conclusions

In this work, peptide fractions obtained by the simulated gastrointestinal digestion of soybean protein extracts were evaluated for antioxidative activity by an intracellular test. Only the most active and non-cytotoxic fractions were fully characterized for their short and medium-sized peptide content. The analysis of the two peptide typologies required two different analytical approaches and two diverse software packages for their identification. In particular, the challenge in the identification of short peptides is the impossibility of following the classical informatics tools generally employed in proteomics analysis.

Among the various peptide sequences identified, five dipeptides, one tripeptide, and one medium-sized peptide had already been reported to possess antioxidative activity in the most up-to-date database of food bioactive peptides. In particular, one dipeptide, the tripeptide, and the medium-sized peptide were already identified in soy or a soy by-product. A further purification of the two active fractions (containing almost the same peptides) could help in identifying the peptides with the highest antioxidant function. This could be particularly interesting for the short peptides, which are less frequently investigated for the known issues related to their analysis, and which have not been fully elucidated in soy yet. Nevertheless, it is important to keep in mind that the amino acid sequences could exert their bioactivity only in combination or with a synergic effect. Furthermore, the short peptides could be tested for assessing other bioactivities.

Nowadays, soy cultivation is widespread in several countries, mainly for feed production. Nonetheless, the economic benefits derived from its intensive cultivation are controversial, because of the negative ecological impact on soil, forests, and other plant cultivation. For this reason, the possibility of maximizing the exploitation of this plant and its by-products by extracting the most active amino acid sequences for several industrial applications, including nutraceuticals, could support its sustainable employment.

**Supplementary Materials:** The following are available online at <https://www.mdpi.com/article/10.3390/antiox10050734/s1>, Table S1: Short peptide identification, Table S2: Short peptide bioactivity prediction by PeptideRanker, Table S3: Medium-sized peptides identified in fraction 2, Table S4: Medium-sized peptides identified in fraction 3, Table S5: Medium-sized peptide (fraction 2) bioactivity prediction by PeptideRanker, Table S6: Medium-sized peptides (fraction 3) bioactivity prediction by PeptideRanker.

**Author Contributions:** Conceptualization, A.L.C. and A.L.; methodology, P.C., S.E.A. and A.M.I.M.; software, C.M.M., S.P. and P.C.; validation, A.C. and R.C.; formal analysis, C.C. and A.L.C.; investigation, C.M.M., A.C. and P.C.; resources, C.C. and R.C.; data curation, P.C. and C.M.M.; writing—

original draft preparation, C.C., R.C. and C.M.M.; writing—review and editing, S.P.; visualization, A.M.I.M. and S.E.A.; supervision, A.L.C. and R.C.; project administration, A.L. and R.C.; funding acquisition, A.L.C. All authors have read and agreed to the published version of the manuscript.

**Funding:** This research received no external funding.

**Institutional Review Board Statement:** Not applicable.

**Informed Consent Statement:** Not applicable.

**Data Availability Statement:** Data is contained within the article.

**Conflicts of Interest:** The authors declare no conflict of interest.

#### Appendix A. Comparison of Three Protein Extraction Protocols

Protocol I: soy flour (2.7 g) was added to 1 mL of extraction buffer, i.e., 50 mmol L<sup>-1</sup> Tris (pH 8.8), 15 mmol L<sup>-1</sup> KCl, 20 mmol L<sup>-1</sup> dithiothreitol (DTT), and 1% (w/v) sodium dodecyl sulfate (SDS) [27]. Then, the sample was placed on ice for 1 h, and vortexed for 1 min every 15 min. Insoluble matter was removed by centrifugation at 4 °C for 15 min at 11,000× g. The supernatant was collected, and the proteins were precipitated overnight at −20 °C by adding four volumes of acetone. After centrifugation at 11,000× g at 4 °C for 30 min, the pellet was dried and dissolved in 6 mol L<sup>-1</sup> of urea and 10 mmol L<sup>-1</sup> Tris-HCl (pH 8).

Protocol II: proteins were extracted from soy flour with the aid of glass beads [28]. A 25 mg soy sample was added to 150 mg glass microbeads and 1 mL lysis buffer (60 mmol L<sup>-1</sup> Tris pH 9, 15 mmol L<sup>-1</sup> KCl, 20 mmol L<sup>-1</sup> DTT, 2% (w/v) SDC). The sample was placed in an ultrasonic bath for 4 h, under agitation for 1 h every 30 min. Then, the sample was incubated at 100 °C for 30 min; centrifugation at 4 °C at 11,000× g for 15 min allowed us to remove insoluble matter. The supernatant was collected as proteins precipitated, as described above.

Protocol III: this is reported in the experimental section, and was used for this work.

#### References

1. Wang, W.; de Mejia, E.G. A New Frontier in Soy Bioactive Peptides that May Prevent Age-related Chronic Diseases. *Compr. Rev. Food Sci. Food Saf.* **2005**, *4*, 63–78. [\[CrossRef\]](#) [\[PubMed\]](#)
2. Daroit, D.J.; Brandelli, A. In vivo bioactivities of food protein-derived peptides—A current review. *Curr. Opin. Food Sci.* **2021**, *39*, 120–129. [\[CrossRef\]](#)
3. Fernández-Tomé, S.; Hernández-Ledesma, B. Gastrointestinal Digestion of Food Proteins under the Effects of Released Bioactive Peptides on Digestive Health. *Mol. Nutr. Food Res.* **2020**, *64*, 2000401. [\[CrossRef\]](#) [\[PubMed\]](#)
4. Ashaolu, T.J. Health Applications of Soy Protein Hydrolysates. *Int. J. Pept. Res. Ther.* **2020**, *26*, 2333–2343. [\[CrossRef\]](#)
5. Capriotti, A.L.; Caruso, G.; Cavaliere, C.; Samperi, R.; Ventura, S.; Zenezini Chiozzi, R.; Laganà, A. Identification of potential bioactive peptides generated by simulated gastrointestinal digestion of soybean seeds and soy milk proteins. *J. Food Compos. Anal.* **2015**, *44*, 205–213. [\[CrossRef\]](#)
6. Piovesana, S.; Capriotti, A.L.; Cavaliere, C.; La Barbera, G.; Montone, C.M.; Zenezini Chiozzi, R.; Laganà, A. Recent trends and analytical challenges in plant bioactive peptide separation, identification and validation. *Anal. Bioanal. Chem.* **2018**, *410*, 3425–3444. [\[CrossRef\]](#)
7. Matemu, A.; Nakamura, S.; Katayama, S. Health Benefits of Antioxidative Peptides Derived from Legume Proteins with a High Amino Acid Score. *Antioxidants* **2021**, *10*, 316. [\[CrossRef\]](#)
8. Zenezini Chiozzi, R.; Capriotti, A.L.; Cavaliere, C.; La Barbera, G.; Piovesana, S.; Samperi, R.; Laganà, A. Purification and identification of endogenous antioxidant and ACE-inhibitory peptides from donkey milk by multidimensional liquid chromatography and nanoHPLC-high resolution mass spectrometry. *Anal. Bioanal. Chem.* **2016**, *408*, 5657–5666. [\[CrossRef\]](#) [\[PubMed\]](#)
9. Capriotti, A.L.; Cavaliere, C.; Piovesana, S.; Samperi, R.; Laganà, A. Recent trends in the analysis of bioactive peptides in milk and dairy products. *Anal. Bioanal. Chem.* **2016**, *408*, 2677–2685. [\[CrossRef\]](#)
10. Piovesana, S.; Capriotti, A.L.; Cavaliere, C.; La Barbera, G.; Samperi, R.; Zenezini Chiozzi, R.; Laganà, A. Peptidome characterization and bioactivity analysis of donkey milk. *J. Proteomics* **2015**, *119*, 21–29. [\[CrossRef\]](#)
11. Capriotti, A.L.; Cavaliere, C.; Foglia, P.; Piovesana, S.; Samperi, R.; Zenezini Chiozzi, R.; Laganà, A. Development of an analytical strategy for the identification of potential bioactive peptides generated by in vitro tryptic digestion of fish muscle proteins. *Anal. Bioanal. Chem.* **2015**, *407*, 845–854. [\[CrossRef\]](#)

12. Halim, N.R.A.R.A.; Yusof, H.M.M.; Sarbon, N.M.M. Functional and bioactive properties of fish protein hydrolysates and peptides: A comprehensive review. *Trends Food Sci. Technol.* **2016**, *51*, 24–33. [\[CrossRef\]](#)
13. Singh, B.P.; Vij, S.; Hati, S. Functional significance of bioactive peptides derived from soybean. *Peptides* **2014**, *54*, 171–179. [\[CrossRef\]](#)
14. Xu, Z.; Wu, C.; Sun-Waterhouse, D.; Zhao, T.; Waterhouse, G.I.N.; Zhao, M.; Su, G. Identification of post-digestion angiotensin-I converting enzyme (ACE) inhibitory peptides from soybean protein isolate: Their production conditions and in silico molecular docking with ACE. *Food Chem.* **2021**, *345*, 128855. [\[CrossRef\]](#)
15. Zhang, Q.; Tong, X.; Li, Y.; Wang, H.; Wang, Z.; Qi, B.; Sui, X.; Jiang, L. Purification and Characterization of Antioxidant Peptides from Alcalase-Hydrolyzed Soybean (*Glycine max* L.) Hydrolysate and Their Cytoprotective Effects in Human Intestinal Caco-2 Cells. *J. Agric. Food Chem.* **2019**, *67*, 5772–5781. [\[CrossRef\]](#) [\[PubMed\]](#)
16. Liu, T.X.; Zhao, M. Physical and chemical modification of SPI as a potential means to enhance small peptide contents and antioxidant activity found in hydrolysates. *Innov. Food Sci. Emerg. Technol.* **2010**, *11*, 677–683. [\[CrossRef\]](#)
17. Tonolo, F.; Moretto, L.; Grinzato, A.; Fiorese, F.; Folda, A.; Scalcon, V.; Ferro, S.; Arrigoni, G.; Bellamio, M.; Feller, E.; et al. Fermented Soy-Derived Bioactive Peptides Selected by a Molecular Docking Approach Show Antioxidant Properties Involving the Keap1/Nrf2 Pathway. *Antioxidants* **2020**, *9*, 1306. [\[CrossRef\]](#) [\[PubMed\]](#)
18. Cerrato, A.; Capriotti, A.L.; Capuano, F.; Cavaliere, C.; Montone, A.M.I.; Montone, C.M.; Piovesana, S.; Zenezini Chiozzi, R.; Laganà, A. Identification and Antimicrobial Activity of Medium-Sized and Short Peptides from Yellowfin Tuna (*Thunnus albacares*) Simulated Gastrointestinal Digestion. *Foods* **2020**, *9*, 1185. [\[CrossRef\]](#) [\[PubMed\]](#)
19. Caliceti, C.; Capriotti, A.L.; Calabria, D.; Bonvicini, F.; Zenezini Chiozzi, R.; Montone, C.M.; Piovesana, S.; Zangheri, M.; Mirasoli, M.; Simoni, P.; et al. Peptides from Cauliflower By-Products, Obtained by an Efficient, Ecosustainable, and Semi-Industrial Method, Exert Protective Effects on Endothelial Function. *Oxid. Med. Cell. Longev.* **2019**, *2019*, 1–13. [\[CrossRef\]](#) [\[PubMed\]](#)
20. Montone, C.M.; Zenezini Chiozzi, R.; Marchetti, N.; Cerrato, A.; Antonelli, M.; Capriotti, A.L.; Cavaliere, C.; Piovesana, S.; Laganà, A. Peptidomic approach for the identification of peptides with potential antioxidant and anti-hypertensive effects derived from Asparagus by-products. *Molecules* **2019**, *24*, 3627. [\[CrossRef\]](#)
21. Cuomo, P.; Papaiani, M.; Fulgione, A.; Guerra, F.; Capparelli, R.; Medaglia, C. An Innovative Approach to Control *H. pylori*-Induced Persistent Inflammation and Colonization. *Microorganisms* **2020**, *8*, 1214. [\[CrossRef\]](#)
22. Cerrato, A.; Aita, S.E.; Cavaliere, C.; Laganà, A.; Montone, C.M.; Piovesana, S.; Zenezini Chiozzi, R.; Capriotti, A.L. Comprehensive identification of native medium-sized and short bioactive peptides in sea bass muscle. *Food Chem.* **2021**, *343*, 128443. [\[CrossRef\]](#)
23. Montone, C.M.; Capriotti, A.L.; Cerrato, A.; Antonelli, M.; La Barbera, G.; Piovesana, S.; Laganà, A.; Cavaliere, C. Identification of bioactive short peptides in cow milk by high-performance liquid chromatography on C18 and porous graphitic carbon coupled to high-resolution mass spectrometry. *Anal. Bioanal. Chem.* **2019**, *411*, 3395–3404. [\[CrossRef\]](#) [\[PubMed\]](#)
24. Piovesana, S.; Montone, C.M.; Cavaliere, C.; Crescenzi, C.; La Barbera, G.; Laganà, A.; Capriotti, A.L. Sensitive untargeted identification of short hydrophilic peptides by high performance liquid chromatography on porous graphitic carbon coupled to high resolution mass spectrometry. *J. Chromatogr. A* **2019**, *1590*, 73–79. [\[CrossRef\]](#)
25. Cerrato, A.; Aita, S.E.; Capriotti, A.L.; Cavaliere, C.; Montone, C.M.; Laganà, A.; Piovesana, S. A new opening for the tricky untargeted investigation of natural and modified short peptides. *Talanta* **2020**, *219*, 121262. [\[CrossRef\]](#)
26. Niedermeyer, T.H.J.; Strohm, M. mMass as a Software Tool for the Annotation of Cyclic Peptide Tandem Mass Spectra. *PLoS ONE* **2012**, *7*, e44913. [\[CrossRef\]](#)
27. Capriotti, A.L.; Cavaliere, C.; Piovesana, S.; Stampachiachiere, S.; Ventura, S.; Zenezini Chiozzi, R.; Laganà, A. Characterization of quinoa seed proteome combining different protein precipitation techniques: Improvement of knowledge of nonmodel plant proteomics. *J. Sep. Sci.* **2015**, *38*, 1017–1025. [\[CrossRef\]](#) [\[PubMed\]](#)
28. Montone, C.M.; Capriotti, A.L.; Cavaliere, C.; La Barbera, G.; Piovesana, S.; Zenezini Chiozzi, R.; Laganà, A. Peptidomic strategy for purification and identification of potential ACE-inhibitory and antioxidant peptides in *Tetrademus obliquus* microalgae. *Anal. Bioanal. Chem.* **2018**, *410*, 3573–3586. [\[CrossRef\]](#)
29. Yu, S.; Bech Thoegersen, J.; Kragh, K.M. Comparative study of protease hydrolysis reaction demonstrating Normalized Peptide Bond Cleavage Frequency and Protease Substrate Broadness Index. *PLoS ONE* **2020**, *15*, e0239080. [\[CrossRef\]](#) [\[PubMed\]](#)
30. Park, S.Y.; Lee, J.-S.S.; Baek, H.-H.H.; Lee, H.G. Purification and characterization of antioxidant peptides from soy protein hydrolysate. *J. Food Biochem.* **2010**, *34*, 120–132. [\[CrossRef\]](#)
31. Darmawan, R.; Bringe, N.A.; de Mejia, E.G. Antioxidant Capacity of Alcalase Hydrolysates and Protein Profiles of Two Conventional and Seven Low Glycinin Soybean Cultivars. *Plant Foods Hum. Nutr.* **2010**, *65*, 233–240. [\[CrossRef\]](#) [\[PubMed\]](#)
32. Jiménez-Escrig, A.; Alaiz, M.; Vioque, J.; Rupérez, P. Health-promoting activities of ultra-filtered okara protein hydrolysates released by in vitro gastrointestinal digestion: Identification of active peptide from soybean lipoxigenase. *Eur. Food Res. Technol.* **2010**, *230*, 655–663. [\[CrossRef\]](#)
33. Yi, G.; ud Din, J.; Zhao, F.; Liu, X. Effect of soybean peptides against hydrogen peroxide induced oxidative stress in HepG2 cells via Nrf2 signaling. *Food Funct.* **2020**, *11*, 2725–2737. [\[CrossRef\]](#)
34. Pizzino, G.; Irrera, N.; Cucinotta, M.; Pallio, G.; Mannino, F.; Arcoraci, V.; Squadrito, F.; Altavilla, D.; Bitto, A. Oxidative Stress: Harms and Benefits for Human Health. *Oxid. Med. Cell. Longev.* **2017**, *2017*, 1–13. [\[CrossRef\]](#)

35. Koskinen, V.R.; Emery, P.A.; Creasy, D.M.; Cottrell, J.S. Hierarchical clustering of shotgun proteomics data. *Mol. Cell. Proteomics* **2011**, *10*, M110.003822. [\[CrossRef\]](#)
36. Minkiewicz, P.; Iwaniak, A.; Darewicz, M. BIOPEP-UWM Database of Bioactive Peptides: Current Opportunities. *Int. J. Mol. Sci.* **2019**, *20*, 5978. [\[CrossRef\]](#)
37. Huang, W.Y.; Majumder, K.; Wu, J. Oxygen radical absorbance capacity of peptides from egg white protein ovotransferrin and their interaction with phytochemicals. *Food Chem.* **2010**, *123*, 635–641. [\[CrossRef\]](#)
38. Liu, R.; Zheng, W.; Li, J.; Wang, L.; Wu, H.; Wang, X.; Shi, L. Rapid identification of bioactive peptides with antioxidant activity from the enzymatic hydrolysate of *Mactra veneriformis* by UHPLC–Q-TOF mass spectrometry. *Food Chem.* **2015**, *167*, 484–489. [\[CrossRef\]](#) [\[PubMed\]](#)
39. Suetsuna, K.; Ukeda, H.; Ochi, H. Isolation and characterization of free radical scavenging activities peptides derived from casein. *J. Nutr. Biochem.* **2000**, *11*, 128–131. [\[CrossRef\]](#)
40. Chen, H.M.; Muramoto, K.; Yamauchi, F.; Nokihara, K. Antioxidant Activity of Designed Peptides Based on the Antioxidative Peptide Isolated from Digests of a Soybean Protein. *J. Agric. Food Chem.* **1996**, *44*, 2619–2623. [\[CrossRef\]](#)
41. Yokomizo, A.; Takenaka, Y.; Takenaka, T. Antioxidative Activity of Peptides Prepared from Okara Protein. *Food Sci. Technol. Res.* **2002**, *8*, 357–359. [\[CrossRef\]](#)
42. Mooney, C.; Haslam, N.J.; Pollastri, G.; Shields, D.C. Towards the Improved Discovery and Design of Functional Peptides: Common Features of Diverse Classes Permit Generalized Prediction of Bioactivity. *PLoS ONE* **2012**, *7*, e45012. [\[CrossRef\]](#) [\[PubMed\]](#)
43. Torres-Fuentes, C.; del Mar Contreras, M.; Recio, I.; Alaiz, M.; Vioque, J. Identification and characterization of antioxidant peptides from chickpea protein hydrolysates. *Food Chem.* **2015**, *180*, 194–202. [\[CrossRef\]](#)
44. Zou, T.-B.; He, T.-P.; Li, H.-B.; Tang, H.-W.; Xia, E.-Q. The Structure-Activity Relationship of the Antioxidant Peptides from Natural Proteins. *Molecules* **2016**, *21*, 72. [\[CrossRef\]](#)
45. Ji, D.; Udenigwe, C.C.; Agyei, D. Antioxidant peptides encrypted in flaxseed proteome: An in silico assessment. *Food Sci. Hum. Wellness* **2019**, *8*, 306–314. [\[CrossRef\]](#)



# Beclin-1-mediated activation of autophagy improves proximal and distal urea cycle disorders

Leandro R Soria<sup>1</sup>, Sonam Gurung<sup>2</sup>, Giulia De Sabbata<sup>3</sup>, Dany P Perocheau<sup>2</sup>, Angela De Angelis<sup>1</sup>, Gemma Bruno<sup>1</sup>, Elena Polishchuk<sup>1</sup>, Debora Paris<sup>4</sup>, Paola Cuomo<sup>4</sup>, Andrea Motta<sup>4</sup>, Michael Orford<sup>2</sup>, Youssef Khalil<sup>2</sup>, Simon Eaton<sup>2</sup>, Philippa B Mills<sup>2</sup>, Simon N Waddington<sup>2,5</sup>, Carmine Settembre<sup>1</sup>, Andrés F Muro<sup>3</sup>, Julien Baruteau<sup>2,6</sup> & Nicola Brunetti-Pierri<sup>1,7,\*</sup>

## Abstract

Urea cycle disorders (UCD) are inherited defects in clearance of waste nitrogen with high morbidity and mortality. Novel and more effective therapies for UCD are needed. Studies in mice with constitutive activation of autophagy unravelled Beclin-1 as *drug-gable* candidate for therapy of hyperammonemia. Next, we investigated efficacy of cell-penetrating autophagy-inducing Tat-Beclin-1 (TB-1) peptide for therapy of the two most common UCD, namely ornithine transcarbamylase (OTC) and argininosuccinate lyase (ASL) deficiencies. TB-1 reduced urinary orotic acid and improved survival under protein-rich diet in *spf-ash* mice, a model of OTC deficiency (proximal UCD). In *As<sup>fluo/neo</sup>* mice, a model of ASL deficiency (distal UCD), TB-1 increased ureagenesis, reduced argininosuccinate, and improved survival. Moreover, it alleviated hepatocellular injury and decreased both cytoplasmic and nuclear glycogen accumulation in *As<sup>fluo/neo</sup>* mice. In conclusion, Beclin-1-dependent activation of autophagy improved biochemical and clinical phenotypes of proximal and distal defects of the urea cycle.

**Keywords** argininosuccinic aciduria; autophagy; OTC deficiency; Tat-Beclin-1 peptide; urea cycle disorders

**Subject Categories** Autophagy & Cell Death; Genetics, Gene Therapy & Genetic Disease

DOI 10.15252/emmm.202013158 | Received 22 July 2020 | Revised 23 November 2020 | Accepted 25 November 2020

EMBO Mol Med (2020) e13158

## Introduction

Autophagy is highly active in liver. Proteins, glycogen and lipid droplets are degraded by autophagy in liver cells to release amino

acids, glucose and free fatty acids that can be reused for synthesis of new proteins and macromolecules, or can enter the tricarboxylic acid (TCA) cycle to generate ATP (Kaur & Debnath, 2015). Liver autophagy was recently found to support ammonia detoxification by furnishing the urea cycle with intermediates and energy that increase urea cycle flux under conditions of excessive ammonia (Soria *et al.*, 2018). Liver-specific deficiency of autophagy impaired ammonia detoxification whereas its enhancement resulted in increased urea synthesis and protection against hyperammonemia (Soria *et al.*, 2018). Therefore, drugs enhancing autophagy have potential for treatment of urea cycle disorders (UCD) (Soria & Brunetti-Pierri, 2018, 2019). In a previous study (Soria *et al.*, 2018), we showed that rapamycin reduces orotic acid in *spf-ash* mice, a mouse model of the ornithine transcarbamylase (OTC) deficiency that carries a single nucleotide mutation in the fourth exon of the *Otc* gene resulting in a splicing defect and 10% of residual enzyme activity (Hodges & Rosenberg, 1989). Although it has been efficiently used to promote autophagy, rapamycin does not completely inhibit its target, the mechanistic target of rapamycin kinase complex 1 (mTORC1), and affects several biological processes besides autophagy (Li *et al.*, 2014). Therefore, drugs targeting autophagy more specifically are attractive because they are expected to have less side effects. Tat-Beclin-1 (TB-1) is an engineered cell-permeable peptide that potently and specifically induces autophagy (Shoji-Kawata *et al.*, 2013). TB-1 is formed by the HIV-1 Tat protein transduction domain attached via a diglycine linker to a peptide derived from Beclin-1 (*Becn1*), a key component of the autophagy induction machinery (Shoji-Kawata *et al.*, 2013). In summary, TB-1 is an attractive therapeutic candidate for its specificity and at least in mice, it has shown great potential for treatment of various diseases, including several types of cancer, infections, cardiac dysfunction, skeletal disorders and axonal injuries (Cinque *et al.*, 2015; He *et al.*, 2016; Pietroluca *et al.*, 2016; Bartolomeo *et al.*, 2017;

<sup>1</sup> Telethon Institute of Genetics and Medicine, Pozzuoli, Italy

<sup>2</sup> UCL Great Ormond Street Institute of Child Health, London, UK

<sup>3</sup> International Centre for Genetic Engineering and Biotechnology, Trieste, Italy

<sup>4</sup> Institute of Biomolecular Chemistry, National Research Council, Pozzuoli, Italy

<sup>5</sup> Wits/SAMRC Antiviral Gene Therapy Research Unit, Faculty of Health Sciences, University of the Witwatersrand, Johannesburg, South Africa

<sup>6</sup> Metabolic Medicine Department, Great Ormond Street Hospital for Children NHS Foundation Trust, London, UK

<sup>7</sup> Department of Translational Medicine, Federico II University, Naples, Italy

\*Corresponding author. Tel: +39 081 19230661; Fax: +39 081 5609877; E-mail: brunetti@tigem.it



Song *et al*, 2018; Sun *et al*, 2018; Vega-Rubin-de-Celis *et al*, 2018). In the present study, we investigated the therapeutic potential of TB-1 for treatment of UCD.

## Results

### Constitutional hyperactivation of Beclin-1 enhances ammonia detoxification

Beclin-1 is a central player in autophagy and regulates autophagosome formation and maturation (Liang *et al*, 2008). To investigate *Becn1* functions *in vivo*, a knock-in mouse model carrying a *Becn1* mutation (*Becn1*<sup>F121A</sup>) resulting in constitutively active autophagy has been recently generated (Rocchi *et al*, 2017). In these mice, Phe121 is mutated into alanine resulting in disruption of the BECN1-BCL2 binding and constitutive activation of BECN1 and autophagy in multiple tissues, including liver (Rocchi *et al*, 2017; Fernandez *et al*, 2018; Yamamoto *et al*, 2018). In these mice, we investigated ammonia detoxification by measurements of blood ammonia levels during acute hyperammonemia induced by an ammonia challenge. Despite no changes in blood ammonia at baseline, *Becn1*<sup>F121A</sup> mice showed 32% reduction in blood ammonia at 30 min after intraperitoneal (i.p.) injection of ammonium chloride compared to age-matched wild-type (WT) mice (Fig 1A). Accordingly, *Becn1*<sup>F121A</sup> mice showed enhanced ureagenesis compared to WT controls, as shown by increased blood levels of <sup>15</sup>N-labelled urea from <sup>15</sup>N-ammonium chloride (Fig EV1A). Improved ammonia clearance was not dependent on increased expression of urea cycle enzymes in *Becn1*<sup>F121A</sup> mice that showed similar enzyme levels by Western blotting compared to WT controls (Fig EV1B and C). Therefore, consistent with previous findings (Soria *et al*, 2018), gain-of-function mutation of the autophagy activator *Becn1* protects against acute hyperammonemia *in vivo*, suggesting that Beclin-1 is a *druggable* candidate for therapy of hyperammonemia.

### Tat-Beclin-1 improves the phenotype of OTC-deficient mice

To investigate the therapeutic efficacy of *Becn1*-mediated induction of autophagy in mouse models of UCD, we injected TB-1 i.p. in *spf-ash* mice (Hodges & Rosenberg, 1989), a model of OTC deficiency, the most common UCD. Body weights were unaffected by TB-1 (Fig EV2A). Although not normalized, in *spf-ash* mice the levels of the biochemical hallmark of OTC deficiency, urinary orotic acid, were significantly reduced by TB-1 (Fig 1B). Consistent with its autophagy enhancer activity, TB-1 increased the hepatic autophagic flux, as showed by reduced protein levels of the autophagosome marker LC3-II, and the two main autophagy cargo receptors, namely p62 and NBR1 (Fig 1C and D). Notably, OTC residual enzyme activity was unaffected by TB-1 (Fig EV2B), thus excluding reduction of urinary orotic acid as a consequence of increased residual OTC activity induced by TB-1. To further investigate the efficacy of TB-1-mediated increased liver autophagy for therapy of OTC deficiency, *spf-ash* mice were fed for 10 days with a high protein diet and were either treated with TB-1 or left untreated. Consistent with previous reports (Yang *et al*, 2016; Kurtz *et al*, 2019), *spf-ash* mice showed marked mortality under high protein diet compared to control WT mice (Fig 1E). An approximately 30% weight loss was observed in

all *spf-ash* mice fed with the high protein diet, independently of TB-1 treatment (Fig EV2C). Although it did not significantly improve survival as single treatment, when combined with an ammonia scavenger drug (Na-benzoate) and L-arginine (L-Arg), TB-1 increased survival whereas ammonia scavengers and L-Arg did not affect survival of *spf-ash* mice under high protein diet (Fig 1E). Consistent with the increased survival, blood ammonia levels measured after 4 days with high protein diet (a time-point prior to mortality) were significantly lower in *spf-ash* mice treated with the combination of TB-1 and Na-benzoate and L-Arg compared to untreated *spf-ash* mice (Fig 1F). TB-1 alone decreased slightly but not significantly blood ammonia whereas Na-benzoate and L-Arg significantly reduced blood ammonia levels, consistent with the human data (Enns *et al*, 2007; Fig 1F). Notably, Na-benzoate and L-Arg treatment did not affect the levels of urinary orotic acid increased by the high protein diet whereas TB-1 either alone or in combination with Na-benzoate and L-Arg efficiently blunted the increase in urinary orotic acid induced by the high protein diet (Fig EV2D). Taken together, these results support the therapeutic potential of activation of liver autophagy by TB-1 in combination with conventional treatments, such as ammonia scavenger drugs and L-Arg (Enns *et al*, 2007; Haberle *et al*, 2019), for treatment of OTC deficiency, the most common UCD.

### Tat-Beclin-1 enhances ureagenesis and corrects metabolic abnormalities of argininosuccinic aciduria

To investigate the efficacy of autophagy enhancement for therapy of argininosuccinic aciduria (ASA), the second most frequent UCD (Baruteau *et al*, 2019a), we investigated TB-1 treatment in the hypomorphic murine model of argininosuccinate lyase (ASL) deficiency (*Asl*<sup>Neo/Neo</sup>) that expresses approximately 16% of residual enzyme activity and recapitulates the main biochemical and clinical abnormalities of ASA patients (Erez *et al*, 2011; Nagamani *et al*, 2012; Baruteau *et al*, 2018; Burrage *et al*, 2020). Besides impaired urea synthesis and ammonia detoxification, systemic manifestations of ASA, such as reduced body weight, increased blood pressure, and reduced survival are also associated with nitric oxide (NO)-deficiency (Erez *et al*, 2011; Nagamani *et al*, 2012; Baruteau *et al*, 2018; Kho *et al*, 2018). *Asl*<sup>Neo/Neo</sup> mice treated with TB-1 but without any additional treatment showed increased survival compared to vehicle-treated controls that started dying by 10 days of age (Fig 2A). Weight gain was unaffected by TB-1 (Fig EV3A). Consistent with our previous work (Soria *et al*, 2018), TB-1-mediated activation of autophagy in *Asl*<sup>Neo/Neo</sup> mice was associated with increased incorporation of <sup>15</sup>N into urea (+88%, *P* < 0.05) indicating enhanced ureagenesis (Fig 2B). Consistent with the increased ureagenesis, blood ammonia levels were lowered by TB-1 in *Asl*<sup>Neo/Neo</sup> mice (Fig EV3B). As expected, autophagic flux was enhanced in livers of *Asl*<sup>Neo/Neo</sup> mice injected with TB-1, as shown by reduced LC3-II and decreased autophagy substrates (p62 and NBR1) in livers (Fig 2C and D), whereas residual ASL enzyme activity was unaffected (Fig EV3C). Argininosuccinic acid levels were reduced in dried blood spots (Fig 2E) in TB-1-treated *Asl*<sup>Neo/Neo</sup> mice. Consistent with this reduction, hepatic content of <sup>15</sup>N-labelled argininosuccinic acid was also reduced in mice treated with TB-1 (Fig 2F). Metabolomic analysis by <sup>1</sup>H-NMR spectroscopy (Soria *et al*, 2018) showed that the whole-liver metabolome of vehicle-treated *Asl*<sup>Neo/Neo</sup> mice was

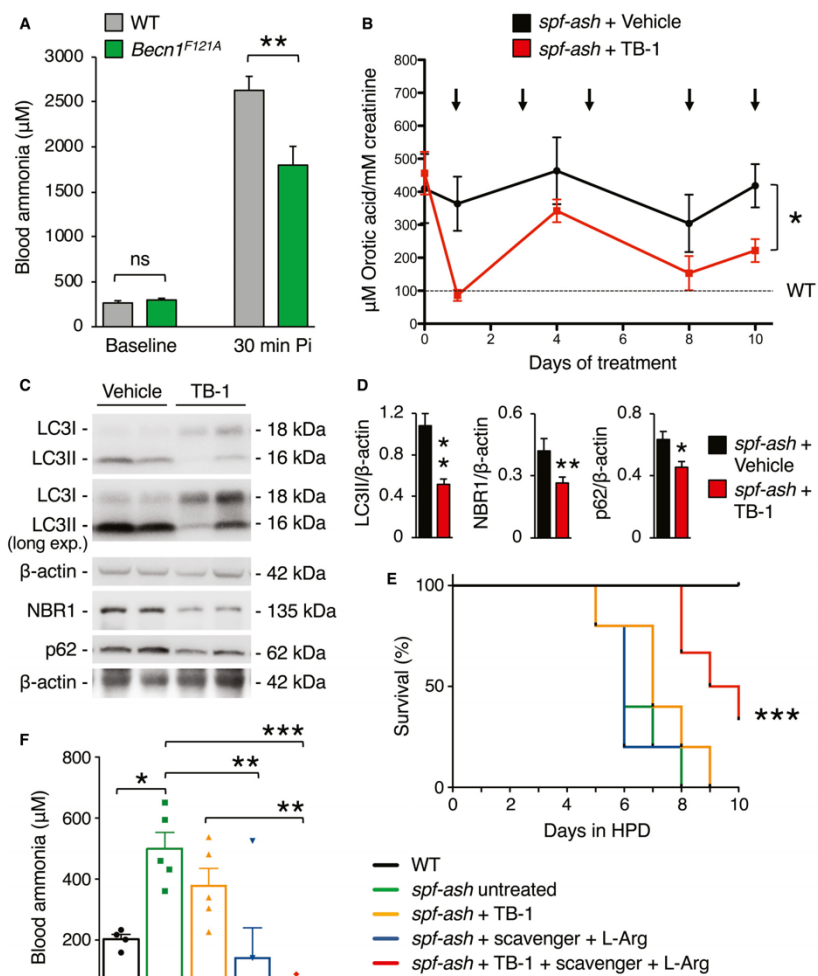


Figure 1.



**Figure 1. Hyperactive Beclin-1 protects against hyperammonemia, and activation of hepatic autophagy improves the phenotype of OTC-deficient mice.**

- A Blood ammonia in 8–9-week-old C57BL/6J wild-type (WT) mice ( $n = 8$ ) and *Becn1*<sup>L224A</sup> mice with constitutive activation of autophagy ( $n = 8$ ) at baseline and 30 min after i.p. injection of  $\text{NH}_4\text{Cl}$  (10 mmol/kg). \*\* $P < 0.01$  (Unpaired t-test), ns: not statistically significant difference.
- B Urinary orotic acid of 12-week-old *spf-ash* mice treated with TB-1 (15 mg/kg, i.p.) or vehicle at various times as indicated by the arrows ( $n = 5$  mice/group). \* $P < 0.05$  (Two-way ANOVA).
- C, D Western blotting and densitometric quantifications of autophagy markers (LC3II: autophagosomes; p62 and NBR1: cargo receptors) in livers of *spf-ash* mice harvested after 10 days of treatment with TB-1 or vehicle.  $\beta$ -actin was used as loading control.  $n = 5$  mice/group. \*\* $P < 0.01$ , \* $P < 0.05$  (Unpaired t-test).
- E Survival curves of *spf-ash* mice fed with a high protein diet (HPD) for 10 days and treated with TB-1 alone or combined with scavenger drug (Na-benzoate) and L-Arginine, or treated with scavenger drug (Na-benzoate) and L-Arginine, or left untreated. WT control were included ( $n = 5$ /group). \*\*\* $P < 0.001$  (Log-rank Mantel–Cox test).
- F Blood ammonia levels determined after 4 days under HPD ( $n = 5$  mice/group). \*\*\* $P < 0.001$ , \*\* $P < 0.01$ , \* $P < 0.05$  (One-way ANOVA).

Data information: Treatments in (E, F): Scavenger (Na-benzoate 250 mg/kg/day, i.p.) and L-arginine (L-Arg, 250 mg/kg/day, i.p.), TB-1 (15 mg/kg every 2 days, i.p.). WT mice were age-, gender- and strain (C3H)-matched. All values are shown as averages  $\pm$  SEM. Exact  $P$  values are reported in Appendix Table S1.

Source data are available online for this figure.

well separated from healthy WT controls but it was shifted towards non-diseased WT controls in *Asl*<sup>Neo/Neo</sup> mice injected with TB-1 (Fig 2G and Appendix Fig S1), suggesting that TB-1 corrects at least partially the liver metabolic deregulation caused by ASL deficiency. Notably, NMR confirmed that liver content of argininosuccinate, along with its two precursors citrulline and aspartate, was reduced (Fig EV4). Moreover, levels of key compounds of the TCA cycle (fumarate and succinate) and glucose were rescued by TB-1 (Fig EV4). In summary, TB-1 improved several biochemical alterations of ASA, confirming the efficacy of autophagy enhancer molecules for therapy of UCD.

#### Tat-Beclin-1 reduces injury and abnormal glycogen deposition in livers with ASL deficiency

Chronic hepatocellular injury is a common complication in patients with ASL deficiency (Mori et al, 2002; Yapito-Lee et al, 2013; Baruteau et al, 2017; Ranucci et al, 2019). Despite the underlying mechanism triggering the liver disease remains unclear, evidence in human and mouse suggests that it is related to massive accumulation of cytoplasmic glycogen (Badizadegan & Perez-Atayde, 1997; Bigot et al, 2017; Burrage et al, 2020). Moreover, because activation of autophagy was found to be effective in clearance of glycogen storage in glycogen storage diseases (Ashe et al, 2010; Spanpanato et al, 2013; Martina et al, 2014; Farah et al, 2016), we investigated whether TB-1 promotes glycogen clearance in ASA livers. To this end, *Asl*<sup>Neo/Neo</sup> mice received protein-restricted diet and daily administration of Na-benzoate and L-Arg in combination with either TB-1 or vehicle, started on day 10 of life and lasting for 3 weeks. Consistent with previous data (Erez et al, 2011; Ashley et al, 2018; Baruteau et al, 2018; Burrage et al, 2020), vehicle-treated *Asl*<sup>Neo/Neo</sup> mice showed vacuolated hepatocyte cytoplasm by haematoxylin and eosin (H&E) staining in contrast to WT mice, whereas TB-1 treatment markedly improved the microscopic changes of liver architecture (Fig 3A). Although body weight was unaffected (Fig EV5A), TB-1 treatment resulted in a trend of reduction in hepatomegaly (Fig EV5B) and a mild decrease in serum alanine aminotransferase (ALT) levels in *Asl*<sup>Neo/Neo</sup> mice (Fig EV5C). Moreover, *Asl*<sup>Neo/Neo</sup> mice treated with TB-1 showed partial reduction of liver glycogen storage by periodic acid Schiff (PAS) staining (Fig 3A and B) and glycogen quantification (Fig 3C) compared to controls. Notably, glycogen accumulation was not observed in livers of *spf-ash* mice (Fig EV5D). Glycogen in hepatocytes is catabolized either in cytosol

by the coordinated action of enzymes involved in glycogenolysis or in the lysosome by the acid glucosidase (Prats et al, 2018). Hepatic expression of glycogen phosphorylase (PYGL), the enzyme that catalyses the rate limiting step of glycogenolysis, was recently found to be reduced in *Asl*<sup>Neo/Neo</sup> mice, suggesting a mechanism responsible for aberrant glycogen accumulation in ASA (Burrage et al, 2020). We confirmed reduced PYGL protein levels in livers of *Asl*<sup>Neo/Neo</sup> mice, but they were unaffected by TB-1 (Fig 3D), suggesting that reduction of glycogen by TB-1 does not occur through rescue of the cytosolic glycogen degradation pathway. Moreover, when autophagy flux is increased by TB-1, glycogen degradation in lysosomes is efficiently achieved, as confirmed by electron microscopy (EM) analysis showing clearance of cytoplasmic glycogen accumulation (Fig 3E). Moreover, glycogen accumulation in *Asl*<sup>Neo/Neo</sup> mice resulted in displacement of organelles to the cell membrane as previously reported (Burrage et al, 2020), that is relieved by TB-1 (Fig 3E). Surprisingly, EM analysis also showed abundant intranuclear glycogen deposition in hepatocytes of *Asl*<sup>Neo/Neo</sup> mice, that was partially reduced by TB-1 (Fig 4A and B). In summary, in addition to promoting urea synthesis, TB-1 reduced abnormal glycogen storage in cytosol and nuclei of ASL-deficient hepatocytes.

## Discussion

UCD are inborn errors of metabolism due to impaired clearance of toxic nitrogen. Despite current therapies, cumulative morbidity is still high in patients with UCD and thus, several experimental therapies have been investigated to improve clinical outcomes (Soria et al, 2019). We recently showed a role of hepatic autophagy in promoting ureagenesis and ammonia detoxification (Soria et al, 2018) that can be exploited for the development of novel therapies for hyperammonemia and UCD (Soria et al, 2018; Soria & Brunetti-Pierri, 2018, 2019). In the present study, we investigated the efficacy of TB-1 peptide, a potent and specific agent that can activate autophagy *in vivo*, in two well-established mouse models of proximal and distal UCD. Induction of liver autophagy was found to improve several clinically relevant endpoints in these mice, supporting autophagy enhancement as a therapeutic strategy for UCD.

Autophagy plays a key role in liver physiology by supporting metabolism and promoting adaptation to stress. Specific modulation of autophagy has been recognized as a potential therapeutic strategy in various liver diseases (Allaire et al, 2019; Hazari et al, 2020).

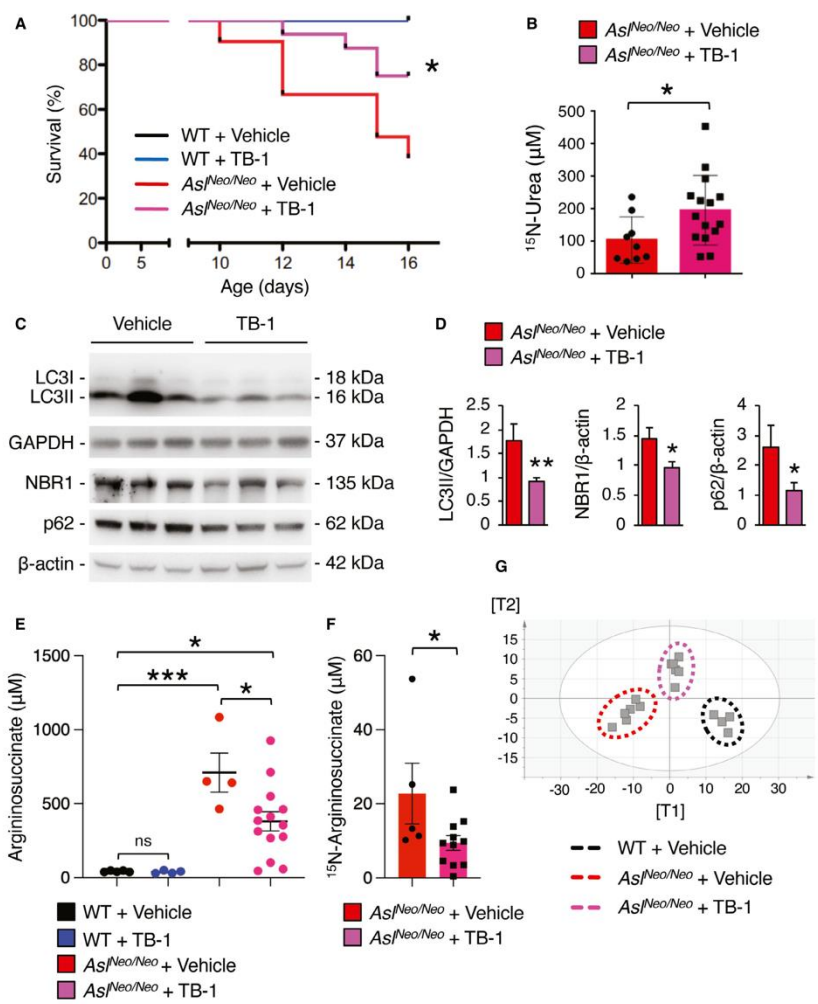


Figure 2.

**Figure 2. Enhancement of liver autophagy improves survival, increases ureagenesis, and corrects metabolic defects of ASL-deficient mice.**

- A Survival curves of *Asl<sup>flx/Neo</sup>* mice and age-matched wild-type (WT) controls treated with TB-1 (15 mg/kg, i.p., every 48 h starting at day 10 of age) or vehicle. WT + Vehicle *n* = 8; WT + TB-1 *n* = 8; *Asl<sup>flx/Neo</sup>* + Vehicle *n* = 20; *Asl<sup>flx/Neo</sup>* + TB-1 *n* = 16. \**P* < 0.05 (Log-rank Mantel-Cox test).
- B Isotopic enrichment of <sup>15</sup>N-labelled urea in blood, 20 min after i.p. injection of <sup>15</sup>NH<sub>4</sub>Cl tracer (4 mmol/kg) in *Asl<sup>flx/Neo</sup>* mice treated with TB-1 (*n* = 15) or vehicle (*n* = 9). \**P* < 0.05 (Unpaired t-test).
- C Representative Western blotting bands of LC3, p62 and NBR1 in livers of *Asl<sup>flx/Neo</sup>* mice treated with TB-1 or vehicle. GAPDH and β-actin were used as loading controls.
- D Densitometric quantifications. *Asl<sup>flx/Neo</sup>* + Vehicle *n* = 5; *Asl<sup>flx/Neo</sup>* + TB-1 *n* = 9. \*\**P* < 0.01, \**P* < 0.05 (Unpaired t-test).
- E Argininosuccinate in dried blood spots of WT and *Asl<sup>flx/Neo</sup>* mice injected with TB-1 or vehicle (*n* = 4–14 mice/group). \*\*\**P* < 0.001, \**P* < 0.05 (One-way ANOVA).
- F Isotopic enrichment of <sup>15</sup>N-labelled argininosuccinate in livers of *Asl<sup>flx/Neo</sup>* mice treated with TB-1 (*n* = 11) or vehicle (*n* = 5). \**P* < 0.05 (Unpaired t-test).
- G Orthogonal Projection to Latent Structure-Discriminant Analysis (OPLS-DA) score plot obtained from high-resolution <sup>1</sup>H-NMR spectroscopy performed on livers of vehicle-treated *Asl<sup>flx/Neo</sup>* mice (*n* = 6), WT controls (*n* = 4) and *Asl<sup>flx/Neo</sup>* mice injected with TB-1 (*n* = 6). A statistical model with *R*<sup>2</sup> = 0.78 (goodness of fit), *Q*<sup>2</sup> = 0.57 (power in prediction) and *P* = 0.0056 was obtained. See also Appendix Fig S1.

Data information: All values are shown as averages ± SEM. ns: not statistically significant difference. Exact *P* values are reported in Appendix Table S1. Source data are available online for this figure.

Obtaining specific modulation of autophagy has been a major challenge for clinical translation of autophagy enhancer molecules (Allaire et al., 2019). Being an essential regulator of autophagosome synthesis and maturation, Beclin-1 is an attractive target for autophagy-inducing drugs and small peptides affecting Beclin-1 interactions, such as TB-1 and its derivatives have been developed (Shoji-Kawata et al., 2013; Peraro et al., 2017). Moreover, drugs affecting post-translational modifications of Beclin-1 altering its function are also attractive (Hill et al., 2019). The *Becn1<sup>F121A</sup>* mouse model used in this work mimics the condition of disrupted interaction of Beclin-1 with BCL2. In these mice, we found improved ureagenesis and increased ammonia detoxification capacity. Within the context of a normal functioning ureagenesis, the increase detected in *Becn1<sup>F121A</sup>* mice was relatively mild and corresponded to about 20–30%. Nevertheless, such increase is still expected to provide significant clinical benefit in UCD. Additionally, the increased ureagenesis of *Becn1<sup>F121A</sup>* mice validates the inhibitors of the Beclin-1-BCL2 complex (Chiang et al., 2018) as targets for increasing ammonia detoxification.

We next investigated the efficacy of TB-1-mediated activation of hepatic autophagy for therapy of proximal and distal UCD using the most relevant mouse models for these disorders, the *spf-ash* and the *Asl<sup>flx/Neo</sup>* mice for OTC and ASL deficiency, respectively (Moscioni et al., 2006; Priev et al., 2018; Kurtz et al., 2019; Soria et al., 2019). In *spf-ash* mice treated with TB-1, we detected reduced urinary orotic aciduria under standard and high protein diet. Importantly, combined with clinically available drugs enhancing ammonia excretion (Na-Benzothate) and urea synthesis (L-Arg), TB-1 was also effective in increasing survival of *spf-ash* mice challenged with a high

protein diet. These data suggest that liver autophagy enhancement cooperates with current treatment in improving the phenotype of OTC deficiency. In *ASA* mice, we also found that hepatic enhancement of autophagy increased ureagenesis and survival, and reduced argininosuccinate levels along with generalized rescue of the metabolic derangement, as suggested by liver metabolomic analyses. In summary, TB-1 improved the phenotypes of two UCD animal models, supporting the potential of autophagy enhancement for therapy of hyperammonemia due to defects of the urea cycle.

Increased liver autophagy by TB-1 provides amelioration but not a cure for UCD. The therapeutic potential of TB-1 could be especially exploited in newborns or infants with UCD in their early disease stages before more definitive treatments, such as liver transplantation or gene therapy can be safely and effectively performed. For liver-directed gene therapy with adeno-associated viral (AAV) vectors, efficacy is gradually lost during mouse growth as a consequence of dilution of episomal vector genomes in dividing hepatocytes (Cunningham et al., 2009; Baruteau et al., 2018). Hence, TB-1 can be viewed as a bridge treatment until affected infants reach an age that permits sustained transgene expression by gene therapy. Interestingly, co-administration of autophagy enhancers with AAV vectors markedly improved transgene expression (Hosel et al., 2017) and thus, TB-1 could have the dual action of increasing AAV transduction and improving metabolic control. Moreover, onset of hepatic gene expression by AAV typically requires 2–3 weeks, and thus, TB-1 might also treat the metabolic defect until high levels of gene expression are achieved.

Interestingly, in *ASA* mice TB-1 also resulted in increased clearance of intracellular glycogen accumulation. Disposal of

**Figure 3. Enhancement of autophagy reduces hepatocellular injury and glycogen storage in ASL-deficient mice.**

- A Haematoxylin and eosin (H&E, upper panels) and periodic acid Schiff (PAS, lower panels) staining of liver samples harvested from wild-type (WT) and *Asl<sup>flx/Neo</sup>* mice treated with TB-1 or vehicle. Scale bars: 500 μm.
- B Computational analysis of PAS staining (*n* ≥ 4 mice/group). \*\**P* < 0.01, \**P* < 0.05 (One-way ANOVA).
- C Quantification of hepatic glycogen in vehicle (*n* = 6)- and TB-1-treated *Asl<sup>flx/Neo</sup>* mice (*n* = 12) compared to WT (*n* = 5) controls. \*\**P* < 0.01, \**P* < 0.05 (One-way ANOVA).
- D Representative Western blotting bands and densitometric quantification of PYGL in livers of WT and *Asl<sup>flx/Neo</sup>* mice treated with either with TB-1 or vehicle (*n* = 4 mice/group). \**P* < 0.05 (One-way ANOVA). GAPDH was used as loading control.
- E Representative electron microscopy images of liver samples harvested from WT and *Asl<sup>flx/Neo</sup>* mice treated with TB-1 or vehicle. Scale bar: 900 nm.

Data information: All values are shown as averages ± SEM. Exact *P* values are reported in Appendix Table S1. Source data are available online for this figure.

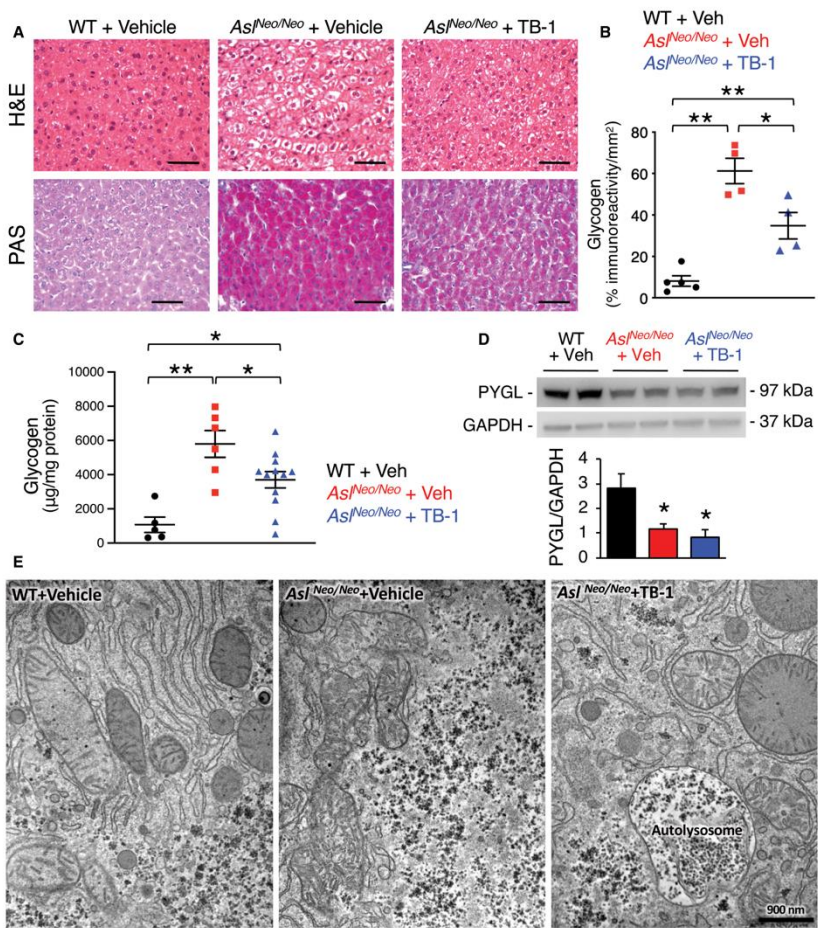
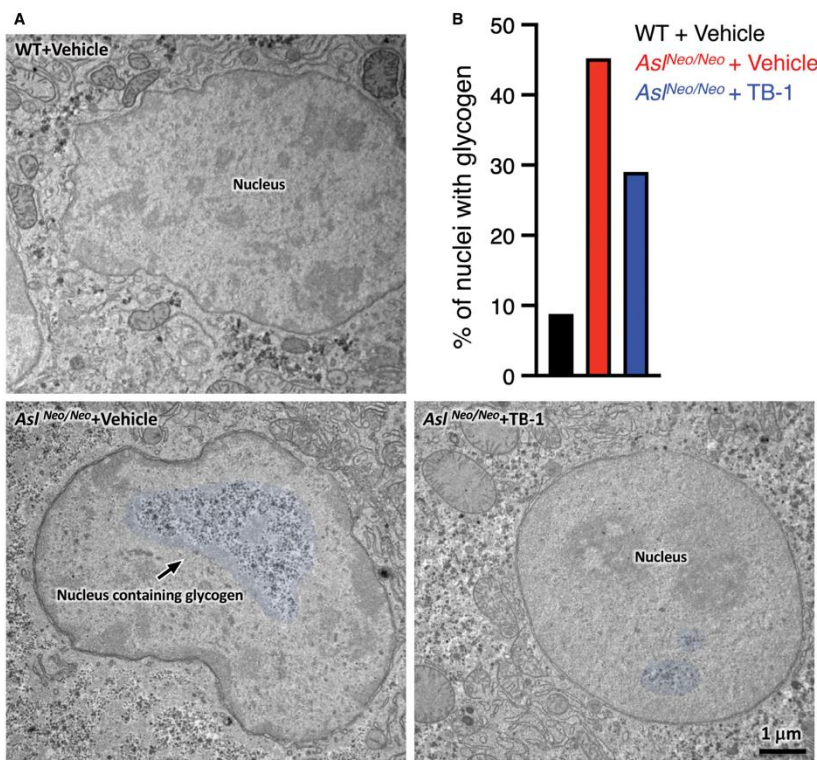


Figure 3.

carbohydrates such as glycogen via autophagy plays a crucial role in glucose homeostasis (Karsli-Uzunbas et al, 2014). This finding is consistent with previous studies in glycogen storage diseases type 1 and 2 showing that either genetic or pharmacologic activation of

autophagy reduced glycogen storage (Ashe et al, 2010; Spanpanato et al, 2013; Martina et al, 2014; Farah et al, 2016). Consistent with a previous study (Burrage et al, 2020), we found that PYGL was reduced in *ASL*-deficient mice and thus, increased glycogen





**Figure 4. TB-1 reduces intra-nuclear glycogen deposition in ASL-deficient mice.**  
A Representative electron microscopy images of liver samples harvested from wild-type (WT) and *Asl*<sup>Neo/Neo</sup> mice treated with TB-1 or vehicle. False colour on the images indicates glycogen within the nuclei. Scale bar: 1 μm.  
B Quantification of nuclei containing glycogen (approx. 180 nuclei were analysed in total per condition, *n* = 3 mice/group).  
Data information: All values are shown as averages ± SEM. ns: not statistically significant difference.  
Source data are available online for this figure.

degradation mediated by TB-1 occurred independently from impaired cytosolic PYGL-dependent degradation of glycogen. Glycogen clearance induced by TB-1 restored physiologic organelle distribution within the cell. Abnormal glycogen deposition in UCD livers occurs independently from metabolic syndrome (Bigot *et al*, 2017) and has been reported in patients with OTC deficiency and other UCD (Badizadegan & Perez-Atayde, 1997; Mori *et al*, 2002; Yapito-Lee *et al*, 2013; Baruteau *et al*, 2017; Bigot *et al*, 2017;

Ranucci *et al*, 2019). However, *spf-ash* mice showed normal hepatic glycogen storage. Intriguingly, we found glycogen accumulation also in nuclei of ASA hepatocytes. Nuclear accumulation of glycogen was recently associated to epigenetic changes in gene expression and cancer (Sun *et al*, 2019). In normal cells, nuclear glycogenolysis provides a carbon pool for proper histone acetylation, whereas in cancer cells suppression of nuclear glycogen catabolism is associated with changes in histone acetylation and gene expression, and

cancer progression (Sun *et al*, 2019). Liver cancer is an emerging feature of UCD (Wilson *et al*, 2012; Koo *et al*, 2017; Wang *et al*, 2019). Therefore, besides improved ureagenesis, the reduced cytoplasmic and intra-nuclear glycogen mediated by TB-1 might provide further long-term clinical benefits preventing progression of chronic liver damage. However, this hypothesis would need further investigation and available mouse models of UCD have not been reported to have an increased frequency of liver cancer. The newly generated OTC knock-out mouse model that develops liver fibrosis and chronic liver damage (Wang *et al*, 2017) might be a suitable model to investigate this issue in long-term studies.

We previously found that TB-1 increases ureagenesis by furnishing the urea cycle with key intermediate metabolites and preventing ammonia-induced depletion of ATP (Soria *et al*, 2018). Whether this mechanism is also responsible for increased ureagenesis in ASL deficiency cannot be established. *Asl<sup>Nes/Neo</sup>* mice have massive accumulation of argininosuccinate secondary to deficiency of ASL that breaks down argininosuccinate into arginine and fumarate. In *Asl<sup>Nes/Neo</sup>* mice, TB-1 increased ureagenesis and reduced argininosuccinate despite the lack of increased ASL activity. Although no changes in ASL enzyme activity were detected, the enzyme assay might not reflect the enzyme *in vivo* activity. Alternatively, other mechanisms can be hypothesized. For instance, TB-1 might improve metabolic channelling, i.e. reversible specific assembly of enzyme clusters that accelerate processing of metabolite intermediates (Castellana *et al*, 2014; Pareek *et al*, 2020). Notably, channelling of urea cycle intermediates has been found between mitochondria and cytosol where ureagenesis takes place (Cheung *et al*, 1989; Cohen *et al*, 1992). This channelling could be particularly affected in *Asl<sup>Nes/Neo</sup>* mouse hepatocytes displaying aberrant distribution of their sub-cellular compartments that is partially corrected by TB-1, as confirmed by the ultrastructural studies performed in this work.

In conclusion, this study shows a key role of liver autophagy in nitrogen homeostasis and indicates that Beclin-1 as a *druggable* target for therapy of hyperammonemia and UCD. Moreover, these findings show that enhancement of hepatic autophagy is beneficial in UCD through: (i) correction of the underlying metabolic abnormalities by supporting residual ureagenesis activity and, (ii) reduction of the aberrant intracellular (cytosolic and nuclear) glycogen burden that might prevent long-term hepatotoxicity.

## Materials and Methods

### Mouse studies

All mouse procedures were performed in accordance with regulations and were authorized by either the Italian Ministry of Health or the UK Home Office. *Becn1<sup>F121A</sup>* (B6.129(Cg)-Becn1<sup>tm1.1Hec/J</sup>) mice were previously described (Rocchi *et al*, 2017; Fernandez *et al*, 2018) and were maintained on a C57BL/6 background. Wild-type (WT) littermates were used as controls. For acute ammonia challenges, male and female WT and *Becn1<sup>F121A</sup>* mice were starved overnight before the i.p. injection of 10 mmol/kg of <sup>15</sup>N-labelled ammonium chloride (98% enriched in <sup>15</sup>N, Sigma) dissolved in water. Blood samples were collected by retro-orbital bleedings at baseline, 5, 15, and 30 min post-injection. The amount of <sup>15</sup>N-labelled urea in sera was quantified by gas chromatography–mass

spectrometry (GC-MS) analysis at the Metabolic Core of The Children's Hospital of Philadelphia (Philadelphia, PA). Mice were sacrificed by cervical dislocation, and liver samples were harvested for analyses. Breeding pairs of *spf-ash* mice (B6EiC3Sn a/A-OTC<sup>Spf-Ash/J</sup>) were purchased from Jackson Laboratories (Cat# 001811) and housed in individually ventilated cages, maintaining a temperature of 22°C (± 2°C), relative humidity of 55% (± 10%), 15–20 air exchanges per hour and 12-h light/12-h dark cycle and receiving a standard chow diet and water *ad libitum*. 12-week-old male *spf-ash* mice received an i.p. injection of TB-1 D-11 retroinverso form peptide (Novus Biologicals; Cat# NBP2-49888) at the dose of 15 mg/kg [dissolved in phosphate buffer saline (PBS)] every 48 h for a total period of 10 days. Animals were daily monitored and weighted. Urine samples were collected at the indicated time points to measure orotic acid. A control group of *spf-ash* animals were injected with vehicle only. For high protein diet challenge, 12-week-old male *spf-ash* mice were maintained on a 51%-protein diet (U8959 version 142, Safe-diets) for 10 days. TB-1 peptide was delivered by i.p. injection at the dose of 15 mg/kg every 48 h. 60 mg/ml Na-Benzothate (Sigma; Cat# 18106) and 60 mg/ml L-Arg (Sigma, Cat# A5006) dissolved in PBS were i.p. injected at the dose of 250 mg/kg Na-Benzothate, 250 mg/kg L-Arg every 24 h. As controls, a group of *spf-ash* mice were injected with vehicle only and a group of WT mice were used. Animals were daily monitored and weighted. Blood samples were collected by submandibular bleeding at day 4 to measure ammonia concentration. Urines were collected at baseline and day 4 for measurements of orotic acid.

*Asl<sup>Nes/Neo</sup>* mice (B6.129S7-*Asl<sup>tm1Btle/J</sup>*) were purchased from Jackson Laboratory (Bar Harbor, ME) and maintained on standard rodent chow (Harlan 2018, Teklab Diets, Madison, WI; protein content 18%) with free access to water in a 12 h light/12 h dark environment. For mouse genotyping, DNA extraction from tail clips was performed as described previously (Barreau *et al*, 2018). For long-term experiment, all WT and *Asl<sup>Nes/Neo</sup>* mice received a supportive treatment modified (Barreau *et al*, 2018) including a reduced-protein diet (SCR4, Labdiet, St Louis, MO; protein content 14.1%) and daily i.p. injections of Na-benzoate (0.5 g/kg/day) and L-Arg (0.5 g/kg/day) from day 10 to day 30. Treated *Asl<sup>Nes/Neo</sup>* mice received 15 mg/kg of TB-1 i.p. three times per week (Monday, Wednesday, Friday). Control animals received vehicle (i.e. PBS). Male WT and *Asl<sup>Nes/Neo</sup>* mice received three i.p. injections over 5 or 20 days with either PBS or TB-1 from 10 days old onwards. Concomitantly, these mice received daily supportive treatment to improve survival until day 30. WT littermates were used as controls. For all experiments, WT and *Asl<sup>Nes/Neo</sup>* littermates were housed in the same cages. WT and mutant pups remained in cages with their mothers until day 30. Pups and their mothers were fed with the same diet. Mice had free access to diet and were not fasted before sacrifice.

### Biochemical measurements

Blood ammonia levels were measured by ammonia colorimetric assay kits (BioVision Incorporated; Cat# K370-100 or Sigma; Cat#AA0100) according to the manufacturer's instructions. Circulating ALT levels were analysed with a Fuji Dri-Chem NX500 (FUJIFILM, Tokyo, Japan). Orotic acid was purchased from Sigma-Aldrich. The isotopically labelled internal standard orotic acid was purchased from Cambridge Isotope Laboratories, Inc. The

quantitative experiments were done using as internal standard the isotopically labelled 1,3- $^{15}\text{N}_2$  orotic acid in 200  $\mu\text{M}$  concentration both for calibration curve and samples. A typical calibration curve ranged from 15 to 300  $\mu\text{M}$  with excellent linearity ( $R^2 > 0.99$ ). A Bruker (Bremen, Germany) amaZon SL bench-top ion trap mass spectrometer, equipped with an electrospray source, was employed for this study. The source was operated in negative ion mode with a needle potential of 4,500 V and a gas flow of 12 l/min of nitrogen with heating at 200°C. The chromatographic separations for quantitative experiments were performed using a series 1260 Agilent Technologies (Waldbronn, Germany) HPLC with auto sampler controlled from the Bruker Hystardata system. A Phenomenex (Torrance, USA) HPLC column Gemini C18 5  $\mu\text{m}$ , 110 Å, 2  $\times$  150 mm was employed. Column flow rate was 0.4 ml/min and elution was performed using 5 min wash time after 10  $\mu\text{l}$  injection and a 3 min gradient from water with 0.1% formic acid to 90% acetonitrile with 0.1% formic acid. The tandem mass spectrometry (MS/MS) transitions used for the quantitative experiments (multiple reaction monitoring, MRM) were  $m/z$  155.1–111.1 (orotic acid) and 157.1 to 113.1 (1,3- $^{15}\text{N}_2$  orotic acid). The acquired data were processed using the Bruker Compass Data Analysis proprietary software. Creatinine was measured using the Mouse Creatinine Kit (Crystal Chem; Cat# 80350) following the manufacturer's guidelines and used to normalize orotic acid values in the urine.

Mass spectrometry analysis of argininosuccinic acid in dried bloodspots was performed as previously described (Baruteau *et al*, 2019b). Briefly, blood spots on a Guthrie card were dried at room temperature for 24 h. 3 mm-diameter punch from dried blood spots were used to measure argininosuccinic acid by liquid chromatography-tandem mass spectrometry (LC-MS/MS). A punch was incubated for 15 min in sonicating water bath in 100  $\mu\text{l}$  of methanol containing stable isotopes used as internal standards. A 4:1 volume of methanol was added to precipitate contaminating proteins. The supernatant was collected and centrifuged at 16,000 g for 5 min before separation on a Waters Alliance 2795 LC system (Waters, Midford, USA) using a XTerra<sup>®</sup> RP18, 5  $\mu\text{m}$ , 3.9  $\times$  150 mm column (Waters, Midford, USA). The mobile phases were (A) methanol and (B) 3.7% acetic acid. Detection was performed using a tandem mass spectrometer Micro Quattro instrument (Micromass UK Ltd, Cheshire, UK) using multiple reaction monitoring in positive ion mode. Data were analysed using Masslynx 4.1 software (Micromass UK Ltd, Cheshire, UK).

Mass spectrometry analysis of  $^{15}\text{N}$ -labelled argininosuccinic acid in liver samples was adapted from Prinsen *et al* (2016). Briefly, liver samples were homogenized in 400  $\mu\text{l}$  of mixture of ice-cold methanol:acetonitrile:water (ratio of 5:3:2) containing internal standard (2 nmol/l, L-citrulline-d7, CDN Isotopes, Pointe-Claire, Quebec) and centrifuged at 17,000 g for 20 min at 4°C. Supernatants were dried using Eppendorf<sup>®</sup> Concentrator Plus and resuspended in 0.05 M HCl. 80  $\mu\text{l}$  of the resuspended mixture was mixed with 280  $\mu\text{l}$  of solvent A (10 mM ammonium formate, 85% Acetonitrile + 0.15% formic acid), centrifuged at 17,000 g for 5 min and filtered with 0.2  $\mu\text{m}$  PTFE membrane filter (Thermo-Fisher Scientific, Rockford, IL, USA) before analysis by hydrophilic interaction liquid chromatography coupled with tandem mass spectrometry. Amino acid chromatography separation was performed in Acquity Ultra-Pure Liquid Chromatography (UPLC)-system (Waters, Manchester, UK) using Acquity UPLC BEH Amide column (2.1  $\times$  100 mm,

1.7  $\mu\text{m}$  particle size) and Van Guard<sup>™</sup> UPLC BEH Amide pre-column (2.1  $\times$  5 mm, 1.7  $\mu\text{m}$  particle size) (Waters Limited, UK). The mobile phases were (A) 10 mM ammonium formate in 85% acetonitrile and 0.15% formic acid and (B) 15 mM ammonium formate containing 0.15% formic acid, pH 3.0. Detection was performed using a tandem mass spectrometer Xevo TQ-S (Waters, UK) using multiple reaction monitoring in positive ion mode. The dwell time was set automatically with MRM-transition of 292.2 > 116.98 and 274.2 > 70.2 for  $^{15}\text{N}$ -ASA and  $^{15}\text{N}$ -ASA anhydrides, respectively. L-Citrulline-d7 was used as internal standard control. Argininosuccinate data were analysed using Masslynx 4.2 software (Micromass UK Ltd, Cheshire, UK).

#### *In vivo* $^{15}\text{N}$ -ureagenesis in $\text{Asl}^{\text{Neo/Neo}}$ mice

Vehicle- and TB-1-treated  $\text{Asl}^{\text{Neo/Neo}}$  mice received an i.p. injection of 4 mmol/kg of  $^{15}\text{N}$ -labelled ammonium chloride ( $^{15}\text{NH}_4\text{Cl}$ , Cambridge Isotope Laboratories) 20 min before terminal blood collection via cardiac puncture. Blood was collected in 1:10 volume of sodium citrate and centrifuged at 13,000 g for 5 min. Plasma was collected and snap-frozen in dry ice.  $^{13}\text{C}$ ,  $^{15}\text{N}_2$ -urea (Sigma) was added to all samples as an internal standard, and samples were derivatized in a two-stage procedure. Firstly, urea was cyclized with 1,1,3,3-Tetramethoxypropane (Sigma-Aldrich) under acidic conditions to obtain 2-hydroxypyrimidine (2HP). 2HP was then coupled with 2,3,4,5,6-Pentafluorobenzyl bromide (Sigma-Aldrich) to yield a derivative that, upon negative ion chemical ionization gas chromatography mass spectrometry, yields a negatively charged 2-HP fragment that includes the nitrogen and carbon atoms of the starting urea. Ions of mass/charge 95 (2HP from  $^{12}\text{C}$ ,  $^{14}\text{N}_2$ -urea), 96 ( $^{12}\text{C}$ ,  $^{15}\text{N}$ ,  $^{14}\text{N}$ -urea derived from  $^{15}\text{N}$ -ammonium chloride or  $^{13}\text{C}$ ,  $^{14}\text{N}_2$ -urea) and 98 ( $^{13}\text{C}$ ,  $^{15}\text{N}_2$ -urea internal standard) were analysed, and quantified with suitable standard curves (95/98 for unlabelled urea, 96/98 for  $^{15}\text{N}$ -urea). Unlabelled urea concentration was calculated from the 95/98 ratio, the contribution of unlabelled urea to mass 96 calculated from the natural abundances of the atoms in the fragment ( $\text{C}_4\text{H}_3\text{N}_2\text{O}^-$ ), and  $^{15}\text{N}$ -urea calculated from the 96/98 ratio minus the contribution of unlabelled urea to mass 96.

#### Metabolite profiling of liver tissue by $^1\text{H}$ -NMR

Livers were mechanically disrupted to extract the metabolites of interest (lipids, carbohydrates, amino acids, and other low-molecular weight metabolites) while leaving other compounds (DNA, RNA, and proteins) in the tissue pellet. Homogenization of 200 mg of frozen tissue samples was carried out in cold methanol (8 ml/g of tissue, wet weight), and cold water (1.7 ml/g of tissue, wet weight) with UltraTurrax for 2 min on ice. Four ml of chloroform per g of tissue (wet weight) were added and the homogenate was gently stirred and mixed on ice for 10 min (the solution must be monophasic). Then, additional 4 ml of chloroform per g of tissue (wet weight), and 4 ml of water per g of tissue (wet weight) were added and the final mixture was well shaken and centrifuged at 12,000 g for 15 min at 4°C. This procedure separates three phases: water/methanol on the top (aqueous phase with the polar metabolites), denatured proteins and cellular debris in the middle, and chloroform at the bottom (lipid phase with lipophilic compounds). The upper and the lower layers were transferred into glass vials, the solvents



removed under a stream of dry nitrogen, and stored at  $-80^{\circ}\text{C}$  until analysis. Polar extracts were resuspended in 700  $\mu\text{l}$  PBS, pH 7.4 with 10%  $\text{D}_2\text{O}$  for lock procedure, and then transferred into an NMR tube. High-resolution one-dimensional (1D) spectra were recorded at 600.13 MHz on a Bruker Avance III-600 spectrometer (Bruker BioSpin GmbH, Rheinstetten, Germany) equipped with a TCI CryoProbe<sup>™</sup> fitted with a gradient along the Z-axis, at a probe temperature of  $27^{\circ}\text{C}$ , using the excitation sculpting sequence for solvent suppression. Spectra were referenced to internal 0.1 mM sodium trimethylsilylpropionate, assumed to resonate at  $\delta = 0.00$  ppm.

#### NMR data processing and statistical analysis

The spectral 0.50–9.40 ppm region of the  $^1\text{H}$ -NMR spectra was automatically data reduced to integrated regions (buckets) of 0.04-ppm each using the AMIX 3.6 package (Bruker Biospin GmbH, Rheinstetten, Germany). The residual water resonance region (4.72–5.10 ppm) was excluded, and the integrated region was normalized to the total spectrum area. To differentiate liver tissues through NMR spectra, we carried out a multivariate statistical data analysis using projection methods as previously reported (Soria *et al*, 2018).

#### Enzyme activity assays

OTC enzyme activity was determined in total liver protein extracts as reported previously (Ye *et al*, 1996) with minor modifications. One  $\mu\text{g}$  of total liver protein extract (in lysis buffer: 0.5% Triton-X, 10 mM Hepes pH 7.4, 2 mM DTT) was added to 350  $\mu\text{l}$  of reaction mixture (5 mM ornithine, 15 mM carbamyl phosphate and 270 mM triethanolamine, pH 7.7) and incubated at  $37^{\circ}\text{C}$  for 30 min. The reaction was then stopped by adding 125  $\mu\text{l}$  of 3:1 phosphoric/sulphuric acid solution followed by 25  $\mu\text{l}$  of 3% 2,3-butanedione monoxime and incubated at  $95^{\circ}\text{C}$  for 15 min in the dark. Citrulline production was determined by measuring the absorbance at 490 nm.

For ASL activity, liver samples were snap-frozen in dry ice at time of collection. Protein extraction was performed on ice. Liver samples were homogenized with the Qiagen Bead Tissue Lyser (Qiagen Manchester Ltd, Manchester, UK) in 500  $\mu\text{l}$  of 50 mM phosphate buffer (pH 7.4) with EDTA-free proteinase inhibitor cocktail (Roche, Basel, Switzerland) at a frequency of 30 for 30 s. Homogenates were centrifuged at 13,000 g for 10 min at  $4^{\circ}\text{C}$ . Protein quantification of the supernatant was performed using the Pierce<sup>™</sup> BCA protein assay kit (Thermo-Fisher Scientific, Rockford, IL, USA) according to the manufacturer's instructions. ASL activity was measured by synthesis of fumarate in an excess of argininosuccinate as previously described (Baruteau *et al*, 2018). Fumarate was measured with the Fumarate Assay Kit (Sigma; Cat# MAK060) according to manufacturer's instructions.

#### Periodic acid Schiff staining

The staining was performed according to the Standard Operating Procedure protocol at the Histopathology laboratory, Great Ormond Street Hospital, London. Sections were dewaxed in xylene, hydrated down through graded alcohol solutions to water, incubated for 10 min in 0.5% periodic acid, rinsed in distilled water, stained for 10 min with Schiff reagent, then rinsed in distilled water. Sections

were then washed for 5 min in running tap water and counter-stained in 1% eosin for 1 min, rinsed briefly in running tap water and dehydrated through ascending grades of alcohol. Sections were then cleared in xylene and mounted. For haematoxylin and eosin (H&E) staining, liver sections were processed according to standard protocols.

For quantitative PAS staining quantification, ten random images per liver section were captured with a microscope camera (DFC420; Leica Microsystems, Milton Keynes, UK) and software (Image Analysis; Leica Microsystems). Quantitative analysis was performed with thresholding analysis using the Image-Pro Premier 9.1 software (Rockville, MD, USA).

#### Hepatic glycogen determination

Liver content of glycogen was determined by using a colorimetric glycogen assay kit (Sigma-Aldrich; Cat# MAK016). Liver lysates were made by homogenization following the manufacturer's instructions using a Tissue Lyser (Qiagen). Hepatic glycogen levels were normalized for protein concentrations determined by Bradford Reagent (Bio-Rad).

#### Western blotting

Liver specimens were homogenized in RIPA buffer in the presence of complete protease inhibitor cocktail (Sigma), incubated for 20 min at  $4^{\circ}\text{C}$  and centrifuged at 16,800 g for 10 min. Pellets were discarded and cell lysates were used for western blots. Total protein concentration in cellular extracts was measured using the Bradford Reagent (Bio-Rad). Protein extracts were separated by SDS-PAGE and transferred onto polyvinylidene difluoride (PVDF) membranes. Blots were blocked with TBS-Tween-20 containing 5% non-fat milk for 1 h at room temperature followed by incubation with primary antibody overnight at  $4^{\circ}\text{C}$ . The primary antibodies used were: rabbit anti-LC3B (Novus Biologicals; Cat# NB-100-2220; dilution: 1/1,000), mouse anti-p62 (Abnova; Cat# H00008878-M01; dilution: 1/1,000), mouse anti-NBR1 (Abnova; Cat# H00004077-M01; dilution: 1/1,000), rabbit anti-PYGL (Proteintech; Cat# 15851-1-AP; dilution: 1/1,000), rabbit anti-NAGS (Abcam; Cat# ab65536; dilution: 1/1,000), rabbit anti-CPS1 (Abcam; Cat# ab45956; dilution: 1/1,000), rabbit anti-OTC (Novus Biologicals; Cat# NBP1-31582; dilution: 1/1,000), mouse anti-ASS1 (Abcam; Cat# ab124465; dilution: 1/1,000), rabbit anti-ASL (Abcam; Cat# ab201026; dilution: 1/1,000), rabbit anti-ARG1 (Abcam; Cat# ab91279; dilution: 1/1,000), mouse anti- $\beta$ -actin (Novus Biologicals; Cat# NB600-501; dilution: 1/3,000), and mouse anti-GAPDH (Santa Cruz Biotechnology; Cat# sc-32233; dilution: 1/3,000). Proteins of interest were detected with horseradish peroxidase (HRP)-conjugated goat anti-mouse or anti-rabbit IgG antibody (GE Healthcare). Peroxidase substrate was provided by ECL Western Blotting Substrate kit (Pierce). Densitometric analyses of the western blotting bands were performed using ImageJ Software (Fiji 2).

#### Electron microscopy

For EM analyses, liver specimens were fixed in 1% glutaraldehyde in 0.2 M HEPES buffer. Small blocks of liver tissues were then post-fixed in  $\text{OsO}_4$  and uranyl acetate.

**The paper explained****Problem**

Urea cycle disorders have high morbidity and mortality and require development of novel and more effective therapies. Ornithine transcarbamylase (OTC) and argininosuccinate lyase (ASL) deficiencies are the two most common urea cycle disorders.

**Results**

Mice carrying a Beclin-1 activating mutation have increased ammonia detoxification and treatment with the cell-penetrating autophagy-inducing Tat-Beclin-1 peptide improved phenotypic and biochemical abnormalities of mouse models of OTC and ASL deficiencies.

**Impact**

Drugs activating Beclin-1 have potential for therapy of UCD.

After dehydration through a graded series of ethanol solutions and propylene oxide tissue samples were embedded in epoxy resin and polymerized at 60°C for 72 h. From each sample, thin sections were cut with a Leica EM UC7 ultramicrotome and images acquired by FEI Tecnai – 12 (FEI, Eindhoven, The Netherlands) EM equipped with Veleta CCD camera for digital image acquisition.

**Statistical analyses**

Data were analysed using GraphPad Prism 5.0 software, San Diego, CA, USA. Comparisons of continuous variables between two and more experimental groups were performed using the two-tailed unpaired Student's *t*-test or one-way ANOVA with Tukey's or Dunnett's *post hoc* tests. Two-way ANOVA and Tukey's *post hoc* tests were performed to compare two groups relative to two factors. Kaplan–Meier survival curves were compared with the log-rank test. No statistical methods were used to predetermine the sample size. A minimum of *n* = 5 per group was included, and the sample size was increased if needed to achieve statistical significance. No formal randomization procedure was used but assignment of mice to treatment groups was based on mouse identification numbers, and the investigators were not blinded. Number of replicates is reported in the figure legends. Data are expressed as means ± SEM. *P* values < 0.05 were considered statistically significant.

**Data availability**

This study includes no data deposited in external repositories. All data reported in the paper are included in the manuscript or available in the Appendix.

**Expanded View** for this article is available online.

**Acknowledgements**

We thank Edoardo Nusco and Carmen Lanzara (TIGEM) for technical assistance with mouse studies. This work was supported by grants of Fondazione Telethon Italy (to N.B.-P.), MIUR (PRIN2017 to N.B.-P.), NIHR Great Ormond Street Hospital Biomedical Research Centre (to J.B. and S.E.), Nutricia Metabolic

Research Grant (to J.B.), London Advanced Therapy/Confidence in Collaboration award 2CIC017 (to J.B.), Medical Research Council, Grant/Award Number: MR/T008024/1 (to J.B.) and Innovate UK Biomedical Catalyst Early stage award 14720 (to J.B.). The views expressed are those of the author(s) and not necessarily those of the NHS, the NIHR or the Department of Health.

**Author contributions**

LRS performed study concept and design, acquisition of data, analysis, interpretation of data and wrote the manuscript; SG performed ASL activity assay and argininosuccinate determinations; GDS performed studies in *spf-ash* mice; DPP performed studies in *As<sup>fluo/neo</sup>* mice; ADA performed some Western blots; GB performed studies on *Becn1<sup>T22A</sup>* mice; EP performed EM; DP analysed <sup>3</sup>H-NMR data; PC performed <sup>3</sup>H-NMR; AM supervised <sup>3</sup>H-NMR studies; YK and PBM performed <sup>15</sup>N-argininosuccinate determinations, MO, SE and SNW participated to studies in *As<sup>fluo/neo</sup>* mice; CS supervised studies on *Becn1<sup>T22A</sup>* mice; AFM supervised studies in *spf-ash* mice; JB supervised studies in *As<sup>fluo/neo</sup>* mice; NB-P supervised the study, performed study concept and design, analysis and interpretation of data, and wrote the manuscript.

**Conflict of interest**

The authors declare no that they have no conflict of interests.

**References**

- Allaire M, Rautou PE, Codogno P, Lotersztajn S (2019) Autophagy in liver diseases: time for translation? *J Hepatol* 70: 985–998
- Ashe KM, Taylor KM, Chu Q, Meyers E, Ellis A, Jingozyan V, Klinger K, Finn PF, Cooper CG, Chuang WL et al (2010) Inhibition of glycogen biosynthesis via mTORC1 suppression as an adjunct therapy for Pompe disease. *Mol Genet Metab* 100: 309–315
- Ashley SN, Nordin JML, Buza EL, Greig JA, Wilson JM (2018) Adeno-associated viral gene therapy corrects a mouse model of argininosuccinic aciduria. *Mol Genet Metab* 125: 241–250
- Badizadegan K, Perez-Atayde AR (1997) Focal glycogenosis of the liver in disorders of ureagenesis: its occurrence and diagnostic significance. *Hepatology* 26: 365–373
- Bartolomeo R, Cinque L, De Leonibus C, Forrester A, Salzano AC, Monfregola J, De Gennaro E, Nusco E, Azario I, Lanzara C et al (2017) mTORC1 hyperactivation arrests bone growth in lysosomal storage disorders by suppressing autophagy. *J Clin Invest* 127: 3717–3729
- Baruteau J, Jameson E, Morris AA, Chakrapani A, Santra S, Vijay S, Kocadag H, Beesley CE, Grunewald S, Murphy E et al (2017) Expanding the phenotype in argininosuccinic aciduria: need for new therapies. *J Inher Metab Dis* 40: 357–368
- Baruteau J, Perocheau DP, Hanley J, Lorvellec M, Rocha-Ferreira E, Karda R, Ng J, Suff N, Diaz JA, Rahim AA et al (2018) Argininosuccinic aciduria fosters neuronal nitrosative stress reversed by Asl gene transfer. *Nat Commun* 9: 3505
- Baruteau J, Diez-Fernandez C, Lerner S, Ranucci G, Gissen P, Dionisi-Vici C, Nagamani S, Erez A, Haberle J (2019a) Argininosuccinic aciduria: recent pathophysiological insights and therapeutic prospects. *J Inher Metab Dis* 42: 1147–1161
- Baruteau J, Khalil Y, Grunewald S, Zancolli M, Chakrapani A, Cleary M, Davison J, Footitt E, Waddington SN, Gissen P et al (2019b) Urea cycle related amino acids measured in dried bloodspots enable long-term in vivo monitoring and therapeutic adjustment. *Metabolites* 9: 275

- Bigot A, Tchan MC, Thoreau B, Blasco H, Mailliot F (2017) Liver involvement in urea cycle disorders: a review of the literature. *J Inherit Metab Dis* 40: 757–769
- Burrage LC, Madan S, Li X, Ali S, Mohammad M, Stroup BM, Jiang MM, Cela R, Bertin T, Jin Z et al (2020) Chronic liver disease and impaired hepatic glycogen metabolism in argininosuccinate lyase deficiency. *JCI Insight* 5: e132342
- Castellana M, Wilson MZ, Xu Y, Joshi P, Cristea IM, Rabinowitz JD, Gitai Z, Wingreen NS (2014) Enzyme clustering accelerates processing of intermediates through metabolic channeling. *Nat Biotechnol* 32: 1011–1018
- Cheung CW, Cohen NS, Rajiman L (1989) Channeling of urea cycle intermediates in situ in permeabilized hepatocytes. *J Biol Chem* 264: 4038–4044
- Chiang WC, Wei Y, Kuo YC, Wei S, Zhou A, Zou Z, Yehl J, Ranaghan MJ, Skepner A, Bittker JA et al (2018) High-throughput screens to identify autophagy inducers that function by disrupting Beclin 1/Bcl-2 binding. *ACS Chem Biol* 13: 2247–2260
- Cinque L, Forrester A, Bartolomeo R, Svelto M, Venditti R, Montefusco S, Polishchuk E, Nusco E, Rossi A, Medina DL et al (2015) FGF signalling regulates bone growth through autophagy. *Nature* 528: 272–275
- Cohen NS, Cheung CW, Sijuwade E, Rajiman L (1992) Kinetic properties of carbamoyl-phosphate synthase (ammonia) and ornithine carbamoyltransferase in permeabilized mitochondria. *Biochem J* 282(Pt 1): 173–180
- Cunningham SC, Spinoulas A, Carpenter KH, Wilcken B, Kuchel PW, Alexander IE (2009) AAV2/8-mediated correction of OTC deficiency is robust in adult but not neonatal Spf(ash) mice. *Mol Ther* 17: 1340–1346
- Enns GM, Berry SA, Berry GT, Rhead WJ, Brusilow SW, Hamosh A (2007) Survival after treatment with phenylacetate and benzoate for urea-cycle disorders. *N Engl J Med* 356: 2282–2292
- Erez A, Nagamani SC, Shchelochkov OA, Premkumar MH, Campeau PM, Chen Y, Garg HK, Li L, Mian A, Bertin TK et al (2011) Requirement of argininosuccinate lyase for systemic nitric oxide production. *Nat Med* 17: 1619–1626
- Farah BL, Landau DJ, Sinha RA, Brooks ED, Wu Y, Fung SYS, Tanaka T, Hirayama M, Bay BH, Koerber DD et al (2016) Induction of autophagy improves hepatic lipid metabolism in glucose-6-phosphatase deficiency. *J Hepatol* 64: 370–379
- Fernandez AF, Sebt S, Wei Y, Zou Z, Shi M, McMillan KL, He C, Ting T, Liu Y, Chiang WC et al (2018) Disruption of the beclin 1-BCL2 autophagy regulatory complex promotes longevity in mice. *Nature* 558: 136–140
- Haberle J, Burlina A, Chakrapani A, Dixon M, Karall D, Lindner M, Mandel H, Martinelli D, Pintos-Morell G, Santer R et al (2019) Suggested guidelines for the diagnosis and management of urea cycle disorders: first revision. *J Inherit Metab Dis* 42: 1192–1230
- Hazari Y, Bravo-San Pedro JM, Hetz C, Galluzzi L, Kroemer G (2020) Autophagy in hepatic adaptation to stress. *J Hepatol* 72: 183–196
- He M, Ding Y, Chu C, Tang J, Xiao Q, Luo ZG (2016) Autophagy induction stabilizes microtubules and promotes axon regeneration after spinal cord injury. *Proc Natl Acad Sci USA* 113: 11324–11329
- Hill SM, Wrobel L, Rubinstein DC (2019) Post-translational modifications of Beclin 1 provide multiple strategies for autophagy regulation. *Cell Death Differ* 26: 617–629
- Hodges PE, Rosenberg LE (1989) The sphash mouse: a missense mutation in the ornithine transcarbamylase gene also causes aberrant mRNA splicing. *Proc Natl Acad Sci USA* 86: 4142–4146
- Hosel M, Huber A, Böhlen S, Lucifora J, Ronzitti G, Puzzo F, Boisgerault F, Hacker UT, Kwanten WJ, Kloting N et al (2017) Autophagy determines efficiency of liver-directed gene therapy with adeno-associated viral vectors. *Hepatology* 66: 252–265
- Karsli-Uzunbas G, Guo JY, Price S, Teng X, Laddha SV, Khor S, Kalaany NY, Jacks T, Chan CS, Rabinowitz JD et al (2014) Autophagy is required for glucose homeostasis and lung tumor maintenance. *Cancer Discov* 4: 914–927
- Kaur J, Debnath J (2015) Autophagy at the crossroads of catabolism and anabolism. *Nat Rev Mol Cell Biol* 16: 461–472
- Kho J, Tian X, Wong WT, Bertin T, Jiang MM, Chen S, Jin Z, Shchelochkov OA, Burrage LC, Reddy AK et al (2018) Argininosuccinate lyase deficiency causes an endothelial-dependent form of hypertension. *Am J Hum Genet* 103: 276–287
- Koo M, Lipshutz GS, Cederbaum SD, Lassman C (2017) Biopsy-proven hepatocellular carcinoma in a 53-year-old woman with arginase deficiency. *Pediatr Dev Pathol* 20: 517–521
- Kurtz CB, Millet YA, Puurunen MK, Perreault M, Charbonneau MR, Isabella VM, Kotula JW, Antipov E, Dagon Y, Denney WS et al (2019) An engineered *E. coli* Nissle improves hyperammonemia and survival in mice and shows dose-dependent exposure in healthy humans. *Sci Transl Med* 11: eaau7975
- Li J, Kim SG, Blenis J (2014) Rapamycin: one drug, many effects. *Cell Metab* 19: 373–379
- Liang C, Lee JS, Inn KS, Gack MU, Li Q, Roberts EA, Vergne I, Deretic V, Feng P, Akazawa C et al (2008) Beclin1-binding UVRAG targets the class C Vps complex to coordinate autophagosome maturation and endocytic trafficking. *Nat Cell Biol* 10: 776–787
- Martina JA, Diab HI, Lishu L, Jeong AL, Patange S, Raben N, Puertollano R (2014) The nutrient-responsive transcription factor TFE3 promotes autophagy, lysosomal biogenesis, and clearance of cellular debris. *Sci Signal* 7: ra9
- Mori T, Nagai K, Mori M, Nagao M, Imamura M, Iijima M, Kobayashi K (2002) Progressive liver fibrosis in late-onset argininosuccinate lyase deficiency. *Pediatr Dev Pathol* 5: 597–601
- Moscioni D, Morizono H, McCarter RJ, Stern A, Cabrera-Luque J, Hoang A, Sanmiguel J, Wu D, Bell P, Gao GP et al (2006) Long-term correction of ammonia metabolism and prolonged survival in ornithine transcarbamylase-deficient mice following liver-directed treatment with adeno-associated viral vectors. *Mol Ther* 14: 25–33
- Nagamani SC, Campeau PM, Shchelochkov OA, Premkumar MH, Guse K, Brunetti-Pierri N, Chen Y, Sun Q, Tang Y, Palmer D et al (2012) Nitric-oxide supplementation for treatment of long-term complications in argininosuccinic aciduria. *Am J Hum Genet* 90: 836–846
- Pareek V, Tian H, Winograd N, Benkovic SJ (2020) Metabolomics and mass spectrometry imaging reveal channelled *de novo* purine synthesis in cells. *Science* 368: 283–290
- Peraro L, Zou Z, Makwana KM, Cummings AE, Ball HL, Yu H, Lin YS, Levine B, Kritzer JA (2017) Diversity-oriented stapling yields intrinsically cell-penetrant inducers of autophagy. *J Am Chem Soc* 139: 7792–7802
- Pietrocola F, Pol J, Vacchelli E, Rao S, Enot DP, Baracco EE, Levesque S, Castoldi F, Jacquolot N, Yamazaki T et al (2016) Caloric restriction mimetics enhance anticancer immunosurveillance. *Cancer Cell* 30: 147–160
- Prats C, Graham TE, Shearer J (2018) The dynamic life of the glycogen granule. *J Biol Chem* 293: 7089–7098
- Prieve MG, Harvie P, Monahan SD, Roy D, Li AG, Blevins TL, Paschal AE, Waldheim M, Bell EC, Galperin A et al (2018) Targeted mRNA therapy for ornithine transcarbamylase deficiency. *Mol Ther* 26: 801–813
- Prinsen H, Schiebergen-Bronkhorst BGM, Roeleveld MW, Jans JJM, de Sain-van der Velden MGM, Visser G, van Hasselt PM, Verhoeven-Duif NM (2016) Rapid quantification of underivatized amino acids in plasma by

- hydrophilic interaction liquid chromatography (HILIC) coupled with tandem mass-spectrometry. *J Inherit Metab Dis* 39: 651–660
- Ranucci G, Rigoldi M, Cotugno G, Bernabei SM, Liguori A, Gasperini S, Goffredo BM, Martinelli D, Monti L, Francalanci P et al (2019) Chronic liver involvement in urea cycle disorders. *J Inherit Metab Dis* 42: 1118–1127
- Rocchi A, Yamamoto S, Ting T, Fan Y, Sadleir K, Wang Y, Zhang W, Huang S, Levine B, Vassar R et al (2017) A Becl1 mutation mediates hyperactive autophagic sequestration of amyloid oligomers and improved cognition in Alzheimer's disease. *PLoS Genet* 13: e1006962
- Shoji-Kawata S, Sumpter R, Leveno M, Campbell GR, Zou Z, Kinch L, Wilkins AD, Sun Q, Pallau K, MacDuff D et al (2013) Identification of a candidate therapeutic autophagy-inducing peptide. *Nature* 494: 201–206
- Song X, Zhu S, Chen P, Hou W, Wen Q, Liu J, Xie Y, Liu J, Kliensky DJ, Kroemer G et al (2018) AMPK-Mediated BECN1 phosphorylation promotes ferroptosis by directly blocking system Xc(-) activity. *Curr Biol* 28: 2388–2399.e5
- Soria LR, Allegri G, Melck D, Pastore N, Annunziata P, Paris D, Polishchuk E, Nusco E, Thony B, Motta A et al (2018) Enhancement of hepatic autophagy increases ureagenesis and protects against hyperammonemia. *Proc Natl Acad Sci USA* 115: 391–396
- Soria LR, Brunetti-Pierri N (2018) Targeting autophagy for therapy of hyperammonemia. *Autophagy* 14: 1273–1275
- Soria LR, Ah Mew N, Brunetti-Pierri N (2019) Progress and challenges in development of new therapies for urea cycle disorders. *Hum Mol Genet* 28: R42–R48
- Soria LR, Brunetti-Pierri N (2019) Ammonia and autophagy: an emerging relationship with implications for disorders with hyperammonemia. *J Inherit Metab Dis* 42: 1097–1104
- Spampinato C, Feeney E, Li L, Cardone M, Lim JA, Annunziata F, Zare H, Polishchuk R, Puertollano R, Parenti G et al (2013) Transcription factor EB (TFEB) is a new therapeutic target for Pompe disease. *EMBO Mol Med* 5: 691–706
- Sun Y, Yao X, Zhang QJ, Zhu M, Liu ZP, Ci B, Xie Y, Carlson D, Rothermel BA, Sun Y et al (2018) Beclin-1-dependent autophagy protects the heart during sepsis. *Circulation* 138: 2247–2262
- Sun RC, Dukhande VV, Zhou Z, Young LEA, Emanuelle S, Brainson CF, Gentry MS (2019) Nuclear glycogenolysis modulates histone acetylation in human non-small cell lung cancers. *Cell Metab* 30: 903–916.e7
- Vega-Rubin-de-Celis S, Zou Z, Fernandez AF, Ci B, Kim M, Xiao G, Xie Y, Levine B (2018) Increased autophagy blocks HER2-mediated breast tumorigenesis. *Proc Natl Acad Sci USA* 115: 4176–4181
- Wang L, Bell P, Morizono H, He Z, Pumbo E, Yu H, White J, Batshaw ML, Wilson JM (2017) AAV gene therapy corrects OTC deficiency and prevents liver fibrosis in aged OTC-knock out heterozygous mice. *Mol Genet Metab* 120: 299–305
- Wang L, Wang L, Zhu S, Zhang M, Dong Y, Wang FS (2019) A 6-year-old child with citrin deficiency and advanced hepatocellular carcinoma. *Pediatrics* 143: e20181931
- Wilson JM, Shchelochkov OA, Gallagher RC, Batshaw ML (2012) Hepatocellular carcinoma in a research subject with ornithine transcarbamylase deficiency. *Mol Genet Metab* 105: 263–265
- Yamamoto S, Kuramoto K, Wang N, Situ X, Priyadarshini M, Zhang W, Cordoba-Chacon J, Layden BT, He C (2018) Autophagy differentially regulates insulin production and insulin sensitivity. *Cell Rep* 23: 3286–3299
- Yang Y, Wang L, Bell P, McMenamin D, He Z, White J, Yu H, Xu C, Morizono H, Musunuru K et al (2016) A dual AAV system enables the Cas9-mediated correction of a metabolic liver disease in newborn mice. *Nat Biotechnol* 34: 334–338
- Yapito-Lee J, Chow CW, Boneh A (2013) Histopathological findings in livers of patients with urea cycle disorders. *Mol Genet Metab* 108: 161–165
- Ye X, Robinson MB, Batshaw ML, Furth EE, Smith I, Wilson JM (1996) Prolonged metabolic correction in adult ornithine transcarbamylase-deficient mice with adenoviral vectors. *J Biol Chem* 271: 3639–3646



**License:** This is an open access article under the terms of the Creative Commons Attribution License, which permits use, distribution and reproduction in any medium, provided the original work is properly cited.



## Article

# Bacteriophage-Resistant *Salmonella rissen*: An In Vitro Mitigated Inflammatory Response

Rosanna Capparelli <sup>1,\*</sup>, Paola Cuomo <sup>1</sup>, Marina Papaiani <sup>1</sup>, Cristina Pagano <sup>2</sup>,  
Angela Michela Immacolata Montone <sup>3</sup>, Annarita Ricciardelli <sup>4</sup> and Domenico Iannelli <sup>1</sup>

- <sup>1</sup> Department of Agriculture, University of Naples "Federico II", 80055 Naples, Italy; paola.cuomo@unina.it (P.C.); marina.papaiani@unina.it (M.P.); domenico.iannelli1935@gmail.com (D.I.)  
<sup>2</sup> Department of Molecular Medicine and Medical Biotechnology, University of Naples "Federico II", 80055 Naples, Italy; pagano.cris@gmail.com  
<sup>3</sup> Department of Food Inspection, Istituto Zooprofilattico Sperimentale del Mezzogiorno, 80055 Naples, Italy; angela.montone@izsmporciti.it  
<sup>4</sup> Department of Marine Biotechnology, Stazione Zoologica "Anton Dohrn", Villa Comunale, 80121 Naples, Italy; annarita.ricciardelli@gmail.com  
\* Correspondence: capparel@unina.it



**Citation:** Capparelli, R.; Cuomo, P.; Papaiani, M.; Pagano, C.; Montone, A.M.I.; Ricciardelli, A.; Iannelli, D. Bacteriophage-Resistant *Salmonella rissen*: An In Vitro Mitigated Inflammatory Response. *Viruses* **2021**, *13*, 2468. <https://doi.org/10.3390/v13122468>

Academic Editor: Terje Dokland

Received: 8 November 2021

Accepted: 8 December 2021

Published: 9 December 2021

**Publisher's Note:** MDPI stays neutral with regard to jurisdictional claims in published maps and institutional affiliations.



**Copyright:** © 2021 by the authors. Licensee MDPI, Basel, Switzerland. This article is an open access article distributed under the terms and conditions of the Creative Commons Attribution (CC BY) license (<https://creativecommons.org/licenses/by/4.0/>).

**Abstract:** Non-typhoid *Salmonella* (NTS) represents one of the major causes of foodborne diseases, which are made worse by the increasing emergence of antibiotic resistance. Thus, NTS are a significant and common public health concern. The purpose of this study is to investigate whether selection for phage-resistance alters bacterial phenotype, making this approach suitable for candidate vaccine preparation. We therefore compared two strains of *Salmonella enterica* serovar *Rissen*:  $R^R$  (the phage-resistant strain) and  $R^W$  (the phage-sensitive strain) in order to investigate a potential cost associated with the bacterium virulence. We tested the ability of both  $R^R$  and  $R^W$  to infect phagocytic and non-phagocytic cell lines, the activity of virulence factors associated with the main Type-3 secretory system (T3SS), as well as the canonical inflammatory mediators. The mutant  $R^R$  strain—compared to the wildtype  $R^W$  strain—induced in the host a weaker innate immune response. We suggest that the mitigated inflammatory response very likely is due to structural modifications of the lipopolysaccharide (LPS). Our results indicate that phage-resistance might be exploited as a means for the development of LPS-based antibacterial vaccines.

**Keywords:** phage-resistance; bacterial virulence; lipopolysaccharide

## 1. Introduction

*Salmonella enterica* (*S. enterica*) is a Gram-negative bacterium, causing salmonellosis, one of the major threats to human health. Approximately 2500 *Salmonella* serovars have been identified [1] and classified as typhoid or non-typhoid strains, according to host specificity and clinical manifestation [2,3].

Non-typhoid *Salmonella* (NTS) species—specifically the *S. Typhimurium* or *Enteritidis*—are the most frequent cause of worldwide foodborne gastroenteritis, causing 155,000 deaths every year [4]. In the last decades, *S. Rissen*—so far a rare serotype—has been reported to play a significant role in the onset of foodborne diseases [5]. Even though self-limiting gastroenteritis is the main clinical manifestation of *Salmonella* infection, more severe complications—such as extra-intestinal infections or bacteremia—can occur in immunocompromised patients [5]. Antimicrobial agents are the primary strategy to counteract infectious diseases. However, the increased resistance of *Salmonella* to traditional antimicrobial drugs makes it difficult to prevent *Salmonella* infections. In this context, vaccination may represent a valid alternative.

Vaccines are designed to prevent infections and reduce the associated morbidity and mortality [6]. In detail, vaccines train the host immune system to recognize and neutralize



the pathogen [7], promoting all the steps of the immune response and the production of cellular mediators responsible for the occurrence of the disease symptoms. Further, vaccines initiate a measured immune response, well tolerated by the host, which does not cause immunopathology.

So far, a vaccine protecting against NTS is not yet available [8].

Bacteriophages are viruses specifically targeting bacteria [9]. They represent the most numerous organisms in the biosphere [10], and their competitive coevolution with the host has contributed to the development, by the host, of many resistance mechanisms [11,12]. Bacteria can evade phage attacks by using different strategies. One of these consists of preventing phage adsorption modifying surface structures (usually referred to as phage receptors) [12–14]. Such modification has a cost for the bacterium, consisting of altering its virulence. However, a limit for the bacterium may result in an advantage for the host, becoming a potential tool for vaccine development [15–17].

The lipopolysaccharide (LPS) plays an important role in both phage adsorption and infection of Gram-negative bacteria [18,19]. In a previous study, we demonstrated differences in the LPS biosynthesis and morphology between the bacteriophage-sensitive ( $R^W$ ) and the resistant *S. Rissen* strains ( $R^R$ ) [20]. More specifically, we detected reduced expression levels of the *phosphomannomutase1* and *phosphomannomutase2* genes in the  $R^R$  resistant strain, compared to that of  $R^W$ . Thus,  $R^R$  was shown to produce a LPS lacking mannose in the O-antigen portion. Furthermore, LPS is a pathogen-associated molecular pattern known to interact with the host Toll-like receptor 4 (TLR4) and activate a strong defense immune response [21]. At the same time, several studies have demonstrated that modified LPSs are poor stimulators of TLR4 and trigger a mild immune response—properties which make them useful for a good candidate vaccine [22]. In this context, we compared in vitro the host inflammatory response following infection with  $R^R$  or  $R^W$  strains.  $R^W$  displayed a stronger inflammation compared to  $R^R$ , potentially attributable to differences in the LPS structure between the two strains. Based on these findings, modified LPS of the phage-resistant *S. Rissen* could represent a potential candidate for vaccine development.

## 2. Materials and Methods

### 2.1. Bacterial Strains and Culture Conditions

Non-typhoid *Salmonella enterica* subsp. *enterica* serovar *Rissen* strain  $R^W$ , *Salmonella bongori*, *Salmonella nottingham* and *Salmonella typhimurium* were isolated from a food matrix and characterized by Istituto Zooprofilattico Sperimentale Del Mezzogiorno (Portici, Naples, Italy). The *S. Rissen* strain  $R^R$  was derived from the  $R^W$  strain following selection for resistance to phage  $\phi 1$ , as previously described [17]. Both the *Salmonella* strains were grown in Nutrient Broth (Scharlab, S.L., Barcelona, Spain) at 37 °C under vigorous agitation (200 rpm).

### 2.2. Cell Lines and Culture Conditions

AGS (human Caucasian gastric adenocarcinoma) and HT-29 (human Caucasian colon adenocarcinoma) cells were grown in Dulbecco's modified Eagle's medium, high glucose (DMEM; Microtech, Pozzuoli, Naples, Italy), and supplemented with 10% fetal bovine serum (FBS; Microtech, Pozzuoli, NA, Italy), 1% penicillin/streptomycin (Gibco, Waltham, MA, USA) and 1% L-glutamine (Gibco, Waltham, MA, USA). U937 (human myeloid leukemia) cells were grown in RPMI-1640 (Microtech, Pozzuoli, NA, Italy) and supplemented with 10% fetal bovine serum (FBS; Microtech, Pozzuoli, NA, Italy), 1% penicillin/streptomycin (Gibco, Waltham, MA, USA) and 1% L-glutamine (Gibco, Waltham, MA, USA). All cell lines were maintained in 5% CO<sub>2</sub> at 37 °C. U937 cells were induced to differentiate into macrophages by exposing them to phorbol-12-myristate-13-acetate (PMA, 100 ng/mL; Sigma Aldrich, St. Louis, MO, USA) for 48 h. Cells were then washed twice, and the culture medium was replaced with RPMI-1640 without PMA, followed by a resting period of 24 h.

### 2.3. *Salmonella* Invasion Assay

All the *Salmonella* strains were analyzed for their capacity to colonize the following human cell lines: AGS and HT-29 (non-phagocytic epithelial cell lines), and U937 differentiated into macrophages (phagocytic cell line). Cells were seeded at the density of  $1 \times 10^6$  per well in 12-well plates and incubated overnight at 37 °C in the presence of 5% CO<sub>2</sub> and without antibiotics. *Salmonella* invasion capabilities were evaluated as previously described [20]. Briefly, cell monolayers were infected with  $10^8$  CFU/mL in a 12-well plate, at MOI (multiplicity of infection) = 1:100 and incubated for 2 h at 37 °C. After incubation, cell monolayers were washed with PBS (Phosphate buffered saline) and incubated in the presence of 100 µg/mL gentamicin for 30 min. Again, cells were washed with PBS (pH 7.3) and lysed in 1 mL of fresh PBS by scraping. Viable intracellular bacteria were counted after plating serial dilutions in nutrient broth. Results were expressed as the mean  $\pm$  standard error of the mean (SEM) of the number of intracellular bacteria, expressed in Log<sub>10</sub> CFU/mL. Experiments were performed in duplicate and repeated at least three times.

### 2.4. Expression Levels of Virulence Genes

The presence of 7 genes related to the virulence of *Salmonella* spp. was detected in R<sup>W</sup> and R<sup>R</sup> strains by end-point PCR and electrophoretic run on an automated qiaxcel instrument (Qiagen, Hilden, Germany). Their expression levels were evaluated by qRT-PCR at 2, 4 and 6 hpi on the AGS cell line. The selected virulence factors are related to the presence of prophages (*groA*, *gogB*, *sspH1*, *sodC1*, *gtgE*) or plasmids (*spvC*) [21].

### 2.5. Infection on AGS Cell Line

Cells were seeded at the density of  $1 \times 10^6$  per well in 12-well plates and incubated overnight at 37 °C in the presence of 5% CO<sub>2</sub>, without antibiotics. The next day, cells were infected with R<sup>R</sup> or R<sup>W</sup> strains (MOI 1:100) for 2 h, 4 h and 6 h. After infection, cells were washed with PBS, and gentamicin (100 µg/mL) was added for 30 min. AGS cells were then lysed and collected using 1 mL of TRIzol LS reagent (Thermo Fisher Scientific, Waltham, MA, USA); whereas bacteria were collected and lysed using scraping and 500 µL of TRIzol reagent. All the samples were stored at −80 °C until the analysis.

### 2.6. RNA Extraction and RT-qPCR

Total RNA extraction was performed using TRIzol LS reagent (Thermo Fisher Scientific, Waltham, MA, USA) following the manufacturer's instructions. The quality and quantity of RNA was estimated using NanoDrop 2000 c (Thermo Fisher Scientific, Waltham, MA, USA) and then reverse-transcribed using the high-capacity cDNA Reverse transcription kit (Thermo Fisher Scientific, Waltham, MA, USA). Gene transcript levels were measured using Power SYBR Green PCR Master Mix (Applied Biosystem, Waltham, MA, USA) on a StepOne Real-Time PCR System (Thermo Fisher Scientific, Waltham, MA, USA), according to the standard mode thermal cycling conditions, as indicated by Spatuzza et al. [22]. Relative expression levels of analyzed genes were determined using probes listed in Table S1. The  $2^{-\Delta\Delta CT}$  method was used to calculate relative changes in gene expression determined from real-time quantitative PCR experiments [23,24]. Target gene expression levels were normalized using housekeeping genes (*recA* for *Salmonella* and *GAPDH* for AGS cell line).

### 2.7. Cytokine Determination by Bio-Plex Assay

Bio-Plex Pro Human Th17 Cytokine Assay (BioRad, Hercules, CA, USA) was performed to detect the level of cytokines in supernatants of AGS cells infected with the R<sup>R</sup> or R<sup>W</sup> strain. The assay detects multiple analytes simultaneously in a single sample [25,26].



### 2.8. Western Blotting Analysis

AGS cells were infected with R<sup>W</sup> or R<sup>R</sup> strains for 1 h and 2 h. Total proteins were extracted with RIPA lysis buffer (50 mM Tris-HCl, 150 mM NaCl, 0.5% Triton X-100, 0.5% deoxycholic acid, 10 mg/mL leupeptin, 2 mM phenylmethylsulfonyl fluoride and 10 mg/mL aprotinin containing protease and phosphatase inhibitors (Sigma Aldrich, St. Louis, MO, USA)). Samples were quantified using Protein Analysis Dye Reagent Concentrate (BioRad, Hercules, CA, USA). Equal quantities of protein were separated by SDS-PAGE gel and transferred to PVDF membranes using a Trans-Blot Turbo (BioRad). The membranes were blocked with 5% fat-free milk in Tris saline buffer containing 0.1% Tween-20 (TBST) at room temperature for 1 h, incubated with primary antibodies (1:1000) at 4 °C overnight, and incubated with horseradish peroxidase (HRP)-conjugated secondary antibodies (1:2000) (BioRad) at room temperature for 1 h. The signals were detected using the BioRad ChemiDoc MP image sensor after the membranes were soaked in enhanced ECL reagents (ECLTM Prime Western Reagents for Blotting Detection, Amersham, GE Healthcare, Buckinghamshire, UK). Protein bands were detected by chemiluminescence HRP substrate (Millipore, Burlington, MA, USA) and analyzed by Image J software (National Institutes of Health, version 2.1.0/1.53c). Total extracts were normalized using an anti- $\beta$ -actin antibody. The following antibodies were used for the Western blot analysis: Mouse monoclonal anti-human  $\beta$ -actin antibody and anti-AKT mouse monoclonal antibody were purchased from Santa Cruz Biotechnology (Santa Cruz, CA, USA); anti-pNFKB rabbit monoclonal antibody, anti-NFKB rabbit monoclonal, anti-IKB $\alpha$  rabbit monoclonal antibody, anti-pSTAT3 rabbit monoclonal antibody, anti-STAT3 rabbit monoclonal antibody and anti-pAKT rabbit monoclonal antibody were from Cell Signaling Technology (Danvers, MA, USA). The following were used as secondary antibodies: Goat Anti-Rabbit and Goat Anti-Mouse HRP (BioRad, Hercules, CA, USA). The company and concentrations of all antibodies used are presented in Table S2.

### 2.9. Statistical Analysis

Statistical analysis was performed using GraphPad Prism 8.0 software (San Diego, CA, USA). All data were compared using two-way ANOVA multiple comparisons. Experimental data are presented as mean  $\pm$  SD of three independent experiments, performed in triplicate. Statistical analysis was considered statistically significant when  $p < 0.05$ .

## 3. Results

### 3.1. R<sup>W</sup> and R<sup>R</sup> Strains Display the Same Antigenic and Antibiotic Resistance Profiles

The slide agglutination test displayed both strains having the same antigenic determinants of the LPS O-chain (O6, O7) and of flagella (Hf, Hg). The two lines also displayed the same antibiotic profile: both were resistant to cefoxitin and sensitive to the same 20 antibiotics (Table S3). Recent studies have shown that, in bacteria, acquisition of phage resistance is often associated with loss of antibiotic resistance [27]. The R<sup>R</sup> strain instead remained resistant to cefoxitin (Table S3).

### 3.2. The R<sup>W</sup> and R<sup>R</sup> Strains Both Exhibit the Same Capacity to Colonize Host Cells

Colonization is a major property of *Salmonella* [28]. Therefore, we tested the two strains (R<sup>R</sup> and R<sup>W</sup>) for their capacity to colonize the host. The AGS (epithelial gastric adenocarcinoma) and U937 (macrophage) cell lines were incubated for 1 and 2 h with the R<sup>W</sup> or R<sup>R</sup> strain. The U937 and AGS cell lines both displayed the capacity to internalize R<sup>W</sup> and R<sup>R</sup> bacterial strains to the same extent (Figure 1A). Instead, the HT-29 cell line was not colonized by R<sup>R</sup> or R<sup>W</sup>, both at 1 and 2 h. In addition, no serovar-specific differences in HT-29 cells' colonization were observed. We repeated the experiment using additional *Salmonella* serovars (*S. typhimurium*, *bongori*, *enteritidis* and *nottingham*). All *Salmonella* strains exhibited no capacity to colonize the HT-29 cell line (Figure 1A,B). According to the literature, studies have shown that, in bacteria, acquisition of phage resistance is associated

with defects in the host cell colonization [13]. The  $R^R$  strain instead behaved exactly as the wildtype (Figure 1A).

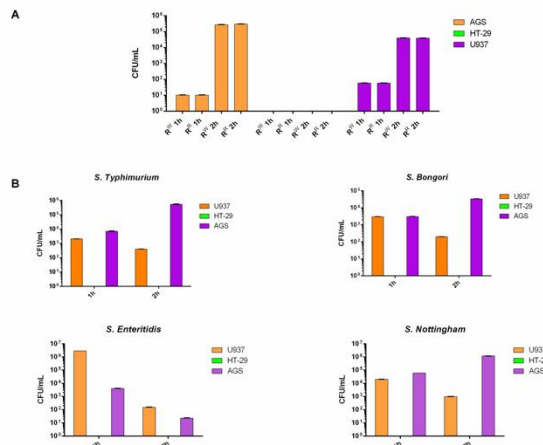


**Figure 1.**  $R^R$  and  $R^W$  host cell colonization. (A) AGS, U937 and HT-29 cell lines were infected with the bacteriophage-resistant  $R^R$  or  $R^W$  strains for 1 and 2 h. (B) AGS, U937 and HT-29 cell lines were infected with *Salmonella typhimurium*, *bongori*, *enteritidis* or *nottingham* for 1 and 2 h. Results are reported as Log<sub>10</sub> CFU/mL and represent the mean  $\pm$  SD of three experiments, each performed in triplicate.

### 3.3. $R^W$ and $R^R$ Strains Exhibit Different Virulence Profiles

The virulence of  $R^R$  and  $R^W$  strains was tested, incubating the epithelial AGS cell line with both strains for 2, 4 and 6 h. The expression levels of the virulence genes (*invA*, *sspH1*, *sodC1*, *gtgE*, *groA*, *spvC*, *gogB*) were measured by RT-qPCR. The *invA* gene—controlling colonization of epithelial cells [29]—was equally expressed in both strains (Figure 2). This result exactly concurs with the one reported in Figure 1A, displaying no difference in the colonization of the epithelial AGS cell line by  $R^R$  or  $R^W$ . Instead, using the same AGS cell line, significant differences between  $R^W$  and  $R^R$  were detected regarding *sodC1*, *gogB*, *spvC*, *sspH1*, *groA*, *gtgE* (Figure 2). *SodC1* protects the bacterium from oxidative burst [30], while *gogB* protects the host tissue integrity [31]. Both of these genes were expressed at a 100 $\times$  higher level in  $R^R$  compared to  $R^W$ . *SpvC* and *sspH1* inhibit NF- $\kappa$ B [32]. *GroA* and *gtgE* help the bacteria survive in the host [33]. Both of these genes (*spvC-sspH1* and *groA-gtgE*) were found significantly expressed in  $R^R$  only at 6 hpi compared to  $R^W$ , while *groA* was found significantly more expressed in  $R^R$  already after 4 h of incubation. Taken together, these results indicate: (1) that  $R^R$  and  $R^W$  have clear different virulence profiles, and (2) that phage-resistance contributes to bacterial persistence in host cells.

### 3.4. $R^W$ and $R^R$ Strains Induce a Different Inflammatory Host Response

Bioplex analysis indicated that  $R^W$  elicits a stronger pro-inflammatory response (higher levels of IL-6, IL-8, G-CSF, MCP-1, MIP-1 $\beta$  and TNF- $\alpha$ ) than  $R^R$ . At the same time, both strains produce low and very close levels of IL-10 (Figure 3A). Western blot analysis confirmed these results. NF- $\kappa$ B, Akt and STAT3 were significantly more activated in  $R^W$  than in  $R^R$  infected cells (Figure 3B). Interestingly,  $R^R$  infected cells displayed a reduced

expression level of STAT3 and a similar expression level of NF- $\kappa$ B, compared to control cells. NF- $\kappa$ B, Akt and STAT3 pathways are known to play a critical role in the inflammatory response triggered by infections [34,35]. These data show that the phage-resistant strain  $R^R$  induces a significantly lower pro-inflammatory response than  $R^W$ .

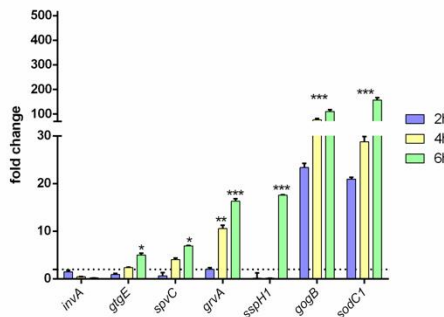


**Figure 2.** Virulence profile of the  $R^R$  phage-resistant strain. *invA*, *glgE*, *spvC*, *groA*, *sspH1*, *groB* and *sodC1* gene expression levels were measured in the epithelial AGS cell line infected with  $R^R$  or  $R^W$  for 2, 4 and 6 h. Results are reported as mean  $\pm$  SD of three independent experiments, each performed in triplicate and labeled with asterisks (\*  $p < 0.05$ ; \*\*  $p < 0.01$ ; \*\*\*  $p < 0.001$ ). Relative gene expression was normalized to  $R^W$ .

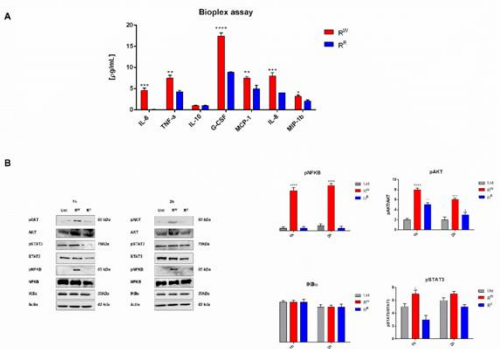


**Figure 3.** Phage-resistance curbs AGS-induced inflammatory response. (A) Cytokines IL-6, TNF- $\alpha$ , IL-10, G-CSF, MCP-1, MIP-1 $\beta$  and IL-8 were measured by Bio-plex assay in AGS cells culture medium after incubation for two hours with  $R^R$  or  $R^W$  strains. Results are expressed as pg of cytokines secreted in mL of cell medium. Values were normalized to the basal activity (CTR) and represent mean  $\pm$  SD of at least three independent experiments, each performed in triplicate (\*  $p < 0.05$ ; \*\*  $p < 0.01$ ; \*\*\*  $p < 0.001$ ; \*\*\*\*  $p < 0.0001$ ). (B) Western blot and densitometric analysis of the ratio pNF- $\kappa$ B/NF- $\kappa$ B; pAkt/Akt; pSTAT3/STAT3. Actin was used for normalization. Graphs report the result of three independent experiments and represent mean  $\pm$  SD (\*  $p < 0.05$ ; \*\*  $p < 0.01$ ; \*\*\*  $p < 0.001$ ; \*\*\*\*  $p < 0.0001$ ).

### 3.5. $R^W$ and $R^R$ Strains Display a Different *LpxR* and *TLR4* Gene Expression Level

The *lpxR* gene is involved in de-acylation of lipid A portion of LPS [36]. A time course RT-PCR experiment displayed that *lpxR* is upregulated in  $R^R$  and downregulated in  $R^W$  (Figure 4A). The same experiment displayed also that upregulation of *lpxR* increases together with incubation time (Figure 4A). A high expression of *lpxR* gene in  $R^R$  could potentially reflect a higher level of de-acylation of the lipid A of the mutant  $R^R$  strain. Instead, the low level of *lpxR* gene expression of the  $R^W$  strain suggests that this strain has the classic hexa-acylated lipid A structure. A further confirmation of this conclusion is provided by an independent experiment carried out on additional *Salmonella* strains (*S. bongori* or *enteritidis*). Again, *lpxR* was found upregulated in  $R^R$  compared to *S. bongori* and *enteritidis*, which instead expresses a level of *lpxR* comparable to  $R^W$ . The expression of *TLR4* is negatively modulated by the presence of deacylated lipid A portion of LPS [37]. In this study, the evidence that *TLR4* gene is downregulated in cells incubated with  $R^R$  (Figure 4B) represents one more independent proof that  $R^R$  has acquired resistance to phage  $\phi 1$  by modification of the LPS.

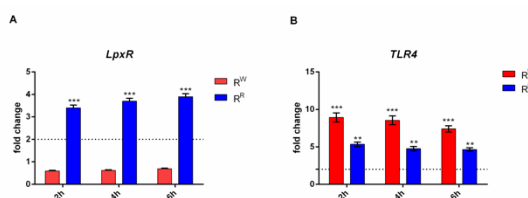


**Figure 4.**  $R^R$  and  $R^W$  strains show a different *TLR4* activation. (A) Relative gene expression of *lpxR* was determined by quantitative real-time PCR (RT-qPCR), performed on RNA isolated from AGS cells cultured with  $R^R$  or  $R^W$  for 2, 4 and 6 h. (\*\*\*\*  $p < 0.001$ ). (B) Relative gene expression of *TLR4* was determined by quantitative real-time PCR (RT-qPCR), performed on RNA isolated from AGS cells cultured with  $R^R$  or  $R^W$  for 2, 4 and 6 h. All samples were normalized to GAPDH as a reference housekeeping gene. Furthermore, relative gene expression was normalized to basal activity (CTR), in order to obtain relative fold expression. Graphs report the results of at least three independent experiments, represented as means  $\pm$  SD (\*\*  $p < 0.01$ ; \*\*\*\*  $p < 0.001$ ).

## 4. Discussion

The frequent and often inappropriate use of antibiotics in medicine and intensive farming has favored the selection of antibiotic-resistant bacteria, causing serious consequences for human health. This drawback was further emphasized by the phenomenon of phage-resistant bacteria. Any host fighting against a drug or a parasite inevitably evolves strategies to evade the antagonist and survives.

In the present study, we compare two strains of *Salmonella enterica* serovar Rissen,  $R^R$  (the phage-resistant strain) and  $R^W$  (the phage-sensitive strain), in order to know, first, whether the changes associated with the acquisition of phage-resistance affects the host cell physiology and, second, the potential mechanisms responsible for the different host-bacteria interaction.

We firstly evaluated the property of both  $R^R$  and  $R^W$  strains to colonize host cells. Both  $R^R$  and  $R^W$  were found to colonize AGS and U937 cell lines to the same extent (Figure 1A). To establish the host colonization, *Salmonella* uses the Type 3 Secretion System (T3SS), a complex machinery encoded by *Salmonella* pathogenicity islands (SPIs) [37,38], and consists of a cluster of virulence genes [39].

Therefore, to investigate the effect of acquisition of phage-resistance on bacteria virulence, we infected the epithelial AGS cell line separately with one of these two strains and analyzed some of the most representative SPIs-virulence genes. As expected, we observed

similar expression levels of *invA*, indicating the same capacity of  $R^R$  and  $R^W$  to colonize AGS cells (Figure 2). Instead, marked differences were detected with *gtgE*, *sodC1* and *groVA*, which were all upregulated in  $R^R$  compared to  $R^W$  (Figure 2), suggesting that upregulation might favor the survival of  $R^R$  in AGS compared to  $R^W$  [30,40]. Interestingly, we also noted increased expression levels of *gogB*, *spvC* and *sspH1* genes in the  $R^R$  strain (Figure 2). These data provide evidence about the capacity of  $R^R$  to infect the host more efficiently, compared to  $R^W$ , by modulating the host's innate immune response and surviving longer within the host.

Upon bacterial infection, innate immunity initiates a defensive response, which leads to inflammation. Bacteria have developed strategies to elude the host immune clearance and curb the inflammatory response. Our data indicate that the above statement extends to the  $R^R$  strain. In accordance with the upregulation of the *sspH1* and *spvC* genes inhibiting NF- $\kappa$ B [32] in the  $R^R$  strain, we found reduced activation of the nuclear transcription factor- $\kappa$ B (NF- $\kappa$ B) and of its activator Akt in the cells infected with  $R^R$  (Figure 3B). NF- $\kappa$ B is a critical modulator of inflammation; it initiates the transcription of numerous genes, including cytokines and chemokines [41]. Consistent with this finding, we also detected reduced expression levels of pro-inflammatory cytokines and chemokines in  $R^R$  infected cells (Figure 3A). More specifically, we observed lower levels of: (1) IL-8, MCP-1 and MIP-1 $\beta$ , responsible for the recruitment of neutrophils, monocytes and lymphocytes at the site of infection [42,43]; (2) IL-6 and TNF- $\alpha$ , directly involved in the early stage of pathogen-induced inflammatory response; and (3) GCS-F, involved in cell growth and differentiation [44–46]. Cytokines, in turn, are known to induce the activation of the transcriptional factor STAT3 [47]. Finally, in  $R^R$  infected cells, we detected reduced activation of the STAT3 protein (Figure 3B). We can conclude that our data indicate the  $R^R$  strain, as a potential candidate vaccine, modulates the immune response curbing inflammation.

In order to organize the immune defense against the pathogen, evolution has selected ancient receptors that recognize pathogen-associated molecular patterns (PAMPs). Lipopolysaccharide (LPS), the most important Gram-negative PAMP, has also been reported to interact with phage proteins, acting as a phage receptor [48]. Bacteria—including *Salmonella* species—can alter genes of the LPS biosynthesis pathway, modifying the LPS structure and inhibiting phage adsorption [49]. In a previous work, we demonstrated differences between  $R^R$  and  $R^W$  strains in the expression levels of two genes (phosphomannomutase1 and phosphomannomutase2) involved in the LPS biosynthetic pathway. Precisely, a comparative analysis showed that  $R^R$  produces an LPS lacking mannose sugar in the O-antigen portion [17]. Further, lipid A, a principal component of the LPS [50], induces the inflammatory reaction following interaction with Toll-like receptor 4 (TLR4). Based on these considerations, we investigated whether modifications of the  $R^R$  phenotype could be attributed to alterations of the LPS-lipid A portion. *Salmonella* species can synthesize enzymes able to covalently alter the lipid A portion, such as the 3'-O-deacetylase, encoded by the *lpxR* gene, which is upregulated in  $R^R$  (Figure 4A). The 3'-O-deacetylated form of the lipid A is a poor stimulator of TLR4 [51], which favors bacteria in evading the host immune response. The downregulation of the TLR4 gene in  $R^R$  infected cells (Figure 4B) further supports the idea that the phage-resistant strain has acquired the resistance by modifying the LPS structure. Before testing  $R^R$  in vivo, as a potential candidate vaccine, we will further confirm biochemically that  $R^R$  displays an altered LPS-lipid A portion.

## 5. Conclusions

In conclusion, this study reports a bacteriophage-resistant *Salmonella rissen* strain, which increases its pathogenicity, most likely due to the potential modification of the LPS-lipid A portion. Literature reports several studies describing vaccines based on modified lipid A portion [52]. Here, we propose a valid alternative to the LPS-synthetic vaccines, consisting of exploiting the capacity of phage-resistant bacteria to modify naturally the LPS-toxic portion.

**Supplementary Materials:** The following are available online at <https://www.mdpi.com/article/10.3390/v13122468/s1>, Table S1: Primers used for RT-qPCR, Table S2: Antibody used for Western blot and Table S3: Antibody used for Western blot.

**Author Contributions:** Conceptualization, R.C.; methodology, M.P. and C.P.; validation, R.C.; formal analysis, A.M.I.M., A.R. and P.C.; data curation, M.P.; writing—original draft preparation, P.C. and M.P.; writing—review and editing, D.L.; supervision, R.C. All authors have read and agreed to the published version of the manuscript.

**Funding:** This research received no external funding.

**Institutional Review Board Statement:** Not applicable.

**Informed Consent Statement:** Not applicable.

**Data Availability Statement:** The data presented in this study are available within the article.

**Conflicts of Interest:** The authors declare no conflict of interest.

## References

- Chattaway, M.A.; Langridge, G.C.; Wain, J. Salmonella nomenclature in the genomic era: A time for change. *Sci. Rep.* **2021**, *11*, 1–8. [\[CrossRef\]](#)
- Gal-Mor, O.; Boyle, E.C.; Grassl, G.A. Same species, different diseases: How and why typhoidal and non-typhoidal Salmonella enterica serovars differ. *Front. Microbiol.* **2014**, *5*, 391. [\[CrossRef\]](#) [\[PubMed\]](#)
- Wemyss, M.; Pearson, J.S. Host Cell Death Responses to Non-typhoidal Salmonella Infection. *Front. Immunol.* **2019**, *10*, 1758. [\[CrossRef\]](#)
- Crump, J.A.; Sjölund-Karlsson, M.; Gordon, M.; Parry, C.M. Epidemiology, clinical presentation, laboratory diagnosis, antimicrobial resistance, and antimicrobial management of invasive salmonella infections. *Clin. Microbiol. Rev.* **2015**, *28*, 901–937. [\[CrossRef\]](#) [\[PubMed\]](#)
- Campos, J.; Mourão, J.; Peixe, L.; Antunes, P. Non-typhoidal salmonella in the pig production chain: A comprehensive analysis of its impact on human health. *Pathogens* **2019**, *8*, 19. [\[CrossRef\]](#) [\[PubMed\]](#)
- Micoli, F.; Bagnoli, F.; Rappuoli, R.; Serruto, D. The role of vaccines in combatting antimicrobial resistance. *Nat. Rev. Genet.* **2021**, *19*, 287–302. [\[CrossRef\]](#) [\[PubMed\]](#)
- Jansen, K.U.; Knirsch, C.; Anderson, A.S. The role of vaccines in preventing bacterial antimicrobial resistance. *Nat. Med.* **2018**, *24*, 10–19. [\[CrossRef\]](#)
- Worsena, C.R.; Miller, A.S.; King, M.A. Salmonella Infections. *Pediatr. Rev.* **2019**, *40*, 543–545. [\[CrossRef\]](#) [\[PubMed\]](#)
- Clokic, M.R.J.; Millard, A.D.; Letarov, A.V.; Heaphy, S. Phages in nature. *Bacteriophage* **2011**, *1*, 31–45. [\[CrossRef\]](#)
- Hatfull, G.F. Dark Matter of the Biosphere: The amazing world of bacteriophage diversity. *J. Virol.* **2015**, *89*, 8107–8110. [\[CrossRef\]](#) [\[PubMed\]](#)
- Koskella, B.; Brockhurst, M.A. Bacteria–phage coevolution as a driver of ecological and evolutionary processes in microbial communities. *FEMS Microbiol. Rev.* **2014**, *38*, 916–931. [\[CrossRef\]](#)
- Rostøl, J.T.; Marraffini, L. (Ph)ighting Phages: How bacteria resist their parasites. *Cell Host Microbe* **2019**, *25*, 184–194. [\[CrossRef\]](#)
- Oechslin, F. Resistance development to bacteriophages occurring during bacteriophage therapy. *Viruses* **2018**, *10*, 351. [\[CrossRef\]](#) [\[PubMed\]](#)
- Labrie, S.J.; Samson, J.E.; Moineau, S. Bacteriophage resistance mechanisms. *Nat. Rev. Microbiol.* **2010**, *8*, 317–327. [\[CrossRef\]](#)
- Filippov, A.A.; Sergueev, K.V.; He, Y.; Huang, X.-Z.; Gnade, B.T.; Mueller, A.J.; Fernandez-Prada, C.M.; Nikolich, M.P. Bacteriophage-Resistant Mutants in *Yersinia pestis*: Identification of Phage Receptors and Attenuation for Mice. *PLoS ONE* **2011**, *6*, e25486. [\[CrossRef\]](#)
- Capparelli, R.; Nocerino, N.; Lanzetta, R.; Silipo, A.; Amoresano, A.; Giangrande, C.; Becker, K.; Blaiotta, G.; Evidente, A.; Cimmino, A.; et al. Bacteriophage-resistant staphylococcus aureus mutant confers broad immunity against staphylococcal infection in mice. *PLoS ONE* **2010**, *5*, e11720. [\[CrossRef\]](#)
- Capparelli, R.; Nocerino, N.; Iannaccone, M.; Ercolini, D.; Parlato, M.; Chiara, M.; Iannelli, D. Bacteriophage Therapy of Salmonella enterica: A Fresh Appraisal of Bacteriophage Therapy. *J. Infect. Dis.* **2010**, *201*, 52–61. [\[CrossRef\]](#)
- Rakhuba, D.V.; Kolomiets, E.I.; Dey, E.S.; Novik, G.I. Bacteriophage receptors, mechanisms of phage adsorption and penetration into host cell. *Pol. J. Microbiol.* **2010**, *59*, 145–155. [\[CrossRef\]](#)
- Kulikov, E.E.; Golomidova, A.K.; Prokhorov, N.; Ivanov, P.A.; Letarov, A.V. High-throughput LPS profiling as a tool for revealing of bacteriophage infection strategies. *Sci. Rep.* **2019**, *9*, 1–10. [\[CrossRef\]](#)
- Papaiani, M.; Contaldi, F.; Fulgione, A.; Woo, S.L.; Casillo, A.; Corsaro, M.M.; Parrilli, E.; Marcolungo, L.; Rossato, M.; Delledonne, M.; et al. Role of phage  $\phi$ 1 in two strains of Salmonella rissen, sensitive and resistant to phage  $\phi$ 1. *BMC Microbiol.* **2018**, *18*, 208. [\[CrossRef\]](#)
- Ematsuura, M. Structural modifications of bacterial lipopolysaccharide that facilitate gram-negative bacteria evasion of host innate immunity. *Front. Immunol.* **2013**, *4*, 109. [\[CrossRef\]](#)



22. Zariri, A.; Van Der Ley, P. Biosynthetically engineered lipopolysaccharide as vaccine adjuvant. *Expert Rev. Vaccines* **2015**, *14*, 861–876. [\[CrossRef\]](#)
23. Roche, S.M.; Gracieux, P.; Milohanic, E.; Albert, I.; Virlogeux-Payant, I.; Témoïn, S.; Grépinet, O.; Kerouanton, A.; Jacquet, C.; Cossart, P.; et al. Investigation of specific substitutions in virulence genes characterizing phenotypic groups of low-virulence field strains of *Listeria monocytogenes*. *Appl. Environ. Microbiol.* **2005**, *71*, 6039–6048. [\[CrossRef\]](#) [\[PubMed\]](#)
24. Borriello, G.; Lucibelli, M.G.; Pesciaroli, M.; Carullo, M.R.; Graziani, C.; Ammendola, S.; Battistoni, A.; Ercolini, D.; Pasquali, P.; Galiero, G. Diversity of *Salmonella* spp. serovars isolated from the intestines of water buffalo calves with gastroenteritis. *BMC Vet. Res.* **2012**, *8*, 201. [\[CrossRef\]](#)
25. Spatuzza, C.; Schiavone, M.; Di Salle, E.; Janda, E.; Sardiello, M.; Fiume, G.; Fierro, O.; Simonetta, M.; Argiriou, N.; Faraonio, R.; et al. Physical and functional characterization of the genetic locus of IBtk, an inhibitor of Bruton's tyrosine kinase: Evidence for three protein isoforms of IBtk. *Nucleic Acids Res.* **2008**, *36*, 4402–4416. [\[CrossRef\]](#) [\[PubMed\]](#)
26. Livak, K.J.; Schmittgen, T.D. Analysis of relative gene expression data using real-time quantitative PCR and the 2<sup>−ΔΔC<sub>T</sub></sup> method. *Front. Plant Sci.* **2001**, *25*, 402–408. [\[CrossRef\]](#) [\[PubMed\]](#)
27. Hu, N.; Qian, L.; Hu, Y.; Shou, J.-Z.; Wang, C.; Giffen, C.; Wang, Q.-H.; Wang, Y.; Goldstein, A.M.; Emmert-Buck, M.; et al. Quantitative real-time RT-PCR validation of differential mRNA expression of SPARC, FADD, Fascin, COL7A1, CK4, TGM3, ECM1, PPL and EVPLin esophageal squamous cell carcinoma. *BMC Cancer* **2006**, *6*, 33. [\[CrossRef\]](#)
28. Iannelli, D.; D'Apice, L.; Cottone, C.; Viscardi, M.; Scala, F.; Zoina, A.; Del Sorbo, G.; Spigno, P.; Capparelli, R. Simultaneous detection of cucumber mosaic virus, tomato mosaic virus and potato virus Y by flow cytometry. *J. Virol. Methods* **1997**, *69*, 137–145. [\[CrossRef\]](#)
29. Lotze, M. *Measuring Immunity: Basic Biology and Clinical Assessment*; Elsevier Academic Press: San Diego, CA, USA; London, UK, 2005; ISBN 978-1-42-375541-8.
30. Burmeister, A.R.; Fortier, A.; Roush, C.; Lessing, A.J.; Bender, R.G.; Barahman, R.; Grant, R.; Chan, B.K.; Turner, P.E. Pleiotropy complicates a trade-off between phage resistance and antibiotic resistance. *Proc. Natl. Acad. Sci. USA* **2020**, *117*, 11207–11216. [\[CrossRef\]](#)
31. Zhou, D.; Galán, J. *Salmonella* entry into host cells: The work in concert of type III secreted effector proteins. *Microbes Infect.* **2001**, *3*, 1293–1298. [\[CrossRef\]](#)
32. Galán, J.E.; Ginocchio, C.; Costeas, P. Molecular and functional characterization of the *Salmonella* invasion gene *invA*: Homology of *InvA* to members of a new protein family. *J. Bacteriol.* **1992**, *174*, 4338–4349. [\[CrossRef\]](#)
33. Ho, T.D.; Schlauch, J.M. Characterization of *grvA*, an Antivirulence Gene on the Gifsy-2 Phage in *Salmonella enterica* Serovar Typhimurium. *J. Bacteriol.* **2001**, *183*, 611–620. [\[CrossRef\]](#) [\[PubMed\]](#)
34. Wang, M.; Qazi, I.H.; Wang, L.; Zhou, G.; Han, H. *Salmonella* Virulence and Immune Escape. *Microorganisms* **2020**, *8*, 407. [\[CrossRef\]](#) [\[PubMed\]](#)
35. Ho, T.D.; Figueroa-Bossi, N.; Wang, M.; Uzzau, S.; Bossi, L.; Schlauch, J.M. Identification of GtgE, a Novel Virulence Factor Encoded on the Gifsy-2 Bacteriophage of *Salmonella enterica* Serovar Typhimurium. *J. Bacteriol.* **2002**, *184*, 5234–5239. [\[CrossRef\]](#)
36. Ranade, K.; Poteete, A.R. Superinfection exclusion (*sieB*) genes of bacteriophages P22 and lambda. *J. Bacteriol.* **1993**, *175*, 4712–4718. [\[CrossRef\]](#) [\[PubMed\]](#)
37. Lu, R.; Zhang, Y.-G.; Sun, J. STAT3 activation in infection and infection-associated cancer. *Mol. Cell. Endocrinol.* **2017**, *451*, 80–87. [\[CrossRef\]](#)
38. Reynolds, C.M.; Ribeiro, A.A.; McGrath, S.C.; Cotter, R.J.; Raetz, C.R.H.; Trent, M.S. An Outer Membrane Enzyme Encoded by *Salmonella typhimurium* *lpxR* That Removes the 3'-Acylxyacyl Moiety of Lipid A. *J. Biol. Chem.* **2006**, *281*, 21974–21987. [\[CrossRef\]](#) [\[PubMed\]](#)
39. Lou, L.; Zhang, P.; Piao, R.; Wang, Y. *Salmonella* Pathogenicity Island 1 (SPI-1) and Its Complex Regulatory Network. *Front. Cell. Infect. Microbiol.* **2019**, *9*, 270. [\[CrossRef\]](#) [\[PubMed\]](#)
40. Park, D.; Lara-Tejero, M.; Waxham, M.N.; Li, W.; Hu, B.; Galán, J.E.; Liu, J. Visualization of the type III secretion mediated *Salmonella*-host cell interface using cryo-electron tomography. *eLife* **2018**, *7*. [\[CrossRef\]](#)
41. Que, F.; Wu, S.; Huang, R. *Salmonella* Pathogenicity Island 1 (SPI-1) at Work. *Curr. Microbiol.* **2013**, *66*, 582–587. [\[CrossRef\]](#)
42. Rushing, M.D.; Schlauch, J.M. Either periplasmic tethering or protease resistance is sufficient to allow a SodC to protect *Salmonella enterica* serovar Typhimurium from phagocytic superoxide. *Mol. Microbiol.* **2011**, *82*, 952–963. [\[CrossRef\]](#) [\[PubMed\]](#)
43. Santoro, M.; Rossi, A.; Amici, C. New embo member's review: NF-kappaB and virus infection: Who controls whom. *EMBO J.* **2003**, *22*, 2552–2560. [\[CrossRef\]](#)
44. Mukaida, N.; Harada, A.; Matsushima, K. Interleukin-8 (IL-8) and monocyte chemotactic and activating factor (MCAF/MCP-1), chemokines essentially involved in inflammatory and immune reactions. *Cytokine Growth Factor Rev.* **1998**, *9*, 9–23. [\[CrossRef\]](#)
45. Maurer, M.; von Stebut, E. Macrophage inflammatory protein-1. *Int. J. Biochem. Cell Biol.* **2004**, *36*, 1882–1886. [\[CrossRef\]](#)
46. Lissoni, P.; Messina, G.; Pelizzoni, E.; Rovelli, F.; Brivio, F.; Monzon, A.; Crivelli, N.; Lissoni, A.; Tassoni, S.; Sassola, A.; et al. The Fascination of Cytokine Immuno-logical Science. *J. Infect. Rev. Artic.* **2020**, *3*, 18–28.
47. Arango Duque, G.; Descoteaux, A. Macrophage Cytokines: Involvement in Immunity and Infectious Diseases. *Front. Immunol.* **2014**, *5*, 491. [\[CrossRef\]](#) [\[PubMed\]](#)
48. Eckmann, L.; Kagnoff, M.F. Cytokines in host defense against *Salmonella*. *Microbes Infect.* **2001**, *3*, 1191–1200. [\[CrossRef\]](#)



49. Steward-Tharp, S.M.; Laurence, A.; Kanno, Y.; Kotlyar, A.; Villarino, A.V.; Sciume, G.; Kuchen, S.; Resch, W.; Wohlfert, E.A.; Jiang, K.; et al. A mouse model of HIES reveals pro- and anti-inflammatory functions of STAT3. *Blood* **2014**, *123*, 2978–2987. [[CrossRef](#)]
50. León, M.; Bastias, R. Virulence reduction in bacteriophage resistant bacteria. *Front. Microbiol.* **2015**, *6*, 343. [[CrossRef](#)] [[PubMed](#)]
51. Jarrell, K.F.; Kropinski, A. Isolation and characterization of a bacteriophage specific for the lipopolysaccharide of rough derivatives of *Pseudomonas aeruginosa* strain PAO. *J. Virol.* **1981**, *38*, 529–538. [[CrossRef](#)]
52. Nijland, R.; Hofland, T.; Van Strijp, J.A.G. Recognition of LPS by TLR4: Potential for Anti-Inflammatory Therapies. *Mar. Drugs* **2014**, *12*, 4260–4273. [[CrossRef](#)] [[PubMed](#)]